



HAL
open science

Drying of mixes of dairy protein using single and monodisperse droplet experiments

Ming Yu

► **To cite this version:**

Ming Yu. Drying of mixes of dairy protein using single and monodisperse droplet experiments. Food and Nutrition. Agrocampus Ouest, 2022. English. NNT : 2022NSARB354 . tel-03711335

HAL Id: tel-03711335

<https://theses.hal.science/tel-03711335>

Submitted on 1 Jul 2022

HAL is a multi-disciplinary open access archive for the deposit and dissemination of scientific research documents, whether they are published or not. The documents may come from teaching and research institutions in France or abroad, or from public or private research centers.

L'archive ouverte pluridisciplinaire **HAL**, est destinée au dépôt et à la diffusion de documents scientifiques de niveau recherche, publiés ou non, émanant des établissements d'enseignement et de recherche français ou étrangers, des laboratoires publics ou privés.

THESE DE DOCTORAT DE

L'INSTITUT NATIONAL D'ENSEIGNEMENT SUPERIEUR POUR L'AGRICULTURE, L'ALIMENTATION ET
L'ENVIRONNEMENT
ECOLE INTERNE AGROCAMPUS OUEST

ECOLE DOCTORALE N° 600
Ecole doctorale Ecologie, Géosciences, Agronomie et Alimentation
Spécialité : Sciences des Aliments

Ming YU

« Séchage de gouttes uniques et monodisperses de mélanges de protéines laitières »

« Drying of mixes of dairy protein using single and monodisperse droplet experiments »

Thèse présentée et soutenue à RENNES, le 19 janvier 2022

Unité de recherche : INRAe, L'institut Agro, UMR 1253 Science & Technologie du Lait & de l'Œuf

Thèse N° : B-354 _ 2022-2

Rapporteurs avant soutenance :

Martine Meireles Directrice de recherche CNRS, LGC Université Toulouse III
Guillaume Delaplace Directeur de recherche INRAe, UMET Villeneuve d'Ascq

Composition du Jury :

Martine Meireles	Directrice de recherche CNRS, LGC Université Toulouse III	Rapporteure
Guillaume Delaplace	Directeur de recherche INRAe, UMET Villeneuve d'Ascq	Rapporteur
Nan Fu	Professeure, Soochow University, Suzhou	Examinatrice
Thierry Ruiz	Professeur, Qualisud, Université de Montpellier	Examineur
Romain Jeantet	Professeur, STLO L'institut Agro - Rennes	Directeur de thèse
Cécile Le Floch-Fouéré	Professeure, STLO, L'institut Agro - Rennes,	Co encadrante
Luca Lanotte.	Chargé de recherche INRAE, STLO, Rennes,	Co encadrant

SECHAGE DE GOUTTES UNIQUES ET MONODISPENSES DE MELANGES DE PROTEINES LAITIERES

Résumé : Afin de garantir les propriétés des formules infantiles, un parfait contrôle du séchage est nécessaire. Mais comprendre la transition goutte à particule est difficile au sein d'enceintes fermées et au vu des cinétiques de séchage. Cette thèse vise à étudier la formation de la peau en surface de gouttes de mélange de protéines solubles (WPI) et micelles de caséine (NPC), qui influence la morphologie et les propriétés des particules.

L'influence du rapport WPI/NPC (WPI%R) sur la formation de la peau, la morphologie des particules et la cinétique de séchage a été démontrée sur goutte unique. Au-delà d'un WPI%R critique, les protéines solubles contrôlent les caractéristiques interfaciales, depuis la transition sol-gel jusqu'à solidification complète. 4 morphologies caractéristiques ont été observées selon un diagramme de phase validé en séchage monodisperse et fonction de la concentration protéique globale (C_p) et du WPI%R. Ainsi, l'augmentation de C_p induit une transition sol-gel précoce, réduisant la contraction volumique et la délamination des particules. Par ailleurs, le remplacement des NPC par des caséinates de sodium dans les mélanges conduit à un comportement intermédiaire induit par leurs caractéristiques physico-chimiques et de taille. Enfin, un modèle préliminaire a été établi pour prédire la transition de phase des gouttelettes lors du séchage par atomisation.

Ce travail permet de mieux comprendre la phénoménologie du séchage des colloïdes laitiers, et plus généralement la physique de la structuration de l'interface de systèmes polydispersés. Ses perspectives concernent la formation de particules à partir de formulations plus complexes représentatives de produits nutritionnels.

Mots clefs : Séchage - Caséines – Protéines solubles – Peau – Transition sol-gel – Particule

INTRODUCTION GENERALE : POSITIONNEMENT DE LA PROBLEMATIQUE DE RECHERCHE

Le procédé de séchage par atomisation est largement utilisé dans les industries alimentaires, pharmaceutiques et biochimiques pour générer des produits secs sous forme de poudre. En ce qui concerne plus spécifiquement l'industrie laitière, les produits secs sont principalement obtenus à partir de lait de vache, qui constitue une source de protéines et de nutriments de haute qualité. La consommation de produits laitiers secs et, par conséquent, le volume de la production de lait, n'ont cessé d'augmenter avec la croissance démographique et la transition économique des dernières décennies, la production globale atteignant 881 millions de tonnes en 2019. Dans ce contexte de

mondialisation, le procédé de séchage par atomisation permet de prolonger la durée de stockage et de réduire les coûts d'expédition et de stockage.

Selon les besoins du marché, différents types de poudres laitières sont produits aujourd'hui, tels que le lait entier en poudre (*whole milk powder*, WMP), le lait écrémé en poudre (*skim milk powder*, SMP) et le lait infantile en poudre (*infant milk formula*, IMF). Aujourd'hui, de plus en plus de parents accordent une attention particulière à offrir une nutrition de qualité supérieure à leur bébé en termes de santé et de croissance. Le secteur des IMF a ainsi connu une croissance sans précédent et est devenu un des moteurs de croissance principaux de l'industrie laitière mondiale ces dernières années. Sur la base des données de l'industrie, la consommation de poudre IMF est passée de 0,97 à 2,15 millions de tonnes entre 2005 et 2019 (+121,5%) et devrait poursuivre sa croissance d'ici 2024 pour atteindre 2,38 millions de tonnes (+10,8%).

Ce contexte de marché a impulsé en parallèle un effort accru de recherche afin de comprendre les mécanismes de formation des particules de poudre pour mieux contrôler et prédire la qualité de la poudre d'IMF. Les principales étapes du procédé de séchage par pulvérisation sont bien établies. Tout d'abord, la solution d'alimentation concentrée est pulvérisée en gouttelettes micrométriques (typiquement 60-200 microns) ; leur exposition à un flux d'air chaud et sec induit un transfert d'eau rapide permettant de limiter les risques de collage en bas de tour. Bien que cette opération puisse sembler relativement aisée, sa complexité réside dans les transferts simultanés de matière et de chaleur se produisant au sein des particules et dans la chambre de séchage. En particulier, différents phénomènes physiques et mécaniques se produisent à l'interface air-liquide des gouttelettes, tels que des changements de phase (e.g., transition vitreuse et sol-gel) et des instabilités mécaniques, affectant fortement les propriétés finales des particules séchées. Les propriétés physico-chimiques des poudres obtenues à partir d'un sécheur-atomiseur mettent en évidence l'influence de deux catégories de paramètres : i) les caractéristiques de la solution d'alimentation, telles que la composition du concentré et ses concentrations en soluté, affectant la tension superficielle et le comportement rhéologique, et ii) les paramètres du procédé de séchage, tels que la température et le débit d'air, affectant le temps de séjour moyen, etc.

Du fait du contrôle encore relativement empirique du procédé de séchage, des problèmes sont rencontrés à l'échelle industrielle, tant en matière de propriétés du produit (non-conformité par rapport aux propriétés attendues) que de performances du procédé (facteurs limitants tels que le collage en tour). En effet, les mécanismes de formation des particules par séchage par pulvérisation ne sont pas encore entièrement compris car la chambre de séchage est une « boîte noire » rendant impossible l'observation directe et en ligne de la formation des gouttelettes-particules, outre le fait que celles-ci se déplacent. Il est donc nécessaire de croiser différents domaines de connaissances et

de développer de nouveaux outils et méthodes analytiques pour mieux appréhender ces mécanismes. A ce titre, la littérature rapporte de nombreux travaux étudiant le séchage des gouttelettes à l'échelle d'une seule gouttelette.

De plus, le lait est une suspension et une émulsion complexe, comprenant de l'eau, des macroéléments (ex. glucides, lipides, protéines) et des microéléments (ex. minéraux et vitamines), avec une assez grande variété de composition selon la saison, l'alimentation et le système d'élevage. Cette variabilité complique encore plus la compréhension des phénomènes impliqués.

Par conséquent, l'étude de la transition gouttelette-particule, rapportée dans la littérature à différentes échelles (laboratoire, pilote, installation industrielle), s'est focalisée jusqu'à présent et pour l'essentiel sur des systèmes de modèles de lait simplifiés. La grande majorité de ces travaux ont été réalisés sur les protéines du lait (protéines de lactosérum et caséines micellaires), qui représentent des ingrédients hautement nutritionnels et fonctionnels essentiels dans la conception de formules infantiles. L'évolution de la morphologie des gouttelettes a été étudiée à l'échelle du laboratoire grâce à une expérience de séchage d'une seule gouttelette : quelle que soit la protéine, une peau est formée à la surface de la gouttelette une fois la transition sol-gel atteinte au cours de l'évaporation, dont les propriétés affectent pour partie la morphologie et les propriétés d'usage des particules après séchage.

STRATEGIE DE RECHERCHE

Dans ce contexte, l'objectif de ce doctorat est d'explorer le comportement au séchage de mélanges d'isolats de protéines de lactosérum (WPI) et de phosphocasinates natifs (NPC) et notamment les mécanismes de formation des particules, qui impactent directement les propriétés morphologiques et fonctionnelles des poudres finales. Ce projet, exploratoire à certains égards, est basé sur une investigation physique pour représenter et expliquer les phénomènes de séchage (par exemple, flambage et transitions de phase, flux internes, etc.) dans le système de mélanges de protéines laitières. En particulier, nous avons souhaité évaluer l'impact du rapport WPI/NPC sur le comportement de séchage des gouttelettes, pour comprendre les mécanismes de formation et d'évolution de la peau dans les systèmes binaires étendus. Pour atteindre cet objectif, une série de travaux a été conçue pour étudier l'organisation des molécules protéiques à l'interface des gouttelettes. Au début de l'évaporation, nous avons utilisé des modèles théoriques récents et l'évaluation des propriétés rhéologiques interfaciales pour expliquer l'accumulation préliminaire et l'auto-organisation des protéines à l'interface air-liquide. Avec la concentration des molécules de protéines à la surface des gouttelettes et la formation de peau qui en résulte, l'influence de l'auto-arrangement des protéines sur les propriétés viscoélastiques de la peau a été explorée en fonction du temps. En observant la structure de la peau des particules et la forme de celles-ci après solidification

complète, l'impact des propriétés physico-chimiques des protéines sur la réponse mécanique de la peau a été illustré. La dernière partie de ce travail a été consacrée à établir un modèle prédictif de la transition de phase des gouttelettes dans la chambre de séchage par atomisation en couplant l'approche d'ingénierie de réaction (REA) et le modèle de carte énergétique (EMM).

Grâce à cette stratégie, cinq résultats principaux ont été obtenus dans ce travail.

RESULTATS & DISCUSSION

1. FORMATION DE LA PEAU AU COURS DU SECHAGE DE MELANGES DE PROTEINES LAITIÈRES : APPROCHE MORPHOLOGIQUE ET CINÉTIQUE

Tout d'abord, nous avons exploré la formation et l'évolution de la peau au cours du séchage des gouttelettes de mélanges de protéines laitières. Afin d'éclairer les mécanismes de formation de la peau, l'évolution du profil et la cinétique de séchage des gouttelettes ont été étudiées à l'échelle de la goutte unique pour différents ratios WPI / NPC ($WPI\%_R$ = masse de WPI/masse de protéine globale) (**Figure 1**).

Par analogie avec des travaux antérieurs sur le séchage de protéines individuelles, trois étapes d'évaporation différentes ont été observées. Quel que soit le $WPI\%_R$, les gouttelettes présentaient une forme sphérique avec un angle de contact similaire au début du séchage. Dans un second temps, les gouttelettes ont progressivement perdu cette géométrie quasi sphérique du fait du rétrécissement progressif induit par l'évaporation du solvant. En effet, la diminution progressive du volume a favorisé l'accumulation de colloïdes à l'interface air-liquide du fait de la compétition entre la progression du front d'évaporation et les mouvements diffusifs. L'estimation du nombre de Péclet a ainsi permis de prédire que pour nos conditions expérimentales, l'évaporation l'emporte sur les phénomènes de diffusion conduisant à la formation d'une couche colloïdale interfaciale. Successivement, la diminution progressive de l'angle de contact des gouttelettes a entraîné l'apparition d'écoulements capillaires avec une intensité croissante une fois l'angle de contact $\Theta < 90^\circ$. Ce type d'écoulement a amélioré le transport continu des colloïdes vers la ligne triple des gouttelettes, où le taux d'évaporation est maximal. Ainsi, l'accumulation externe de macromolécules WPI et NPC a entraîné la formation d'un pied gélifié conférant une sorte de chapeau mexicain à la goutte. Il convient de souligner que jusqu'à ce stade, les gouttelettes présentaient qualitativement le même comportement quel que soit le $WPI\%_R$, et aucune preuve de formation de peau n'était observée, que ce soit directement ou par son impact sur la cinétique d'évaporation. Cependant, à la fin de la transition sol-gel, les signes de gélification de surface étaient flagrants, conduisant à deux catégories principales de morphologie en fonction de $WPI\%_R$:

- Pour $WPI\%_R \leq 20\%$, les gouttelettes présentaient un processus de flambage typique avec une réduction limitée de leur diamètre,
- Pour $WPI\%_R \geq 50\%$, elles présentaient une surface lisse ronde et un détachement net (c'est-à-dire un délaminage) de la bordure du substrat.

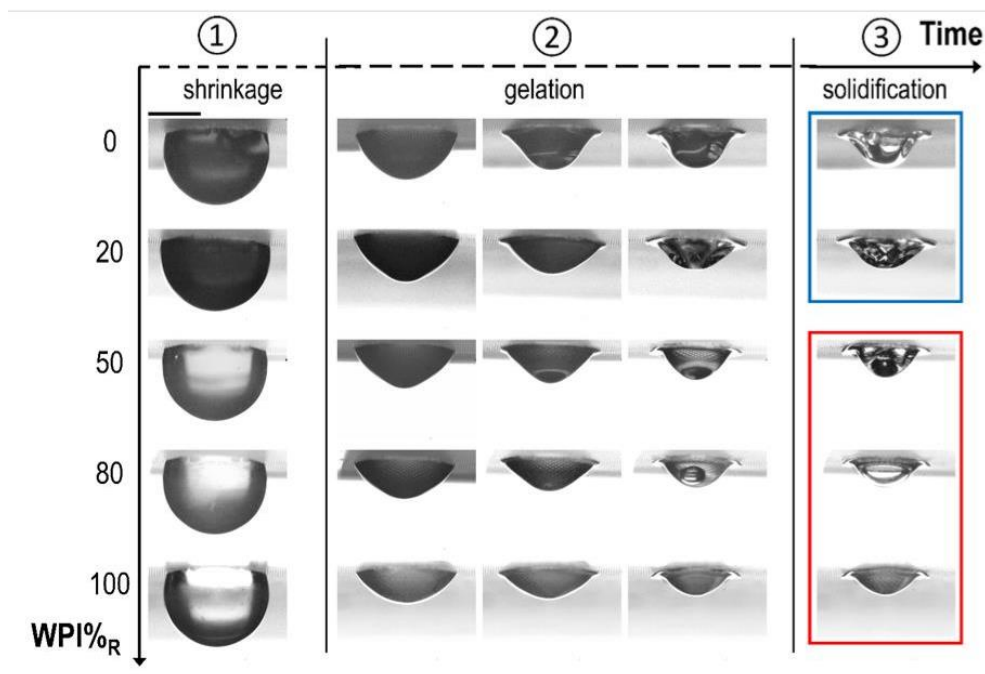


Figure 1 : Évolution morphologique des gouttelettes de WPI/NPC au cours de l'évaporation en fonction du ratio $WPI\%_R$. La barre d'échelle est égale à $500\mu m$.

A la fin du processus d'évaporation, aucune modification de forme n'était plus observée dans les échantillons. En d'autres termes, l'évaporation de l'eau résiduelle ne modifie pas les particules des deux catégories distinguées respectivement par le flambement et la surface lisse : elle s'accompagne en revanche de la formation ou du développement définitif d'une vacuole au cœur de la particule. L'observation de ces deux morphologies ne constitue pas un résultat inhabituel. En fait, la forme ridée (NPC) et ronde (WPI) a souvent été observée dans des travaux antérieurs sur des systèmes colloïdaux modèles et dans des échantillons biologiques, en fonction de la concentration du soluté, de la composition du solvant et des conditions expérimentales (température, humidité). Les phénomènes de flambage sont des instabilités de niveau secondaire qui se produisent lorsque la peau des gouttelettes ne résiste pas à la pression croissante vers l'intérieur qui se développe pendant le séchage. Nos résultats démontrent que les propriétés physico-chimiques du WPI peuvent conférer une plus grande rigidité à l'interface même en présence de NPC. Cette robustesse accrue pourrait dépendre non seulement des propriétés des colloïdes, mais également des caractéristiques structurales de la peau.

Pour résumer, l'analyse qualitative de l'évolution de la forme des gouttelettes a montré que le $WPI\%_R$ a un fort impact sur la dynamique de séchage des gouttelettes des mélanges WPI/NPC, entraînant une transition de forme se produisant à une concentration relative WPI critique ($WPI\%_{RC}$) comprise entre 20% et 50%. De plus, les deux principaux types de morphologie obtenus suggèrent un rôle compétitif joué par les deux catégories de colloïde sur le processus de séchage : en effet, bien que le WPI soit le composant mineur dans les mélanges en termes de fraction volumique, les protéines de lactosérum régissent la forme finale des gouttelettes si elles sont suffisamment représentées dans le système ($WPI\%_R > 50\%$).

À la lumière de ces résultats sur la morphologie des gouttelettes, nous avons cherché à comprendre si l'évolution des propriétés mécaniques de surface dépendait simplement de la concentration en colloïde dans l'échantillon, ou si l'organisation spécifique des WPI et NPC à l'interface air-liquide intervenait également. La cinétique d'évaporation des gouttelettes peut être utilisée comme preuve indirecte pour explorer la structure de la peau des particules dans la mesure où celle-ci affecte la dynamique de transfert de l'eau. Dans tous les échantillons WPI/NPC, des stades de séchage similaires en fonction du taux d'évaporation ont été observés, conformément aux résultats obtenus par observation de la morphologie. D'une part, nous avons détecté une différence évidente entre les comportements NPC et WPI, d'autre part, une relative similitude entre les suspensions de WPI pur et les mélanges avec $WPI\%_R=50\%$. Afin de mieux caractériser la formation de la peau, le temps de demi-vie a été défini comme le moment où le taux d'évaporation atteint la moitié de sa valeur initiale : sa mesure a permis de démontrer l'apparition plus précoce de la gélification de surface dans les dispersions de NPC par rapport à celle de WPI. Ce comportement a été interprété à la lumière d'une concentration massique critique plus faible pour déclencher la transition sol-gel à l'interface air-gouttelette dans le cas du NPC. La raison peut être attribuée à la présence abondante de caséines en suspension, couplée à leurs propriétés physico-chimiques et structurales qui favorisent l'accumulation à l'interface air-liquide des gouttelettes et la formation d'une couche concentrée à haute affinité pour l'eau. De façon étonnante, nous avons également détecté un temps de séchage plus long pour les gouttelettes de NPC que pour celles de WPI. En effet, on pourrait penser que, du fait de leur structure globulaire rigide, les colloïdes de type WPI contribuent au développement d'une peau compacte, alors que les micelles irrégulières et déformables de NPC s'auto-organiseraient en une structure poreuse à mailles plus lâches. Dans ce cas, une peau riche en WPI très compactée, similaire au cas des sphères colloïdales monodisperses, devrait constituer une résistance à l'évaporation de l'eau plus élevée qu'une couche superficielle de NPC clairsemée. En réalité, les NPC s'organisent selon une structure très dense, qui est principalement affectée par la polydispersité autour de leur taille moyenne. L'augmentation supplémentaire de la concentration de l'échantillon induite par des pressions

osmotiques croissantes implique également une compression des micelles et des liaisons intermicellaires conduisant au développement d'un gel compact. Cette organisation différente du WPI et du NPC dans la couche de peau explique le séchage plus rapide des gouttelettes de WPI.

En ce qui concerne l'analogie de comportement dans les mélanges WPI/NPC avec $WPI\%_R \geq 50$, la présence de colloïdes de type WPI est un facteur limitant de la dynamique de séchage. L'impact prépondérant du WPI sur la structure et les propriétés mécaniques de la peau a été expliqué par la possible ségrégation des protéines induite par le séchage et l'accumulation des plus petits colloïdes, ici le WPI, dans les couches externes de la peau (théorie *small-on-top*).

Les détails de la structure de la peau des gouttelettes de mélanges laitiers ont été observés par microscopie électronique à balayage. Les sections sèches de particules de WPI affichaient une structure dense et lisse, tandis que celles de NPC étaient caractérisées par des régions compactes clairsemées de vides, en particulier à proximité de la surface des particules. En effet, la taille quasi monodisperse et la structure rigide et globulaire des colloïdes WPI conduisent à la formation d'une peau homogène et dense, comme on l'observe normalement dans les dispersions colloïdales de sphères dures. En raison de leur polydispersité élevée, de leur déformation et de leur développement de liaison, les micelles de caséines du NPC contribuent à augmenter de manière significative le compactage, mais aussi la formation de pores dispersés de manière irrégulière dans les couches constitutives de la peau. Dans les mélanges avec $WPI\%_R = 50\%$, les propriétés de peau WPI et NPC se retrouvent simultanément en fonction de la distance de la surface. En effet, la couche supérieure présentait une compacité et une porosité homogènes, similaires au WPI, mais la partie interne de la peau présentait des irrégularités et des cavités de type NPC. Cette observation est concordante avec l'hypothèse d'une ségrégation des micelles de caséines et des protéines de lactosérum au cours du séchage. Cette ségrégation de WPI et NPC, sous certaines conditions, a été interprétée à la lumière du modèle ZJD pour les systèmes binaires. Selon cette théorie, l'accumulation de colloïdes à la surface des gouttelettes tout au long de l'évaporation de l'eau conduit à une augmentation de la pression osmotique, favorisant le mouvement de macromolécules plus petites vers l'interface air-liquide. Étonnamment, bien que les WPI et NPC présentent une structure et des propriétés physicochimiques différentes qui pourraient influencer le processus de séchage des gouttelettes, c'est ainsi le rapport de taille des deux protéines qui intervient principalement dans le contrôle de la stratification.

Pour aller plus loin, la ségrégation préférentielle de WPI et NPC a été abordée au moyen d'un tensiomètre à goutte oscillante permettant d'étudier les propriétés rhéologiques interfaciales d'une surface au cours du temps. En raison de l'adsorption continue des protéines laitières, un gradient vertical de concentration de protéines s'est progressivement formé à l'interface des gouttelettes,

généralisant des pressions osmotiques croissantes et conduisant à l'apparition de phénomènes de stratification. Le suivi du module viscoélastique interfacial de l'échantillon de mélange a permis de montrer que les protéines de lactosérum et les micelles de caséine présentaient un comportement différent au cours du processus de vieillissement. Cependant, les courbes de module obtenues pour les échantillons de mélange étaient toutes proches de celle du WPI pur lorsque $WPI\%_R \geq 50\%$. En d'autres termes, les protéines de lactosérum préfèrent s'accumuler à la surface externe de la peau, et impactent par suite les propriétés interfaciales au cours du processus de vieillissement.

Globalement, ce comportement de stratification dans la peau a influencé la cinétique de séchage et la morphologie finale des particules. Le rapport de taille des colloïdes entre WPI et NPC a été déterminé comme un facteur clé induisant une telle stratification spécifique, en accord avec les travaux expérimentaux et théoriques antérieurs sur les systèmes de modèles binaires.

Selon nos observations, la ségrégation des protéines induite par le séchage dans les mélanges WPI/NPC est principalement régie par le rapport de taille WPI/NPC. Cependant, d'autres facteurs pourraient influencer le comportement de séchage des gouttelettes des mélanges de protéines de lactosérum et de micelles de caséine. Pour répondre à cette question, nous avons exploré l'impact possible de la structure des protéines et des propriétés physicochimiques qui en résultent sur le séchage des mélanges laitiers en remplaçant les NPC par des caséinates de sodium (SC). Du point de vue moléculaire, NPC et SC sont tous deux constitués d' α_s , β et κ -caséine. Cependant, ces deux isolats présentent des différences flagrantes en termes de structure. Les micelles de caséine, dont le diamètre moyen varie de 100 à 300 nm dans le lait bovin, peuvent être décrites de manière simpliste comme un réseau de sous-micelles structurées par des nano clusters de phosphates de calcium et de calcium associé au phosphosérines, comprenant au cœur des caséines plus hydrophobes (α_s) et en surface des κ -caséines plus amphiphiles. La déstructuration de la micelle par acidification/neutralisation au cours du procédé d'obtention des caséinates conduit dans le cas des caséinates de sodium à des structures amorphes de rayon moyen plus petit (≈ 10 nm). Fait intéressant, les colloïdes de type WPI et SC ont une taille comparable, ce qui ne permet pas de prédire a priori une auto-stratification par taille pendant le processus de séchage. Dans cette partie, nous avons comparé l'évolution de la morphologie des gouttelettes au cours de l'évaporation dans des mélanges WPI/SC à différents ratios $WPI\%_R$, et effectué une analyse quantitative de la réduction du diamètre des gouttelettes et de la hauteur finale des particules dans des échantillons de mélanges WPI/NPC et WPI/SC. L'étude préliminaire des mécanismes d'évaporation dans les mélanges WPI/SC a permis de mettre en évidence le rôle spécifique de chaque colloïde sur le cours des étapes de séchage et la forme finale des particules. En comparant le processus de séchage de NPC et SC, les résultats ont montré

que, malgré des différences structurelles flagrantes, les caractéristiques physicochimiques comparable des NPC et SC induisent de manière similaire une déformabilité élevée de la peau des gouttelettes et une atténuation significative de la délamination de leur pied. D'autre part, le rétrécissement global des gouttelettes, qui est influencé par la précocité de la transition sol-gel à l'interface air-liquide, a été fortement affecté par la taille moyenne des colloïdes, comme en témoigne la constance de la hauteur finale de l'apex dans Échantillons WPI/SC (protéines de taille comparable) et la diminution significative avec WPI%_R dans les mélanges WPI/NPC. Cependant, la seule observation de l'évolution du profil des gouttelettes au cours du processus de séchage ne permet pas de recueillir des preuves d'une auto-stratification possible dans un mélange WPI/SC, ouvrant ainsi la voie à d'autres investigations en cours (microscopie confocale, à balayage).

2. DIAGRAMME DE PHASE DE MELANGES DE PROTEINES LAITIÈRES OBTENU PAR SECHAGE DE GOUTTELETTE UNIQUE

La composition des protéines n'est pas le seul paramètre à influencer le séchage des gouttelettes. Il est nécessaire de considérer également l'impact de la concentration globale en protéines. De nombreuses études ont été réalisées sur le séchage des protéines laitières en utilisant une approche laboratoire au cours de la dernière décennie. Le séchage des gouttelettes a été exploré dans des solutions de configuration pendantes pour des gouttelettes de WPI ou NPC purs, puis pour des mélanges de protéines en utilisant une stratégie expérimentale similaire. Toutes ces études ont été réalisées sur des dispersions WPI/NPC avec soit différentes concentrations globales de protéines (c_p), soit différentes compositions (WPI%_R), donc sans permettre de dégager un aperçu global des phénomènes. Par conséquent, nous avons exploré dans cette section de la thèse l'effet de c_p (variant de 6 % p/p à 14 % p/p) sur la morphologie des particules de mélanges WPI/NPC pour différents WPI%_R. Nous avons caractérisé la diminution du diamètre des gouttelettes ($\Delta D\%$) et de la hauteur finale relative de l'apex (H_f/H_{max}) en fonction de c_p et de WPI%_R. Les résultats ont montré une réduction décroissante du diamètre des gouttelettes à concentration plus élevée, entraînant une transition du délaminage des bords vers un simple rétrécissement. Ce comportement a été interprété à la lumière de la composition effective des poudres utilisées pour la préparation des échantillons. En effet, les poudres de WPI sont constituées outre les protéines de lactosérum majoritaires environ 5% de caséines. Par conséquent, la quantité de molécules de caséine augmente avec la concentration en protéine des gouttelettes, ce qui favoriserait l'adhérence entre le substrat et le bord des gouttelettes et atténuerait le délaminage. De plus, une hauteur d'apex finale plus élevée a été mesurée dans les gouttelettes séchées à c_p croissante. Cette tendance s'explique par l'apparition plus précoce de la transition sol-gel avec une concentration croissante de protéines, due à l'atteinte d'une concentration critique de colloïdes à la surface des gouttelettes. Dans l'ensemble, ces résultats ont montré que la

composition de l'échantillon ($WPI\%_R$) affecte la dynamique de transition sol-gel à la surface des gouttelettes et à la triple ligne, mais ces phénomènes sont fortement atténués par l'augmentation de la concentration en protéines en raison des effets d'encombrement et des propriétés physico-chimiques de micelles de caséines. Cet aperçu global de l'impact de la composition et de la concentration de la suspension sur la morphologie finale des gouttelettes a conduit à la construction d'un premier diagramme de phase capable de prédire la forme des particules laitières en fonction des caractéristiques de dispersion initiale (c_p et $WPI\%_R$), et identifiant quatre régions principales correspondant à des morphologies spécifiques (**Figure 2**) :

- Région I : particules obtenues de dispersion majoritaire en NPC, et présentent quel que soit c_p une surface ridée typique avec formation de vacuoles et sans délaminage aux bords ;
- Région II : particules présentent une forme hybride (sphérique avec déformations) incluant une vacuole interne et un délaminage important. Elles sont issues de dispersion à valeur intermédiaire de $WPI\%_R$ et faible c_p ;
- Région III : particules présentant une interface lisse avec formation de vacuoles et délaminage aux bords. Elles sont issues de dispersion avec $WPI\%_R > 37\%$ et c_p intermédiaire/élevé ;
- Région IV : particules issues de dispersions majoritaire en WPI et faible c_p . Comme pour la région III, elles présentent une surface lisse typique des échantillons riches en WPI, mais en contraste avec un délaminage important et sans formation de vacuoles.

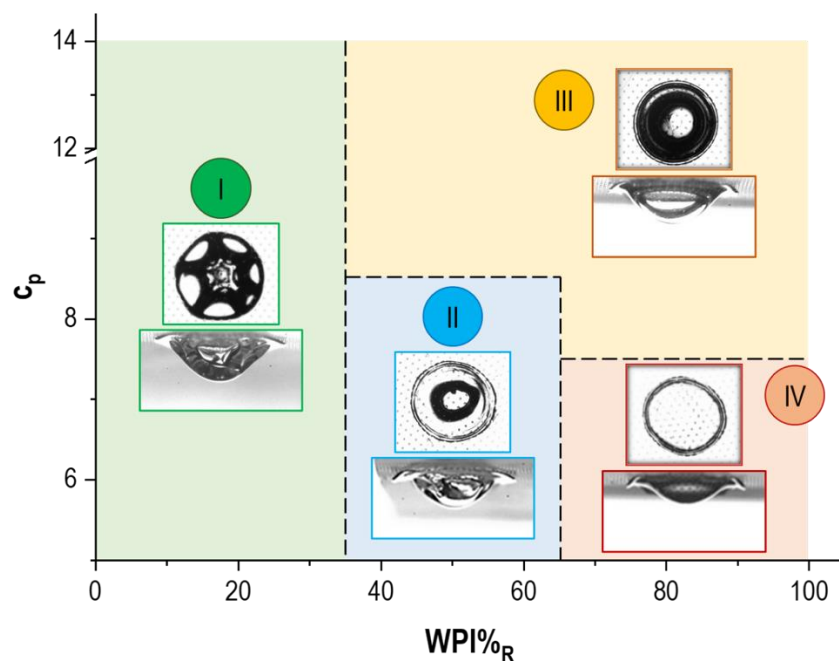


Figure 2. Diagramme de phase des principales morphologies des gouttelettes de WPI/NPC séchées en fonction de la concentration globale de protéines (c_p) et de la composition de l'échantillon ($WPI\%_R$).

3. PROPRIETES DE PARTICULES RESULTANT DE GOUTTELETTES VOLANTES

Pour valider le diagramme de phase obtenu à partir de l'approche de séchage goutte unique, nous avons analysé plus en détail la morphologie des particules de SC, WPI, NPC pures et de mélange WPI/NPC ($c_p = 10\%$ p/p) obtenues par un sécheur monodisperse. L'analyse quantitative des paramètres morphologiques clés des particules sèches (aire de section transversale, circularité et solidité) a été effectuée pour déterminer d'éventuels phénomènes d'organisation à l'interface induits par le séchage, par analogie avec ce qui a été observé à l'échelle d'une goutte unique. Deux résultats principaux ont été mis en évidence.

Tout d'abord, les mélanges WPI/NPC présentaient une forme ronde hybride, avec de légères bosses en surface, donc assez similaires aux poudres WPI pures. Cette similitude a également été confirmée par les valeurs de circularité et de solidité des particules. Par conséquent, il est possible de prédire une ségrégation des protéines et, en particulier, une stratification *small on top* également dans les gouttelettes volantes obtenues par séchage monodisperse, malgré la cinétique beaucoup plus rapide du séchage.

Par ailleurs, les particules sèches NPC et SC, bien qu'à la fois irrégulières et ridées, présentaient des différences évidentes en termes de sphéricité. En effet, la grande majorité des poudres NPC étaient constituées de petites particules ridées en forme d'étoile, tandis que celles de SC étaient principalement composées de particules plus grosses et sphériques, semblables à des ballons dégonflés. Cela pourrait être lié aux différentes propriétés de la peau induites par la taille des protéines dans les dispersions initiales. Les petits colloïdes SC, par analogie avec ceux du WPI, auraient tendance à former une peau compacte régulière capable de résister aux instabilités de surface conduisant aux phénomènes de flambage typiques des micelles de caséine.

Globalement, les résultats obtenus par la méthode de séchage par pulvérisation monodisperse ont montré des similitudes intéressantes avec les résultats observés sur le séchage de gouttelettes simples de suspensions de protéines laitières. Par conséquent, cela ouvre la voie à une étude approfondie et plus systématique au bénéfice d'un meilleur contrôle de la morphologie et des propriétés fonctionnelles des poudres.

4. COUPLAGE DES APPROCHES DE MODELISATION D'INGENIERIE DE LA REACTION ET DE CARTE ENERGETIQUE

La cinétique de séchage et la transition de phase subies par les protéines laitières sont contrôlées à l'interface par des interactions protéine-protéine et protéine-air complexes et hors d'équilibre. La modélisation de ces phénomènes par couplage des approches ingénierie de la réaction (REA) et de carte énergétique (EMM) peut aider à mieux comprendre et contrôler la cinétique de séchage, en établissant le lien entre la transition de phase et la cinétique de séchage. L'approche d'ingénierie de

la réaction met en relation l'énergie d'activation du séchage et la teneur en eau des gouttelettes. Le modèle de carte énergétique décrit le lien entre la pression interfaciale (pression osmotique) et l'énergie à surmonter pour que l'eau migre de l'intérieur de la gouttelette vers l'air ambiant. La courbe maîtresse REA a été établie pendant le séchage de gouttes uniques suspendues de NPC (*glass filament single droplet*). En couplant le REA et l'EMM, nous avons obtenu une équation (REA-EMM) qui représente l'évolution de la pression osmotique interfaciale des gouttelettes avec la teneur en eau au cours du séchage. Cependant, la valeur de pression osmotique calculée avec REA-EMM était 1000 fois supérieure aux données disponibles concernant le diagramme d'état du NPC (évolution de la pression osmotique de NPC en fonction de sa concentration). La pression osmotique de NPC à l'état d'équilibre obtenue à partir de l'isotherme de sorption était plus proche du résultat obtenu à partir de l'équation REA-EMM. Il faut souligner que la solution reconstituée de NPC contient environ 15 % p/p de solutés de plus faible masse molaire que les micelles de caséine (principalement des sels minéraux et du lactose), et que leur concentration au cours du séchage accroît de façon prépondérante la pression osmotique à l'intérieur de la particule. Ainsi, le modèle REA-EMM a surestimé l'évolution de la pression osmotique au cours du processus de séchage en considérant uniquement la pression osmotique interfaciale, et non en considérant la pression osmotique dans la partie centrale des particules. Ce travail ne fournit que quelques résultats préliminaires pour relier à terme la transition de phase à la cinétique de séchage.

CONCLUSION

Ce projet de thèse présente une contribution originale concernant l'évaporation de dispersions colloïdales bidisperses, car les mécanismes d'auto-stratification ont jusqu'à présent rarement été étudiés dans les systèmes biologiques. Nos résultats corroborent les théories les plus récentes sur la ségrégation par taille induite par le séchage. Ce travail est précurseur de futures investigations qui permettront à terme la prédiction de la forme des gouttelettes sèches à partir essentiellement des propriétés colloïdales (par exemple, taille, structure, propriétés mécaniques et charge de surface) et de la composition de solutions polydisperses. De plus, le diagramme de phase obtenu à partir d'expérience de séchage de gouttelettes uniques puis validé sur gouttes volantes monodisperses pourrait ouvrir la voie à des investigations plus approfondies et plus systématiques aboutissant à un contrôle strict de la morphologie et des propriétés fonctionnelles de la poudre.

ACKNOWLEDGMENTS

I have wonderful three-year study life in the lab of Science and Technology of Milk and Eggs (**STLO**). At the end of my Ph.D, I would like to thank all the people who have contributed to the accomplishment of this project. Thanks for the financial support of this project from the **Chinese Scholarship Council**.

First of all, I would like to thank the jury members: **Martine Meireles, Guillaume Delaplace, Nan Fu and Thierry Ruiz**, for agreeing to evaluate my work.

I express my heartfelt thanks to **Romain Jeantet, Cécile Le Floch-Fouéré** and **Luca Lanotte**. Especially thanks for your support and help over these three years, both study and life. I am also greatly indebted to your encouragement and valuable guidance in my work. Your rich expertise and your insightful feedback are critical factors for the smooth running of this project.

I also would like to thank **Arnaud Saint-Jalmes**, who helped and guided me to finish the droplet interfacial rheology test and provided a lot of valuable advice. Thanks to **Ludovic Pauchard** and **Patrice Bachin**, you gave me some constructive suggestions during the discussion when I met some questions about my work. Thanks to the member of my CSI committee, **Paul Menut** and **Thierry Ruiz**, thank you for your encouragement, support and instructive recommendations during my study.

Many thanks to everyone who gives me a hand during my work. I would particularly like to thank **Marie-No Madec, Françoise Boissel**, for the technical support in the experiment. Thanks to all the INRAe STLO members, your help and company made me not feel lonely in a foreign country.

Thank all the doctoral students, post-docs, interns and others that I have had the chance to meet during these three years. Thank you for your appearing in my life, which makes my life more wonderful. And I hope to meet you again somewhere in the world one day. My dear friends, thank you for your concern, support and help. Let me never be alone in the past three years.

I am grateful for my family's unconditional, unequivocal, and loving support. Especially to my parents, thank you for all the efforts and sacrifices that make me a better myself.

TABLE OF CONTENTS

INTRODUCTION	1
CHAPTER 1. ECONOMIC AND SCIENTIFIC CONTEXT	4
1.1. Worldwide dairy market	4
1.2. Composition, structure and physicochemical properties of cow milk	10
1.2.1. Lactose	10
1.2.2. FAT	11
1.2.3. Proteins	11
1.2.4. Minerals	16
1.2.5. Key differences between Human milk and cow milk.....	17
1.3. Infant formula processing and manufacture	20
1.3.1. Raw materials and preparation of the mix	22
1.3.2. Heat treatment	23
1.3.3. Homogenisation.....	24
1.3.4. Concentration by evaporation	25
1.3.5. Spray-drying	25
1.4. Drying mechanisms in droplets of dairy fluids	26
1.4.1. Pilot spray dryers	27
1.4.2. Single droplet approach.....	30
1.4.3. The physics of the drying process in colloidal droplets	33
1.4.4. Skin formation and characterization in dairy protein drying.....	35
CHAPTER 2. EXPERIMENTAL STRATEGY.....	43
2.1. Investigation on skin formation.....	44
2.1.1. Skin formation at the early stage of the drying	45
2.1.2. Later stage of the drying	46
2.1.3. Time evolution of the rheological properties of the skin	46
2.2. Modelling the drying kinetics	47
CHAPTER 3. MATERIAL AND METHODS	48
3.1. Sample preparation	48
3.1.1. Preparation of Whey protein isolates (WPI), Native phosphocaseinate (NPC) and Sodium caseinate (SC) solutions	48

3.1.2. Mixture sample preparation	48
3.2. Single droplet drying experiment	49
3.2.1. Hydrophobic substrate	49
3.2.2. Drying conditions	50
3.2.3. Droplet profile observation.....	50
3.2.4. Droplet top view observation	53
3.2.5. Droplet evaporation rate measurement.....	54
3.2.6. Particle section structure and shell thickness.....	55
3.3. Droplet interfacial properties.....	56
3.3.1. Surface tension measurement.....	56
3.3.2. Optimization of experimental parameters for droplet dilation tests.....	57
3.4. Monodisperse spray drying process	59
3.4.1. Analyzing powder’s shape factors	60
3.5. Glass filament drying experiments	61
3.5.1. Diameter measurement.....	62
3.5.2. Mass measurement	62
3.5.3. The temperature measurement of droplet	62
CHAPTER 4. RESULTS AND DISCUSSION	64
4.1. Skin layer formation in drying droplet of dairy protein mixes	64
4.1.1. Introduction	64
4.1.2. Experiment strategies	66
4.1.3. Results and discussion	66
4.1.4. Complementary results.....	78
4.1.5. Conclusions	81
4.2. Phase diagram of dairy protein mixes obtained by single droplet drying experiments	84
4.2.1. Introduction	84
4.2.2. Experiment strategy.....	84
4.2.3. Results and discussion	84
4.2.4. Conclusions	92
4.3. Exploring the properties of particles obtained from flying droplets.....	93
4.3.1. Introduction	93
4.3.2. Experiment strategies	93

Table of contents

4.3.3. Results and Discussion	94
4.3.4. Conclusions	99
4.4. Coupling Reaction Engineering and Energy Map approaches	100
4.4.1. Introduction	100
4.4.2. Modelling strategies	101
4.4.3. Results and discussion	105
4.4.4. Conclusions	111
GENERAL CONCLUSION AND PERSPECTIVES	113
REFERENCES	118
THESIS OUTPUTS.....	136
LIST OF FIGURES	137
LIST OF TABLES	142

INTRODUCTION

The spray drying process is widely used in food, pharmaceutical and biochemical industries to manufacture dry products in the form of powders. Concerning more specifically the dairy industry, dry products are mainly obtained from cow milk raw materials, which is a source of high-quality proteins and nutrients. For this reason, the consumption and volume of milk production have kept rising with the population growth and economical transition, the overall output reaching 881 million tons in 2019 (IDF, 2020); moreover, volume production is predicted to grow in the future. For these reasons, the spray drying method is largely adopted nowadays to produce dairy powders for the global and local markets, since it allows to extend the storage period and to reduce shipping and storage costs.

According to the different needs of customers, different kinds of dairy powders are produced, such as whole milk powder (WMP), skim milk powder (SMP) and infant milk formula powder (IMF). Since an increasing portion of parents pay significant attention to the premium nutrition of their baby in relation to health and growth issues, the IMF sector experienced an unprecedented growth and became a hot topic in recent years. Based on the industry data, the IMF powder consumption increased from 0.97 to 2.15 million tons between 2005 and 2019 (+121.5%) and a further growth to 2.38 million tons is expected by 2024 (+10.8%). This context clearly drives research to understand dairy particle formation mechanism and further to control and predict the quality of IMF powder.

The main stages of the drying process in a spray dryer are well-established. First, a concentrated feeding solution is sprayed into micrometric droplets and exposed to a hot air flow in order to induce a rapid water loss to avoid stickiness limitations. Although this operation could seem relatively easy, its complexity lies in fundamental and simultaneous mass and heat transfer phenomena occurring in the drying chamber. In particular, various physical and mechanical phenomena are taking place at the droplet air-liquid interface, such as phase changes (e.g., glass / sol-gel transition) and mechanical instabilities, strongly affecting the final properties of the dried particles. The physicochemical properties of powders obtained from a spray dryer highlight the influence of two categories of parameters according to the experimental conditions:

- i) the physicochemical properties of the product in relation to its composition/concentration, affecting surface tension and rheological behavior;
- ii) the drying process parameters, such as the temperature and flow rate of hot air, affecting the mean residence time etc.

Despite the relative empirical control in the operating the powder process, residual problems are still encountered at the industrial scale, especially regarding the product properties and the process

performance. Indeed, the mechanism of particle formation in the spray drying process is not yet fully understood because the drying chamber is a 'black box,' and it is impossible to observe directly the droplet-particle formation process in line. Therefore, it is necessary to cross different knowledge areas and develop new tools and analytical methods to better understand the basic principle of drying. In this way, the literature reports many works studying the droplet drying on a single droplet scale.

However, milk is a complex suspension and emulsion, including water, macro elements (e.g. carbohydrates, fat, proteins) and microelements (e.g., minerals and vitamins), with a fairly large variety of composition according to season, feed and farming system. This variability complicates the understanding of the droplet drying phenomena even more. Moreover, it should be noticed that milk proteins (whey proteins and casein micelles) are the highly nutritionally and functionally essential ingredients in infant formulae, whose properties strongly influence the final quality of the powder. Therefore, in the previous literature works, simplified milk models (pure milk protein, being single whey proteins or native phosphocaseinates, that is to say casein micelles) were used to explore the droplet-particle transition process on multi- scales. The droplet morphology evolution was investigated at the lab scale through single droplet drying experiment: regardless of the protein, a skin layer was formed at the droplet surface once the sol-gel transition was reached in the course of water evaporation, the properties of which, to a certain extent, affect the particle morphology after drying.

In this context, the goal of this Ph.D. project is to explore the drying behavior in WPI/NPC mixes and notably the mechanisms of particle formation, which directly impact the morphological and functional properties of final powders. This project is exploratory in some aspects, and it is based on physical investigation to picture and explain the drying phenomena (e.g., buckling and phase transitions, internal flows, etc.) in dairy protein mixes system. Moreover, it aims at highlighting the impact of the WPI/NPC ratio on droplet drying behavior, providing more information to understand the mechanisms of skin formation in extended binary systems.

The first chapter of this thesis present the economic and scientific context of this PhD project, assembling an overview of the global dairy trade and a literature review on dairy physicochemistry, powder manufacture and droplet drying mechanism of dairy protein (Chapter 1). On this basis, the experimental strategy (Chapter 2) and materials and methods (Chapter 3) of this project are described. The results and discussion are grouped in a single chapter (Chapter 4): First, it explores how the composition (4.1) and concentration (4.2) impact the skin layer formation and the particle shape evolution in the drying process of dairy protein mixes. Moreover, the shape factor of powder produced by monodisperse drying was analyzed (4.3). Last, the reaction engineering approach (REA) model of NPC was first established in order to provide a preliminary coupling of reaction engineering and energy

Introduction

map modelling approaches (4.4). Finally, the main contributions and potential avenues of research are drawn together in the General conclusion and outlook sections.

Chapter 1. ECONOMIC AND SCIENTIFIC CONTEXT

1.1. WORLDWIDE DAIRY MARKET

Dairy products represent one of the most common sources of high-quality proteins, and from a nutritional point of view, with egg white, are considered as products containing reference proteins. The nutritional benefits that result from their consumption and the ongoing globalization push forward the market demand growth, in particular in emerging dairy markets such as milk deficient regions in Asia.

Thereafter, the global milk production reached 881 million tonnes (mlt) all milk species included in 2019, on a steady growth trend of 2.2% close to the average over the last decade (2.4%; (IDF, 2020)). Global milk production is driven by three main world regions, i.e. Asia with 42% total milk followed by Europe and North & Central America with 20% and 15% total milk, respectively. At the same time, the average per capita milk consumption reached 114.7 kg at the global scale in 2019 (+1.1%; **Figure 1**). This parameter does not reflect the strong differences in consumption habit and level existing between the different regions of the world. As an example, milk and fermented products are significantly consumed in India compared to some European countries, contrary to the case of cheese. Moreover, the average milk equivalent per capita annual consumption shows a large dispersion, ranging from 42 kg in Africa to approx. 275 kg in Europe and North America.

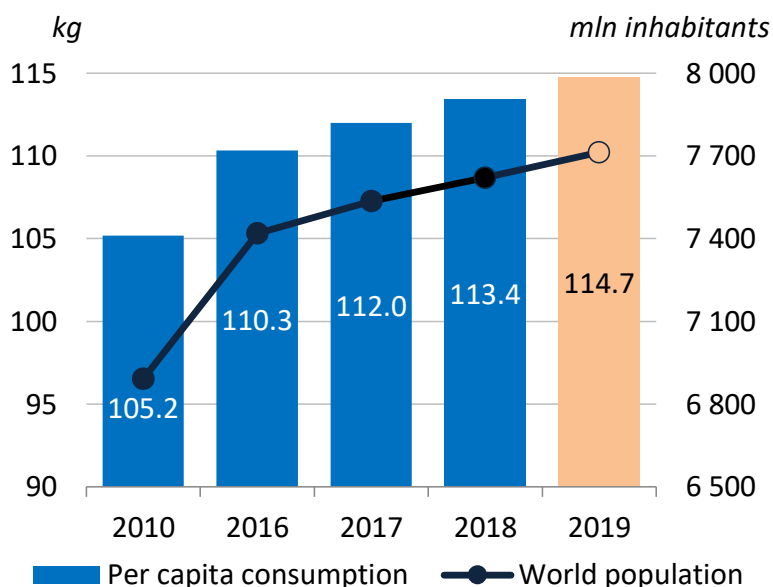


Figure 1. Global milk equivalent per capita annual consumption (left axis; kg/(year.inhabitant)) and world population (right axis; million inhabitant) between 2010 and 2019 (IDF, 2020)

Cow milk represents the main portion of milk production, with 714 million tonnes. The growth is mainly driven by the dynamic trend in both cow and buffalo’s milk production in Asia, in particular in India (188 mlt; +6.5%), China (32 mlt; +4,1%) and Pakistan (48 mlt; +3.3%), whereas traditional excess production regions with regard to local consumption (EU, Oceania, USA) added only marginal volume (**Figure 2**). However, the Asian dairy market is growing faster than its growing milk production, making it challenging for the local production to cover the consumer demand: indeed, the self-sufficiency rate in Asia decreased from 93% in 2010 to 90% in 2019, despite a growth production rate of +4.0% per year on this period.

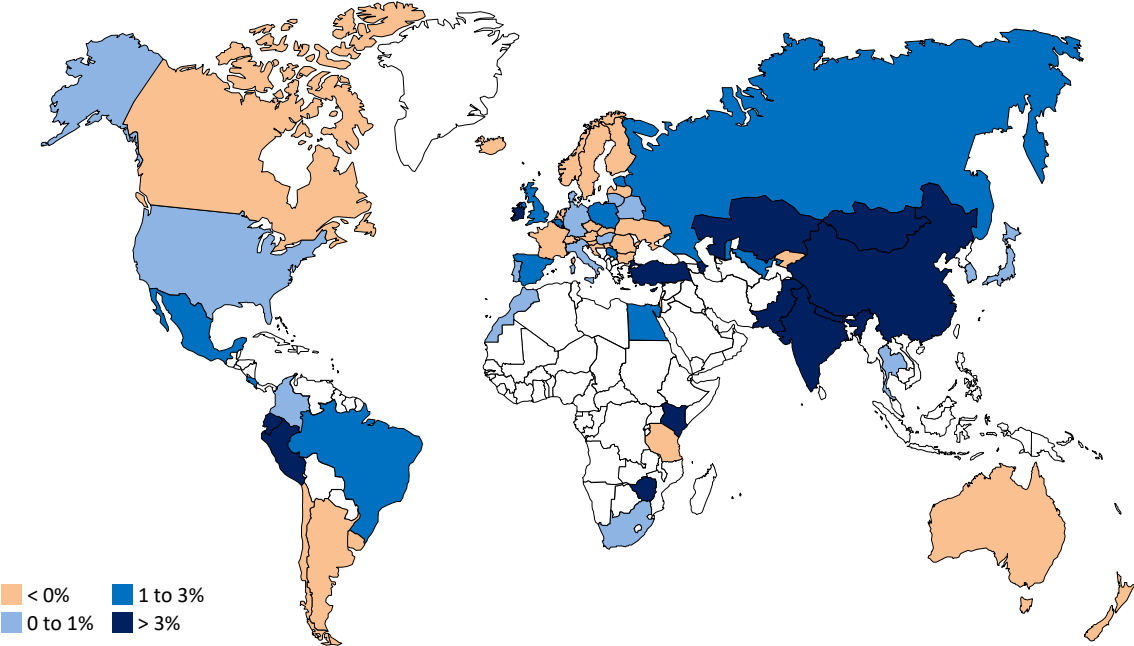


Figure 2. Cow’s milk production growth in 2019 (IDF, 2020)

This milk deficit is the starting point of the development of the dairy world trade to supply the market of regions with high demand, especially developing / emerging countries, from those that have a surplus in milk production in relation to their domestic demand, namely western countries. As such, the world trade is dominated by Oceania (New Zealand and Australia), EU and USA, representing all together 73% of the export shares (**Figure 3**).

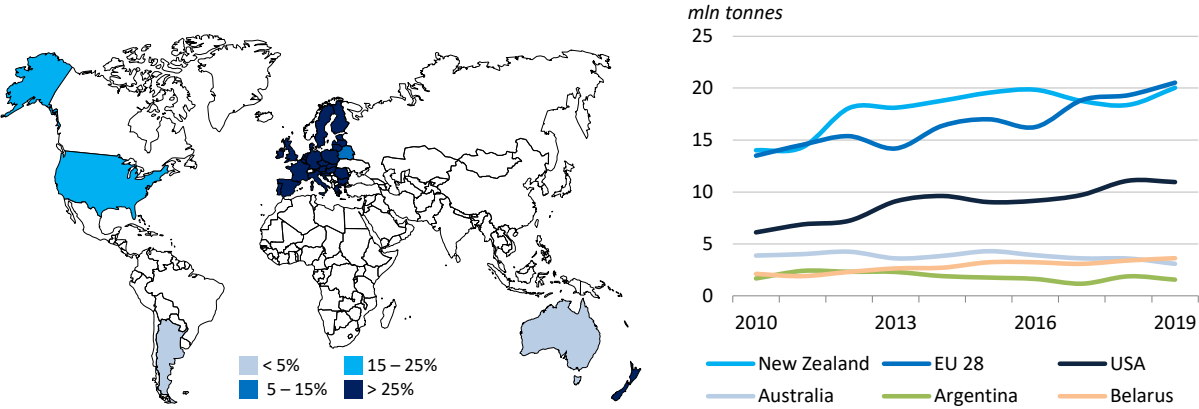


Figure 3.Key exporters at the global scale. Left: market share in 2019; right: top exporters (mlt of milk equivalent) in between 2010 and 2019 (IDF, 2020).

World dairy trade in 2019 grew modestly by just over 1% (compared to the +9% growth since 2015), reaching a volume of about 82.1 million tonnes in milk equivalent and therefore representing close to 9% of global milk production. Thus, exports generally constitute a small proportion of production and most of the global milk is consumed locally without crossing any borders. In order to be exported in safe conditions, milk has first to be processed in a stable form, mostly dairy powders (skim milk powder, SMP; whole milk powder, WMP), cheese and butter. **Figure 4** shows the exported volume of each of these categories: given the conversion factor in milk equivalent, the powder form (including whey powders, not represented on Figure 4 but accounting approx. 14 mlt milk equivalent) represents by far the first share of world trade, close to 69% (FAO, 2021). This can be explained by the fact that powder processing is the major way to stabilize dairy products over long periods of time (up to 2 years) and to reduce their volume (by a factor ranging from 2.5 to 8.0, in the case of milk and whey, respectively) and by consequence the cost of storage and shipping.

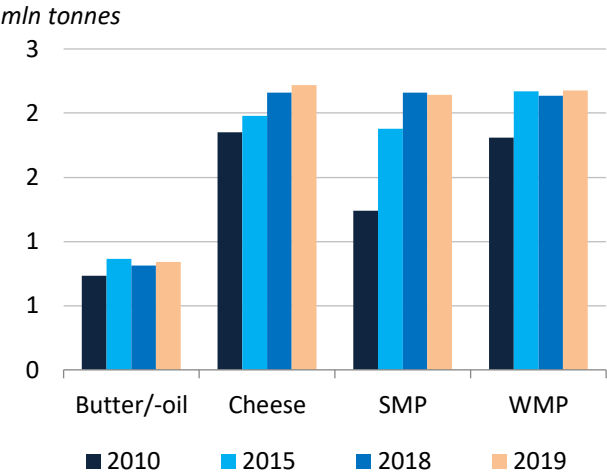


Figure 4. World trade: Main dairy products exported (mlt) in between 2010 and 2019 (IDF, 2020). SMP: skim milk powder; WMP: whole milk powder.

As shown in **Table 1**, the global production of skim and whole milk dairy powders remained stable between 2014 and 2018, while it showed a sharp increase of 29% and 20% in the previous 4 years (2010-2014; (CNIEL, 2016)). In contrast, whey powder production, mainly originating from cheese production regions (EU and North and Central America), continued to grow at a level close to that of the previous period: +8.3% between 2014 and 2018, versus +10% between 2010 and 2014. The growing trend of the whey powders exports is the signature of the demand for nutritional products on the dairy market, especially in Asia. Indeed, the label “whey powders” may cover whey powder for feed or food application, this latter being connected to infant milk formulae (IMF) formulation.

Table 1. Overall production of the main dairy powders between 2014 and 2018 (CNIEL, 2020)

× 1000 tonnes	Skim milk powder (SMP)		Whole milk powders (WMP)		Whey powders (WP)	
	2014	2018	2014	2018	2014	2018
EU (28)	1602	1670	809	853	1974	2103
North & Central America	1134	1176	129	119	394	465
Asia	640	720	1170	1059	-	-
Oceania	657	618	1557	1494	52	48
South America	154	155	842	730	69	80
Total	4187	4339	4507	4255	2489	2696

As an example, the main dry products exported by France in 1988 were whey powders (42% in volume) and WMP (33% in volume); at this time, the share of IMF powders was only 5% in volume (FranceAgriMer, 2019). In 2018, the breakdown still places whey powders as leading product (36% in volume), in front of SMP (26%) and mainly IMF powders (21%). France has therefore gradually turned to the export of products with higher added value, as IMF powders represented in 2018 the main share of income of powder products (43%), 36% of the IMF exports in volume concerning China (CNIEL, 2020). At the global scale, Baker et al. (P. Baker et al., 2021) reported that China accounted for 32.5% of total IMF sales volume at a global scale, close to 0.7 mlt.

Indeed, China is biggest importer since 2008, from which its production level has been kept stable (**Figure 5**), approx. 32 mlt. The imported dairy products can be divided into five categories: whole milk powder (WMP), butter, cheese, skim milk powder (SMP) and other products. In **Figure 5**, their share

in total import is estimated. Before 2008, the total dairy imports lied between 3 and 4 mlt, and other products (namely whey powders, IMF, fresh products, etc.) accounted for about half of imports. Since 2008, the total volume of imported dairy products has been multiplied by a factor of 4, WMP and other products accounting for 40% each of the whole. China represents the world’s second largest infant and young child population (P. Baker et al., 2021). Moreover, a further increase of total dairy imports is predictable due to the second-child policy encouraged recently by the Chinese government.

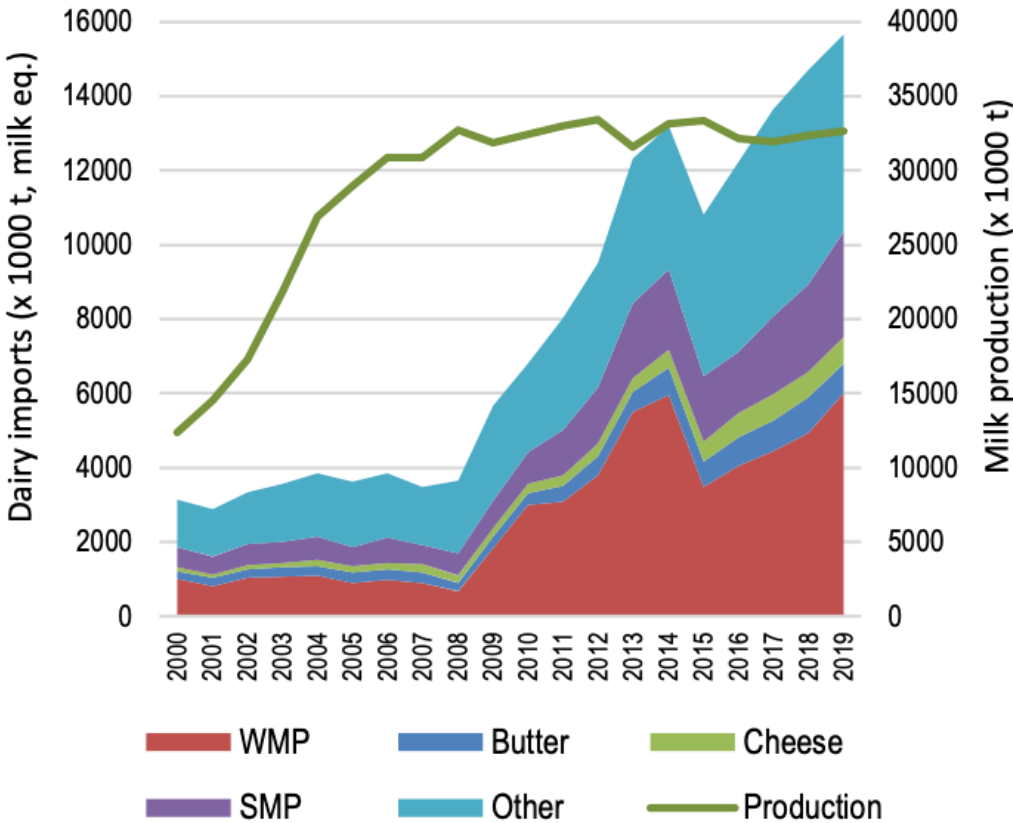


Figure 5. China dairy imports (left axis and coloured areas; x 1000 t milk equivalent) and milk production (right axis and green curve; x 1000 t milk) from 2000 to 2019 (FAO, 2020). SMP: skim milk powder; WMP: whole milk powder.

China’s population and economic growth, increasing wealth of the middle classes and women’s employment (representing 45% of the total labor share) are factors pushing forward the IMF market, as it makes it necessary to access a substitute replacing breast milk for providing all the premium nutrition for baby growth. Recently, Baker et.al (P. Baker et al., 2021) represented the relation between the IMF powder consumption per child in 77 countries from 2005 to 2019 as a function of IMF powder compounding annual growth rate (CAGR) for the different formula categories (standard, follow-up, toddler and special) (Figure 6). Although a wide variation in category sales, growth rates between regions and country income categories, and between countries at the same income level can

be observed, it is clear that much of the IMF sale growth can be attributed to upper-middle income countries (UMIC) with an average CAGR of +8.6% in 2005–19. This growth was led by China with a CAGR around 10% and per child consumption around 20 kg and 25 kg for standard (0-6 month) and follow-up (7-12 month) categories, respectively, and experienced the highest growth rate in special formulas. In contrast, India has remarkably low per child volumes across all categories and negative growth in the standard category, although being the world's largest infant and young child population.



Figure 6. Country milk formula category sales volumes (kg) per child in 2019 v. 14-year compounding annual growth rate (CAGR; %) for 2005–2019; weighted markers represent infant/child population sizes (P. Baker et al., 2021).

During the first half of 2020, dairy world trade showed almost the same level as in the same period of 2019, coming with apparently few COVID-19 impact except for milk powders that suffered a significant declining demand (IDF, 2020). Moreover, Van Tulleken et al. (van Tulleken et al., 2020) reported that IMF industry has been actively exploiting concerns about COVID-19 to increase sales, in violation of the WHO International Code of Marketing of Breast-milk Substitutes and national law in many countries. Large manufacturers have spread messages about unnecessary hygiene measures and the

separation of mothers from their babies, whereas the growing food insecurity coming with the upcoming economic and social crisis makes breastfeeding even more important. On a longer term, and although IMF Chinese market forecast appears to be positively oriented, the main development should concern the refocusing of Chinese domestic demand on IMF products made in China, rather than from abroad as has been the case since the melamine crisis. In 2021 already, major IMF players such as Reckitt (Mead Johnson) and Danone have sold their positions in China, arguing from “sluggish sales caused by intense competition from local Chinese baby formula brands” (Reuters).

1.2. COMPOSITION, STRUCTURE AND PHYSICOCHEMICAL PROPERTIES OF COW MILK

Ruminant milk (cow, goat, sheep) represents a complete natural food ideally suited to the needs of the young. Their composition depends on the species and breed, stage of lactation, herd management, the age of the animal and its health status. Milk provides water (87-88% w / w on average for cow's milk), energy (fat and lactose) and essential nutrients (amino acids, fatty acids, vitamins, etc.) allowing to cover the main physiological functions. First in this section, the different categories of milk components will be reminded (content, structure, physicochemical properties), bovine milk serving as an example and reference. The comparison of human and bovine milk will be then provided.

1.2.1. LACTOSE

Apart from traces of glucose, galactose and a minor fraction of oligosaccharides, lactose is the main carbohydrate and major dry matter constituent of cow's milk with a concentration in between 4.5 and 5.0 w/w % (Jeantet & Croguennec, 2018). In combination with the mineral elements of milk (K^+ , Na^+ , Cl^- for the most part), it helps controlling the osmotic pressure in the mammary gland. From a structural point of view, lactose is a reducing D-galactose / D-glucose disaccharide, present in two configurations (α and β) in thermodynamic equilibrium in solution (mutarotation). Lactose (especially the α form) is a poorly soluble carbohydrate: at 20°C, its solubility limit (saturation) is approximately of 19 g / 100 g of water. Milk is therefore an aqueous solution that is unsaturated with lactose, unlike whey and permeates concentrates obtained by evaporation which are supersaturated. In these concentrates, lactose crystallizes when conditions are favorable according to a mechanism involving two kinetics, that of the formation of stable seed crystals (nucleation) and that of crystal growth (growth). Crystallization takes place under normal conditions in the α form, and greatly reduces the hygroscopicity of the powders finally obtained. Indeed, lactose in the amorphous state is highly hygroscopic, and thermodynamically unstable when it is brought to supersaturation in the dry state, coming with a risk evolution towards a crystalline state in case of humidity uptake or temperature increase, releasing water and inducing caking and non-enzymatic browning of the powders.

1.2.2. FAT

Whole milk is a natural emulsion of fat in an aqueous phase (skimmed milk). The fat represents around 4 w / w % of the overall composition of the milk, and is dispersed in the form of fat globules with an average diameter of around 3 μm and distributed from 1 to 10 μm (Briard et al., 2003). The triglycerides, which represent about 97 w/w % of the total milk fat, are thus protected by a complex biological membrane.

The fatty acid composition of milk fat varies depending on diet, stage of lactation, season and geographic factors (Bornaz et al., 1992; Chilliard et al., 2001). There are over 400 fatty acids, although only 13 of them are present in amounts greater than 1% in mol/kg (JENSEN & NEWBURG, 1995). These are mainly saturated fatty acids (65-75% of total fatty acids). The unsaturated fraction (25-35% of total fatty acids) includes in particular trans fatty acids.

Representing about 2 w/w % of the total milk fat, the fat globule membrane is structured in a triple layer and contains minor proteins (1 w/w % of the fat globule: butyrophilin, xanthine oxidase, etc. ; (Patton & Huston, 1986) and mainly polar milk lipids (0.2 to 1 w/w % of total lipids: phosphatidylcholine, phosphatidylethanolamine, sphingomyelin, etc.). It plays an essential role in maintaining the integrity and preventing the coalescence of fatty globules, as well as acting as a natural physical barrier against oxidation and lipolysis (Jeantet & Croguennec, 2018). However, its fragility allows deep compositional and structural changes during the implementation of technological treatments (e.g., homogenization, heat treatment). During homogenization, the interface of the fatty globules (initially with a surface area of 50 to 110 m^2 per liter of milk) is considerably increased with simultaneous enrichment in milk proteins (casein micelles and whey proteins).

1.2.3. PROTEINS

The protein concentration of bovine milk varies between 3.1 and 3.7 w/w %; even more than the breed, it varies especially from one cow to another depending on genetic, health and food factors (Marshall, 1995). About 80% of the nitrogen fraction in cow's milk corresponds to the casein fraction and 20% to soluble proteins and the non-protein nitrogen fraction (NPN: urea, creatine, uric acids, vitamins, peptides, ammonia, etc.) (Walstra et al., 1999). The concentration of major milk proteins (concentration ≥ 0.01 w/w %) is shown in **Table 2**.

Table 2. Protein composition of cow milk (g.L⁻¹) (adapted from Jeantet & Croguennec, 2018)

Protein	Concentration (w/w %)
α 1 casein	0.97
α 2 casein	0.25
β casein	0.90
κ casein	0.32
γ casein	0.08
β -Lactoglobulin	0.31
α -Lactalbumin	0.12
Bovine Serum Albumin	0.04
Immunoglobulins	0.08
Proteose Peptones, 8F, 8S	0.08
Lactoferrin	0.01
Transferrin	0.01
Fat globule membrane	0.04
Total	3.19

1.2.3.1. CASEINS

Bovine caseins are defined as the fraction of phosphorylated proteins in raw milk which coagulates at pH 4.6 and at 20 ° C (Jenness et al., 1956). The α s1, α s2, β and κ caseins come from distinct genes and present several molecular variants depending on genetic polymorphism and different post-translational modifications (glycosylation and phosphorylation (Holland et al., 2006)). The α s1, α s2 and β caseins exhibit strongly phosphorylated sequences with a high anionic density, called clusters of phosphoserine residues, which have a very high affinity for calcium. κ casein is sensitive to the action of chymosin. Caseins are rich in glutamic acid, glutamine, leucine, proline, lysine and low in tryptophan and cysteine residues (except α s2 and κ caseins). The distribution of amino acids in the sequence generates hydrophilic and hydrophobic areas conferring more or less amphiphilic properties on the caseins. Because of their low level of secondary structure, caseins are rheomorphic proteins: they have

great conformational flexibility and their structure changes depending on physicochemical conditions. The main physicochemical characteristics of caseins are presented in **Table 3**.

Table 3. Physicochemical characteristics of bovine caseins (Jeantet & Croguennec, 2018)

Casein	α 1	α 2	β	κ
Number of variants	8	4	12	11
Amino acids	199	207	209	169
Molecular weight (kDa)	23.6	25.2	24.0	19.0
Phosphoserine residues	8-9	10-13	5	1-2
Cysteine residues	0	2	0	2
Hydrophobicity (KJ.res ⁻¹)	4.89	4.64	5.58	5.12
Charge at pH 6,6 (mV)	-21	-15	-12	-3
Isoelectric point	4.9-5.0	5.0-5.4	5.1-5.6	5.4-5.9
Sensitivity to Ca ²⁺	++	+++	+	-
Sensitivity to chymosin	-	-	+	+++

In bovine milk, 95% of the caseins are organized in a supramolecular structure called the casein micelle, with an average diameter equal to 150 nm (**Figure 7 A**). Casein micelles are composed of 94% protein and 6% colloidal calcium phosphates (CCP), especially located on the phosphoserine clusters, and are also stabilized by hydrogen bonds (De Kruif & Holt, 2003; Walstra, 1990). Several models have been proposed by studying the properties and behavior of individual and micellar caseins, without any consensus to date (Qi, 2007). For example, the nanocluster model (De Kruif & Holt, 2003; Holt, 1992) describes the micelle as a network of proteins which cohesiveness depends on CCPs (**Figure 7 B**). The phosphoserine clusters react with the CCPs to form 2-3 nm nanoclusters. By neutralizing the charges, CCPs allow the hydrophobic interactions at the heart of the micelle to maintain its integrity. More recently, Bouchoux et al. (Bouchoux et al., 2010) relied on a small angle X-ray scattering approach to propose a sponge-like model including 3 structure levels (**Figure 7 C**). In this model, the micelle is made of soft and hard regions of approx. 25 nm in characteristic size. The soft regions are voids filled with solvent and the hard regions contain all the calcium phosphates and protein materials.

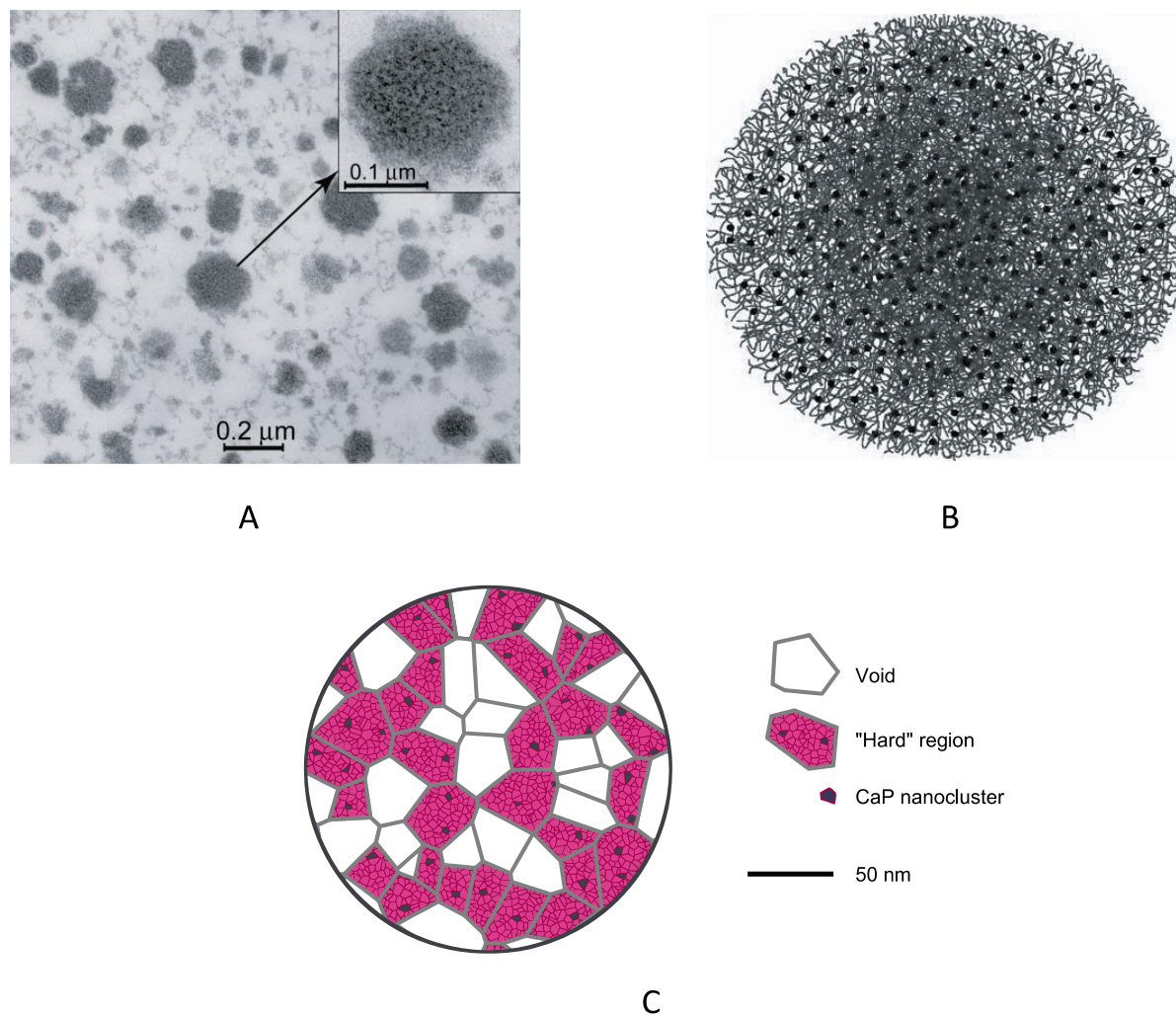


Figure 7. The casein micelle. A : Transmission electron micrograph image of bovine casein micelles (Qi, 2007). **B:** The nanocluster model structure proposed by de Kruif and Holt (2003); black dots correspond to CCP nanoclusters. **C:** Sponge like model structure proposed by Bouchoux et al. (2010).

1.2.3.2. WHEY PROTEINS

Whey proteins include the protein fraction which remains soluble after precipitation of caseins at pH 4.6. It consists of globular proteins with a diameter of around 5 nm, that is to say 20 to 40 times smaller than casein micelles. Beyond the two major soluble proteins in bovine milk, β -lactoglobulin and α -lactalbumin, this fraction also includes many minor proteins (bovine serum albumin, immunoglobulin, lactoferrin, lactoperoxidase, lysozyme, etc.). The physicochemical characteristics of β -lactoglobulin, α -lactalbumin, bovine serum albumin (BSA) and lactoferrin are shown in **Table 4**.

Table 4. Physicochemical characteristics of main bovine whey proteins (Jeantet & Croguennec, 2018)

	β -lactoglobulin	α -lactalbumin	BSA	Lactoferrin
Amino acids	162	123	582	692
Molecular weight (kDa)	18.3	14.2	66.4	83
Isoelectric point	5.2	4.2-5.1	4.8	8.5
Charge at pH 6.6 (mV)	-16	-3.7		
Cysteine residues	5	8	35	34
Disulfide bonds	2	4	17	17
Thiol groups	1	0	1	0
Fixed mineral compound	-	Ca ²⁺	-	Fe ³⁺ (2)
β sheets (%)	50	10-15	18	
α helix (%)	15	25-30	56-83	

β -Lactoglobulin (β -LG) represents about 50% of the total whey protein in cow's milk. Consisting of 162 amino acids (molecular weight of 18.3 kDa), it presents several variants, the most common of which, A and B, differing by the substitution of aspartic acid and valine at positions 64 and 118 (variant A) into glycine and alanine (variant B). The molecular structure of β -LG is well established: it mainly comprises β sheets (50%), which form a pocket at the heart of the protein (**Figure 8 A**) capable of binding hydrophobic ligands (retinol, fatty acids, etc.) (Le Maux et al., 2014). β -LG is stabilized by two disulfide bonds and has a free cysteine residue located at the heart of the structure, which limits its reactivity in the native state. However, the unfolding of the protein on heating (molten globule state) exposes this thiol group and hydrophobic residues, then promoting its aggregation with other whey proteins through intermolecular covalent bonds, disulfide bonds and hydrophobic associations and resulting in loss of solubility at its pHi. β -LG denaturation temperature is estimated at about 77°C (Havea et al., 2001; Relkin, 1996), depending strongly on the chemical environment.

α -Lactalbumin (α -LA) represents 20 to 35% of the soluble proteins in cow's milk. Consisting of 123 amino acids (molecular weight of 14.2 kDa), it has two variants, A and B, which differing by the substitution of glutamine in position 10 (variant A) by arginine (variant B). Its sequence is organized into 25-30% α helix and 10-15% β sheets (**Figure 8 B**). It has 4 disulfide bridges and a specific Ca²⁺ binding site, which stabilizes the protein against thermal denaturation and accelerates its folding (Forge et al., 1999). The denaturation temperature of α -LA is 64°C at pH 6.7 in the presence of calcium (holo form), compared to about 30°C without calcium (apo form) at acidic pH (Griko & Remeta, 1999).

Bovine serum albumin (BSA) is a protein composed of 582 amino acids (molecular weight 66.4 kDa) representing less than 5% of the soluble proteins in cow's milk. Ovoid in shape, it has numerous surface cavities into which hydrophobic ligands can be inserted.

Lactoferrin (LF) is a glycoprotein of 692 amino acids (molar mass 83 kDa) belonging to the transferrin family. Basic protein unlike most whey proteins, its concentration in cow's milk varies from 0.02 to 0.35 g.L⁻¹. It is organized into two lobes stabilized by 17 disulfide bridges and linked by one α helix. Each lobe consists of two domains forming a binding site for Fe³⁺ and a synergistic anion (carbonate under physiological conditions) (E. N. Baker & Baker, 2009). Its ability to bind iron gives LF bacteriostatic properties. It also contains in its structure a basic and hydrophobic peptide (lactoferricin) having lytic activity of the membrane of many microorganisms (bacteria, fungus, yeasts). At pH 6.7, more than 50% of LF would be bound to the casein micelle (Croguennec et al., 2012).

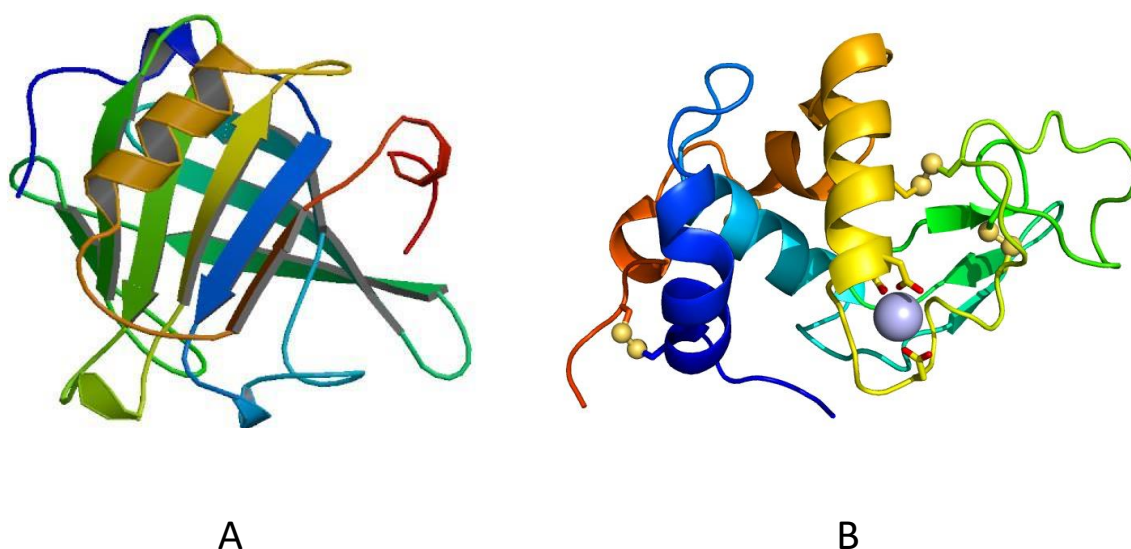


Figure 8. Tridimensional representation of β -lactoglobulin (A) (Brownlow et al., 1997) and α -lactalbumin (B) (Acharya et al., 1991).

1.2.4. MINERALS

Minerals quantitatively represent a minor fraction of milk (ranging between 5.7 w/w % (whole) and 8.4 w/w % (skimmed) of dry matter), although they strongly contribute to its physicochemical, technological and nutritional properties. As already mentioned, they participate in the organization of casein micelles. Furthermore, they condition certain properties of milk and dairy products and more particularly its suitability for the production of a very wide variety of cheese textures. Last, the high concentration of calcium and phosphorus gives nutritional value to milk and its derivatives.

The mineral elements are distributed between the colloidal phase and the solvent phase of the milk (**Table 5**) according to the physicochemical characteristics (in particular the pH and the temperature). The alkaline earth metals (Ca, Mg) associated with phosphate anions are mainly integrated in the colloidal phase. Monovalent ions (Na, K, Cl), which have a low affinity towards caseins, are mainly present in the solvent phase of milk. The main trace elements (Zn, Fe, Mn) are attached to proteins (caseins and whey proteins).

Table 5. Distribution of macroelements (mg.L⁻¹) between the soluble phase and the colloidal phase at pH 6.65 and at room temperature (Jeantet & Croguennec, 2018)

	Total	Soluble	% colloidal
Potassium	1600	1500	6
Sodium	425	400	6
Chlorine	1100	1100	0
Calcium	1200	350	70
Magnesium	115	70	40
Phosphorus	950	420	55
Citrate	1650	1500	11

1.2.5. KEY DIFFERENCES BETWEEN HUMAN MILK AND COW MILK

As presented in **Table 6**, human and bovine milks contain the same variety of macro- and micro-nutrients (proteins, lipids, carbohydrates; minerals and vitamins), but with large differences in their content and fine distribution. From a general perspective, human milk, in comparison to bovine milk, contains:

- A fat content in the same range, but a higher content in polyunsaturated fatty acids (PUFA);
- A higher lactose and oligosaccharides content
- A lower protein content and a different casein:whey protein proportion, emphasizing the part of whey proteins (in particular α -Lactalbumin and lactoferrin);
- Connected to these two last points, a lower mineral content.

Table 6. Human milk composition in comparison to cow milk (data from (1) (Thompkinson & Kharb, 2007), (2) (Brenna et al., 2007), (3) (Bode, 2012), (4) (Gopal & Gill, 2000), (5) (Chatterton et al., 2013), (6) (Farrell Jr et al., 2004), (7) (Cuilliere et al., 1999), (8) (Bacchin et al., 2018))

Constituent	Human milk	Bovine milk	Reference
Fat (g.L⁻¹)	38	37	(1)
PUFA (% fat)	16.2	3.4	(1) (2)
Lactose (g.L⁻¹)	70	48	(1)
Oligosaccharides (g.L ⁻¹)	5-15	0.05	(3) (4)
Protein (g.L⁻¹)	9 - 12	35 - 37	(1) (5)
Casein : Whey protein ratio	40 : 60	80 : 20	(1)
α_s casein (g.L ⁻¹)	0.6	15-19	(5) (6)
β casein (g.L ⁻¹)	2.6-4.4	9-11	(5) (6) (7)
κ casein (g.L ⁻¹)	0.9-1.3	2-4	(5) (6) (7)
α -Lactalbumin (g.L ⁻¹)	1.5-2.5	1.0-1.5	(1) (5)
β -Lactoglobulin (g.L ⁻¹)	0	3.0-4.0	(5)
Bovine Serum Albumin (g.L ⁻¹)	0.4	0.3-0.4	(5) (8)
Immunoglobulins (g.L ⁻¹)	1.2	0.6-1.0	(5)
Lactoferrin (g.L ⁻¹)	1.5	0.1	(1) (8)
Minerals (g.L⁻¹)	2	7.3	(1)

1.2.5.1. FAT CONTENT

Human and bovine milk fat both mostly consist of triglycerids (mass fraction > 95%). However, human milk is 3 to 4 times richer in PUFA, docosahexaenoic acid (DHA) and arachidonic acid (ARA) essential for the retina and brain development (Bindels, 1992; Innis, 1992), that has to be supplemented in IMF. As an example, PUFA source usually consists of vegetable oils (eg, coconut, palm or sunflower oil).

1.2.5.2. CARBOHYDRATES

Regarding carbohydrates, human milk contains a higher lactose and oligosaccharides content. Consequently, IMF production from bovine milk requires its supplementation in lactose and oligosaccharides, that act as prebiotics and promote the growth of bifidus microflora in the gut (Engfer et al., 2000; Goedhart & Bindels, 1994), which is essential for preventing gastrointestinal infections. As a consequence of the growing IMF demand, the global lactose production increased by 4.8% on the last decade. Besides, IMF formulation includes galacto-oligosaccharides (GOS) and fructo-oligosaccharides (FOS), with a GOS:FOS ratio of 90:10 (European Union., 2016).

1.2.5.3. PROTEINS

In relation to the main topic of this thesis, human and bovine milk widely differ on their protein content (overall and individual; **Table 6**) and structure. Indeed, the casein micelles show smaller diameter in human milk (30–75 nm in diameter;(Calapaj, 1968), β -casein accounting for more than 70% of total caseins and α 2-casein being absent (O’Callaghan DM, 2011). Regarding the whey protein fraction as well, the main whey proteins largely differ between bovine and human milks (**Table 6**). α -LA and LF are the main whey protein in human milk, accounting for 14-28% and 14-17% of total proteins. These two proteins have essential biological functions, α -LA being a key source of essential amino acids (eg, lysine, cysteine, tryptophane) and LF being an iron carrier and providing antibacterial effect, as already mentioned (Chierici et al., 1992; W. Heine, 1999). In order to match with human milk composition, bovine milk can be supplemented in both of these proteins. Bovine α -LA enriched whey protein concentrate is an excellent candidate as the amino acid sequences of human and bovine α -LA are very similar (W. E. Heine et al., 1991). On the other hand, and although LF supplementation was first introduced in Japan in 1986 (Ben, 2008), it leads to mixed results from a clinical benefit point of view as human and bovine LF differ from their amino acid sequence, leading to non-recognition of bovine LF by human LF receptors (Chierici et al., 1992). As a consequence, and due to the high cost of LF ingredient, the enrichment of IMF with LF is still limited (O’Callaghan DM, 2011). In contrast, β -LG is absent in human milk while it is the major whey protein in bovine milk (**Table 6**), and therefore consists of one of the major sources of allergy in infants(Wal, 2002). Its removal from bovine milk is complex, in particular with the aim of keeping the other whey proteins functional properties (Lucena et al., 2006), such as the solubility if they are going to be incorporated into liquid products . An alternative option is to hydrolyze bovine β -LG to address these problems, leading to the removal of more than 99% of these proteins.

1.2.5.4. MINERALS

Last, mineral content of human milk is approx. 3.5 times lower than that of bovine milk (**Table 6**). In order to reduce the supply of mineral when producing IMF from bovine source and standardize it at a required human level, demineralised whey or whey protein concentrates / powders are most often used (De Wit, 1998).

1.3. INFANT FORMULA PROCESSING AND MANUFACTURE

In general, powdered infant milk formulae (IMF) can be produced at an industrial scale by two types of processing schemes (McSweeney, 2008; Montagne et al., 2009): wet-mixing or dry blending. Wet-mixing consists of rehydrating ingredients in water to the desired composition and further spray drying of the formula, whereas dry blending involves mixing directly powdered ingredients.

Advantages and drawbacks of these process are summarized in **Table 7**. The main advantage of the wet-mixing over the dry blending is a better control of the microbiological safety thanks to heat treatments steps such as pasteurization or sterilisation. However, in dry blending, the microbiological quality of the final product is dependent on raw material quality as no heat treatment is involved.

Table 7. Advantages and drawbacks of wet-mixing and dry blending (adapted from (Montagne et al., 2009))

	Wet-mixing	Dry blending
Advantages	<ul style="list-style-type: none"> - Possibility of ensuring microbiological quality of final product <i>via</i> heat treatment - Physical properties of final product can be more effectively controlled - Higher level of control over physical properties of final product - Possibility of incorporating oil during process - More homogeneous and less segregated final product 	<ul style="list-style-type: none"> - Less equipment and less consumption of energy - Shorter production time - Easier to avoid bacterial contamination as no water involved.

Drawbacks	- More equipment	- Dependency of
	- Longer production time	microbiological and physical
	- Maintenance is more complicated, costly, and time consuming	properties of final product on raw materials
	- Relatively higher cost	- No possibility of adding oil
		- Risk of segregation or de-blending of ingredients during transport and storage

Taking into account this main advantage of ensuring microbiological quality of the product, the wet-mixing method is more commonly and broadly used than dry blending. Manufacture of wet-mixing IMF can be broken down into several steps (preparation of the mix, heating of the mix to a certain time-temperature combination to achieve microbial sterility, homogenization of the mix, concentration by evaporation, spray-drying of the concentrate and packaging and storage of the final product) (**Figure 9**). The following sections will discuss each of these steps.

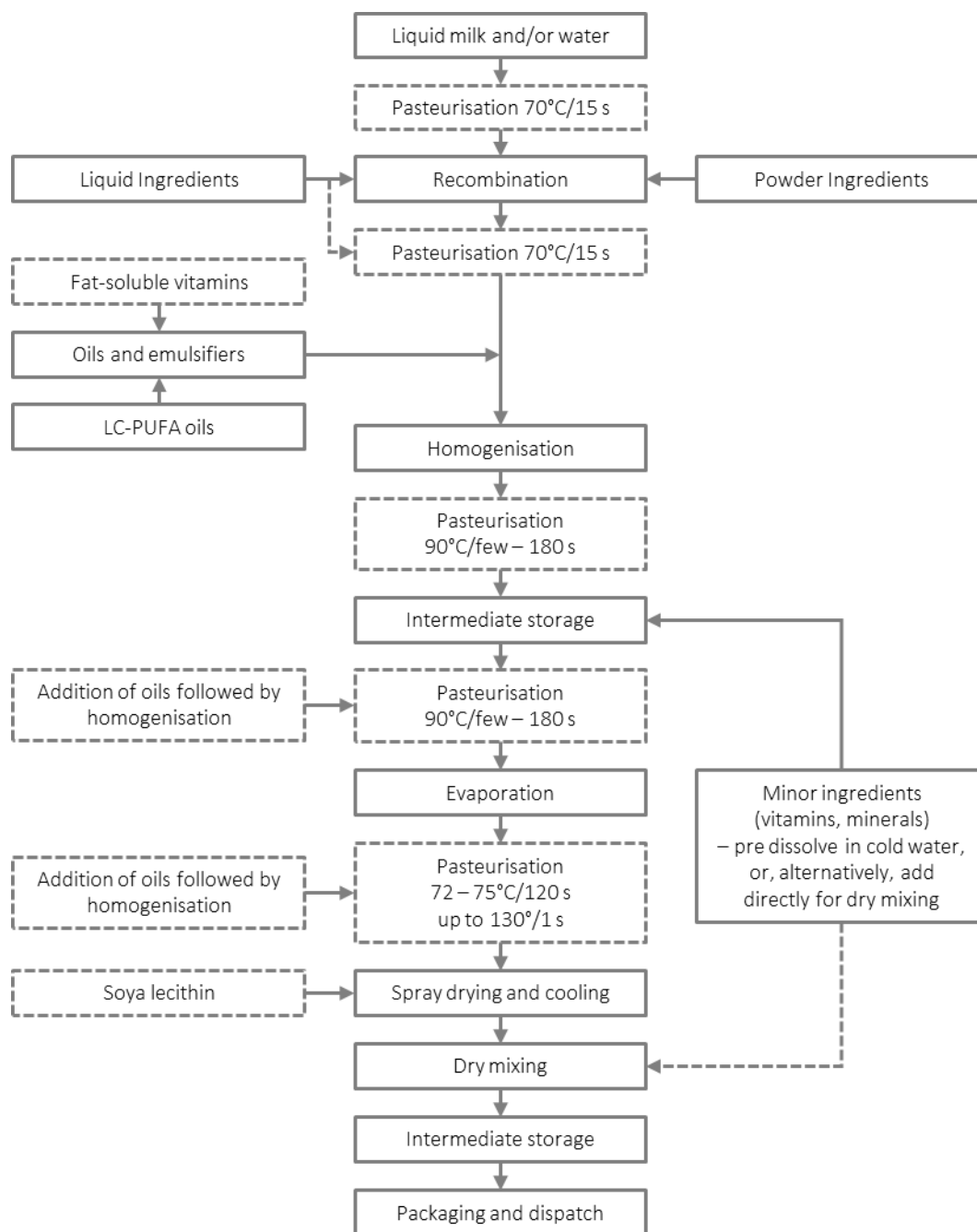


Figure 9. Generalized powdered IMF and manufacturing process (adapted from (Montagne et al., 2009)). Dotted lines indicate alternative processing route.

1.3.1. RAW MATERIALS AND PREPARATION OF THE MIX

Table 8 lists raw materials commonly used for IMF, in connection with human and bovine milk differences presented in 1.2.5. The initial quality and pre-treatment of raw materials influence the physico-chemical properties of the wet mix and of the final product. Typically, skim milk powder (SMP) can be categorized into three qualities (low, medium and high heat) according to the severity of heat treatment during the process (Martin et al., 2007). The classification indirectly shows the extent of

denaturation undergone by whey proteins during manufacture (Y. Lin et al., 2017), as measured through the whey protein nitrogen index (WPNi).

Table 8. Raw materials typically used in infant milk formulae (Adapted from (European Union., 2016; Montagne et al., 2009; Thompson & Kharb, 2007))

Nutrient/additive	Ingredients
Casein Source	Skim milk powder (SMP), evaporated skim milk, acid casein, sodium/calcium/potassium caseinate
Whey Source	Whey protein concentrate, whey protein isolate, demineralized whey powder, partially hydrolyzed whey powder
Alternative protein source	Isolated soy protein, soy milk, locust bean seed protein
Carbohydrates	Lactose, starch, sucrose, corn syrup
Lipids	Vegetable oils, butter oil, cream, alpha-linolenic acid, linoleic acid, DHA, other polyunsaturated fatty acids (PUFAs)
Functional ingredients	Soya lecithin, mono- and di-glycerides as emulsifiers/stabilizers
Major minerals	Calcium carbonate, calcium phosphate, magnesium phosphate, potassium citrate, magnesium chloride
Vitamins	Vitamin A, D, E, K, B3 (niacin), B9 (folic acid), B5 (pantothenic acid)

The preparation of the mix mainly refers to the rehydration of raw materials. The water soluble-ingredients are rehydrated in fresh skim milk or a mixture of water and SMP to the desired composition regarding macro-elements (Cuilliere et al., 1999). High shear devices can be used to disperse raw materials to reduce rehydration time (McCarthy et al., 2012, 2013). Temperature of dispersion is also critical to ensuring adequate rehydration; wettability increases as temperature is increased from 10°C to 50 °C (Bylund, 1995). Then, the system is heat-treated. Heat sensitive micro-ingredients (vitamins) may be added at a later stage (eg, end of drying or even post drying) to limit their degradation. Some other ingredients can be added at different stages according to their functional properties. For example, starches are often sprayed with infant formulas directly in the chamber of the spray dryer in order to limit the viscosity increase during the steps prior to drying (Blanchard et al., 2013).

1.3.2. HEAT TREATMENT

Heat treatment is a critical control point in guaranteeing microbial quality of IMF. As observed in Figure 9, its positioning within the process can be flexible. It can be beneficial to position the heat treatment prior to homogenisation in order to produce a more stable emulsion (Varnam & Sutherland, 1994) as aggregates of fat globules produced during heat treatment (McSweeney et al., 2004) could be disrupted by homogenisation.

Heat treatment can be done either directly (direct contact between heating medium and product, e.g., steam infusion or injection) or indirectly (e.g. use of tubular or plate heat exchangers). Mostly, indirect heating with tubular heat exchangers is applied for the heating of IMF wet-mix (Murphy et al., 2011). The heat treatments applied during infant formula manufacturing are theoretically sufficient to ensure the destruction of at least 8-log units of *Enterobacteriaceae*, including *Salmonella* and *E.sakazakii*, as well as other microorganisms as *L.monocytogenes* or *S.aureus* (World Health Organization, 2006). Depending on the processing conditions, spore-formers such as *B.cereus* and *C.botulinum* are partly inactivated. For example, some authors (Iversen & Forsythe, 2004; NAZAROWEC-WHITE & and Farber, 1999) have shown that standard pasteurisation treatment during infant formula manufacturing is effective for the inactivation of *E.sakazakii*. Pasteurization consists in heating of a medium over 70°C during an appropriate time, with the aim to eliminate the vegetative forms of bacteria, viruses, protozoa, moulds and yeasts can be used. The temperature/time combinations for pasteurisation in dairy industry can be various: 70°C for 15 s for liquid ingredients, milk and water, 90°C from few to 180 s after homogenization and before evaporation, 72 – 75°C for 120 s up to 130°C for 1 s after evaporation (Jeantet, 2016).

1.3.3. HOMOGENEISATION

The oil-soluble phase, composed of a mixture of oils, fat and lipophilic vitamins, is mixed with the water-soluble system after the heat treatment of the non-fat premix, either after its concentration by vacuum evaporation, to form a pre-emulsion. The pre-emulsion is homogenized in order to decrease the lipid droplet size and increase their creaming stability. Homogenization is generally achieved by high-pressure valve- type homogenization (Bylund, 1995). The homogenizing pressure is the pressure drop required to pass through the valve, that generates high shear forces breaking down the original fat droplet into smaller submicronic droplets (Carić, 1994). In many cases, homogenization is carried out using two stages: the first stage reduces the emulsion fat droplet size as a result of high pressure applied (e.g. 14 MPa); it is followed by a lower second stage pressure (e.g. 3 MPa) to prevent and disrupt formation of fat globule clusters (McCarthy et al., 2012). The main process factors affecting homogenization are: pressure, temperature, flow rate and fat content (Phipps, 1985).

As a consequence of the reduction of fat droplet size by two-stage homogenisation, the total surface of the lipid droplets increases, which makes it necessary for milk proteins and other emulsifiers to adsorb on the newly formed surface. The affinity of proteins to adsorb at the oil-water interface depends on many factors such as the nature (caseins, whey proteins), the molecular weight and physical structure (native, denatured) of proteins (Dickinson, 2013).

1.3.4. CONCENTRATION BY EVAPORATION

Concentration by evaporation of IMF is often employed to remove water prior to spray drying (**Figure 9**). Water can be eliminated by evaporation with specific energy costs generally in the range of 10 times lower compared to spray drying (M. Fox et al., 2010). In the dairy industry, falling film evaporators are most commonly used. During falling film evaporation, the mix flows downwards by gravity through a multitude of tubes in parallel, forming a thin film (thickness of a few mm) on the inside of each tube. Live steam is applied to the outside of the tubes causing evaporation of water from the wet-mix. Evaporation is carried out under vacuum (~ 50 to 70 °C) which allows for the evaporation of heat sensitive wet-mixes. The extent of concentration achievable is determined by viscosity increase; in order for efficient drying to subsequently take place, that comes with controlled spraying conditions, post-evaporation viscosity of whole milk should not exceed 60 – 100 mPa s (Westergaard, 2004). In addition to changes in viscosity, evaporation can affect the physical state of wet-mix constituents. Liu et al. (D. Z. Liu et al., 2012) reported that concentration of skim milk affected micellar hydration, aggregation and the amount of calcium associated with the micelle. Transfer of calcium phosphate from soluble to colloidal micellar state and increase in ionic strength reduces pH during evaporation (Singh, 2007). McCarthy et al. (McCarthy et al., 2012) observed an increase in fat globule size of IMF emulsions during evaporation.

1.3.5. SPRAY-DRYING

Spray drying is the last step of IMF production, and it results in the conversion of the liquid concentrate into dried powders. In typical drying towers, concentrated dairy solutions are fed to a nozzle atomizer that breaks the liquid stream into a spray of droplets with almost homogeneous size, normally ranging from 100 to 400 μm (Kelly et al., 2003; Westergaard, 2004). The resulting drops are characterized by a high surface to volume ratio, which favors the rapid solvent evaporation in conditions of high temperature and low vapor partial pressure and their progressive shrinkage toward final particle state. The water removal leads to skin/crust formation and finally to complete solidification (residence time in the tower, $t_{\text{dry}} \approx 5$ s). Powdered infant formulas are generally produced using multiple stage spray dryer technique, consisting of a large drying chamber where the bulk water is removed, followed by

supplementary drying stages realized by an internal and/or an external fluidized bed (**Figure 10**). Tuning the main operating parameters of a spray drying setup, it is possible to modulate IMF specific physico-chemical properties (Sharma et al., 2012; Singh, 2007), such as rehydration (Selomulya & Fang, 2013) and nutrient encapsulation ability (Schuck et al., 2016). However, due to the multiple factors involved in the process, linked both to environmental conditions (e.g. temperature, relative humidity and flow rate of the hot air stream) and feed concentrate, optimizing the evaporation capacity and the thermal efficiency of the dryer represents a complex challenge despite recent technological advances (Anandharamakrishnan & Ishwarya, 2015). From this point of view, the main open question regards the characterization of the milk drying dynamics at the molecular scale, which have not yet been fully elucidated due to spatial and structural limitations. Indeed, it is difficult to follow and investigate the shape evolution of single droplets in industrial closed system, not to mention that these tests implicate also considerable economic costs.

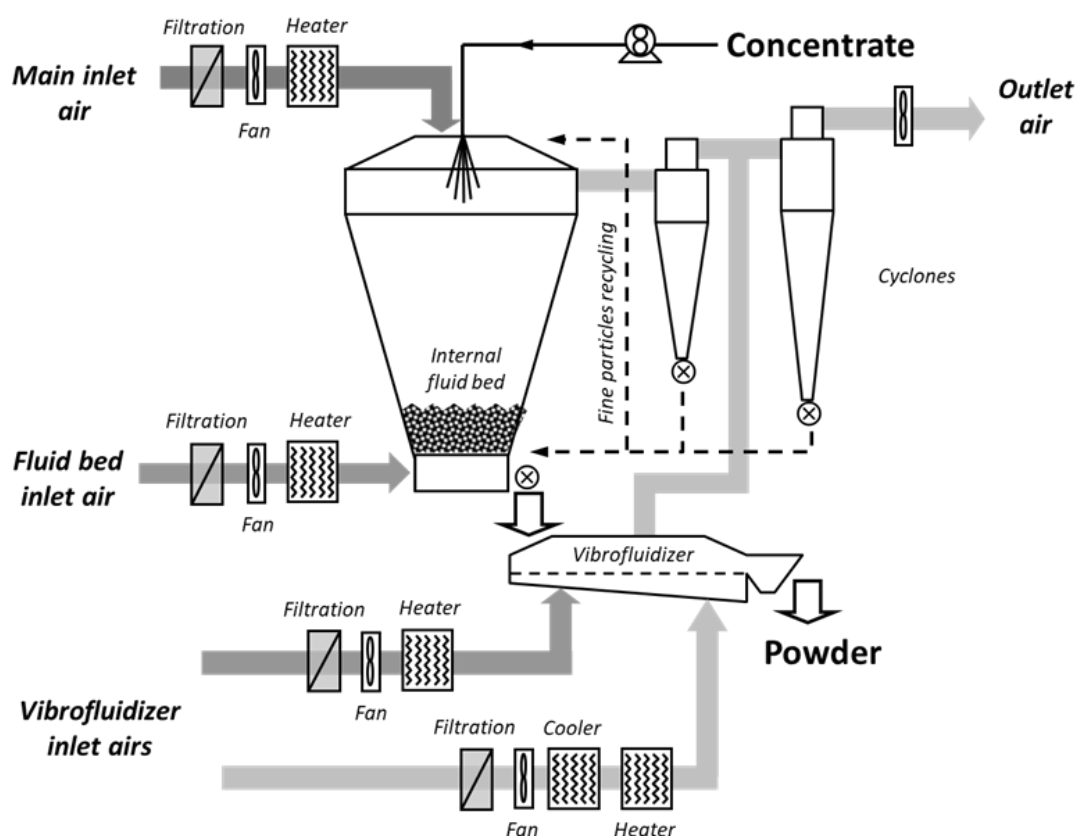


Figure 10. Illustrative scheme of an industrial plant for the production of dairy powders.

1.4. DRYING MECHANISMS IN DROPLETS OF DAIRY FLUIDS

Despite the considerable advances made during the last decade, the operations linked to IMFs production still present some technological limitations that prevent further quality improvements. For example, and with regards to the spray drying technique, the high viscosity of the feeding solution

often affects its pulverization in a microdroplet size distribution, thus influencing the stability of the overall process (Roos, 2002). Indeed, a non-complete evaporation of water during the droplet trajectory towards the exit of the drying chamber can cause the occurrence of the so-called caking and sticking phenomena on the walls of the dryers (Bhandari & Howes, 1999; Fitzpatrick et al., 2007; Özkan et al., 2003). The onset of these inconveniences during the drying stages has also a negative impact on the packing and storage of the powders, causing an alteration of the final product characteristics (Min et al., 1989). These longstanding technological issues limit the tight control of powder functional properties (*e.g.*, rehydration, nutritional characteristics), which is a crucial concerning the increasing customer expectation toward IMFs quality (Chever et al., 2017; Gaiani et al., 2007; Sharma et al., 2012). All in all, the spray drying process limitations are mainly related to the lack of knowledge about the physics of the phenomena taking place in industrial dairy facilities. The main arising question is: how thoroughly do we know the mechanisms governing the physics of drying in dairy products? From a very simplistic point of view, the spray drying equipment used to produce IMFs can be considered as black boxes. The main characteristics of the final product, such as shape and size of the dry particles, are observed post drying and currently tuned by controlling the feeding parameters (*e.g.*, solute concentration, flow rate) and the process environmental conditions (temperature, pressure, relative humidity). However, a direct observation of the droplet sol-gel transition in a drying chamber and, thus, an on-line monitoring of the process efficiency is still not possible due to the quick evaporation (≈ 4 -5 seconds), the challenge of tracking flying droplets and the non-transparent material of the equipment walls. Therefore, new experimental approaches have been explored to close this gap by coupling the process engineering competences with the most recent studies on the physico-chemical phenomena related to droplet evaporation. These emerging strategies can be classified in two main categories: i) the design of pilot spray dryers to test new formulas and to evaluate the impact of environmental parameters on final powder properties, and ii) the single-droplet approach, consisting of the detection of the main drying stages at the microscopic scale by coupling different laboratory methods. The differences between the industrial and the laboratory scales are definitely glaring in terms of quantity of elaborated fluids, experimental conditions, and temporal and spatial scales. Nevertheless, the investigation of the drying mechanisms at the microscale using a physico-chemical point of view represents a useful opportunity for shedding light on the dynamics of dry particle formation (Lanotte, 2020).

1.4.1. Pilot spray dryers

Different prototypes of pilot spray dryers (PSDs) have been designed to offer technological alternatives to the traditional industrial facilities for milk drying, to reduce energy consumption and feedstock waste, and to improve at the same time the quality of the products (Mansouri et al., 2016; Piatkowski

et al., 2015). Indeed, despite above-mentioned differences in terms of operating temperatures and air/concentrate flow rate, such pilot systems represent a good compromise to simulate the drying process in industrial facilities taking advantage of a facilitated control of the main process parameters involved. Well instrumented PSDs are nowadays often used to develop new formulas and innovative products due to these favorable conditions. Among the different prototypes developed over the years, the one designed in the 2000s at the University of Monash (Australia), and then technologically improved at Soochow University (China) in the group of Prof. X.D. Chen, represents a high point of innovation (Patel & Chen, 2007; Wu et al., 2007). This pilot dryer was developed employing ink-jet method for obtaining droplets, and consequently dry particles, of homogeneous size (**Figure 11 A**). In short, the dairy solution is fed to a nozzle equipped with a narrow orifice (adjustable diameter d in the range 50 to 200 μm) and the jet is fractioned in homogeneous droplets by a piezo-electric transducer (atomization). The drops dispersed into the chamber undergo the same drying (time/temperature) history, resulting into particles with same average size and properties. Over the years, monodisperse droplet spray dryers (MDSDs) have been used to investigate a wide range of dairy products, from full fat milk to whey protein solutions, and to foster the modeling of the drying process due to high operational stability and repeatability.

The first pioneering work was presented in the late 90 s by Chen and Xie, who developed a reaction engineering approach (REA) to investigate the air-drying in thin films and small drops (Chen & Xie, 1997). Starting from a mass transfer model describing the transport of water to surface, they studied not only the evaporation rate of the investigated object, but also its morphological evolution. The REA approach was first validated using a single droplet suspended in a uniform and well-controlled air stream by a glass filament (Chen & Lin, 2005). Successively, it has proven to be a powerful tool to predict the events occurring in monodisperse dryers and, with necessary precautions, also at the larger industrial scale (Chen, 2008).

The MDSD prototypes have been also employed to investigate the droplet sol-gel transition dynamics. In this regard, one could expect a similar spherical shape both for sprayed droplets and particles in dry powders since it is likely to predict a homogenous shrinkage induced by the quick solvent evaporation. However, the dry particles obtained by MDSD from milk samples with different fat content (0.3-33 w/w %) usually exhibit significantly wrinkled and irregular surface (You et al., 2014). Only a minor fraction of the whole powder population displays a spherical morphology and a vacuole in the core, as well as a quite larger size compared to the average of the sample. Rogers *et al.* showed that the percentage of such “puffed” particles (**Figure 11 B**) increases with the operating temperature in the chamber (normally from 120°C to 180°C), possibly because reaching in such conditions the boiling

point of the internal moisture (Rogers et al., 2012). Mostly, the authors interpreted the transition from spherical droplet to wrinkled particle (**Figure 11 C**) because of the outstanding surface stresses occurring throughout the drying process. In this light, the interfacial skin does not withstand the interfacial stress and deform at similar rate as water removal (buckling phenomenon). Therefore, it is crucial to characterize the development with time of skin properties and its organization at the microscopic scale.

Starting from the observation of milk dry particle morphology, monodisperse pilot systems have been also used to investigate the distribution of fat, proteins, and other solid components (*e.g.*, minerals, lactose) in the crust (Foerster et al., 2016). Due to their different physicochemical properties, milk components could therefore influence dry skin mechanical behavior, and even powder nutritional characteristics, depending on their organization at the interface. The authors carried out experiments in both skim and full fat milk. The observation of the particles (scanning electron microscopy, SEM), coupled with the elemental analysis of their surface (X-ray photoelectron spectroscopy, XPS), showed that lipids tend to accumulate at the air-droplet interface more than proteins and lactose. Nijdam and Langrish obtained similar results using a different MDSD prototype (Nijdam & Langrish, 2006). Such behavior results in a higher stickiness tendency toward drying chamber walls and enhanced caking of the powders when processing fat-rich milk solutions. Lipid over-representation on particle surface could be explained by the onset of internal flows originating from local concentration gradients at the air-liquid interface. The higher diffusivity of smaller molecules, such as proteins, minerals, lactose, should enhance fat stratification on droplet top surface. However, Foerster *et al.* (Foerster et al., 2016), investigating cryogenic flash-frozen droplets after atomization by MDSD, found that the air-liquid interface was already covered of lipids immediately after droplet formation, thus giving greater weight to surface tension phenomena compared to the development of internal dynamics.

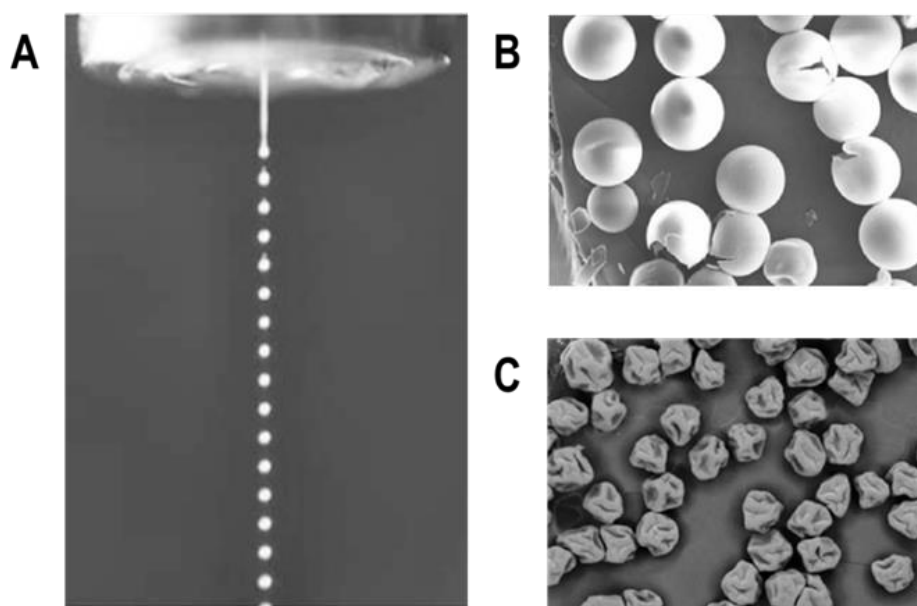


Figure 11. A) Generation of monodisperse droplets in MDSD spray dryers. (Foerster 2016) B) Puffed and C) wrinkled dry particles obtained by monodisperse dryers varying feeding solution composition and operating parameters (e.g. temperature) (Rogers et al., 2012).

All in all, understanding the drying stages of the droplet sol-gel transition in model spray dryers remains an open question, as well as predicting their impact on skin formation and particle final shape. From this point of view, the strong limitation of PSDs lies in the impossibility of following droplet morphological evolution in real time. Therefore, the research on this topic is currently oriented to the use of a so-called single-droplet approach at the laboratory scale.

1.4.2. SINGLE DROPLET APPROACH

1.4.2.1. LEVITATING DROPS

Compared to the pilot scale, the single-droplet approach allows performing much easier and extensive tests concomitantly less expensive, due to the small amount of volumes required and the relatively long duration of the observations with regard to industrial drying. Moreover, the investigation at the micro-scale shows a considerable repeatability since all droplets undergo the same drying history. In the case of drying of dairy products, an efficient single-droplet setup should reproduce the same environmental and flow conditions experienced by droplets while flying in industrial drying towers after atomization. In this regard, some pioneering works have been realized reproducing the typical drop free-falling conditions in a setup based on the so-called “levitated droplet” approach (Adhikari et al., 2000). This experimental strategy is based on the application of acoustic waves or air/gas streams to suspend drops of different size and to observe their morphological evolution, as highlighted in

different studies in the literature on fluids of different nature (Nuzzo et al., 2015; Zang et al., 2017). However, these methods are complex, imply strong deformations and non-uniform evaporation of the droplets, and do not allow the visualization of drying-induced internal flows and the monitoring of drying kinetics. Therefore, the ultimate goal of developing non-intrusive methodologies for investigating milk droplet drying had to be set aside for the moment, in favor of less “mimicking” setups but with better reliability.

1.4.2.2. GLASS FILAMENT METHOD

In the last two decades, the glass filament method (GFM) has been extensively used for investigating milk drying stages (S. X. Q. Lin & Chen, 2002). This setup consists of a Teflon filament (average diameter, $d=30-100\ \mu\text{m}$) with a glass knob at the extremity ($100-200\ \mu\text{m}$) for holding microdroplets (volume $V=2-5\ \mu\text{l}$) (**Figure 12**). The filament is placed in a drying chamber where the droplet is subjected to air stream with controlled flow rate, temperature, and relative humidity (Chen & Lin, 2005). The GFM approach was initially used to quantify the shrinkage induced by water removal in droplets of both fresh and skim milk. In this light, the impact of sample composition was investigated through drying kinetics and diameter reduction throughout the evaporation process. In the wake of these first preliminary works, Fu *et al.* used the same setup for the detection of main droplet drying stages in milk samples and corroborated their outcomes using the already mentioned REA method. The authors pointed out the occurrence of an early sol-gel transition at droplet surface, highlighted by an immediate falling drying rate (N. Fu et al., 2013). Due to the fast water removal and the early crust formation, the existence of internal flows throughout droplet drying process was not considered plausible. However, another work of the same group highlighted the presence of convective motions in milk droplets during the evaporation by GFM. Such convective flows resulted in the preferential fat segregation at the air-liquid interface and then in the surface wrinkling irrespective of the lipid content (N. Fu et al., 2011), in agreement with the above-mentioned observation in dry powders produced at a pilot scale (Foerster et al., 2016). The morphological characteristics of the suspended dry particles proved to be strongly depending on the overall solute content in the samples and on temperature. For instance, increasing the drying temperature from 70°C to 110°C both reduced shrinkage and buckling, thus suggesting that higher temperatures possibly foster skin formation and hinder solute diffusion. The GFM setup has been also used to investigate the evaporation of emergent products, such as noni juice and noni acacia (Zhang et al., 2019).

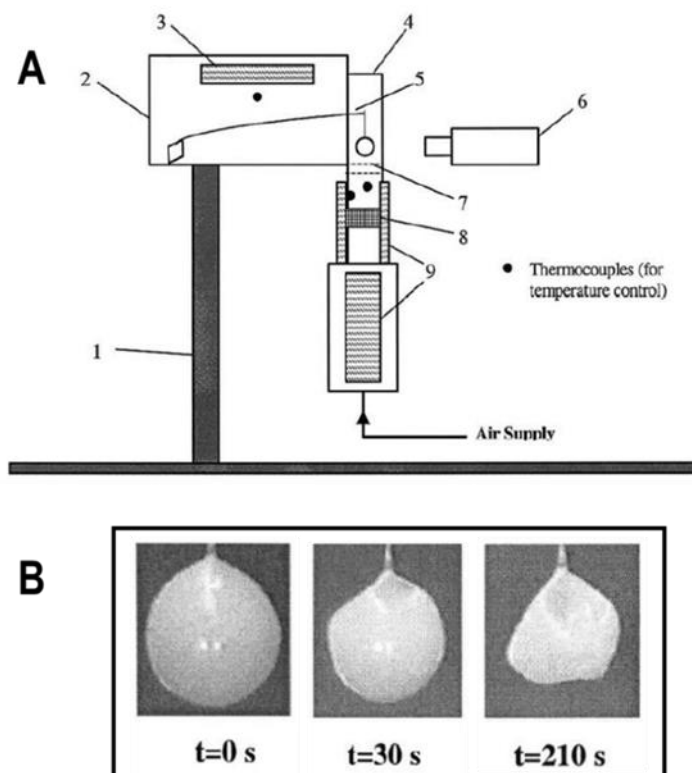


Figure 12. A) GFM setup: 1- Main support; 2- Glass filament box; 3- Heater for temperature control; 4- Drying chamber; 5- Glass filament; 6- Video camera; 7- By-pass switch; 8) Mesh block; 9- Heaters. B) Milk droplet shrinkage with time and skin formation (S. X. Q. Lin & Chen, 2002).

Despite its reliability for detecting the main evaporation stages in dairy droplets and suggesting possible dynamics of drying-induced segregation, the GFM is not efficient to clarify the physical interpretation of these phenomena. In fact, providing a direct observation of the mechanisms at the micro-scale would be crucial to elucidate the role of each dairy component (*i.e.*, lipids, proteins) in drying-induced crust formation. Nevertheless, this represents a real scientific challenge due to the multiple parameters involved and the high complexity of milk system. The need of a further strategy simplification resulted in studies focusing on the investigation at the lab-scale of simplified dairy models (*e.g.*, dairy protein solutions) using the well-known sessile and pendant droplet configurations. In recent years, this choice contributed to highlighting the considerable interdisciplinary nature of milk drying studies, involving physics, chemistry, and biology in addition to process engineering, and to benefiting from the introduction of experimental methods already reliable for other biological systems.

1.4.2.3. SESSILE/PENDANT CONFIGURATION

The study of the drying process of droplets in sessile or pendant configuration consists of two steps. First, the droplets are deposited on top or underside a substrate with different mechanical and chemical characteristics (*e.g.* deformability, hydrophobicity) and, afterwards, the dynamics of the

evaporation are investigated by visualizing droplet shape evolution with time until the complete solidification. The presence of a solid-liquid interface makes this experimental approach far from the real drying conditions of milk droplets despite the use of superhydrophobic substrates that reduce its contact area with the drop. However, the simplicity of the setup enables the monitoring of the internal flows, the drying stages, and the drying kinetics through microscopy methods (bright field, phase contrast, fluorescence). In the field of dairy science, different research groups have extensively studied the evaporation of sessile and/or pendant droplets in solutions of dairy proteins in the last decade. For example, the team of Food Processing Engineering of Wageningen (The Netherlands) observed the evaporation process in whey protein (WPI) sessile droplets (Bouman et al., 2016) deposited on a hydrophobic substrate (polypropylene membrane) under controlled environmental conditions (temperature $T=20-80^{\circ}\text{C}$, relative humidity $\text{RH}\approx 0\%$, air flow $\approx 0.2\text{ m s}^{-1}$). In parallel, the team of Science and Technology of Milk and Eggs of Rennes (France) proposed a thorough investigation of the evaporation in WPI and micellar caseins (native phosphocaseinates, NPC) droplets (Sadek et al., 2013, 2016). These works were carried out by observing the drying-induced morphological transition of pendant droplets of such dairy proteins after deposition on hydrophobic substrates (polydimethylsiloxane, PDMS) under constant temperature ($T=20^{\circ}\text{C}$) and relative humidity ($\text{RH}<3\%$). Both setups proved to be useful to detect the main evaporation stages, in agreement with what has been already mentioned for PSD and GFM approaches. Mostly, these typical examples of single droplet setups stressed a profoundly different behavior between WPI and NPC during the drying process that will be highlighted in the next paragraphs. The scenario is even more complex when studying the evaporation in mixes of dairy proteins, since it is likely to predict competitive dynamics involving the formation of the skin and, consequently, its rheological properties. From this point of view, it is necessary to provide a systematic investigation at the molecular scale and, thus, to integrate the study of WPI/NPC mixes in the wide domain of the evaporation and drying in colloidal systems.

1.4.3. THE PHYSICS OF THE DRYING PROCESS IN COLLOIDAL DROPLETS

The drying of a colloidal droplet is characterized by mass and energy transfers phenomena that govern the sol-gel transition and determine the final particle morphology. Once deposited on a substrate (either in pendant or in sessile configuration), the droplet evaporation is characterized by the onset of internal flows. Due to the pinned contact line, the free surface pushes the fluid outwards to refill with liquid the region in the vicinity of the triple line where the evaporation is more significant. However, such capillary flows also have the effect of carrying the solute phase towards borders, resulting in the so-called “coffee ring” effect and the formation of a gelled foot (Deegan, 2000; Deegan et al., 1997). At the same time, the evaporation at the air-liquid interface induces the development of local

concentration and thermal gradients, fostering the onset of Marangoni-Bénard flows (Hu & Larson, 2005; Nguyen & Stebe, 2002). These convective motions continuously mix the colloidal suspension in an attempt of keeping homogenous temperature and solute concentration. Therefore, on the one hand, the receding of the air-liquid interface leads to increasing colloid concentration at the surface; on the other, typical Brownian diffusive motions tend to oppose these events and to re-distribute homogeneously the colloids (**Figure 13**). When the evaporation rate is significantly higher than diffusion, a layer of macromolecules forms on droplet top layer, until a critical concentration is achieved and sol- gel transition events take place (Trueman, Lago Domingues, Emmett, Murray, & Routh, 2012). A global picture of the drying-induced surface gelation is provided by the Péclet number (Pe) that is defined as the ratio between the characteristic times related to diffusion (τ_d) and evaporation (τ_{ev}). The Pe estimation has been largely used in the literature to investigate the evaporation of colloidal films (Fortini et al., 2016), whereas the mechanisms of evaporation have been less explored in droplets (W. Liu et al., 2019) despite multiple potential applications. The onset of surface gelation marks that of skin formation. As the evaporation process progresses, the thickening of the crust corresponds to the development of inward stresses, whose intensity increases with time. Consequently, depending on its viscoelastic properties, the skin bends and buckles until complete solidification is achieved (Pauchard & Allain, 2003). Furthermore, due to the increasing interfacial forces, the already mentioned external foot undergoes inward solicitations leading often to stress release in the form of border detachment (delamination). The delamination occurs when the stored elastic strain overcomes the adhesion energy of the gel in contact with the substrate (Giorgiutti-Dauphiné & Pauchard, 2016; Pauchard, 2006). The process stops when the elastic strain induced by border detachment becomes lower than the adhesion force.

The vast majority of the works on the drying of colloidal suspensions has been realized on model systems (silica and/or polystyrene nano-beads). All in all, these studies highlighted that the morphology of dry colloid droplets, *i.e.* external foot and skin, is strongly affected by colloid size and volume fraction in the initial dispersion. In the case of dairy proteins, in addition to these crucial parameters, it is likely to predict an impact also of the molecular structure and the surface charges on the development of the drying process. In this regard, an overview of the main results obtained by single-droplet and MDS approaches on the investigation of colloid fingerprint on the mechanisms of skin formation in drying dairy protein mixes will be presented in the next paragraph.

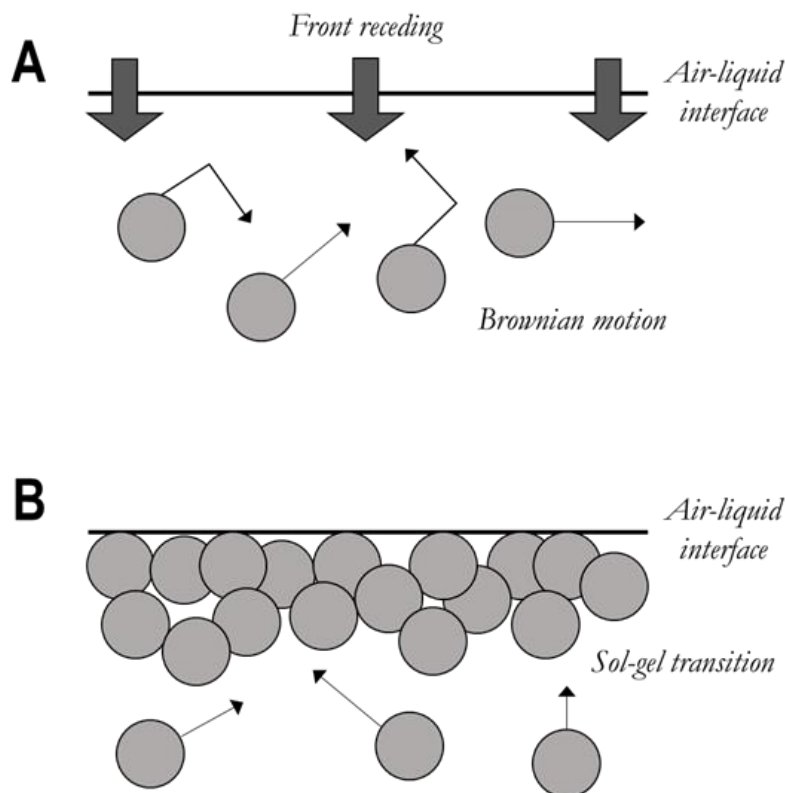


Figure 13. A) Competition between diffusive Brownian motion and drying-induced front receding at droplet air-liquid interface. B) Onset of interfacial sol-gel transition for high evaporation rates (Lanotte, 2020).

1.4.4. SKIN FORMATION AND CHARACTERIZATION IN DAIRY PROTEIN DRYING

1.4.4.1. SINGLE PROTEIN DROPLETS

As previously mentioned, in the last decade a systematic investigation of the drying mechanisms in droplets of single proteins (WPI or NPC) has been performed at the STLO laboratory using a multi-scale approach, from the single droplet to the scale up at the semi-industrial scale. First, the main stages of the droplet-to-particle transition were characterized by observing the shape evolution and the drying kinetics in drying single droplets (Sadek et al., 2013, 2016). Afterwards, WPI and NPC powder samples were produced by monodisperse dryer to tightly control the droplet drying history, collect homogeneous and abundant amounts of particles and statistically analyze their morphological properties. Finally, these results were validated by comparison with those of industrial spray dryers. The striking result of these works was that single protein dry particles exhibit the same morphology, irrespective of the experimental setup (*i.e.*, different temperature, relative humidity, droplet size): spherical hollow particles in the case of WPI, wrinkled irregular and puffed ones in the case of NPC.

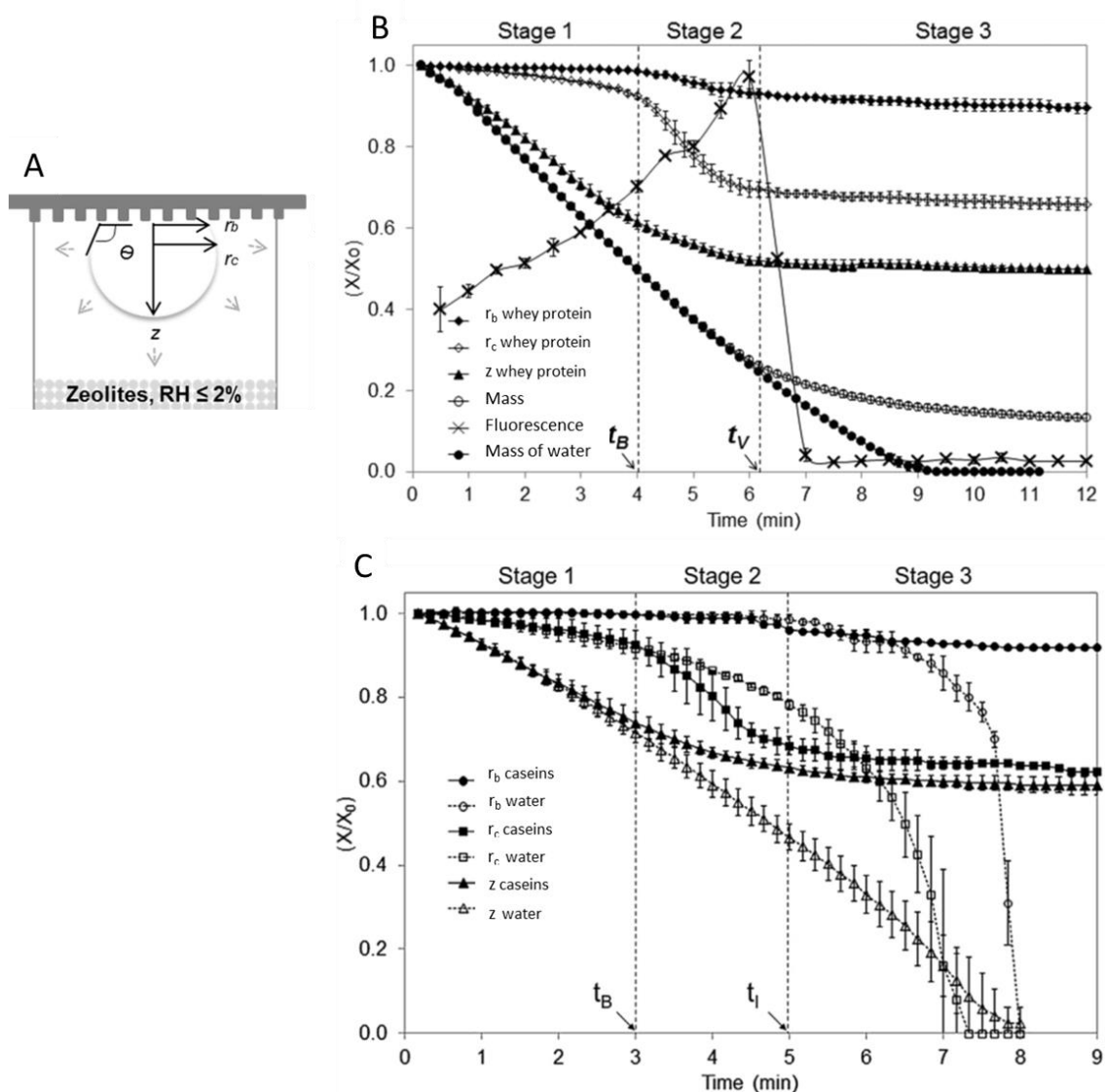


Figure 14. A) Schematic representation of a pendant drying droplet and definition of its base radius (r_b), cap radius (r_c) and apex height (z). B) Representation of dimensionless values (X/X_0) for base radius, cap radius, height, and mass of single droplet of WPI (filled dots). C) Representation of dimensionless values (X/X_0) for base radius, cap radius, height of single droplet of NPC (filled dots) and a single droplet of pure water (empty dots). Characteristic times represent the beginning of the buckling of droplet at t_B , and vacuole formation at t_V . Adapted from Sadek et al. (2013, 2016).

Regarding the single-droplet experiments, the drying stages were detected by monitoring the evolution with time of three key shape parameters (*i.e.*, base radius, cap radius and apex height) and of droplet mass, as showed in **Figure 14** B and C for WPI and NPC samples, respectively. Once deposited on the hydrophobic PDMS support, both WPI and NPC droplets exhibited a typical hemispherical shape (contact angle $\approx 106^\circ$) and were characterized by a progressive shrinkage (stage 1). This homogeneous volume reduction corresponded to a linear decrease of the height and the cap radius (even if very

slight), whereas the base diameter remained constant due to the self-pinning of the so-called triple line (**Figure 15**). At the same time, the droplet mass decreased linearly, characteristic of constant rate drying as for pure water, the protein solutions being diluted enough to be considered as pure fluids. During this first stage, it is likely to predict that the drying dynamics is controlled by water diffusion from droplet surface to the surrounding air and the consequent development of solute local concentration gradient at the air-liquid interface.

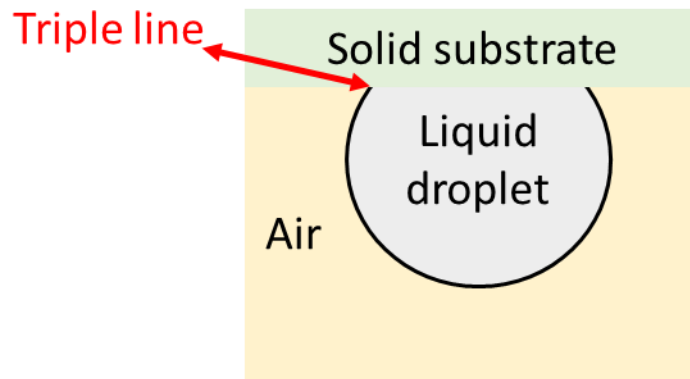


Figure 15. Sketch of the triple line as a boundary of solid substrate, liquid droplet and surrounding air.

The continuous accumulation of colloids at droplet surface, induced by the competition between evaporation front receding and Brownian motions, and at droplet borders, due to the already mentioned capillary flows, resulted in the formation of increasingly concentrated layers leading to:

- i) the occurrence of sol-gel transition phenomena at the air-liquid interface (*i.e.*, skin formation) once a critical protein concentration is achieved, resulting in high surface deformations defining buckling time (t_B),
- ii) and the development of a gelled external ring in the vicinity of droplet borders (also called “foot”).

The occurrence of these two fundamental shape modifications was characterized by evident changes in all the shape parameters, *e.g.* the slowdown of the height reduction and the sudden reduction of the cap radius (stage 2). At this stage of the evaporation, the samples of whey proteins and casein micelles started to display significant mechanical and morphological differences. Indeed, the gelation events occurred much earlier in NPC droplets than in WPI ones, as stressed by their different buckling time ($t_{B_NPC} \approx 3$ min; $t_{B_WPI} \approx 4$ min) (Sadek, Pauchard, et al., 2015). This could be explained in the light of the molecular structure of the two proteins, since NPC micelles are natural examples of microgels whereas WPI are smaller and rather globular structures. The skin formation corresponds also to the onset of increasing interfacial inward stresses, which act contrary to adhesion forces between gelled

foot and substrate. When the stresses passed a threshold level, NPC droplet surface underwent a surface instability (buckling) characterized by the partial folding of the skin (**Figure 16B**). On the contrary, WPI kept a round rigid shell until the end of the evaporation (**Figure 16A**). However, when the process was significantly advanced, whey protein samples displayed an evident delamination as possible clue of stress release, whereas casein micelle droplets showed just a slight diameter reduction. Interestingly, the onset of surface gelation did not affect the evaporation rate at this stage, as underlined by the identical behavior of WPI and pure water mass curves in **Figure 14A**. This could mean that the skin is not able to hinder water evaporation until a compact porous structure is formed.

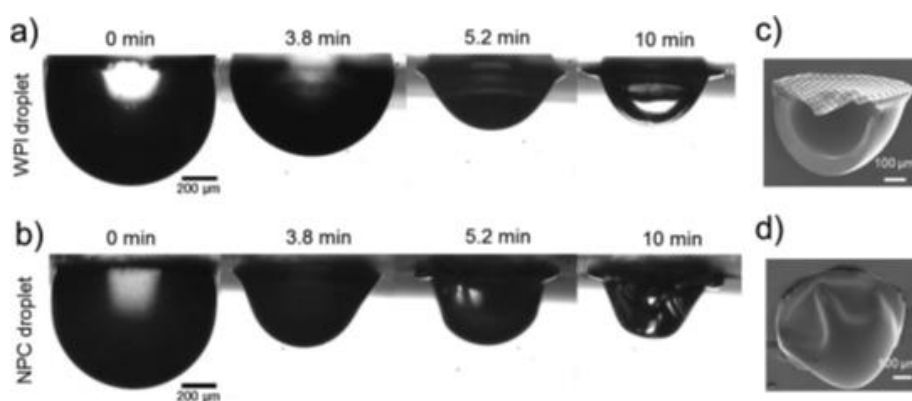


Figure 16. WPI (A) and NPC (B) shape evolution with time. Final particle of WPI (c) and NPC(d) observation by SEM (Sadek, Pauchard, et al., 2015).

During the final drying stage, droplet shape no longer evolved and, as a result, all the shape parameters reached a plateau. Only the mass kept slightly decreasing, thus suggesting the evaporation of the last water fraction in the droplets. At this point, when the complete solidification is almost achieved, the formation of a vacuole was observed especially in WPI samples (vacuole time, t_v), filling all the space beneath the shell. Arai and Doi (Arai & Doi, 2012) reported that the skin layer formation is a necessary condition for vacuole appearance, since it enhances the pressure difference between the liquid inside the droplet and the atmosphere until the air diffuses inside through the solid shell.

The detection of the main drying stages in WPI and NPC droplets represents an indirect characterization of the evolution of skin mechanical properties with time and highlights once more the key role played by colloid physico-chemical properties and their organization at the air-liquid interface during the evaporation. This global picture has been efficiently summarized by Sadek et al. (Sadek, Schuck, et al., 2015), where the different rheological regimes characterizing WPI and NPC surface during the drying process are illustrated (**Figure 17**). The sol-gel transition marks transition from the viscous to the elastic regime; as already mentioned, it occurs when a critical concentration resulting from the gradual accumulation of proteins at droplet surface is achieved. Such critical concentration

was estimated from droplet visualization and drying kinetics in confined conditions and significantly differed in whey proteins (41.4 w/w %) and casein micelles (15.6 w/w %), in good correlation with the difference in terms of t_B showed in **Figure 14**. Such a fundamental phase transition has been investigated also in previous studies in the literature. For example, Loveday et al. studied the protein phase transitions at increasing osmotic pressures, showing a good agreement with the outcomes obtained in confined droplets (Loveday et al., 2007). In other experimental works, the rheological behavior of whey protein and casein micelles have been explored by oscillatory tests, measuring the evolution of storage (G') and loss (G'') moduli. In this case, the critical concentration for sol-gel transition was estimated equal to 60 w/w % for WPI (Brownsey et al., 2003) and 19 w/w % for NPC (Dahbi et al., 2010) thus comparable to what the study of Sadek et al. When the interface is almost completely solidified, the skin exhibits a plastic behavior leading to possible mechanical instabilities to counteract the increasing inward stresses. The yield stress in dry WPI and NPC films has been measured by indentation tests (Sadek, Schuck, et al., 2015) in order to evaluate the peculiar plasticity of the two different layers. NPC dry skin layers displayed a lower yield stress compared to WPI ones (30 MPa against 52 MPa, respectively), thus reflecting a higher deformability and explaining the development of a wrinkled surface. On the other hand, the higher resistance of WPI skin to the interface stresses and the increasing osmotic pressures led to the formation of a brittle rigid shell at the end of the process.

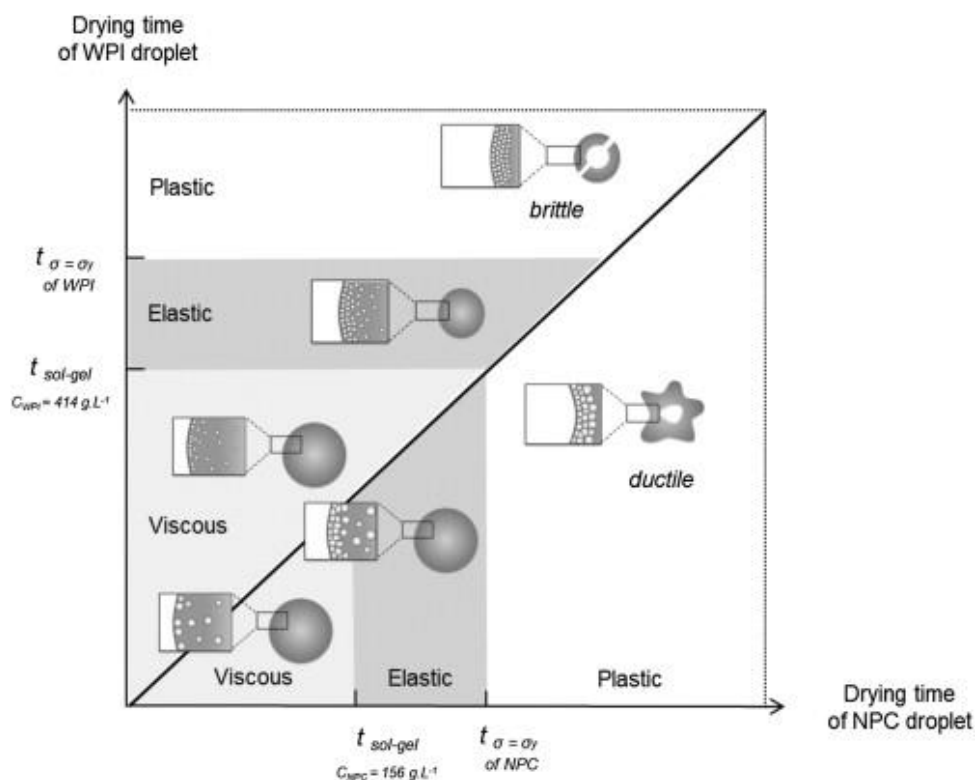


Figure 17. Diagram WPI and NPC skin rheological regimes as a function of the drying time (Sadek et al, 2015).

The investigation of surface rheology in drying suspensions of single dairy proteins suggested that the significant differences between WPI and NPC skin mechanical behavior are ascribable to their different structure at the molecular scale. Indeed, whey proteins, and especially β -LG, have been often considered equivalent to hard nano-spheres in previous works, in analogy to other globular proteins (*e.g.*, BSA;(Brownsey et al., 2003; Loveday et al., 2007)). In this light, the repulsive excluded-volume interactions are the predominant dynamics for high WPI concentrations at the air-liquid interface, resulting in a jammed layer with volume fraction ≈ 0.58 . Such a compact structure allows to resist to the drying-induced stresses until the occurrence of a crack when the yield stress is achieved, as often observed in WPI dry particles at the end of the process. On the other hand, casein micelles have been mainly theorized as self-assembled highly deformable microgels, whose structure strongly depends on the increasing concentration and osmotic pressure throughout the evaporation (Bouchoux et al., 2010). Therefore, it is likely to predict a deviation from the hard sphere behavior, especially in dense conditions, leading to the squeezing of the micellar structure above close packing and the gradual irreversible merging into a continuous gel (Dahbi et al., 2010).

1.4.4.2. DRYING OF DROPLETS OF DAIRY PROTEIN MIXES

In addition to the production of single WPI and NPC powders, the MDSD approach has been employed also to carry out preliminary studies on the drying of dairy protein mixes with different WPI/NPC ratio and fixed overall protein concentration (Sadek et al., 2014). The dry particles have been analyzed via their density, size and shape, and rehydration properties. The micrographs presented in **Figure 18 A** as a function of WPI/NPC allowed to highlight how the morphology of the particles is strongly affected by the major component in the mixture, as clearly noticeable in WPI-rich (WPI/NPC equal to 100/0 and 80/20) and NPC-rich samples (WPI/NPC equal to 20/80 and 0/100). However, when WPI and NPC are dispersed in the suspensions in comparable amount, two main outcomes were obtained: i) the presence of hybrid morphology, displaying a round but partially wrinkled surface, and ii) the formation of single WPI and NPC-like dry particles, thus suggesting sort of protein segregation during the drying process. The comparison with dry WPI/NPC samples obtained by single droplet approach (**Figure 18 B**) did not point out the development of these three shape categories, thus suggesting the possible influence of the drying temperature on the development of the drying stages ($\approx 100^\circ\text{C}$ dry temperature in the MDSD setup, 20°C for the single droplet evaporation). The other outcomes present in the literature on the spray drying of dairy mixes (Alamilla-Beltran et al., 2005; Nijdam & Langrish, 2006; Rogers et al., 2012) are mostly qualitative and based on the off-line analysis of powders. Part of these works (Alamilla-Beltran et al., 2005) predicts the formation of spherical particles due to the high evaporation rate in the drying chambers and the consequent rapid crust formation. Conversely (Sadek

et al., 2014), the authors suggested the formation of wrinkled irregular particles in case of slow drying conditions, such as in the single-droplet setup, which favor droplet shrinkage, deformation and surface collapse. These contradictory results highlight the need of a systematic investigation of the drying mechanisms in dairy protein mixes in order to shed light on the specific role of different parameter, such as the drying rate, the colloid properties and the composition of the solutions.

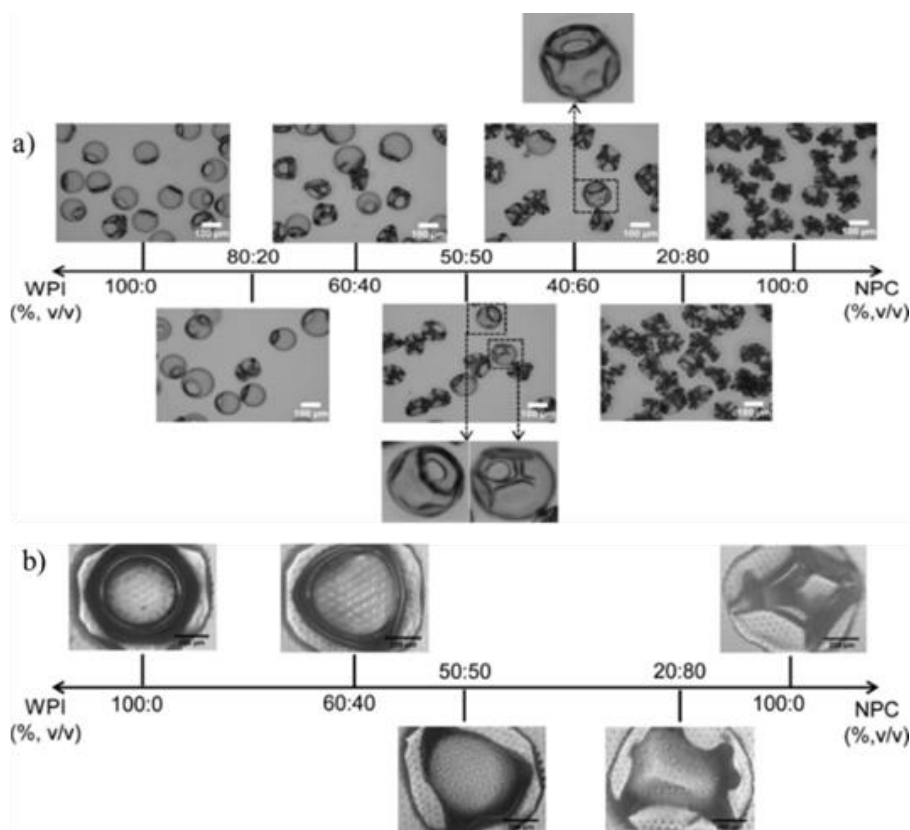


Figure 18. A) Micrographs of different WPI/NPC particles obtained by MSD drying (objective: $\times 10$, scale bar = $100\ \mu\text{m}$); B) Image of WPI/NPC particle obtained by pendant single droplet drying experiment (objective: $\times 10$, scale bar = $200\ \mu\text{m}$) (Sadek et al., 2014).

From this point of view, the work realized by Lanotte et al., (Lanotte et al., 2018) studying the drying dynamics in droplets of WPI/NPC mixes, paved the way to further ongoing investigation and this thesis project. Using the same single-droplet experimental approach implemented for single WPI and NPC droplets, the authors showed that the shape of dry particles of WPI/NPC mixes presents significant similarities with that of the most represented protein in the sample. However, an elemental analysis (EDS) was also performed by scanning electron microscopy (SEM) on the skin of the dry particles (**Figure 19 A**) in search of NPC key elements, such as calcium (Ca) and phosphorus (P). In particular, the authors compared Ca mass concentration on the internal and the external layer of the shell, as illustrated in **Figure 19 B**. This revealed the overrepresentation of the whey proteins on the external

side of the skin shell. The accumulation of the smaller proteins on droplet top surface is in good agreement with recent studies on the evaporation in model colloidal systems. In these works, the evaporation process has been investigated in films and droplets of dispersions consisting of hard nano-beads differing by size to shed light on the mechanisms of drying-induced organization at the air-liquid interface and, thus, on skin formation (Schulz & Keddie, 2018). The outcomes of these studies highlighted that surface colloid deposit strongly depends on their characteristics (*e.g.*, component size ratio), and on evaporation rate (*e.g.*, temperature, relative humidity). Under certain experimental conditions, a preferential colloid stratification was observed, which led to the accumulation of the smaller nano-beads on the external part of the skin layer (small-on-top theory) (Fortini et al., 2016; W. Liu et al., 2019). Such a behavior is not intuitively explicable, since, according to what already mentioned before on the dynamics of skin formation, larger macromolecules should be “trapped” faster in the gelling surface front due to their lower diffusivity. The most recent hypothesis relates the skin self-organization at the colloidal scale to the interplay between two driving forces: interfacial osmotic pressures (Zhou et al., 2017) and diffusiophoresis motions linked to the development of local concentration gradients (Sear & Warren, 2017). Despite the evident progress of last years, the question regarding interface rheology and skin formation in complex colloidal systems is far from being fully clarified. Therefore, these promising preliminary results on WPI/NPC droplet drying underlined the necessity of a further accurate investigation at the micro-scale to explore the mechanisms of skin formation and the evolution of its viscoelastic properties throughout the evaporation process.

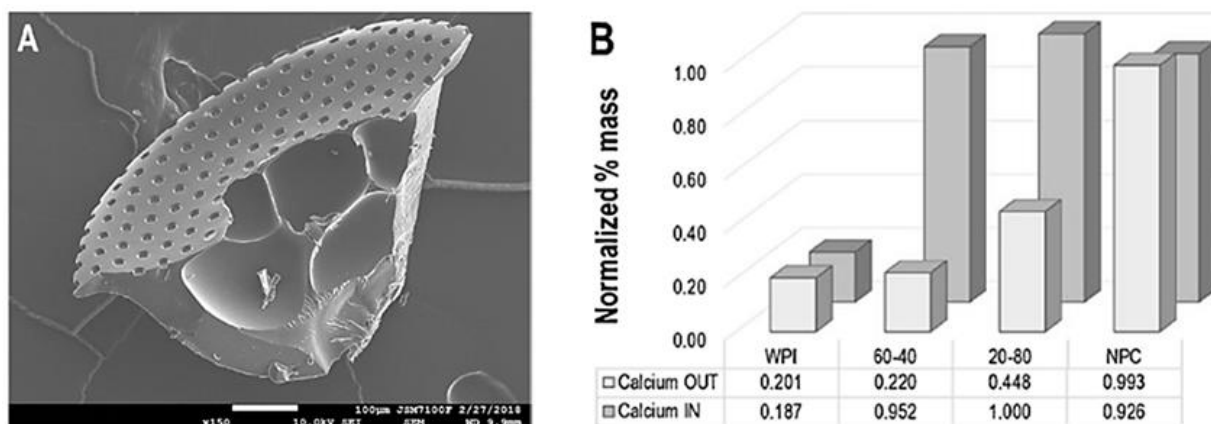


Figure 19. A) Internal part of dry WP skin layer observed by SEM. B) Normalized Ca mass percentage on the internal (IN) and the external (OUT) part of WP/CM mixes skin layer (Lanotte et al., 2018).

Chapter 2. EXPERIMENTAL STRATEGY

The literature review pointed out the need of a better understanding of the mechanisms leading the formation of dry particles to fully master the properties of products as complex as IMF powders and more generally nutritional dairy products (*e.g.*, sports nutrition, elderly nutrition), which has been representing for about fifteen years the main engine of growth of the dairy industry at the global scale. Nevertheless, these phenomena take place in closed systems and at such fast kinetics that their observation and decryption *in situ* is not possible. These practical difficulties can be circumvented by implementing:

- Experimental approaches at the scale of a single drop deposited on hydrophobic surfaces, which favor the visualization of the drop / particle conversion over extended times by different analytical means (*e.g.*, imaging, optical and confocal microscopy);
- Trains of mono-dispersed flying droplets resulting in characterizable particles (internal structure, local composition), all having undergone the same thermal history during the drying process and thus with identical morphology, as opposed to industrial systems which lead to large particle size distributions.

As mentioned in Chapter 1, STLO research group validated the genericity of the results obtained through both of these approaches upon scale up (industrial spraying cone droplets), that led to similar morphologies and structure of the particles although obtained in different drying environments (drying temperature between 20°C and 190°C and relative humidity (RH) ranging from 40% to 2%; (Sadek et al., 2013, 2016; Sadek, Schuck, et al., 2015)). As well, it is already known that when drying pure solutions of whey proteins (WPI) or micellar caseins (NPC), the formation of the outer skin layer particle occurred at a critical protein concentration at the interface, leading to specific particle shapes and governing the powder properties. However, while it is possible to make the connection for pure colloids between the onset of skin formation and the achievement of the critical sol-gel transition concentration, this is much more complex in the case of mixtures of colloids. Nevertheless, and from an application point of view, it is such mixtures which are used in the formulation of the nutritional dairy products mentioned above.

For these reasons, this study will focus on the physical mechanisms leading the droplet / particle transition in the case of mixes of WPI and NPC. In order to breakdown the complexity of the drying phenomenon, the now established multiscale strategy, including the single droplet (and eventually a

confined droplet), the mono-dispersed droplets and the semi-industrial spraying cone (benchmark) scales, will be implemented. The two aims of this PhD project will be (**Figure 20**):

- On the one hand, to highlight the key physical phenomena (buckling and phase transitions, internal flows, etc.) at a single drop scale in the case of WPI / NPC mixes, so to shed light on the mechanisms of skin formation. This part of the work has been conducted in the frame of the well-established collaboration with FAST laboratory (Orsay; L. Pauchard) and IPR laboratory (Rennes; A. Saint Jalmes);
- On the other hand, to model the drying kinetics by coupling the Reaction Engineering Approach (REA), developed by X.D. Chen team (Soochow University) and the Energy Map Model (EMM), developed by P. Bacchin team (LGC Toulouse).

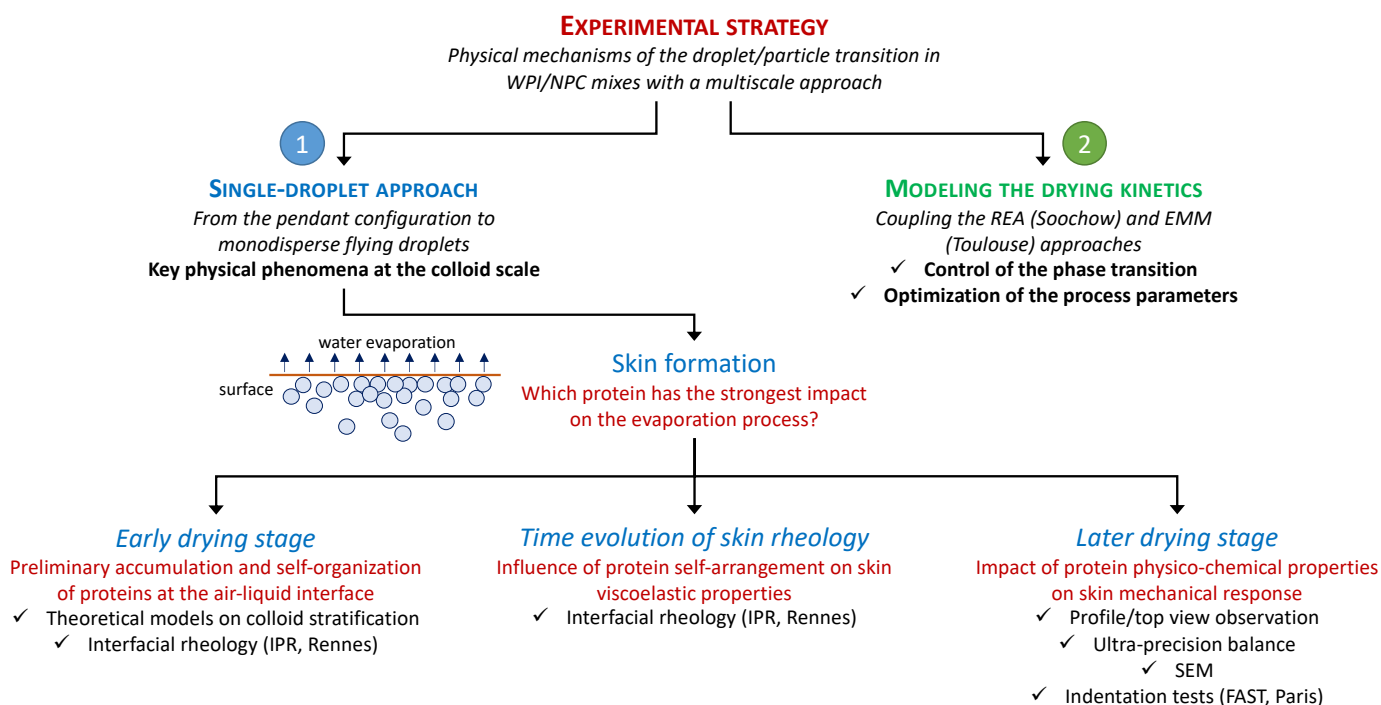


Figure 20. Research strategy of the PhD project

2.1. INVESTIGATION ON SKIN FORMATION

As already mentioned, the formation of the skin marks the onset of the droplet / particle transition. While it is possible to relate this event to the sol-gel transition in the case of pure colloids, colloid mixtures raise the question of their competition and their location in relation to the structural organization of the interface. **The central research question of this work is therefore to understand, in the case of WPI / NPC mixes, whether one of these colloids primarily drives the transition at the interface and therefore the skin mechanical properties.** In order to answer this question, the drying dynamics will be investigated in this thesis by varying separately or simultaneously the proportion of each of these colloids in solution and the total protein concentration.

The single pendant-droplet setup available at STLO will be employed to provide information about the separate role of WPI and NPC during the drying process and their location at the interface. After that, the dry skin structure and its composition will be observed by Scanning Electron Microscopy (SEM) to reveal any eventual self-organization phenomena induced by the evaporation. Additionally, the results by single droplet approach will be consolidated by the production of WPI/NPC particles by MDSD (Mono-Disperse Single droplets, available at the pilot scale at STLO) to clarify the different particle shape distribution previously reported. In particular, this method will make it possible to gain more information about the cohabitation of whey proteins and casein micelles and on a specific signature depending on the WPI/NPC ratio for free flying droplets (that is to say out of the influence of the substrate).

Moreover, some preliminary tests will be presented to track the drying-induced protein motion within the droplets by specifically labelling milk proteins. The observation was carried out by confocal microscopy, first considering WPI and NPC separately and then using different WPI/NPC mixtures. For selective protein labelling we used the method proposed by Nigen et al. (Nigen et al., 2010) based on the pH adjustment of proteins to 8.5 to favor covalent binding with fluorescent probes, followed by extensive dialysis to remove free probes. Previous studies have shown good results for the labelling of β -lactoglobulin with Fluorescein isothiocyanate (FITC) and the labelling of α s1-casein with Rhodamine B isothiocyanate (RITC). These probes can be used jointly, as their excitation wavelengths are 488 and 543 nm, respectively, while their emission wavelengths are 525 and 580 nm, respectively.

2.1.1. SKIN FORMATION AT THE EARLY STAGE OF THE DRYING

Due to the double simultaneous action of the receding of the evaporation front and the colloid Brownian motion, WPI and NPC accumulate at droplet air-liquid interface since the early stage of the drying process. The main experimental questions to deal with are, thus: **is it possible to observe an eventual protein distribution at droplet surface at the occurrence of the gelation (*i.e.*, when the skin is forming)? If so, what are the parameters affecting this molecular organization?** The single pendant-droplet setup does not allow to investigate the early stage of the drying process, when the interfacial sol-gel transition is already ongoing and the droplet is merely characterized by a homogeneous shrinkage. Thus, two alternative approaches will be here implemented:

- Comparison with the outcomes of recent theoretical models on the evaporation in model colloid binary systems and evaluation of their feasibility to our experiments on protein mixtures (environmental conditions, protein physico-chemical properties);

- Interfacial rheology by oscillatory drop setup to estimate the viscoelastic properties of WPI/NPC surfaces, with different protein concentration and WPI/NPC ratio, before significant gelation (collaboration with the IPR laboratory – A. Saint-Jalmes).

2.1.2. LATER STAGE OF THE DRYING

Later-on during the drying process, the development of the skin is defined as the formation of a medium mechanically withstanding stress. From a structural point of view, the orientation symmetry of the medium is broken and a structural anisotropy is generated at this point, when the particles have been concentrated by the flow to the point so that they are caged by their neighbors into a soft, deformable network.

In the light of a possible protein specific organization at droplet surface, a systematic analysis will be presented to answer the question: **how skin composition and structure at the molecular scale influence skin rheological behavior and, consequently, the final morphology of the dry WPI/NPC particles?** In order to achieve this goal, the observation of single pendant-droplet shape evolution is a precious tool to detect the main morphological modifications linked to the progress of the drying process. Therefore, this setup will be used to investigate whether one of the two dairy proteins has a predominant effect on dry particle shape. For the same reason, in parallel, the drying kinetics in WPI/NPC droplets will be measured using the same configuration by ultra-precision balance.

To further study the paradigm linking colloid properties at the molecular scale to particle macroscopic characteristics, the dry samples will be observed by SEM. In particular, the section of dry WPI/NPC droplets with different WPI/NPC ratio will be explored to find the evidence of colloid self-organization. Moreover, the rheological properties of dry films of whey proteins and casein micelles will be estimated by micro-indentation tests in the frame of the collaboration with the FAST laboratory (L. Pauchard) to evaluate the impact of skin composition and structure on its mechanical response.

At a later stage, the role of protein characteristics (size, structure, deformability) on the organization at the interface will be explored by realizing a full investigation of the drying process replacing casein micelles in the mixes with smaller amorphous sodium caseinates.

2.1.3. TIME EVOLUTION OF THE RHEOLOGICAL PROPERTIES OF THE SKIN

The rheological properties of the outer skin evolve with time. As a result, the skin exhibits viscous, elastic and plastic behaviors. The rheological properties of the drying medium will be evaluated as a response to oscillatory solicitations at different instants. In continuity with the tests carried out for the

early-stage characterization of the skin properties, interfacial rheology experiments will be realized on WPI/NPC mixtures overnight to highlight the evolution of surface viscoelastic behavior.

2.2. MODELLING THE DRYING KINETICS

The drying kinetics and the phase transitions undergone by the milk proteins are controlled by a complex non-equilibrium interplay between protein-protein and protein-air interface interactions and mechanical stresses. This coupling is responsible of mass transport in the droplet leading to the skin formation (2.1.1) and to buckling phenomena (2.1.2). The modelling of these phenomena can help to unravel these mechanisms and to have a better understanding and control of the drying kinetics.

The originality of the approach proposed in this PhD will be to implement the interaction between the proteins and the gas-liquid interface in modelling approaches already developed in the participating team: the Reaction Engineering Approach (X.D. Chen team, Suzhou University) and the Energy Map Model (P. Bacchin team, LGC Toulouse). These protein-air interface interactions are modifying the water activity at the interface and are then responsible of changes in the drying kinetics. Moreover, these interfacial interactions can be the cause of interfacially driven transport (as Marangoni flow inside the drying droplet; section 1.4) that can change the mass transport inside the droplet.

The implementation of the protein-interface interactions will be done in modelling approach based on a coupling of momentum and mass balances for the protein and the water. At the end, the complete model will be able to account for the physico-chemical properties of the milk (with the protein/protein and the protein/interface interactions) and the mechanical stresses (hydrodynamic and internal solid stresses respectively before and after the liquid/solid transition). This modelling approach should then help to control the phase transition in the drop leading to skin or cracking and to have a better link between the physicochemical milk properties and the drying kinetics. This model should also allow to define new experimental conditions to test in order to identify the limiting phenomena in the process.

Chapter 3. MATERIAL AND METHODS

3.1. SAMPLE PREPARATION

3.1.1. PREPARATION OF WHEY PROTEIN ISOLATES (WPI), NATIVE PHOSPHOCASEINATE (NPC) AND SODIUM CASEINATE (SC) SOLUTIONS

WPI, NPC and SC powders with respective protein content equal to 86 w / w %, 82 w / w % and 91 w / w % were obtained from industrial sources. Dispersions of single WPI, NPC proteins with overall protein concentration (c_p) ranging from 6 w / w % to 14 w / w %, and SC dispersions with $c_p = 8$ w / w %, were prepared by dissolving the commercial powders in deionized water containing 0.02 w / w % of sodium azide (NaN_3) as a bacteriostatic agent. The WPI, NPC and SC suspensions were then stirred at 600 rpm for 48 h at 20°C to ensure full dissolution.

3.1.2. MIXTURE SAMPLE PREPARATION

The mixture samples were prepared by mixing NPC or SC and WPI solutions, respectively, and adjusting the final composition to obtain relative WPI percentages ($\text{WPI}\%_R$, defined according to the Eq.1) of 0, 20, 50, 80 and 100 w / w %:

$$\text{WPI}\%_R = \frac{m_{\text{WPI}}}{m_{\text{protein}}} \quad (\text{Eq. 1})$$

With m_{WPI} the mass of WPI and m_{protein} the total mass of the proteins. These mixture solutions were stirred at 400 rpm for 1 h at 20°C. Due to the different voluminosity of WPI and NPC macromolecules, which is equal to 0.74 mL.g⁻¹ (Mylonas & Svergun, 2007) and 4.4 mL.g⁻¹ (Bouchoux, Cayemitte, et al., 2009) (**Table 9**) respectively, the final WPI/NPC mixes exhibited significant differences in terms of overall volume fraction (ϕ_p) and WPI volume fraction (ϕ_{WPI}) as a function of c_p and $\text{WPI}\%_R$, as summarized in **Table 9**.

Table 9 : Overall volume fraction (ϕ_p) and WPI volume fraction (ϕ_{WPI}) as a function of overall protein concentration c_p and WPI percentage $WPI\%_R$

c_p (w / w %)	ϕ_p					ϕ_{WPI}				
	WPI $\%_R$					WPI $\%_R$				
	0	20	50	80	100	0	20	50	80	100
6	0.22	0.19	0.14	0.09	0.05	0	0.008	0.020	0.035	0.045
8	0.28	0.24	0.18	0.11	0.06	0	0.010	0.026	0.046	0.060
10	0.33	0.29	0.22	0.14	0.08	0	0.012	0.032	0.057	0.076
12	0.38	0.33	0.26	0.17	0.09	0	0.013	0.037	0.067	0.092
14	0.42	0.37	0.29	0.19	0.11	0	0.015	0.042	0.078	0.108

3.2. SINGLE DROPLET DRYING EXPERIMENT

3.2.1. HYDROPHOBIC SUBSTRATE

The hydrophobic substrate was produced by mixing polydimethylsiloxane (PDMS) and curing agent (Dow Corner) agent with the mass ratio of 10:1 (g:g) in a beaker. Due to its high viscosity, the homogenization of the mixture was obtained by manual stirring with a plastic rod. In order to get rid of the numerous bubbles formed after strong mixing, the beaker was left for 1 hour in a vacuum glass dryer at room temperature. Afterwards, a thin PDMS film was poured into a Petri dish on a silicon wafer specifically designed with cylindrical micropillars (20 μm diameter, 10 μm height) (**Figure 21**) and then put in an oven at 55°C for 3-4 h. Such a patterned hydrophobic support reduced the contact surface and conferred to the droplets an almost hemispherical shape (initial contact angle close to 105°) at the early stage of the evaporation, making it possible to maintain a quasi-spherical shape of droplets and limiting the substrate impact on droplet drying dynamics during the drying process.

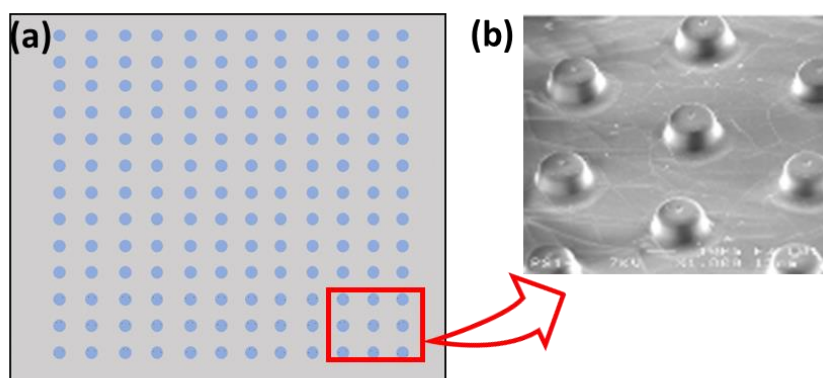


Figure 21. (a) Top view of the PDMS substrate, cylindrical pillars (blue circle) were separated from each other by a 50 μm center-to-center distance. (b) a scanning electron microscopy image of the cylindrical pillars (20 μm diameter, 10 μm height (Sadek et al., 2013).

3.2.2. DRYING CONDITIONS

The drying temperature was kept at $20 \pm 1^\circ\text{C}$ and the relative humidity (RH) was regulated to 2% by using zeolites (HG2-DES-3, Rotronic) for ensuring a constant drying force. The zeolites were heated in an oven at 105°C for 48 hours before use. It should be highlighted that the moisture of the environment around the droplet plays an important role in the drying process since the diffusion of vapor into the surrounding air is driven by the difference between the saturation and vapor pressure. Therefore, the lower humidity of the surrounding air favors the vapor migration from droplet to ambient in order to balance the vapor pressure.

3.2.3. DROPLET PROFILE OBSERVATION

3.2.3.1. EXPERIMENTAL SET UP

The profile view setup consisted of a high-speed camera (Fastcam MC2 10,000 NB, Photron) to capture droplet profile evolution, a drying chamber and a background light (Phlox 100/100 LLub), as shown in **Figure 22**. The background light was placed in the opposite direction of the camera to get a uniform background and enhance the quality of image contrast. The sealed drying chamber was designed to reduce the atmospheric disturbance during droplet evaporation.

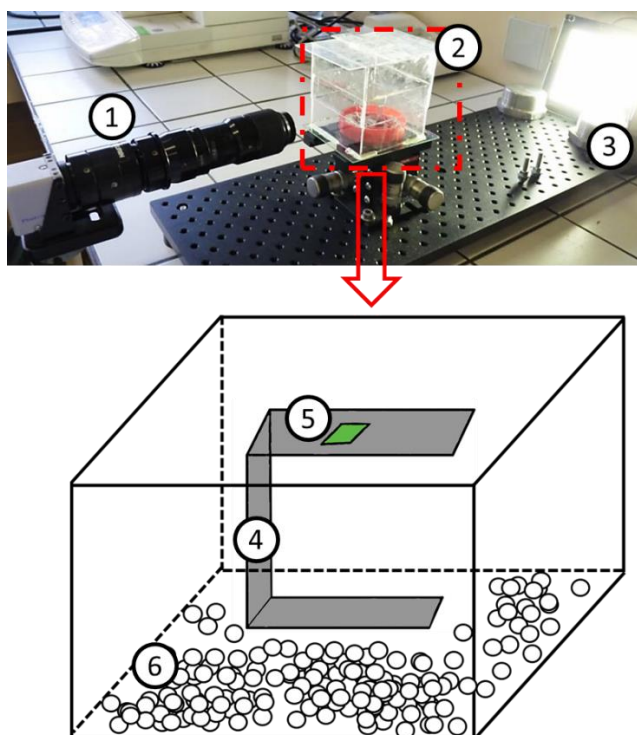


Figure 22. Profile observation device, ① high-speed camera, ② drying glass chamber ($8*8*8\text{ cm}^3$), ③ background light, ④ glass support (grey area), ⑤ PDMS substrate (green square), ⑥ zeolites (empty circle).

3.2.3.2. MEASUREMENT PROCESS

Before droplet deposit, the PDMS substrate was cleaned with water and dried. Remaining insoluble particles on the substrate were cleaned off by tape. Then, the PDMS was put on a glass support. A droplet of 0.5 μL was generated with a microsyringe (0.5 μL syringe, SEG Analytical Science) and deposited onto the hydrophobic substrate. The glass support was reversed to ensure a pendant configuration and then quickly moved into the drying chamber. The morphology profile history during the evaporation process was recorded (fps = 0.2) by a high-speed camera. The experiments were repeated 8 to 10 times for each sample.

3.2.3.3. DROPLET MORPHOLOGICAL ANALYSIS

The image sequences acquired throughout the evaporation were subsequently analyzed by a custom image analysis software (Image J). The initial contact angle (θ) of the droplet, defined as the angle between the substrate plane and the tangent one originating from the droplet triple line, ranged from 103° to 110° . The droplet profile changes were characterized by two shape indicators: the base diameter (D) and the apex height (H). The evolution of these indicators normalized by their maximum values (D_{max} , H_{max}) was monitored throughout the entire drying process.

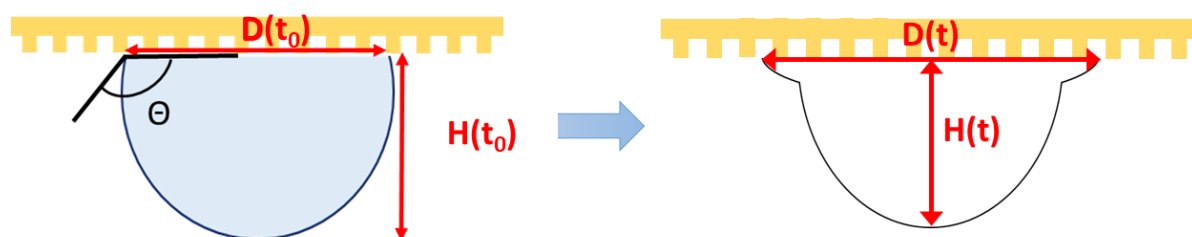


Figure 23 . A pendant droplet on the substrate. Base diameter (D) is the radius at contact line with substrate and the apex height (H) is the maximum height from the substrate to the top of the droplet.

3.2.3.4. DRYING DROPLET PHYSICAL CHARACTERIZATION

In addition to the quantitative characterization of the key shape indicators, an evaluation of the main forces involved in the evaporation process was further provided by the estimation of two adimensional numbers: the Bond number (Bo) and the already mentioned Péclet number (Pe).

The Bond number is defined as the ratio between the gravitational force and surface tension in order that it appears quite evident that this number control the integrity if droplet when subjected to external force (limited here to gravitational force). And Bo number provides an evaluation of droplet sphericity under the external action of gravity. It is expressed as:

$$Bo = \frac{\rho \cdot g \cdot R_0^2}{\gamma} \quad (\text{Eq. 2})$$

where ρ is droplet density, g is gravity acceleration, R_0 is the initial droplet radius (μm) and γ stands for droplet surface tension. Bo provides an estimation of the relative impact of gravity and surface tension on droplet morphology. In the present study, Bo was calculated for all the samples at the beginning of the drying process.

Pe is a precious tool to characterize the relative contribution of advection and diffusion to colloid motion during the evaporation. In other words, it could be defined as the ratio of the rate of advective physical quantity initiated by the flow to the rate of diffusion of the same quantity driven by an appropriate gradient. In this study, the estimation of Pe for WPI (Pe_{WPI}) and NPC (Pe_{NPC}) was carried out using the work of Liu et al. (W. Liu et al., 2019) on the drying of binary colloidal droplets as main reference. For spherical droplets, Pe is defined as the ratio between the characteristic times related to diffusion (τ_d) and evaporation (τ_{ev}). The characteristic diffusion time is equal to:

$$\tau_d = \frac{R_0^2}{D_p} \quad (\text{Eq. 3})$$

where D_p is the colloid diffusion coefficient. This parameter was calculated through the Stokes-Einstein relation, approximating WPI and NPC proteins to spherical particles at the early drying stage:

$$D_p = \frac{k \cdot B \cdot T}{3 \cdot \pi \cdot \eta \cdot d} \quad (\text{Eq. 4})$$

Here, $k \cdot B \cdot T$ is the system thermal energy, η is the suspension viscosity, and d is the average particle diameter, i.e. WPI (d_{WPI}) and NPC (d_{NPC}) average size in this case. On the other hand, the evaporation characteristic time can be expressed as:

$$\tau_{ev} = \frac{R_0}{v_{ev}} \quad (\text{Eq. 5})$$

Where v_{ev} is the evaporation rate intended as droplet volume variation with time. This evaporation rate can be obtained by the expression:

$$v_{ev} = \frac{1}{2} \times \left(\frac{3}{4\pi}\right)^{\frac{2}{3}} \times \frac{a}{R_0} \quad (\text{Eq. 6})$$

where a ($\mu\text{m}^2 \cdot \text{s}^{-1}$) refers to the rate of surface reduction. The parameter a has been determined by image analysis, evaluating the droplet volume variation with time, and also calculated using the equation proposed by Picknett and Bexon (Batchelor & Shen, 1985) for sessile droplets with spherical cap shape (not reported here for the sake of simplicity). In the latter case, we considered that the

differences with our setup are geometrically negligible from the drying point of view. At the beginning of the drying process ($50 \text{ s} < t < 100 \text{ s}$), typical values for the evaporation rate in WPI and NPC droplets were $\approx 0.13 \mu\text{m}\cdot\text{s}^{-1}$. To summarize, the equation used here for Pe calculation at the early evaporation stage was:

$$Pe = \frac{\tau_d}{\tau_{ev}} = \frac{1}{2} \times \left(\frac{3}{4\pi}\right)^{\frac{2}{3}} \times \frac{a}{D_p} \quad (\text{Eq. 7})$$

3.2.4. DROPLET TOP VIEW OBSERVATION

3.2.4.1. TOP VIEW OBSERVATION SETUP

An optical microscope (OLYMPUS, BX51) was used to observe the sol-gel transition and the morphology of dried samples from the top view. In analogy to the profile view tests, a glass drying box ($9 \times 9 \times 2 \text{ cm}^3$) was employed for the observation, placed between the objective and condenser, as shown in **Figure 24**. A layer of zeolites on the bottom of the box allowed keeping a low RH and favored the evaporation process. In the center of the box, a glass support was used to hold the PDMS substrate (green square) fixed to a glass coverslip (yellow rectangle) to investigate the evaporation in pendant configuration.

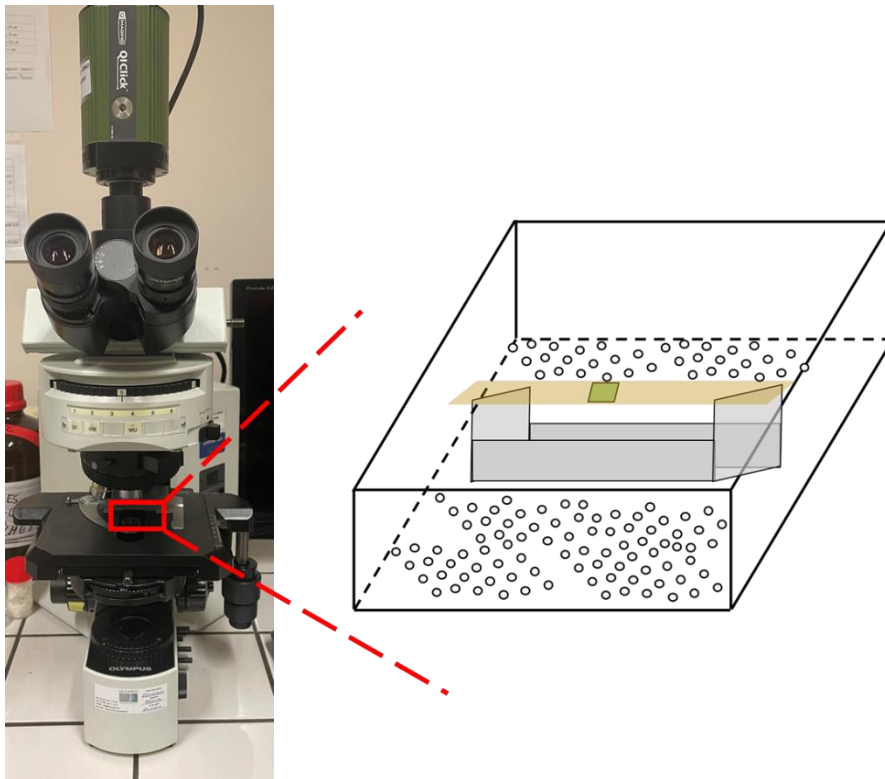


Figure 24: Droplet top view setup. Zeolites (circle shape) were put on the bottom of the box, the support (grey rectangle) was used to provide droplet pendant configuration. PDMS substrate (green square) and glass slide (yellow rectangle) were used to hold droplets.

3.2.4.2. OBSERVATION STRATEGY

After the cleaning procedure already described for the profile view tests, droplets were deposited on the PDMS substrate in pendant configuration, then quickly moved into the glass box under the microscope. After adjusting the focus in the region in proximity to droplet borders, *i.e.* the triple line, the droplet shape evolution was observed with an objective (x4) in bright field and phase contrast. The droplet drying was recorded by a QIClick Digital CCD Camera (fps = 1 s) until the occurrence of border delamination (bright double ring in **Figure 25**), that characterizes the end of the drying process. In particular, the formation and the development of the gelled foot were observed as a function of time. Indeed, contrary to the profile observation, the top view favored the measurement of the foot final width (W_f), consisting of the external ring (often detached at the end of the drying process) and of an internal portion adjacent to droplet skin. This quantitative analysis was performed at least 3 times for each WPI/ NPC sample.

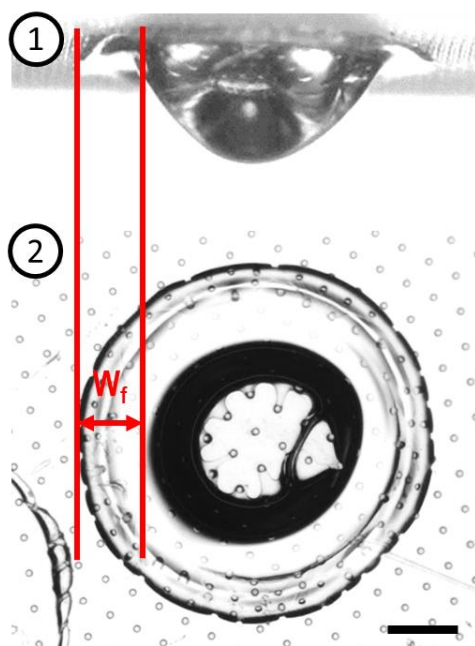


Figure 25. Profile (①) and top (②) view of a WPI particle; W_f refers to the foot width. Scale bar is 200 μm .

3.2.5. DROPLET EVAPORATION RATE MEASUREMENT

The droplet mass measurement device is presented in **Figure 26**. First, the mass of the support and PDMS substrate was tared. Then, a 0.5 μL droplet was deposited on the PDMS and the support was quickly moved into the measurement chamber, in which zeolites controlled the humidity of the

ambient air. The droplet weight (m) was measured using an ultra-micro balance (XP2U, Mettler Toledo) every 5 seconds during the drying process. The droplet's overall drying time (t_{dry}) was defined as the droplet mass kept constant for 15 seconds. In this measurement, the accuracy of a microbalance is $0.1 \mu\text{g}$. The mass loss ($-dm/dt$) was calculated the mass data in order to extract the droplet drying kinetics. The same drying condition as profile observation were used for mass measurements. Experiments were repeated from 8 to 10 times for each WPI/NPC dispersion.

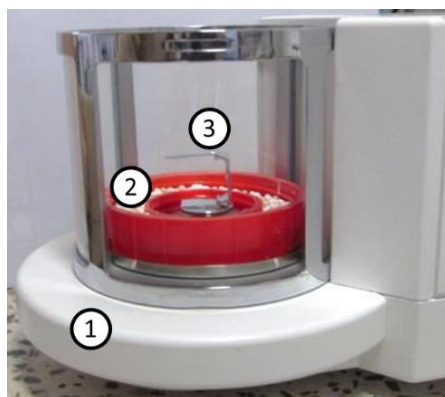


Figure 26 . Droplet mass measurement device, ①micro-balance, ②zeolites, ③ support

3.2.6. PARTICLE SECTION STRUCTURE AND SHELL THICKNESS

After drying, the droplets were cut into two pieces using a small scalpel and moved on conductive tape. In order to have a good view of particle image, the position and direction of particle were controlled, as illustrated in **Figure 27 a**. Then, the sample and substrate were coated with gold/palladium for 5 min and observed by scanning electron microscopy (SEM) at 5 to 10 kV (model 6301, JEOL). The particle section structure and the skin thickness (δ_s) were observed by adjusting the magnification (**Figure 27 b**). At least 5 droplets were investigated for each WPI/NPC dispersion.

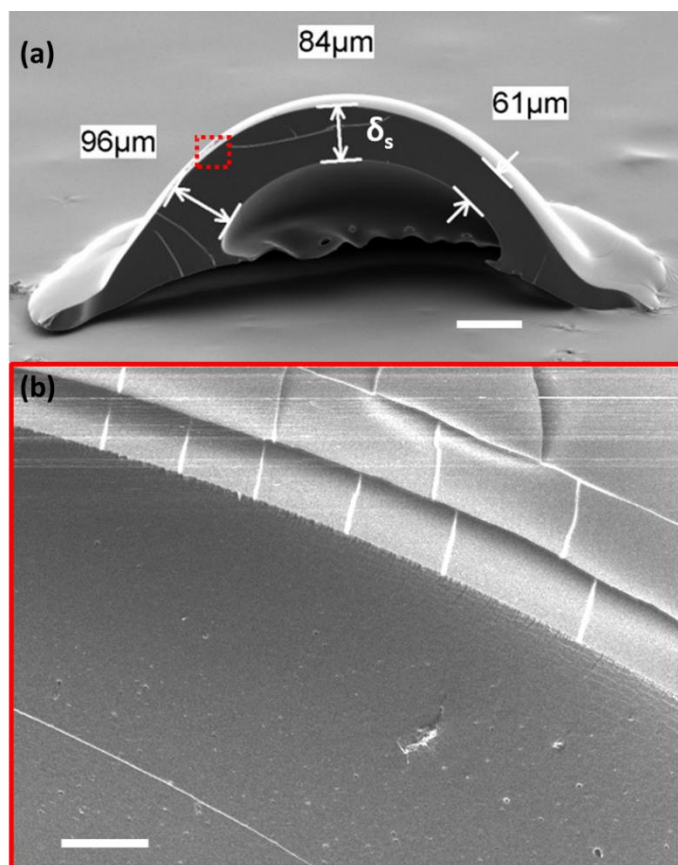


Figure 27 . Image of a dry droplet obtained by SEM. (a) Half particle deposited on the conductive tape, δ_s is the shell thickness of particle. (b) Zoom of the skin section structure. The scale bar of (a) and (b) is 100 μm and 10 μm , respectively.

3.3. DROPLET INTERFACIAL PROPERTIES

A pendant drop tensiometer (Tracker, Teclis-Scientific, France) was used to study both the evolution of the surface tension(γ) and the viscoelastic, elastic and viscous moduli in WPI/NPC mixes with different WPI%_R.

3.3.1. SURFACE TENSION MEASUREMENT

Surface tension (γ) was deduced from evaluating pendant droplet profile shape and evolution. In our experiment, a droplet with an initial volume of 8 μL was extruded from a syringe tip, and a camera captured its profile. The droplet curvature radii and polar angle of the tangent were calculated by a software (Tracker), based on droplet shape. Further, the surface tension was calculated by combination of the Laplace-Young equation and the equation based on the force equilibrium across any horizontal plane. In our tests, the dynamic surface tension was monitored from the first instants after droplet generation to the achievement of an equilibrium stage due to the adsorption of protein on the surface. For each sample, we repeated this protocol at least 5 times.

3.3.2. OPTIMIZATION OF EXPERIMENTAL PARAMETERS FOR DROPLET DILATION TESTS

Droplet dilation tests followed the surface tension measurements since it was likely to predict the formation of a protein layer adsorbed on the droplet surface. We provided an external force to expand and compress the droplet (**Figure 28 a**) and we evaluated simultaneously the mechanical response of the interface, which strictly depended on its organization at the molecular scale. Two parameters were tuned in this kind of experiments, the frequency and the strain amplitude. The frequency was defined as the time needed for one complete cycle of compression and expansion. The strain amplitude referred to the volume difference related to droplet expansion or contraction. Here, the volume variation was estimated by the surface variation since the drops were observed in a profile view. It should be noticed that short frequency leads to rapid droplet dilation. Therefore, protein molecules do not have enough time to migrate towards droplet surface and, subsequently, to self-arrange in any specific structure. This means that surface properties do not evolve. On the other hand, too high strain amplitude result in the breaking of the surface molecular layer. In other words, the frequency and the strain amplitude affect the dilation process and, mostly, the viscoelastic response of the drop surface. Therefore, it was necessary to optimize the choice of these two key parameters in order to explore the droplet interfacial rheological properties. Different frequency and strain amplitudes were tested in these preliminary experiments (**Figure 28 b**). As it concerns the strain amplitude percentage, which has been quantified by measuring the relative area ratio (A/A_0), the control and repeatability of the oscillations were affected by the intrinsic accuracy error of the experimental setup. To summarize, first a frequency was chosen (e.g., 20 s), whereas the interfacial rheology was investigated at different strain amplitude percentage (6.25%, 12.5%, 25%, 37.5%). Then we fixed the amplitude percentage (e.g., 12.5%) and we verified the impact of the frequency (10, 15, 20, and 30 s). The duration of droplet oscillatory tests was 5 mins. The outcomes regarding the real part (E_r) and the imaginary part (E_i) of the viscoelastic modulus (E), summarized in **Figure 29**, allowed to select the optimal coupled amplitude and period time for the oscillatory process in case of WPI/NPC mixes. For each sample, the measurements were repeated at least 3 times.

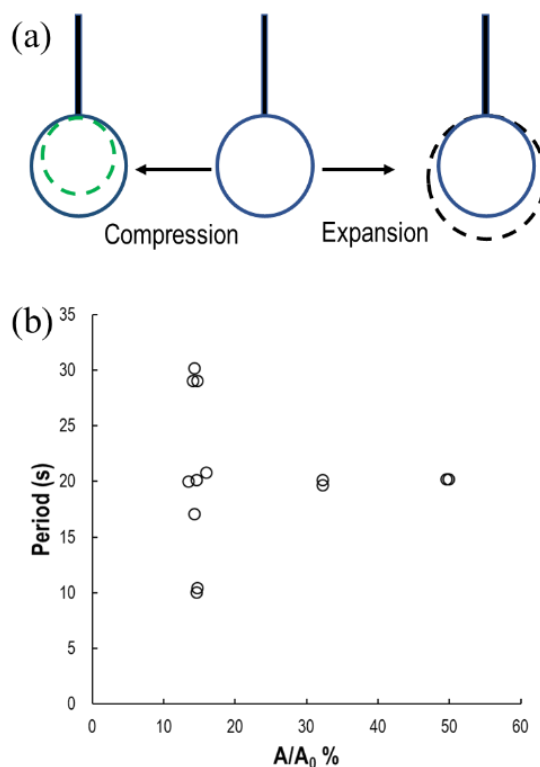


Figure 28. (a) droplet oscillatory process: a droplet (blue circle) first compresses to a smaller volume (green dash circle) and recovers to its initial one, then expands into a big drop (black dash circle). (b) Preliminary oscillatory test of droplets with different frequencies and strain amplitude percentages. The droplet area difference of big and small is defined as A , the initial droplet area is A_0 .

As it concerns the tests at fixed strain amplitude percentage (12.5%), we observed that E exhibits an evident decreasing tendency with higher $WPI\%_R$ when the period changes from 5 s to 20 s. In contrast, the E kept almost constant when the surface area modification induced by the oscillation was slow enough (≥ 20 s), possibly because protein molecules have enough time to move to drops surface and arrange into a stable interface. On the other hand, the variation of E as a function of the amplitude for fixed period (20 s) highlighted that the viscoelastic behavior of droplet interface was not affected by A/A_0 . In other words, no matter how much surface area changed, a stable interface was formed when molecules had enough time to adsorb and re-organize at the drop interface. For the evaluation of the interfacial rheology evolution with time in WPI/NPC mixes, the real part (E_r), imaginary part (E_i) and the viscoelastic modulus (E) were monitored for 1 hour in droplets oscillating at fixed period (30 s) and amplitude percentage (12.5%), i.e. in correspondence of a probable stable interface layer in terms of structure organization.

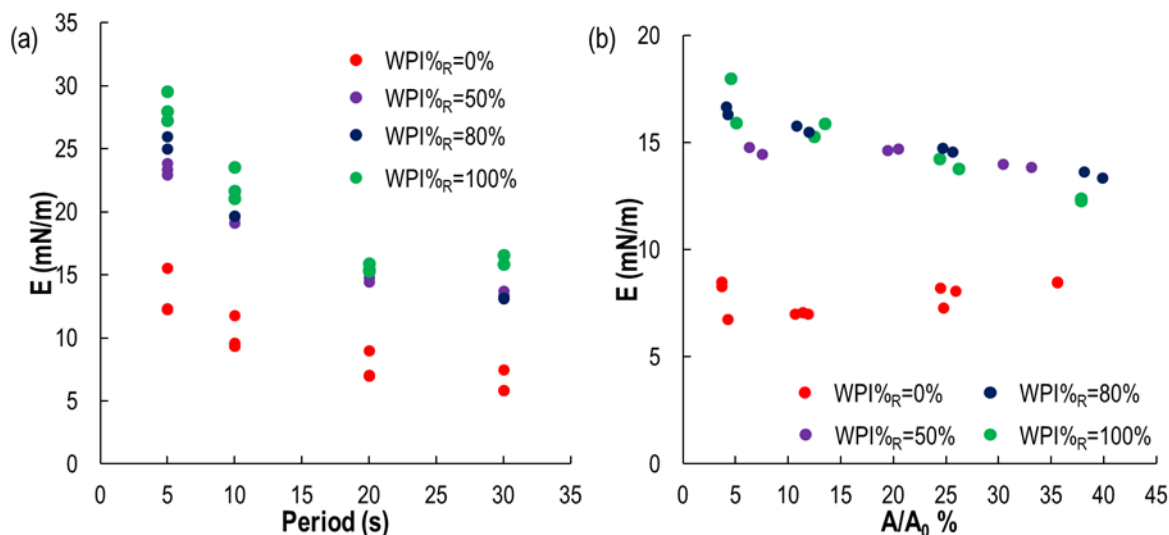


Figure 29. Viscoelastic modulus (E) of WPI/NPC particle variation with frequency when we fix the strain amplitude percentage at 12.5% (a); we fixed the frequency at 20 s, the E changing as function of amplitude percentage(b).

3.4. MONODISPERSE SPRAY DRYING PROCESS

A simple sketch of a monodisperse spray dryer is presented in **Figure 30**. It can be divided into three parts: dispersed droplet generator, spray drying chamber and powder collection plate. Before experiments, the drying chamber was pre-heated for 1 hour at the target drying temperature to obtain a stable drying environment. Before feeding, vacuum filtering was adopted to avoid the protein aggregates or bigger impurities in the solution. An applied pressure allowed to feed the sample at constant flow rate through the nozzle (diameter: 100 μm). The stream liquid line was fractioned into droplets with homogeneous size (monodispersed droplets) by a piezo-electric transducer. The droplet size was controlled by adjusting the wave vibration frequency through an oscillometer. Subsequently, the droplets were fully dispersed by compressed air into the drying chamber to avoid contact and potential merging. The droplets were exposed to hot air flow and underwent fast mass and energy transfer (4-5 s), leading to similar shrinkage and to final monodispersed particles: This is the advantage of this equipment, insofar as each of the particles obtained is strictly comparable to the others not only in terms of drying history, but also in terms of dimensions and morphological characteristics. Finally, the dried powder was collected under the drying chamber. The parameters chosen for the drying of WPI/NPC mixes are shown in **Table 10**.

Table 10. Monodispersed drying conditions.

	Frequency (kHz)	Feeding pressure (kg/cm ³)	Disperse air (L/min)	Chamber temperature (°C)	Inlet temperature (°C)	Outlet temperature (°C)	Air velocity (L/min)
Parameter value	12	0.4	10	270	217±5	89±5	225

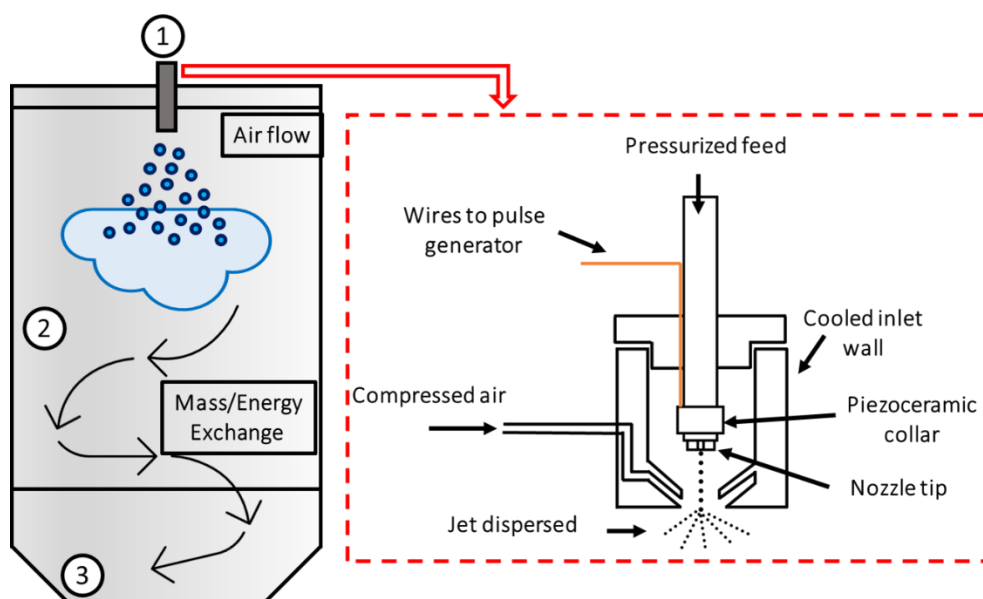


Figure 30. Monodisperse spray dryer sketch. ① droplet generator with the detail components are shown in red rectangle, ② drying chamber and ③ the collection plate.

3.4.1. ANALYZING POWDER’S SHAPE FACTORS

After spray drying, the main shape characteristics of the collected powders were analyzed by characterizing their area (A), circularity and solidity. Circularity ($C_{ir} = \sqrt{\frac{4\pi A}{\text{perimeter}^2}}$) is a shape factor to describe the powder particle’s shape. C_{ir} is defined as the degree to which the particle is similar to a circle. For example, if C_{ir} infinitely approaches 1, it means that powder shape is round (Figure 31 A). Solidity (S) is the measurement of the overall concavity of a particle, and it is defined as the image area divided by the convex hull area. The more S approaches to 1, the smoother the particles (Figure 31 B). The measurement of particle area could help us to estimate the powder size distribution. Firstly, dried powders were scattered on the glass slide, then images were acquired by optical microscope in bright

field. In order to ensure the accuracy of the result, more than 200 particles for each WPI/NPC dispersion were investigated. The dry particle images were analyzed by ImageJ software, using in particular the Analyze Particles function to obtain the circularity and solidity values.

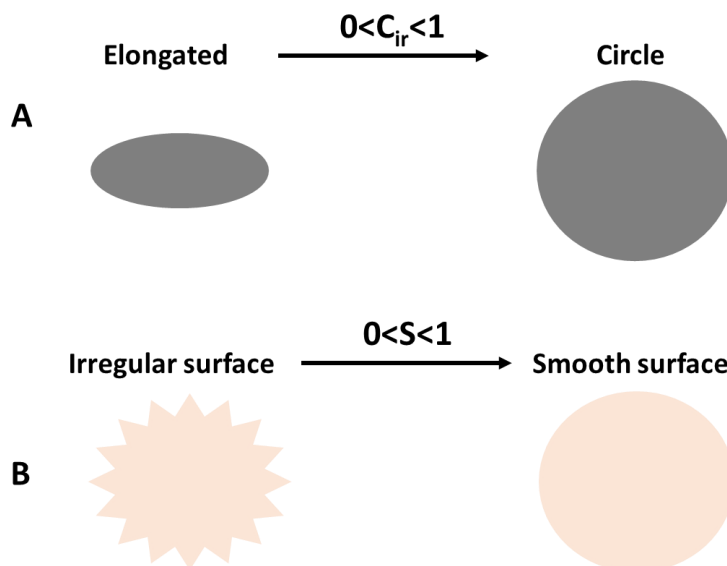


Figure 31. Various shapes at different circularity (A) and solidity (B).

3.5. GLASS FILAMENT DRYING EXPERIMENTS

In this single droplet drying experiment, the droplet diameter, mass and drying temperature at different drying conditions were measured. The drying parameters are presented in **Table 11**. The sketch of the single droplet drying setup (Soochow University, China) is shown in **Figure 32**. An air-compressor was used to compress air to dehumidify the drying-tower (40x50x60 cm). Then the dried air was stored in a gas tank to ensure a stable airflow during drying process. The drying temperature was governed by an electric heater and the temperature controlling system. In order to keep a stable drying environment, the drying chamber was preheated for 1 h at the target temperature. Droplet drying history was recorded by a high-speed camera (3.5.2). The temperature, diameter and weight of droplet during the drying process were measured by three different glass filament modules.

Table 11. Drying parameters of NPC droplet

Air flow	Temperature	70°C, 90°C, 110°C
	Velocity	0.75 m.s ⁻¹
	Moisture content	0.0001 kg water / kg dry air
Droplet	Solute	NPC
	Initial concentration	10 w / w %

3.5.1. DIAMETER MEASUREMENT

A syringe was used to produce a 2 μ L droplet. A transfer glass filament was used to suspend the droplet on the glass knob of the diameter measurement module. The camera recorded the droplet drying process. In order to analyze diameter evolution during the drying process, the videos (fps=1) were converted into images by the Adobe After Effects CS4 software. The real diameter of glass knob was measured by a light microscope. The software ImageJ was used to measure real area of droplet, using the area of the glass knob as a reference. It was assumed that, during the drying process, a drying droplet kept a spherical shape. The diameter evolution of the droplets was then given by the circle area equation.

3.5.2. MASS MEASUREMENT

The droplet weight was measured by a flexible glass filament with a marker (mass measurement module). The initial position of mark of a standard sample was first observed in the hot air. When suspended on the tip of this module, a new marker position was captured by the camera. The difference between these two positions (variation of deflection of the glass filament) was interpreted as the mass variation of the droplet. The standard curve was obtained by measuring the displacement of five standard samples with different weights made of plasticine. The mass of droplets was obtained during the drying process by calculating the deviation of the marker from the baseline in the images.

3.5.3. THE TEMPERATURE MEASUREMENT OF DROPLET

The temperature module was similar to the diameter module with a thermocouple placed under the glass knob. The droplet was suspended on the knob by ensuring the thermocouple was correctly placed

right in the center of the droplet. The droplet drying temperature was recorded by a data acquisition software connected to a thermocouple with the help of a Pico-logger.

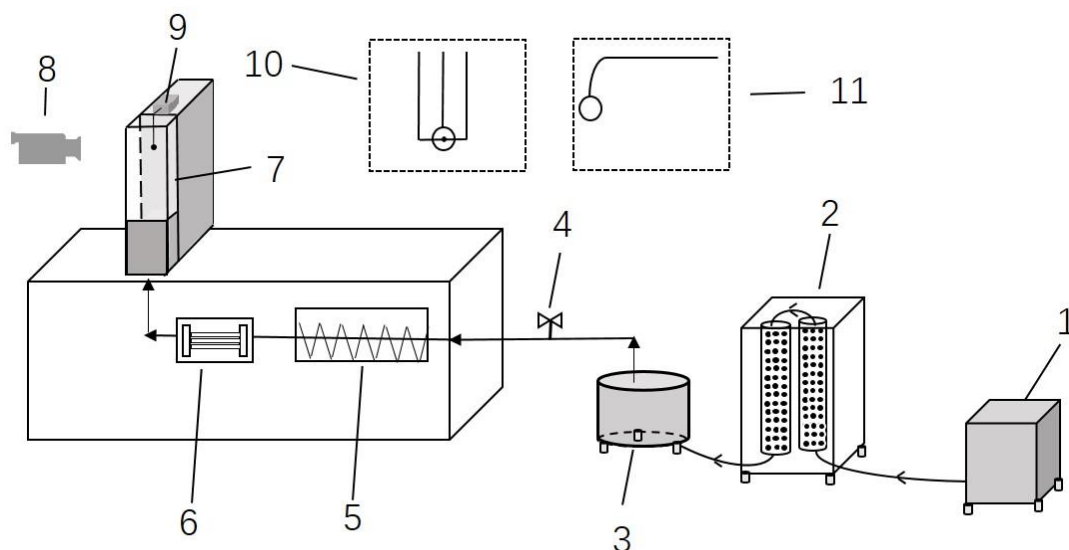


Figure 32. Schematic of single droplet drying setup: 1. Air-pressure controller. 2. Drying tower. 3. Air storage tank. 4. Flow regulator. 5. Heater. 6. Temperature controller of drying air flow. 7. Drying chamber. 8. High-speed camera. 9. Droplet suspension module for droplet diameter measurement. 10. Temperature measuring glass filament. 11. Weight measuring glass filament.

Chapter 4. RESULTS AND DISCUSSION

4.1. SKIN LAYER FORMATION IN DRYING DROPLET OF DAIRY PROTEIN MIXES

4.1.1. INTRODUCTION

As mentioned in Chapter 1, the skin development in the course of drying colloidal systems is essentially due to the competition between evaporation and diffusive Brownian motion. When the surface receding induced by evaporation overcomes the molecule diffusion, the solutes tend to locate at the surface and trigger the sol-gel transition once a solute critical concentration is locally achieved (Fortini et al., 2016; Le Floch-Fouéré et al., 2019). At the end of the evaporation process, the surface of dry samples can display different morphologies depending on solute properties and overall concentration. Indeed, the observation of highly deformed skin (*i.e.* buckling) (Brutin et al., 2012), or conversely of rigid compact external shell (often at the origin of border delamination) (Sadek et al., 2013; Sobac & Brutin, 2014), as well as the formation of cracks (Pauchard et al., 2009; Sibrant & Pauchard, 2017; Sobac & Brutin, 2014), can be considered as a signature of the dynamics occurring at the molecular scale. Thus, shedding light on drying-induced interface mechanisms in solution is clearly valuable to predict macroscopic sample characteristics, such as shape, mechanical response, and, in the case of biological samples, functional properties. At the same time, understanding the physics of skin formation still represents a scientific challenge, especially when investigating complex systems (*e.g.* biological fluids and industrial systems) whose multicomponent can differ by size, structure, and charge.

Most of the experimental works were performed on model colloids, well calibrated, to take advantage of the full characterization of their physico-chemical properties (*e.g.* latex and silica beads) (Koga & Inasawa, 2019). In the case of colloidal binary dispersions, the open question is to understand the impact of particle characteristics and interaction on the deposit and re-arrangement in the vicinity of the air-liquid interface (Schulz & Keddie, 2018). To this purpose, both experimental and theoretical works have been recently conducted on model particles differing merely by size (Fortini et al., 2016; Howard et al., 2017; Makepeace et al., 2017; Sear & Warren, 2017; Trueman, Lago Domingues, Emmett, Murray, Keddie, et al., 2012; Trueman, Lago Domingues, Emmett, Murray, & Routh, 2012). As it concerns the drying of droplets, experiments performed on super hydrophobic substrates (Rastogi et al., 2008) or by acoustic levitation (Raju et al., 2018) suggested the enrichment of small particles on the external region of the shell by evaluating surface mechanical behavior. However, although quite innovative, these studies did not aim at exploring the possible mechanisms of segregation. In this regard, the work of Liu *et al.* of 2019 (W. Liu et al., 2019) is a precious exception. Here, the authors

investigated the mechanisms governing the development of interface structure in drying droplets of bidisperse suspensions by experiments and simulations. Their outcomes revealed that surface self-organization, ranging from random packing to selective stratification of small colloids on the top layer, depends on experimental conditions (*i.e.* evaporation rate (Trueman, Lago Domingues, Emmett, Murray, Keddie, et al., 2012; Trueman, Lago Domingues, Emmett, Murray, & Routh, 2012) and solute properties (size, concentration). Similar scenarios have been observed in thin films, leading to the deduction of increasingly complex predictive models (Fortini et al., 2016; Makepeace et al., 2017; Sear & Warren, 2017; Zhou et al., 2017) of which more accurate analysis will be provided in the following sections. In general, stratification by size has been associated with colloid cross-interactions driven by osmotic pressure (Fortini et al., 2016; Zhou et al., 2017) and, more recently, to the motion in the direction opposite to the surface induced by local particle concentration gradients at the surface (Sear & Warren, 2017). However, due to the multiple crucial parameters involved, these mechanisms have not been fully clarified and need further thorough experimental verification.

In order to understand how the composition of protein suspensions impacts skin layer formation, evolution and final properties, we investigated the evaporation process in pendant droplets consisting of glaring examples of biocolloids, *i.e.* two of the most represented proteins in milk: the whey proteins (in the form of whey protein isolates, WPI) and the caseins (in the form of micellar native phosphocaseinates, NPC). As mentioned in Chapter 1, WPI macromolecules exhibit a globular shape (average size, $d_{\text{WPI}} \approx 10\text{-}20\text{nm}$) (Yano, 2012), whereas NPC are typical sponge-like micelles ($d_{\text{NPC}} = 100\text{-}300\text{nm}$) (Bouchoux et al., 2010). We focused on observing the main drying-induced morphological changes occurring in WPI/NPC mixes in order to extract a possible link between surface colloid organization at the molecular scale and skin rheology evolution. Preliminary studies have been performed on mixes of dairy proteins, revealing WPI over-representation on the top shell layer and, thus, possible stratification (Lanotte et al., 2018).

To verify this hypothesis and its impact on droplet morphology, we propose here a systematic investigation of skin mechanical behavior during the evaporation. We first present a global overview of the drying process in WPI/NPC mixes by droplet profile observation and mass measurements (4.1.3.1). Afterwards, we evaluate surface mechanical properties from shape characteristics and drying characteristic times as a function of the composition of the mixes (4.1.3.2 – 4.1.3.4). Mostly, we provide a direct observation of dry section structure highlighting the clues of possible protein segregation in the skin. We corroborate our findings in the light of previous works on bi-dispersed colloid dispersions, underlining the good agreement with theoretical models in the literature. Finally, we provide further evidence of preferential segregation in WPI/NPC mixes performing tests of

interfacial rheology by the oscillatory drop method (4.1.3.5). These results have been published in *Colloids and Surface A* (Coll Surf A 620, 2021, article 126560). In order to further test the soundness of the hypotheses formulated, additional experiments were carried out on mixtures of WPI and sodium caseinate (SC), in order to identify the contribution of the size of the colloids on the one hand, and their specific properties on the other hand (4.1.4). Indeed, sodium caseinate have a comparable size to that of WPI, being heard that they are composed of casein as for NPC.

4.1.2. EXPERIMENT STRATEGIES

The experimental activity focused on the drying mechanisms in droplets of WPI/NPC mixes with overall protein concentration equal to 8 w / w % and WPI relative percentage (WPI%_R) of 0, 20, 50, 80, 100%. This concentration was chosen in order to maximize the observation of the drying-induced effects on droplet morphology (*i.e.*, diameter reduction, skin deformation).

A single droplet drying approach (see Chapter 3 for the detailed description) was used to explore the droplet profile evolution and drying kinetics during the drying process. This favored the understanding of how WPI relative percentage impacts particle shape, skin layer structure and properties. The dried particle shape and the section structure were further studied by scanning electronic microscopy (SEM) to shed light on the possible organization of WPI and NPC macromolecules in the skin layer. Furthermore, the WPI and NPC adsorption and self-organization at droplet air-liquid interface induced by ageing phenomena was explored by a drop tensiometer. Experiment condition, parameters and measurement protocols were introduced in the previous chapter.

4.1.3. RESULTS AND DISCUSSION

4.1.3.1. MORPHOLOGICAL EVOLUTION OF WPI/NPC DROPLETS

A summary of the drying process in WPI/NPC mixes is presented in **Figure 33**, where the image sequences illustrate the morphological changes occurring in droplets with different WPI%_R throughout the evaporation. This qualitative overview allowed detecting the three main stages of the process, in agreement with previous works in the literature (Lanotte et al., 2018; Sadek et al., 2013, 2016).

1) At the beginning, all droplets showed similar contact angle ($\theta_0 \approx 105^\circ$) due to the hydrophobic properties of the PDMS support. The Bond number (Bo ; Eq. 2) was estimated ≈ 0.08 for all mixes, thus excluding possible gravity-induced deformations. During the first drying stage (referred to as 1 in **Figure 33**), the droplets were characterized by the loss of the nearly spherical geometry and the gradual shrinkage induced by solvent evaporation. As it concerns the bulk, the initial protein volume fraction (ϕ_p) was strongly depending on WPI%_R. Taking into account WPI and NPC voluminosity, which

is equal to 0.74 ml.mg^{-1} (Mylonas, E., 2007) and 4.4 ml.mg^{-1} (Bouchoux, A., 2009) respectively, we estimated that ϕ_p ranged from a minimum of $\phi_{\text{WPI}}=0.06$ for $\text{WPI}\%_{\text{R}}=100\%$ to a maximum of $\phi_p=0.27$ for $\text{WPI}\%_{\text{R}}=0\%$ (Table 12). Therefore, in this first part of the evaporation process, the suspensions were diluted enough to consider protein macromolecules as “hard spheres” with no significant interactions, except in the vicinity of the air-liquid interface (Bouchoux, Cayemitte, et al., 2009). Indeed, the progressive volume reduction possibly favored colloid accumulation at the air-liquid interface as a result of the competition between the receding of the evaporation front and diffusive motions. To verify such hypothesis, we calculated the Péclet number (Pe ; Eq. 7) at the initial conditions for both WPI and NPC and we obtained $Pe_{\text{WPI}}=6$ and $Pe_{\text{NPC}}=100$. This means that, under these experimental conditions, the evaporation prevails on diffusion and the formation of an interfacial colloidal layer is predictable.

Table 12. Overall protein volume fraction (ϕ_p), WPI volume fraction (ϕ_{WPI}), and average surface tension (γ) at the equilibrium in WPI/NPC droplets as a function of $\text{WPI}\%_{\text{R}}$.

$\text{WPI}\%_{\text{R}}$	0%	20%	50%	80%	100%
ϕ_p	0.27	0.24	0.18	0.11	0.06
ϕ_{WPI}	-	0.01	0.03	0.05	0.06
$\gamma(\text{mN.m}^{-1})$	48.4 ± 0.1	48 ± 0.5	49 ± 0.5	48.6 ± 0.4	49.8 ± 1

2) The second stage of the drying process was marked by the evidence of sol-gel transition at droplet surface. First, the decrease of the contact angle (θ) induced by volume shrinkage led to the onset of capillary flows with increasing intensity once $\theta < 90^\circ$. This kind of internal motion has been largely observed in colloidal dispersions (e.g. coffee ring effect) and results in the continuous transport of the solute towards droplet triple line, where the evaporation rate is maximal (Bouchoux, Debbou, et al., 2009; Deegan, 2000). In the present work, the external segregation of WPI and NPC macromolecules resulted in the formation of a gelled “foot” conferring a sort of Mexican cap shape to the droplets (see first two columns of the stage 2 in Figure 33 for the different $\text{WPI}\%_{\text{R}}$). It is worth emphasizing that up to this point in the process all WPI/NPC droplets displayed qualitatively the same behavior irrespective of $\text{WPI}\%_{\text{R}}$ and, mostly, no evidence of skin formation nor of its impact on the evaporation process was observed. It is only at the end of the Stage 2, i.e. when the sol-gel transition was advanced, that the signs of surface gelation became glaring, resulting in two main morphology categories depending on

WPI%_R. For WPI%_R ≤ 20%, the droplets underwent a typical buckling process with slight diameter reduction, whereas, for WPI%_R ≥ 50%, they exhibited a round smooth surface and evident border detachment from the substrate (*i.e.* delamination).

3) During the last stage of the evaporation process (referred to as 3 in **Figure 33**), no shape modifications were observed. The evaporation of the remaining water did not affect the diversification into two shape categories mainly distinguished by buckling (blue frame) and convex smooth surface (red frame) respectively, and it was accompanied by the formation or the definitive development of a vacuole in the nearly solid droplets. The different appearance of the two morphology types is not an unusual outcome. In fact, wrinkled (*e.g.* NPC) and Mexican cap shapes (*e.g.* WPI) have been often observed in previous works on model colloidal systems and in biological samples, depending on solute concentration, solvent composition, and experimental conditions (T, RH) (Pauchard & Allain, 2003). Buckling phenomena are secondary level instabilities occurring when droplet skin does not withstand the increasing inward pressure developing during the drying. Therefore, our observations suggest that WPI physico-chemical properties can confer a higher rigidity to the interface even in the simultaneous presence of NPC. Such enhanced robustness could depend not exclusively on colloid properties, but also on skin structural characteristics. In a previous work, for example, Head suggests that dry shells with homogeneous thickness do not undergo buckling instabilities (Head, 2006). In this light, the outcomes of Sadek *et al.* (Sadek *et al.*, 2013) on the drying of WPI droplets experimentally corroborate this theory, since samples exhibited an almost constant thickness from the base to the apex height for different protein concentrations.

The qualitative picture presented in **Figure 33** provides two points of reflection:

- The drying dynamics in WPI/NPC mixes are strongly affected by sample composition (WPI%_R), resulting in a shape transition occurring at a critical WPI relative concentration (WPI%_{RC}) found between for 20% and 50%. The marked differences between the two observed morphologies possibly suggest a competitive separate role played by the two components on the drying process.
- WPI colloids have a significant impact on evaporation process and interface rheological properties. Indeed, despite being always the minor component in the mixes in terms of volume fraction (*e.g.*, in mixes with WPI%_R = 50%, $\phi_{WPI} = 0.03$ compared to overall $\phi_p = 0.18$), whey proteins govern droplet final shape if sufficiently represented in the system (WPI%_R ≥ 50%).

Starting from these preliminary conclusions, it would be important to understand if the dynamics leading to skin formation in drying WPI/NPC droplets, and consequently the evolution of surface mechanical properties, merely depend on colloid concentration in the sample or if there is any further impact due to a specific organization of WPI and NPC at the air-liquid interface.

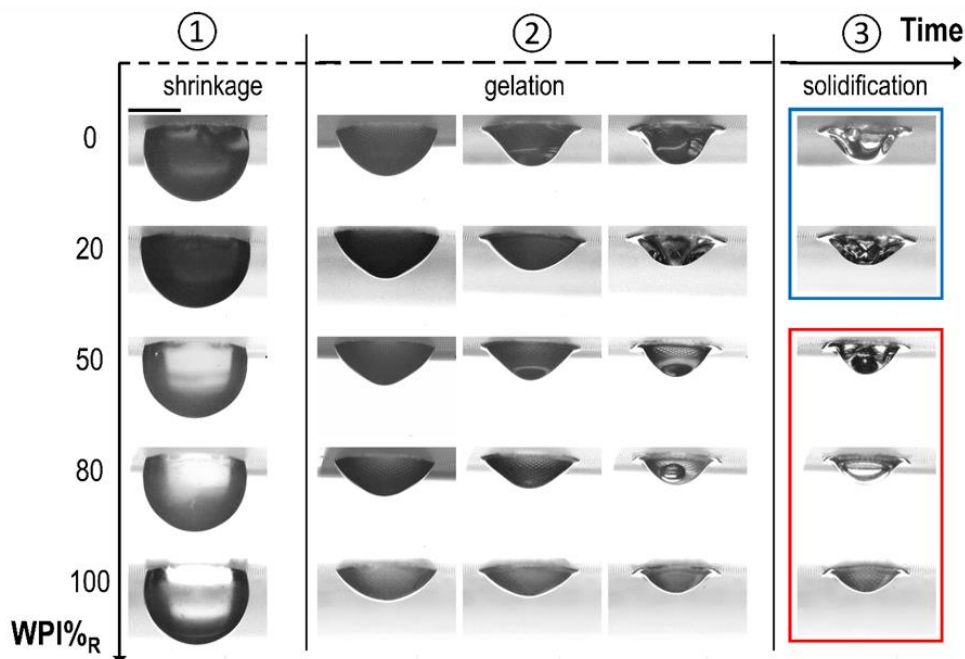


Figure 33. Morphological evolution of WPI/NPC droplets during the evaporation process as a function of WPI%_R. The image sequences are intended only to summarize the main drying-induced shape changes, without providing a quantitative comparison between the duration of the different stages. The scale bar is equal to 500 μm .

4.1.3.2. DRYING KINETICS

The evaporation rate was monitored in all WPI/NPC mixes to investigate the link between droplet morphology evolution and drying kinetics. In **Figure 34**, the mass loss with time ($-\text{dm}/\text{dt}$) is displayed for single protein suspensions, *i.e.* WPI (WPI%_R=100%) and NPC (WPI%_R=0%), and for a mix with WPI%_R=50%. Compared to profile visualization in **Figure 33**, which is limited by the difficulty of detecting early evidence of skin gelation, the evaluation of the kinetics allowed a better characterization of the duration of the different steps of the drying process. After an initial instability following droplet deposition on the substrate ($t \leq 1$ min, light yellow rectangle), the Stage 1, characterized by droplet shrinkage, here corresponded to a slightly decreasing evaporation rate with time. Afterwards, compatibly with the progress of the sol-gel transition at droplet surface, a typical falling drying rate was observed (Stage 2). At the end of this phase, when no significant shape changes were observed, the evaporation rate went rapidly to zero (Stage 3). Upon a first examination, the curves in **Figure 34** point out, on the one hand, the evident difference between NPC and WPI behaviors and, on the other, the drying kinetics curve of WPI%_R=50% close to WPI result. In fact, NPC droplets exhibited an earlier falling drying stage and a retarded achievement of the plateau at the end of the evaporation compared to the other samples. This behavior is further highlighted in the inset of **Figure**

34, where the overall drying time (t_{dry} , black triangles, see the Materials and Methods section for the definition) and the half-life drying time ($t_{1/2}$, blue stars) are displayed as a function of $WPI\%_R$. NPC dispersions were characterized by lower $t_{1/2}$ (*i.e.* earlier sol-gel transition) and longer t_{dry} than WPI-rich samples ($WPI\%_R \geq 50\%$). The earlier occurrence of surface gelation in NPC dispersions has been already experimentally documented in the literature, using both single droplet (C. Sadek, 2016) and confined geometry approaches (C. Sadek, 2015). Such behavior resulted in a lower critical mass concentration required to trigger interfacial sol-gel transition in NPC (16 w/w.%) than in WPI samples (41 w/w.%) (C. Sadek, 2013). The origin of such evident difference can be plausibly attributed to three main factors: i) the higher ϕ_p in NPC dispersions, despite the same fixed mass concentration, ii) the NPC micellar open structure, which is a glaring example of biological microgel retaining water, and iii) $Pe_{NPC} \gg Pe_{WPI}$. In a few words, the abundant presence of casein micelles in the bulk suspension and their physico-chemical and structural properties favor the accumulation at droplet air-liquid interface and the formation of a concentrated layer with high water affinity. If on the one hand, the significant propensity of NPC colloids to foster the formation of a gelled interface finds a solid explanation even in the light of previous works, on the other, the detection of a longer drying time in NPC droplets than in WPI ones may appear striking. Indeed, one could predict that, due to their rigid globular structure, WPI colloids contribute to the development of a compact skin, whereas irregular and deformable NPC micelles would self-organize in a sparse porous structure. Consequently, a highly packed WPI-rich skin, similar to the case of monodisperse colloidal spheres, should represent a higher “resistance” to water evaporation than a sparse NPC surface layer. However, this simplistic, but plausible, point of view neglects some fundamental mechanisms characterizing the interface evolution in NPC suspensions. In a series of works on the rheology of casein micelle dispersions under osmotic stress, Bouchoux *et al.* (Bouchoux, Cayemite, et al., 2009; Bouchoux, Debbou, et al., 2009; Bouchoux et al., 2010) showed that NPC phase characteristics significantly evolve with increasing concentrations. They pointed out that above a specific concentration, comparable to mentioned values related to sol-gel transition in droplets, NPCs organize in a highly packed structure (packing factor ≈ 0.78 higher than in monodisperse hard-sphere fluids). Such a dense arrangement is mainly affected by the polydispersity of average NPC size. The further increase of sample concentration induced by higher osmotic pressures implicates also micelle squeezing and inter-micellar bonds leading to the development of a compact gel. The scenario explored by Bouchoux *et al.* is consistent with the physical events occurring at droplet surface during the evaporation process, thus providing a credible interpretation to the longer t_{dry} measured for NPC samples in **Figure 34**.

As regards the analogy of behavior in WPI/NPC mixes with $WPI\%_R \geq 50\%$ (the $WPI\%_R = 80\%$ curve is not illustrated here for the sake of clarity), in agreement with the outcomes of **Figure 33**, it is evident that

the presence of WPI colloids represents a limiting factor in the drying process. The main open question to address lies in understanding how whey protein physico-chemical properties affect skin structure and mechanical response: is it sort of mechanical reinforcement effect due to WPI macromolecules randomly dispersed in the interfacial layer? Or is it related to some spatial colloid stratification? This latter phenomenon has been frequently observed in polydisperse colloidal systems and it consists of the selective segregation of the components into separate layers having specific rheological and mechanical roles. Numerous experimental studies, as effectively summarized by Schulz and Keddie in a review of 2018 (Schulz & Keddie, 2018), highlighted that the surface region is responsible for defining fundamental properties, such as wetting, hardness, and electrical conductivity. For example, Nunes *et al.* (Nunes *et al.*, 2014) detected greater mechanical resistance in auto-stratified colloidal coatings by enriching the surface in hard particles. In our binary system, WPI colloids can be approximated to hard spherical colloids. Moreover, above the threshold value $WPI\%_{Rc}$ ranging between 20% and 50%, they clearly governed shape transition and skin mechanical properties. Therefore, in the next sections of this work we aimed at exploring possible clues of WPI outer accumulation during the evaporation process.

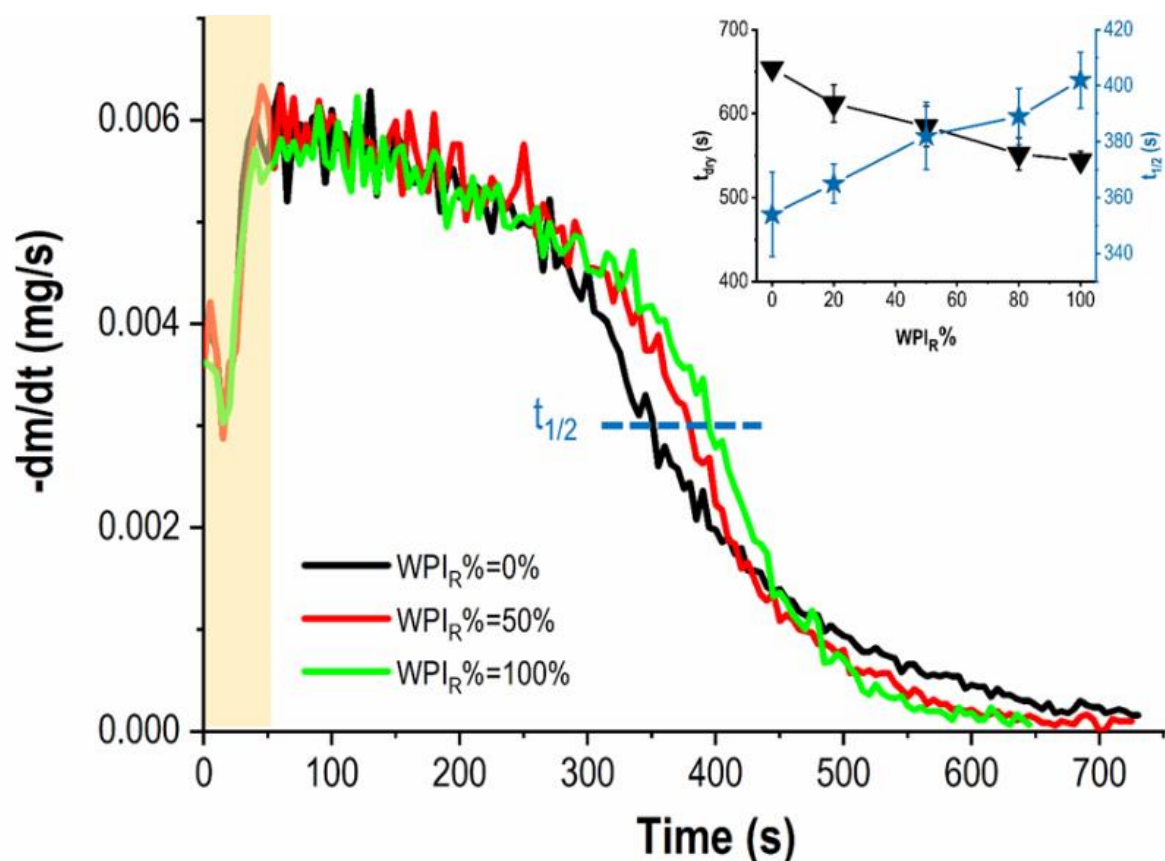


Figure 34: Evolution of the mass loss ($-dm/dt$) with time in WPI/NPC droplets with $WPI\%_R=0\%$, 50% , 100% . In the inset, the black triangles refer to the overall drying time (t_{dry}) and the blue stars to the half-life drying time ($t_{1/2}$) for all the mixes

4.1.3.3. SOL-GEL TRANSITION

To investigate the shape changes in WPI/NPC droplets, we evaluated two main parameters during the evaporation: i) the base diameter, D (*i.e.* the average diameter of the surface adhering to the PDMS substrate), and ii) the apex height, H (*i.e.* the distance from droplet top to substrate). This approach was helpful to characterize sol-gel transition major morphological consequences (Lanotte et al., 2018; Sadek et al., 2013, 2016): skin buckling and border delamination. Such shape modifications occurred in the final part of the Stage 2 (**Figure 33**) and led to the attenuation of H curve slope and, at the same time, to the sudden D reduction (see the curves in the inset of **Figure 35** concerning WPI droplets), with an importance depending on $WPI\%_R$. Indeed, both buckling and delamination represent, in a different way, a reaction to the increasing drying-induced inward pressures and the selective occurrence of either events is related to skin mechanical properties. For $WPI\%_R \leq 20\%$, the abundant NPC amount provided surface deformability, resulting in skin folding. On the other hand, the mixes with $WPI\%_R \geq 50\%$ exhibited such a skin hardness that they resisted to interfacial pressure until stress release by delamination. Here, we defined as Δt_{gel} the gelation time duration corresponding to such significant morphological changes, as illustrated in the inset of **Figure 35**, and we measured its onset and duration as a function of $WPI\%_R$ (purple rectangles in **Figure 35**, values reported in **Table 13**). The dispersions with hard skin and evident delamination ($WPI\%_R \geq 50\%$) exhibited almost identical Δt_{gel} , thus suggesting a similar surface mechanical response to stress even when WPI colloids are minor components in terms of volume fraction. This would corroborate the hypothesis of whey protein accumulation on the external part of droplet surface. On the contrary, the droplets undergoing buckling ($WPI\%_R \leq 20\%$) displayed a longer Δt_{gel} , denoting slower gelation and different rheological behavior. Surprisingly, Δt_{gel} related to mixes with $WPI\%_R = 20\%$ was even longer than in single protein NPC droplets probably due to the impact of the presence of both proteins at the air-liquid interface.

Table 13. Duration of Δt_{gel} and of the final drying of remaining water (Δt_{dry}) as a function of $WPI\%_R$.

$WPI\%_R$	0%	20%	50%	80%	100%
Δt_{gel} (s)	156±27	204±47	114±47	113±27	107±8
Δt_{dry} (s)	130±20	100±39	126±42	76±15	42±11

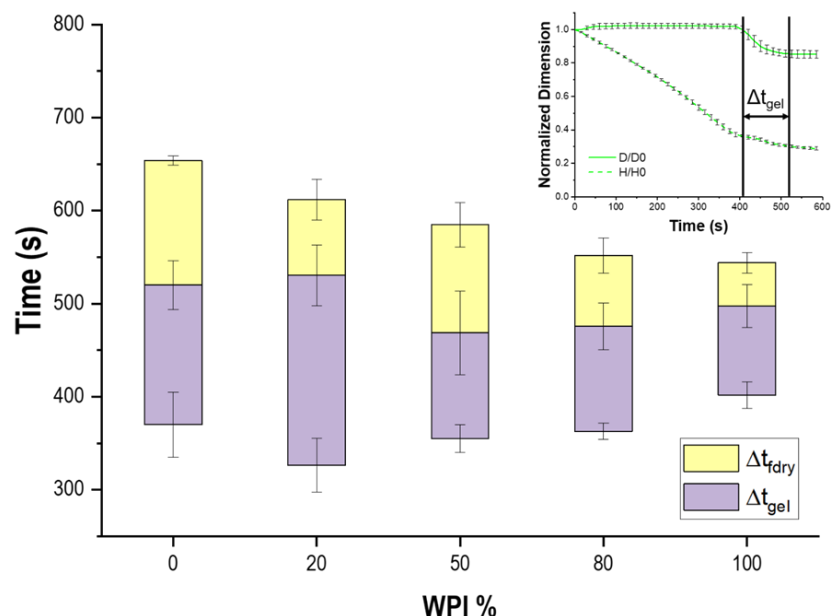


Figure 35. Onset and duration of the buckling stage (Δt_{gel} , purple rectangles), and of the final drying of remaining water (Δt_{dry} , yellow rectangles) as a function of $WPI\%_R$. In the inset, typical curves referring to base diameter (D) and apex height (H) time evolution is presented for WPI suspensions. From these curves, the value of Δt_{gel} has been deduced for all WPI/NPC mixes.

The upper limit of Δt_{gel} corresponded to the achievement of droplet shape invariability for all samples. However, when comparing this value to the overall drying time (t_{dry}) showed in **Figure 35**, it seems evident that the end of gelation events did not reflect the end of the evaporation process. It is likely to predict that, despite skin solidification, some water could be still retained in droplet surface structure. The duration of this further water evaporation (final drying, Δt_{dry}), which provides a quantitative characterization of the Stage 3 in **Figure 33**, was significantly increasing with the amount of casein micelles in the dispersion (see values in **Table 13**). In the case of $WPI\%_R \geq 50\%$, on the one hand droplet shape and skin mechanical behavior suggested WPI segregation on the outer surface region. On the other, the gradual increase of Δt_{dry} with NPC concentration pointed out that casein micelles were, in a certain way, still wet at the end of the process and thus, possibly accumulated in the inner skin layer.

4.1.3.4. STRUCTURE OF DRY DROPLET SECTION

The hypothesis of drying-induced WPI colloid external segregation was further investigated observing the section structure of WPI/NPC dry droplets by SEM. On average, all mixes exhibited similar skin thickness ($\approx 60 \mu m$). Our window of visualization was reduced to the region in the vicinity of the air-liquid interface (white frame in **Figure 36 A**). Starting from the qualitative observation of WPI ($WPI\%_R=100\%$) and NPC ($WPI\%_R=0\%$) peculiarities (e.g. smoothness, porosity), the goal was to address

an eventual protein stratification in mixes with $WPI\%_R=50\%$. Typical WPI droplet dry sections (**Figure 36 B**) displayed a dense, smooth structure, whereas NPC shells (**Figure 36 C**) were characterized by compact regions and sparse empty cells especially in proximity to droplet surface. In fact, the almost monodisperse size and the globular rigid structure of WPI colloids led to the formation of a homogenous, dense skin, as normally observed in hard spheres colloidal dispersions. On the contrary, due to their high polydispersity, deformation and bond development, NPC micelles enhanced significant compaction, but also the formation of pores irregularly dispersed in the shell layer. In mixes with $WPI\%_R=50\%$, both WPI and NPC skin properties were distinguished depending on the distance from the surface (**Figure 36 D**). Indeed, the top layer showed homogeneous compactness and porosity, similar to WPI, but the internal part of the shell exhibited NPC-like irregularities and cavities.

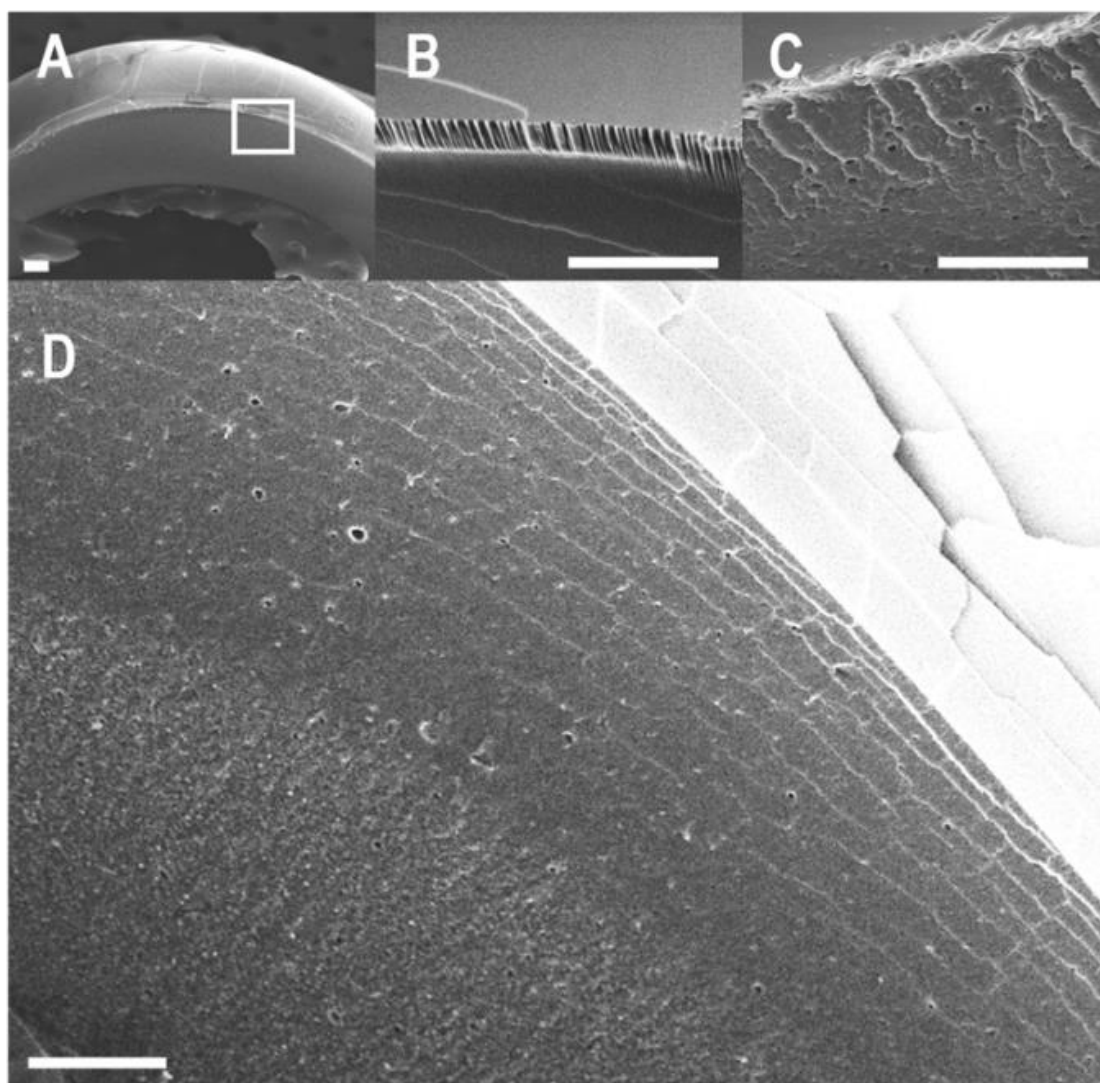


Figure 36 Particle shell structure captured by SEM: A) Skin layer of a dry droplet. The white frame highlights the region of interest for the investigation of skin structure; Shell structure of droplets of WPI (B), NPC (C), and mixes with $WPI\%_R=50\%$ (D). The scale bars correspond to 10 μm .

Considering that $Pe_{NPC} \gg Pe_{WPI} > 1$, we could predict a faster accumulation of NPC micelles at the air-liquid interface during the drying process. Consequently, preferential segregation of the larger colloid on surface top layer should be expected in the binary system investigated in this work. However, the analysis of droplet shape changes with time (**Figure 33**), of drying kinetics (**Figure 34**), of skin mechanical behavior (**Figure 35**) coupled to the direct observation of dry droplet skin structure (**Figure 36**) rather underlines the external segregation of WPI colloids. To shed light on the mechanisms of skin formation in drying WPI/NPC droplets, it is necessary to refer to the rich literature concerning the evaporation in films and droplets of binary colloidal systems. In this respect, numerous experimental and theoretical works have been carried out in the last decade, focusing mainly on the behavior of model colloids differing merely by size (Schulz & Keddie, 2018). According to more recent outcomes, the stratification of the smaller particles on the external part of the skin layer (*i.e.* small-on-top) can take place when the evaporation rate is predominant on diffusive phenomena ($Pe > 1$) for both colloids (Fortini et al., 2016; Makepeace et al., 2017; Sear & Warren, 2017; Zhou et al., 2017), which corresponds to our experimental scenario. In fact, the concentration gradients developing in the direction of the surface during the evaporation result in increasing osmotic pressures, which in turn can induce downward motion especially in larger particles. Starting from this hypothesis and modeling the diffusive cross-interactions between colloids, Zhou, Jiang and Doi (ZJD) (Zhou et al., 2017) identified three crucial parameters to predict a possible stratification by size: the size ratio (α), the Péclet number (Pe_s), and the volume fraction (ϕ_s) associated to the smaller colloid. They also deduced that the necessary condition for the small-on-top stratification to occur is that:

$$C_{ZJD} = \alpha^2(1 + Pe_s)\phi_s > C \quad (\text{Eq. 8})$$

where C is a constant ≈ 1 . In our binary dairy protein system, $\alpha = d_{NPC}/d_{WPI} = 10-30$, $Pe_s = Pe_{WPI} = 6$, and $\phi_s = \phi_{WPI} = 0.01-0.06$. The C_{ZJD} value of WPI/NPC was calculated for the different $WPI\%_R$ (**Table 14**). Therefore, the ZJD criterion is satisfied for all the WPI/NPC mixes investigated in this work but for $WPI\%_R = 20\%$, where the outcome is on the same order of C . This could mean that in this kind of mixes with largely predominant NPC micelles, under these specific environmental conditions, droplet skin does not exhibit evident self-organization, *i.e.* protein stratification could not take place or at least not in the expected way. Despite the ZJD model represents a powerful tool to predict skin structure in binary colloid systems, it neglects hydrodynamic interactions and fluid backflow during the drying process. Sear and Warren (Sear & Warren, 2017), for example, proposed a revised model taking into account diffusiophoretic particle motion driven by concentration gradients, which attenuate the impact of the already mentioned osmotic pressure and, thus, downward flows. All in all, considering diffusiophoresis does not exclude the occurrence of surface stratification, but it implies higher colloid

concentrations and faster evaporation rates. However, full modeling colloidal selective segregation remains a current open question requiring further thorough experimental and theoretical testing. For this reason, the good agreement between our experimental results and the ZJD model corroborates already the hypothesis of WPI colloids on top of NPC micelles in droplet dry skin, at least for higher WPI concentrations (higher than $WPI\%_{RC}$, *i.e.* $0.01 \leq \phi_{WPI} \leq 0.03$, as suggested in previous sections of this work).

Table 14: C value calculated by ZJD model (Eq. 8) with different $WPI\%_R$.

$WPI\%_R$	20%	50%	80%
C_{ZJD}	6.8	14.2	31.1

4.1.3.5. COLLOID ADSORPTION AT DROPLET INTERFACE AND GELATION OVER TIME

In principle, phenomena of self-organization at the air-liquid interface in colloidal systems are not limited to the study of the evaporation. For example, surface gelation can be frequently observed during the investigation of protein adsorption due to gradual ageing. As in the case of drying-induced skin formation, the continuous protein accumulation at the interface leads to the development of concentration gradients and, consequently, of osmotic pressures and, possibly, diffusiophoretic motion. Therefore, the experimental conditions could be favorable for colloid stratification. In the case of WPI/NPC mixes examined in our study, it is interesting to check whether selective protein segregation induced by surface ageing results in interfacial rheological properties consistent with those obtained by drying depending on $WPI\%_R$. Therefore, we explored the time dependence of the interfacial rheological properties of WPI/NPC dispersions by an oscillatory drop tensiometer.

Small sinusoidal variations of the mean drop volume are applied to scan the viscoelastic nature of the interfacial layer. Such measurements reveal surface protein self-arrangement as the interface ages, gradually forming complex gelled layers (Audebert et al., 2019). To reproduce the instantaneous compression rates found in the early stages of the pendant droplet experiments (*i.e.* Stage 1 in **Figure 33**), for the oscillatory experiments we applied an amplitude of area deformation amplitude of 10% and a time period of 30s. In **Figure 37**, we report the evolution of the complex modulus E with time for WPI/NPC droplets with different $WPI\%_R$. At the beginning ($t < 200s$), samples did not exhibit any viscoelasticity ($E' = E'' = 1-5 mN.m^{-1}$), except for $WPI\%_R \geq 80\%$. With time, proteins re-organized and entangled at drop surface and all samples underwent a sol-gel transition, as underlined by the significant increase of E (up to 5-6 times higher than the initial value when $t = 1600s$) and the predominance of the elastic contribution on the viscous one. However, our outcomes also highlighted

that both occurrence and importance of gelation significantly depend on $WPI\%_R$. Indeed, the NPC curve ($WPI\%_R=0\%$) showed to be shifted compared to all others. Samples with $WPI\%_R \geq 50\%$ exhibited a very similar behavior, thus suggesting that WPI colloids control the interfacial rheological properties above a critical concentration in the initial dispersion. It is also worth stressing the surprising behavior observed for $WPI\%_R=20\%$, since E was initially comparable to pure NPC and then increased to higher values than WPI during the measurements. When $t > 1600$ s, the E values increased rapidly due to the onset of surface solidification. The occurrence of these events, which implicate microfracture formation and/or other solid-like irreversible deformations, marked the end of the oscillatory tests. Clearly, these outcomes show significant similarities with those obtained by single droplet drying approach. Thus, in interfacial gelation induced by ageing, as for the gelation induced by drying, WPI colloids dominate skin mechanical properties once their concentration is above a same critical value ($WPI\%_{Rc}$). Also, dispersions with $WPI\%_R=20\%$ confirmed to have unexpected properties, displaying enhanced mechanical response plausibly due to a non-well-defined surface self-arrangement.

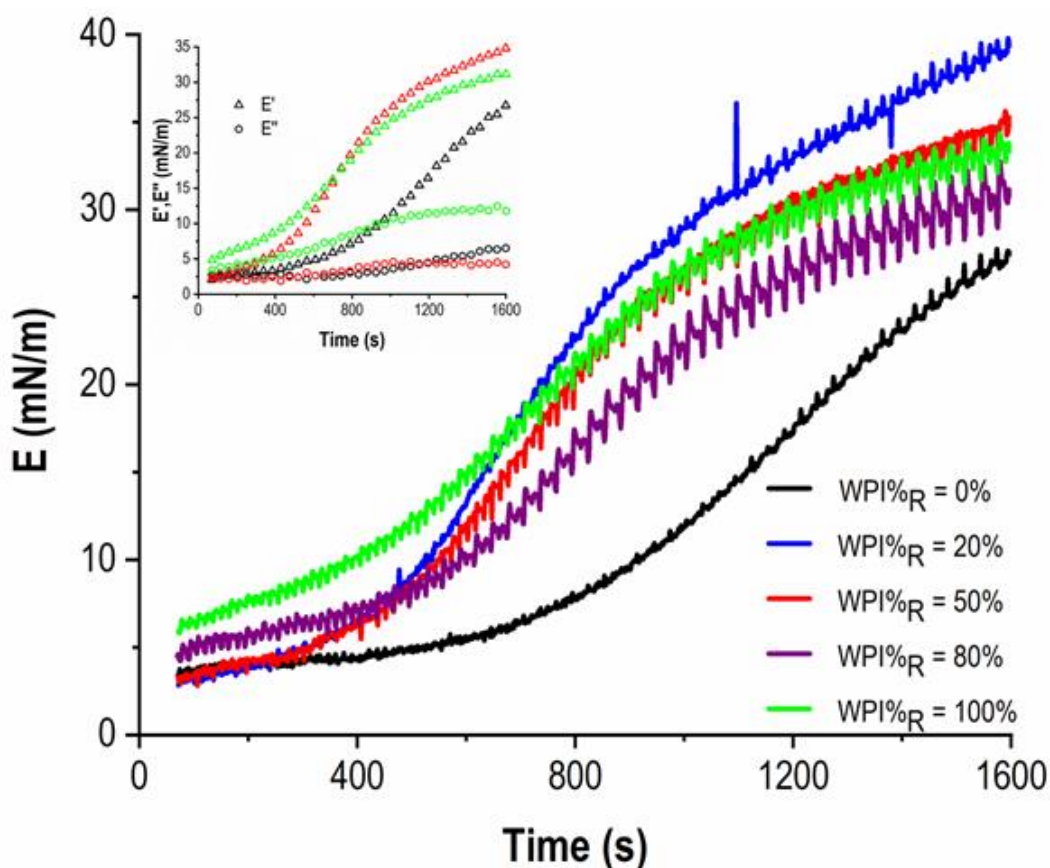


Figure 37. Evolution of the complex viscoelastic modulus (E) with time in WPI/NPC droplets with different $WPI\%_R$. In the inset, the elastic (E') and the viscous part (E'') of the complex modulus are presented for $WPI\%_R=0\%$, 50% , and 100% .

4.1.4. COMPLEMENTARY RESULTS

In the first part of this chapter, we investigated the drying mechanisms in droplets of WPI/NPC mixes, highlighting the segregation/accumulation of the smaller WPI macromolecules on the external side of the droplet skin (small-on-top) at the end of the process. This stratification affected the drying kinetics and the final particle morphology. The colloid size ratio between WPI and NPC was determined as a key factor inducing such a specific stratification, in agreement with previous experimental and theoretical works on binary model systems. In this paragraph, we explore the evaporation in a different type of dairy protein mixture, replacing NPC micelles with sodium caseinates (SC). From the molecular point of view, both NPC and SC consist of α , β , κ -casein (Dalglish & Law, 1988; Walstra et al., 2005). However, they also exhibit glaring differences in terms of structure, as shown in **Figure 38** (Ma & Chatterton, 2021). On the one hand, casein micelles, whose average diameter range from 100 to 300 nm in bovine milk (P. F. Fox & Brodkorb, 2008), can be simplistically described as network of sub-micelles, including a core of Ca-caseins and a κ -casein external layer. On the other, sodium caseinates are organized in amorphous structures consisting of few molecules (isolates) and have a smaller mean radius (≈ 10 nm) (Hemar et al., 2021). This structural difference compared to NPCs is due to the solubilization of calcium phosphate throughout their obtention by acidification, and thus to the significant attenuation of the attractive forces contributing to micelle cohesion. Interestingly, WPI and SC colloids have a comparable size, which means that it is not likely to predict a self-stratification by size during the drying process. In this section, we will provide a preliminary investigation of the evaporation mechanisms in WPI/SC mixes aiming to highlight the specific role of each component on the development of the drying stages and final particle shape.

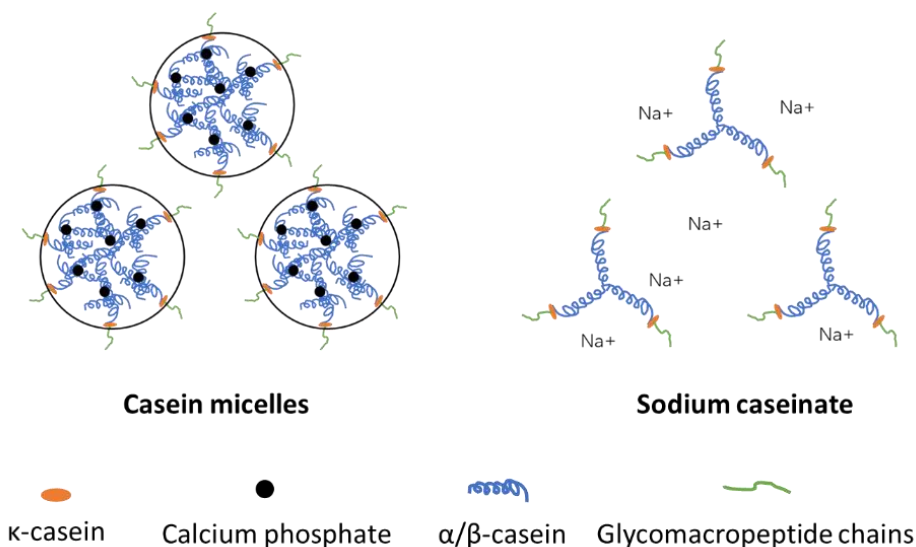


Figure 38. Schematic representation of the molecular structure of casein micelles (NPC) and sodium caseinates (SC).

4.1.4.1. COMPARISON OF WPI/NPC AND WPI/SC DRY PARTICLE MORPHOLOGY

The shape evolution of WPI/SC single droplets was investigated during the evaporation to point out the main stages of the process and, mostly, the eventual morphological differences with WPI/NPC dry samples. In analogy to the experiments on dairy protein mixes with casein micelles described previously, we measured the diameter reduction ($\Delta D\%$) and the normalized final apex height (H/H_0) of the drying WPI/SC droplets to characterize their gradual morphological changes.

From a qualitative point of view, **Figure 39** provides a first overview in which the morphology of dry WPI/SC and WPI/NPC droplets is compared for different $WPI\%_R$. The droplets of SC and NPC ($WPI\%_R=0\%$) displayed evident analogies, exhibiting a typical buckled surface and negligible delamination. When increasing $WPI\%_R$, a transition from wrinkled to round surface was observed irrespective of the kind of binary mixes, even if occurring at different critical $WPI\%_{Rc}$. Indeed, dry WPI/SC droplets with $WPI\%_R=50\%$ were still characterized by surface buckling, whereas WPI/NPC ones showed almost perfectly smooth surface at the same $WPI\%_R$. Although this shape transition was plausibly interpreted in the previous section through the occurrence of protein segregation in WPI/NPC droplets, the question remains to be explored in the case of WPI/SC mixes given their similar colloid size. Finally, we also clearly noticed that the WPI/SC droplets were flatter than WPI/SC ones at the end of the evaporation, thus suggesting a delayed interfacial sol-gel transition compared to what observed in the presence of micellar microgels in the suspensions.

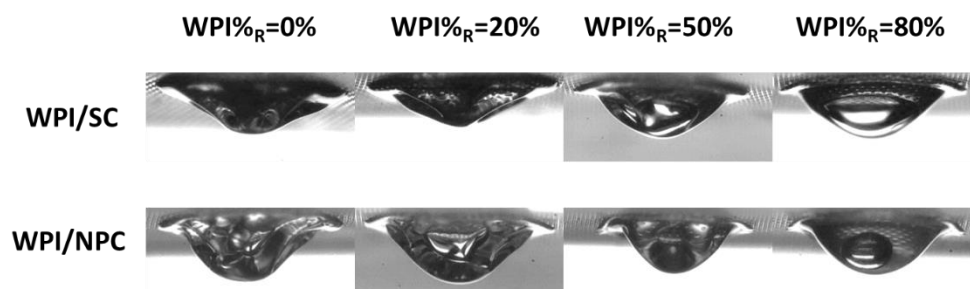


Figure 39. Qualitative comparison between WPI/SC and WPI/NPC dry droplets for different $WPI\%_R$.

4.1.4.2. DROPLET DIAMETER REDUCTION

In **Figure 40**, the diameter reduction in dry droplets of WPI/SC and WPI/NPC mixes is illustrated as a function of $WPI\%_R$. Interestingly, this quantitative comparison highlighted a very similar behavior irrespective of the structure of the casein present in the suspensions, sodium caseinates or casein micelles. An increasing $\Delta D\%$ has been measured for increasing $WPI\%_R$, ranging from $\approx 6\%$ ($WPI\%_R=0\%$) to $\approx 17\%$ ($WPI\%_R \geq 80\%$), with a slightly higher effect observed in WPI/NPC droplets. In fact, the $\Delta D\%$ is influenced by two main factors:

- i) the chemical affinity between the droplet solute and the substrate, resulting in a more or less intense adhesion;
- ii) the mechanical properties of the interfacial skin, leading to increasing inward stresses during the evaporation.

As already mentioned, the critical condition for stress release is achieved when the surface shrinkage force overcomes the adhesion to the substrate (Sobac 2014, Pauchard 2006). In the case of samples rich in sodium caseinates or casein micelles, the increase of interfacial stresses resulted in surface invagination, thus showing significant skin deformability. On the contrary, the development of the rigid skin layer typical of WPI-rich droplets led to border detachment from the substrate when the evaporation process advanced. In WPI/NPC mixes, the rigidity of droplet surface could be further enhanced by WPI accumulation on the top surface, thus explaining the slight difference with WPI/SC samples (Schulz & Keddie, 2018). In this latter case, the skin layer incorporated both caseinate and globular WPI, and thus, its mechanical properties as monitored by $\Delta D\%$ evolution probably depended only on their relative concentration.

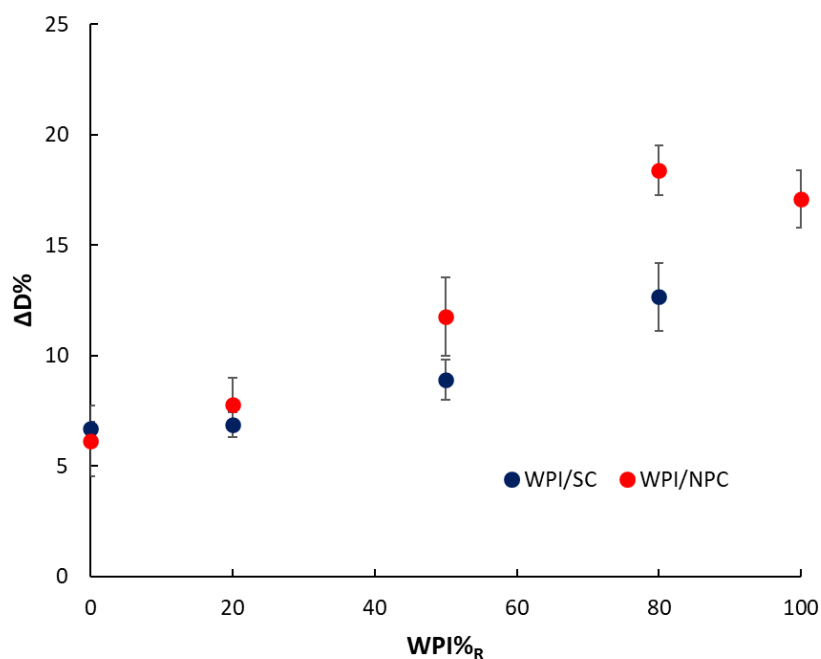


Figure 40. Diameter reduction percentage in WPI/SC and WPI/NPC dry droplets as a function of WPI%_R.

4.1.4.3. DROPLET APEX HEIGHT

Measuring the evolution of WPI/SC apex height during the evaporation allowed to corroborate the previous qualitative observation (**Figure 41**), where droplets containing sodium caseinates seemed to be flatter than casein micelles ones. Here, we compared the normalized final apex height (H/H_0) of WPI/SC and WPI/NPC droplets as a function of sample composition (WPI%_R), as showed in **Figure 41**.

Contrary to what observed for the occurrence of the delamination and, in general, for the diameter reduction, the analysis of droplet height stressed a significant difference with regard to the structure of the casein in the mix, WPI/NPC or WPI/SC. For WPI/NPC, a gradual decrease of H/H_0 was observed for increasing amounts of whey proteins in the droplets. Indeed, $H/H_0=43\%$ in pure NPC samples, whereas in pure WPI ones the height reduction was more evident ($H/H_0=28\%$). For WPI/SC, the final droplet height was almost constant regardless of $WPI\%_R$ ($H/H_0= 33-38\%$), thus on average lower than in WPI/NPC suspensions. In previous works on the evaporation of dairy protein mixes, it has been established that the attenuation of drying-induced droplet shrinkage and the observation of a constant final height is strictly linked to the achievement of a protein critical concentration (c_{gel}) at the air-liquid interface, corresponding to the sol-gel transition. In other words, the later c_{gel} is reached, the lower the height of the droplets. In the case of NPC, SC and WPI, the reported c_{gel} are 16 w / w %, 24 w / w % and 41 w / w % (Bouchoux, Cayemite, et al., 2009; Sadek, Pauchard, et al., 2015), respectively. As a consequence, the increase of $WPI\%_R$ possibly corresponded to a later sol-gel transition at droplet surface (even more if we take into account WPI external segregation) and, thus, to a significant height reduction in WPI/NPC mixes. On the other hand, the higher c_{gel} corresponding to SC colloids and their average size similar to WPI favored the consistency of lower and almost constant H/H_0 values in WPI/SC suspensions.

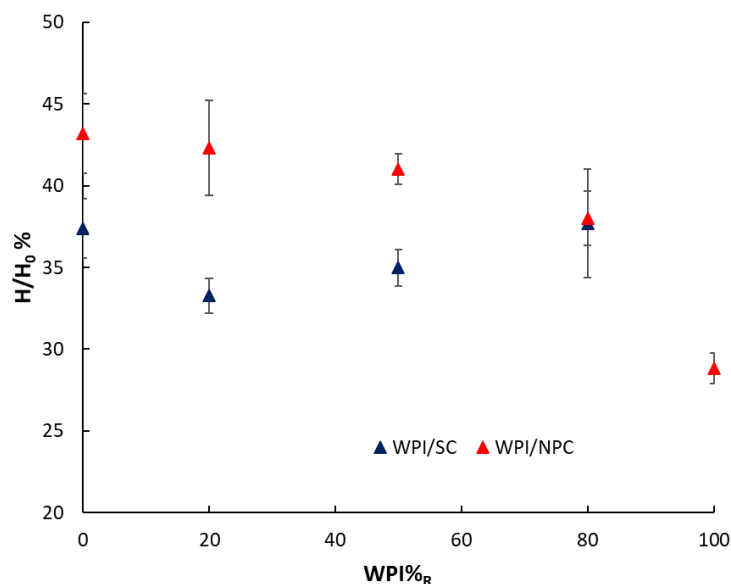


Figure 41. Normalized final apex height of WPI/SC and WPI/NPC dry droplets as a function of $WPI\%_R$.

4.1.5. CONCLUSIONS

In this work, we provided a characterization of the drying process in droplets of a binary colloidal systems consisting on the one hand of whey proteins (WPI) and casein micelles (NPC), and on the other

hand of WPI and sodium caseinate (SC). Compared to most of the previous studies focusing on model colloids, here we dealt with three real proteins types exhibiting significant differences in terms not only of size, but also of structure and mechanical properties.

In the WPI/NPC droplet drying process, the evaluation of droplet profile evolution and drying kinetics with time underlined the crucial role played by WPI in the evaporation dynamics despite being the minor component of the suspension in terms of volume fraction. Indeed, when sufficiently represented in the initial dispersions ($WPI\%_R \geq WPI\%_{RC}$), WPI colloids confer to droplets a rigid skin with high resistance to buckling. Such enhanced mechanical properties suggested possible drying-induced WPI external segregation, as already proposed in previous works on bidisperse non-dairy suspensions. The hypothesis of interfacial protein stratification was confirmed by the direct observation of WPI/NPC droplet skin section by SEM, highlighting WPI accumulation on top surface (small-on-top re-arrangement). The occurrence of WPI preferential segregation under certain conditions was interpreted in the light of the ZJD model for binary systems. According to this theory, the accumulation of colloids at droplet surface foster increasing osmotic pressures, which in turn favor the accumulation of smaller macromolecules at the air-liquid interface. Interestingly, although WPI and NPC exhibit different structure and physico-chemical properties that could influence the evaporation process, the size of the two proteins was the main factor governing the auto-stratification. We also showed by oscillatory drop tensiometer that the small-on-top re-arrangement can be also driven by ageing surface gelation. This suggests that the evaporation is not a prerequisite for colloid auto-stratification, but rather the development of local concentration gradients in proximity to droplet surface.

In the WPI/SC droplet drying process, we aimed to explore the possible impact of protein structure and resulting physico-chemical properties on the drying of binary mixes of whey protein and caseins, replacing the NPC micelles with SC in the suspensions. All in all, the results highlighted that, despite glaring structural differences, the chemical characteristics of NPC and SC macromolecules provided similar high deformability to droplet skin and a significant attenuation of the delamination at the borders. On the other hand, the global shrinkage of the droplets, which is influenced by the achievement of the sol-gel transition at the air-liquid interface, was strongly affected by colloid average size, as evidenced by the consistency of final apex height in WPI/SC samples (proteins with comparable size) and the significant decrease with $WPI\%_R$ in WPI/NPC mixes. However, the observation of droplet profile modification during the drying process does not allow to gather any possible evidence of self-stratification in WPI/SC, thus paving the way to further ongoing investigation (confocal microscopy, SEM).

This study represents a point of novelty in the literature about the evaporation in bidisperse colloidal dispersions, since the mechanisms of auto-stratification have been rarely investigated in biological systems so far. Our outcomes corroborate the most accredited theories about drying-induced segregation by size. Moreover, this work represents a forerunner for further investigations that could favor the prediction of dry droplet shape starting basically from colloidal properties (*e.g.*, size, structure, mechanical properties, and surface charge) and composition in a polydisperse dispersion. This could be fundamental, for example, in dairy industry, mostly concerning the optimization of dairy powder production and the control of their functional properties (*e.g.*, rehydration).

4.2. PHASE DIAGRAM OF DAIRY PROTEIN MIXES OBTAINED BY SINGLE DROPLET DRYING EXPERIMENTS

4.2.1. INTRODUCTION

As already mentioned in the introductory part, the outcomes presented in the section 4.1 are placed in the context of the numerous studies performed on the drying of dairy proteins using a lab-scale approach. The first works have been carried out on single protein droplets in pendant configuration (Sadek et al., 2013; Sadek, Schuck, et al., 2015) and, in the wake of these seminal results, the investigation has turned to protein mixes using similar experimental strategy (Lanotte et al., 2018; Yu et al., 2021). Moreover, all these studies have been performed on WPI/NPC dispersions with different overall protein concentration (c_p) and composition ($WPI\%_R$). For example, Sadek *et al.* investigated the evaporation process in WPI and NPC droplets with $c_p = 10$ w/w %, Lanotte *et al.* focused on WPI/NPC mixes ($WPI\%_R = 20\%$, 60%) with $c_p = 12$ w/w %, whereas Yu *et al.* observed the skin formation in dairy protein mixtures ($WPI\%_R = 0\%$ - 100%) with $c_p = 8$ w/w %. In this section, therefore, the goal has been to further explore on an extended scale the impact of these two crucial parameters on the shape characteristics of the dried droplets and to provide a global picture able to predict the main events taking place during the evaporation process. The results presented in this section have been submitted for publication in *Foods*, in view to contribute to the special Issue "Application of Innovative Spray Drying Technology on Food Engineering".

4.2.2. EXPERIMENT STRATEGY

The experimental activity focused on the drying mechanisms in droplets of WPI/NPC mixes with overall protein concentration ranging from 6 w / w % to 14 w / w % and WPI relative percentage ($WPI\%_R$) of 0, 20, 50, 80, 100%.

The single droplet drying approach (see Chapter 3 for the detailed description) was used to explore the droplet profile evolution and drying kinetics during the drying process. This favored the understanding of how WPI relative percentage impacts particle shape, skin layer structure and properties. The morphology of the dry WPI/NPC droplets was further investigated by SEM (JEOL JSM 7100F) at 5 kV: In particular, the influence of protein concentration on the thickness and the structure of the hemispherical section was verified in WPI-rich samples ($WPI\%_R \geq 50\%$) due to their more regular shape and the facility to be cut.

4.2.3. RESULTS AND DISCUSSION

4.2.3.1. DEFINITION OF THE KEY SHAPE PARAMETERS

The profile view approach allowed to characterize the variation with time of the base diameter (D) and the apex height (H) for all WPI/NPC droplets, in analogy with recent works on the drying of dairy protein dispersions (Lanotte et al., 2018; Sadek et al., 2013; Yu et al., 2021). This kind of quantitative analysis provided indirect evidence of the impact of sample characteristics (c_p , $\text{WPI}\%_R$) on droplet morphology changes induced by the evaporation, here quantified by the diameter reduction and the final apex height. In **Figure 42**, the evolution of D and H normalized by their maximum values (D_{\max} , H_{\max}) is displayed, as a reference, for WPI suspensions ($\text{WPI}\%_R = 100\%$) with different c_p (for the sake of clarity, only the data related to $c_p = 6$ w/w %, 10 w/w % and 14 w/w % are showed here), since in these samples the shape modifications are more evident than in other mixes.

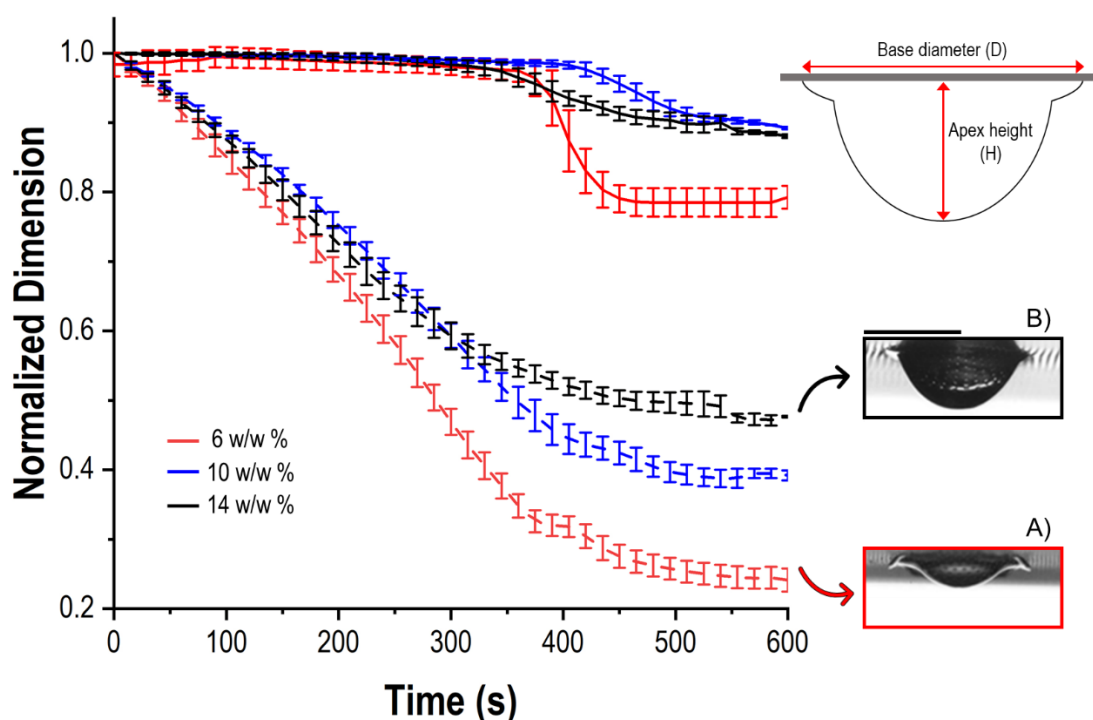


Figure 42. Evolution of normalized droplet base diameter (D/D_{\max} – top curves) and apex height (H/H_{\max} – bottom curves) with time for WPI samples with different protein concentration (c_p).

As it concerns the D/D_{\max} curves, a transition from border detachment (**Figure 42A**) to slighter shrinkage (**Figure 42B**), similar for all WPI droplets when $c_p \geq 10$ w/w %, was observed with increasing initial protein content in the suspensions. The attenuation of the delamination at higher c_p could be explained by the enhanced accumulation of solutes driven by drying-induced outward capillary flows (Deegan et al., 1997). This would lead to the formation of a larger external “foot” able to withstand the surface inward stresses due to its structural robustness and possibly even its improved chemical affinity with the substrate. Indeed, as already stated in the Materials and Methods section, the commercial WPI and NPC powders used for sample preparation contain a minor amount (5-6 w/w %)

of the other protein (that is to say, single caseins for WPI and whey proteins for NPC), as well as a mineral and lactose fraction. In previous studies, NPC colloids have proven to favor the triple line adhesion in drying droplets, resulting in negligible border detachment (Sadek et al., 2016; Sadek, Schuck, et al., 2015). Therefore, it is likely that, for $c_p \geq 10$ w/w %, WPI dispersions include enough casein contributing to the foot anchoring to the PDMS surface. On the other hand, increasing c_p corresponded to gradually larger final apex height and base diameter, that is to say lower shrinkage. Such a behavior could be interpreted in the light of the probable earlier achievement of the surface sol-gel transition conditions, *i.e.*, for colloid critical concentration $c_{gel} = 41$ w/w % (Bouchoux, Cayemite, et al., 2009), resulting in the development of a thicker skin layer.

4.2.3.2 DIAMETER REDUCTION

If the outcomes obtained for WPI droplets lead to linear interpretation, the investigation appeared more complex in case of WPI/NPC mixes, where the coexistence of colloids with different size, structure and mechanical properties results in possible competitive dynamics. To avoid the redundancy of presenting the evolution of D/D_{max} and H/H_{max} for all WPI/NPC dispersions, we focused here on the diameter reduction ($\Delta D\%$) and the final apex height (H_f) as a function of $WPI\%_R$ in droplets with different c_p .

The diameter reduction was defined as:

$$\Delta D\% = \frac{(D_{max} - D_f)}{D_{max}} \quad (\text{Eq. 9})$$

Where D_{max} and D_f refer to the maximum and the final base diameter, respectively (N.B., $D_{max} \neq D_0$, *i.e.*, the initial value, since droplets often expand during the early drying stage). The $\Delta D\%$ values related to all the explored WPI/NPC mixes are reported in **Table 15**, whereas in **Figure 43** only the outcomes for suspensions with $c_p = 6$ w/w %, 10 w/w % and 14 w/w % are displayed for the sake of clarity. The outcomes highlighted that an increasing amount of whey proteins in the binary mix corresponded to a more significant diameter reduction, resulting in delamination ($\Delta D\% \geq 10\%$) under certain conditions ($c_p \leq 8$ w/w %). This is not surprising, since numerous works in the literature showed that, contrary to what already mentioned for NPC, that the brittle character of WPI-rich dry structures fosters border delamination (Sadek et al., 2013; Yu et al., 2021). However, the increase of overall protein concentration led to a strong mitigation of the diameter reduction, down to $\Delta D\% < 10\%$ for $c_p \geq 10$ wt% regardless of $WPI\%_R$. This corroborates the hypotheses of possible thicker foot width and enhanced adhesivity with increasing c_p .

Table 15. Measured values of $\Delta D\%$ and H_f/H_{max} in drying WPI/NPC droplets with different c_p and $WPI\%_R$.

c_p \ $WPI\%_R$	0		20		50		80		100	
	$\Delta D\%$	H_f/H_{max}								
6w/w %	8.7±1.1	0.4±0.03	8.2±0.6	0.38±0.02	13.2±2.3	0.34±0.01	18.9±2.2	0.28±0.01	21.3±1.8	0.24±0.01
8w/w %	6.1±1.6	0.43±0.02	7.8±0.9	0.44±0.02	11.8±1.8	0.41±0.01	18.4±1.1	0.38±0.01	17.5±0.0	0.29±0.01
10w/w %	5.8±0.9	0.42±0.02	8.2±1.2	0.41±0.02	9.6±1	0.40±0.02	11±0.6	0.41±0.01	9.3±0.6	0.39±0.01
12w/w %	6.8±1.8	0.52±0.02	5.3±1.3	0.5±0.01	6.2±1.4	0.48±0.02	9.4±1.4	0.45±0.02	9.3±1.5	0.45±0.03
14w/w %	4.9±1.7	0.6±0.01	4.6±0.4	0.54±0.01	5.2±0.7	0.53±0.01	7.1±0.7	0.50±0.01	10.8±1.3	0.49±0.02

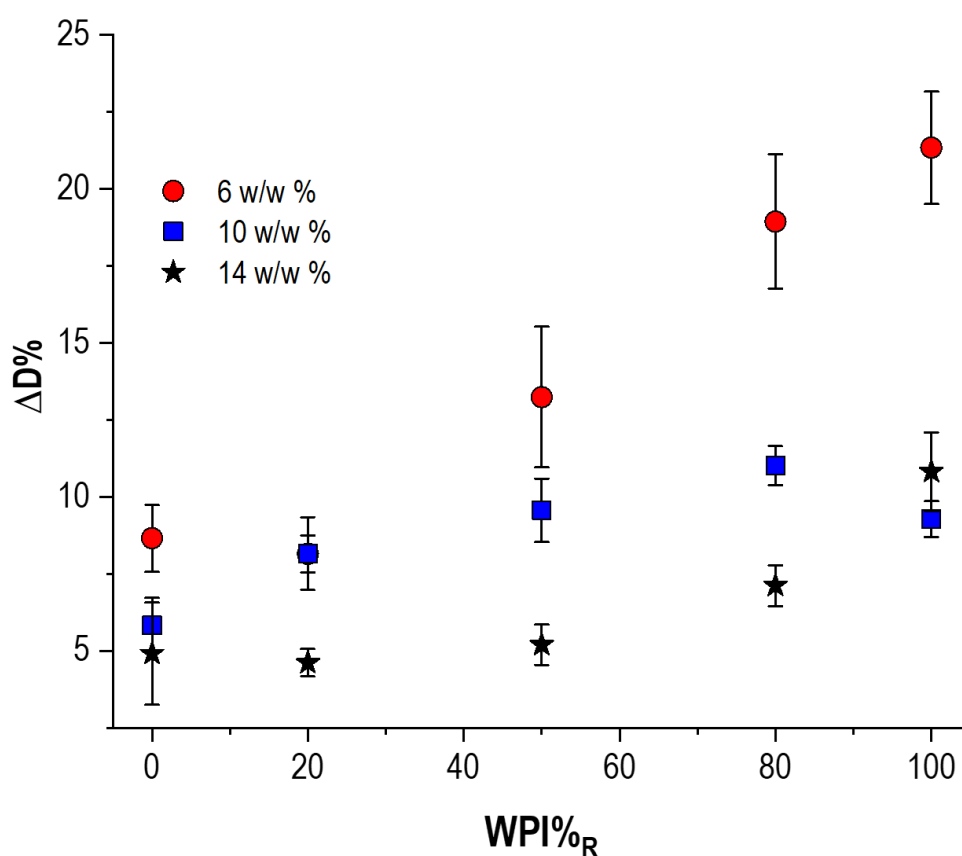


Figure 43. Estimation of the diameter reduction ($\Delta D\%$) as a function of $WPI\%_R$ at the end of the drying process in WPI/NPC droplets with $c_p = 6$ w/w %, 10 w/w %, and 14 w/w %.

In order to investigate the potential dependency of droplet foot width (w_f) on c_p , we performed a quantitative analysis of w_f , whose definition is provided in **Figure 44 A**, as a function of $WPI\%_R$ for $c_p = 8$ w/w % (*i.e.*, droplets exhibiting delamination) and $c_p = 12$ w/w % (*i.e.*, samples displaying slight shrinkage). The results illustrated in **Figure 44 B** highlight once more the strong impact of $WPI\%_R$ on the shape characteristics of WPI/NPC droplets in the course of drying. Indeed, we observed an

increasing w_f with higher $WPI\%_R$, especially in the case of $c_p = 8$ w/w %. This is quite surprising given the respective NPC and WPI colloid average size and volume fraction, that lead at constant mass concentration to higher volume fraction in the dispersion with lower $WPI\%_R$ (**Table 9**). Consequently, a thicker width in NPC-rich droplets (i.e., at lower $WPI\%_R$) should be expected. In addition, droplets with $c_p = 12$ w/w % exhibited, on average, a smaller and almost $WPI\%_R$ -constant foot width compared to those observed at lower overall protein concentration (**Figure 44 B**). A possible explanation to these surprising outcomes could be found in the intensity of the internal flows during the evaporation. In fact, casein micelles are characterized by a slower diffusion than whey proteins, due to their size and structure (Yu et al., 2021). NPC lower motion would lead, on the one hand, to the early gelation at the surface (evaporation front retraction faster than colloid Brownian motion) and, on the other, to the development of weaker capillary flows. In this light, it would be likely to predict the formation of a smaller foot for low $WPI\%_R$. This effect would be even emphasized by the increase of c_p , due to the increase in terms of NPC concentration and of colloid crowding events in general (volume fraction, Table 9), which would further slowdown the internal motions in the droplets.

All in all, the results presented in **Figure 44** underline that the attenuation of the delamination phenomena at higher c_p is not linked to the formation of an external foot with larger size. Therefore, rather than w_f considerations, NPC adhesivity to the PDMS substrate could be the most plausible reason for the inhibition of border detachment at the end of the drying process. This hypothesis is further corroborated if we consider the effective volume fraction “occupied” by casein micelles in the drying dispersions. In fact, starting from the overall ϕ_p reported in **Table 9** and considering casein micelle voluminosity, it is possible to estimate that the NPC volume fraction is higher than the WPI one even when whey proteins are major components in terms of mass concentration. For example, when $WPI\%_R = 80\%$, $\phi_{NPC} = 0.055$ for $c_p = 6$ wt%, and $\phi_{NPC} = 0.11$ for $c_p = 14$ wt%. It is worth pointing out that the values of ϕ_p and ϕ_{NPC} are calculated starting from the ideal assumption of pure initial powders of WPI and NPC, thus without taking into account any minor component. Anyway, the mechanical response to the inward interfacial stresses occurring during the evaporation, which is the main cause of the diameter reduction, is also related to onset of the sol-gel transition at droplet surface and, therefore, to the thickness and the structure of the skin.

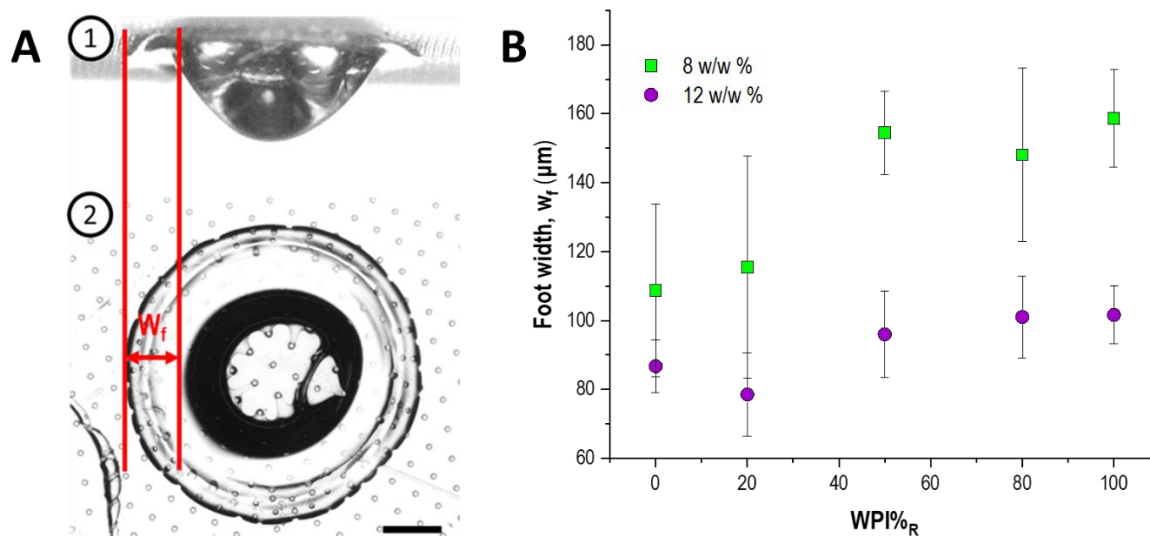


Figure 44. A) Definition of the foot width (w_f) at the end of the evaporation process in WPI/NPC droplets. 1) Profile and 2) top view projections in a WPI droplet. Scale bar equal to 200 μm . B) Measure of w_f as a function of $\text{WPI}\%_R$ for $c_p = 8$ w/w %, and 12 w/w %.

4.2.3.3 DROPLET FINAL HEIGHT

In Table 15, the data referring to H_f normalized by their maximum values (H_f/H_{max}) are reported for WPI/NPC droplets as a function of c_p and $\text{WPI}\%_R$. In **Figure 45**, H_f/H_{max} values as a function of $\text{WPI}\%_R$ are illustrated for $c_p = 6$ w/w %, 10 w/w %, and 14 w/w % for the sake of clarity. This kind of analysis did not provide a characterization of skin morphology at the end of the drying (e.g., buckling instabilities), but rather an evaluation of the impact of sample characteristics (c_p and $\text{WPI}\%_R$) on the occurrence of the gelation at droplet surface and, therefore, of the skin development. At low c_p (≤ 8 w/w %), a significantly lower H_f/H_{max} was measured with increasing $\text{WPI}\%_R$, with a difference between NPC and WPI samples equal to 0.15. Such an evident tendency was in agreement with the hypothesis of later interfacial sol-gel transition in presence of larger amounts of whey proteins. A similar, but mitigated trend was observed in more concentrated samples ($c_p \geq 12$ w/w %), where the difference between H_f/H_{max} in NPC and WPI droplets was reduced to 0.05-0.07. These results could be interpreted once more in the light of a higher concentration of NPC micelles in the dispersions, thus fostering the occurrence of an earlier sol-gel transition compared to more dilute suspensions. Finally, an unexpected behavior was detected for the intermediate $c_p = 10$ w/w %, where the measured values of H_f/H_{max} exhibited a plateau-like tendency irrespective of $\text{WPI}\%_R$.

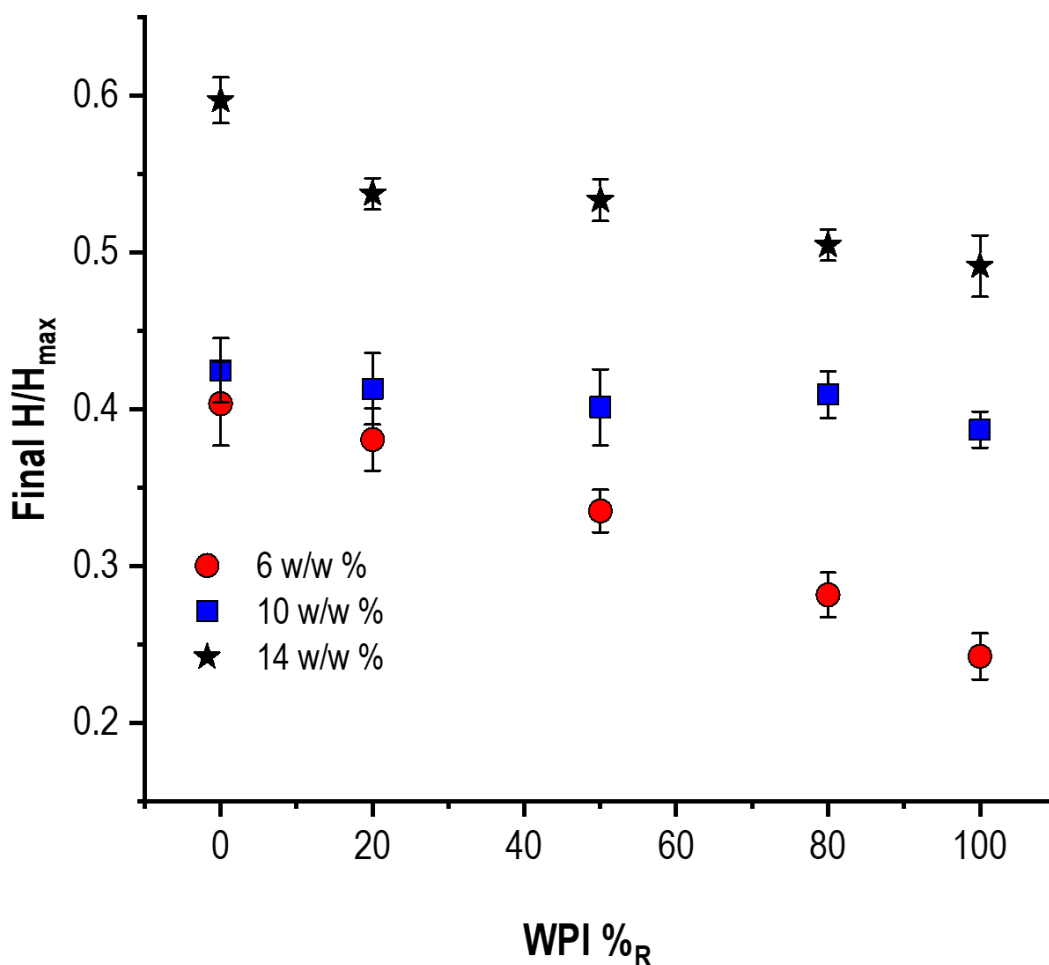


Figure 45. Evaluation of the impact of $WPI\%_R$ on WPI/NPC droplet final normalized height (H_f/H_{max}) for dispersions with $c_p = 6$ w/w %, 10 w/w %, 14 w/w %.

The reason of this almost constant values found for $c_p = 10$ w/w % could be linked to the overestimation of WPI-rich droplet height at intermediate concentrations due to the elastic response of the skin in correspondence of the delamination, and, simultaneously, to the underestimation of H_f/H_{max} in NPC dispersions is due to the collapse of the skin induced by the buckling. However, although plausible, there is not yet experimental evidence of this hypothesis and, mostly, it is not possible to explain why it should happen only for 10 w/w %. Indeed, a systematic study of skin characteristics as a function of solute concentration and composition is currently only at a “embryonic” stage. Indeed, the skin thickness (δ_s) has been measured by SEM in WPI droplets with different c_p . The subsequent step will be to enrich these first experiments with further tests on WPI-rich samples (*i.e.*, $WPI\%_R = 50\%$, 80%). This will allow to evaluate the impact of NPC on colloid self-arrangement and final δ_s , mostly in the light of the outcomes shown in the 4.1 section on the drying-induced protein stratification. It is not likely to perform the same characterization on dispersions with $WPI\%_R \leq 20\%$ since in this case droplets display a very irregular and wrinkled surface and the cutting is, consequently, much more complicated.

4.2.3.4 PHASE DIAGRAM OF DRIED WPI/NPC DROPLETS

The full characterization of droplet base diameter (D) and apex height (H) led to the construction of a preliminary phase diagram for mixes of whey proteins and casein micelles. The purpose of this phase diagram is mainly to predict the main shape characteristics of dry WPI/NPC droplets knowing the initial protein concentration (c_p) and the composition ($WPI\%_R$) of the initial dispersion. In this regard, **Figure 46** displays four main regions corresponding to specific morphologies:

- Region I: Particles comes from NPC major dispersion, irrespective of c_p , and present a typical wrinkled surface developing along with vacuole formation, and no border detachment;
- Region II: Particles show a hybrid shape (round shell with dimples) including an internal vacuole and significant delamination. They correspond to dispersion with intermediate value of $WPI\%_R$ and low c_p ;
- Region III: Particles present a smooth interface, border detachment and vacuole formation. They correspond to dispersion with $WPI\%_R > 37\%$ and intermediate/high c_p ;
- Region IV: Particles comes from WPI major dispersion and low c_p . As for Region III, they show a smooth surface typical of WPI rich samples, but in contrast with significant delamination and without vacuole formation.

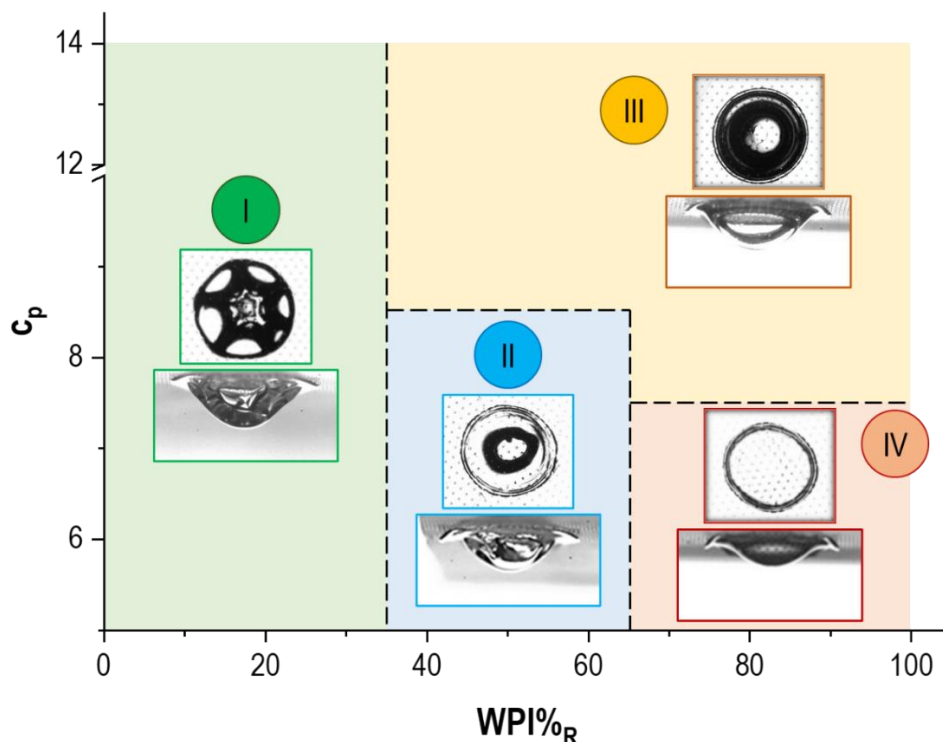


Figure 46. Phase diagram of the main shape characteristics of dried WPI/NPC droplets as a function of protein overall concentration (c_p) and sample composition ($WPI\%_R$). I: Wrinkled surface, no border detachment, vacuole formation; II: Hybrid shape, significant delamination, vacuole formation; III: smooth interface, border detachment, vacuole formation; IV: smooth surface, significant delamination, no vacuole formation.

4.2.4. CONCLUSIONS

In this section, we aimed at providing an overview of the main shape modifications occurring in WPI/NPC droplets during the evaporation in pendant configuration. We characterized the droplet diameter reduction ($\Delta D\%$) and the final apex height (H_f/H_{max}) as a function of protein overall concentration (c_p) in the dispersions and their composition ($WPI\%_R$). The outcomes highlighted how the different physical phenomena typically affected by $WPI\%_R$, such as delamination and rigid round shell formation for $WPI\%_R \geq 50\%$ and high border adhesivity and skin buckling instability, are extremely attenuated or inhibited by the increase of protein concentration in the initial dispersion. This effect has been interpreted in the light of the increase with c_p of NPC volume fraction, in the mixes but also in single WPI suspensions due to the partial impurity of the commercial powders, which enhance the pinning of droplet triple line and favor the earlier onset of the sol-gel transition at the air-liquid interface. Such a global overview of the drying process in WPI/NPC mixes allowed to construct a preliminary phase diagram able to predict the main morphological properties of dried WPI/NPC droplets starting from the initial characteristics of the sample (c_p , $WPI\%_R$). This diagram will be much more accurate in the next future thanks to ongoing experimental tests and it will be validated also at larger scale, first by monodisperse drying and at the semi-industrial scale. Indeed, if confirmed, these results would be very useful to control not only the shape of the obtained powders but mostly their connected functional and nutritional properties.

4.3. EXPLORING THE PROPERTIES OF PARTICLES OBTAINED FROM FLYING DROPLETS

4.3.1. INTRODUCTION

Spray drying is one of the most used manufacturing processes. It has been applied in a wide range of products and industries, including food (Kim et al., 2009), pharmaceutical (Vehring, 2008), ceramic (Stunda-Zujeva et al., 2017), polymer, and chemical (Santos et al., 2018) industries. In the dairy industry, the basic principles of the operation remain essentially the same: a suspension is fed to the dryer, and atomized into a cloud of small drops, which rapidly transform into particles when exposed to the hot air. However, as explained in Chapter 1, the mechanisms governing the droplet-particle formation in the spray drying process have not yet fully elucidated. In the past decades, numerous studies have been focusing on how the drying parameters, feed concentration and solute properties impact the particle properties and notably their final morphology (hollow, dense spherical, wrinkled). This is a crucial point, since powder physico-chemical and morphological characteristics (particle size distribution, shape, and surface composition) strongly affect also their functional and nutritional properties, such as flowability (X. Fu et al., 2012; Habibnejad-korayem et al., 2021; Kim et al., 2005; Sandler & Wilson, 2010) or rehydration (Selomulya & Fang, 2013). Briefly, particle morphology plays a crucial role in the packaging, storage, and application process.

In the previous section, we dealt with the effect of WPI/NPC composition and overall protein concentration on the particle shape. As summarized in **Figure 46**, four different morphology types of dairy particles were observed using the pendant droplet configuration. In addition, in the 4.1 section, we explored by similar experimental setup the influence of the molecular structure of the casein source on particle shape through drying WPI/SC droplets. Therefore, it is of interest to verify if these results could predict dairy particle shape in mixes with different initial composition even at larger scale, comparing the single-droplet approach to the flying droplet one. In this part of the thesis, we performed drying tests on WPI/NPC mixtures and single SC suspensions with a monodisperse spray dryer providing a possible interpretation of the outcomes in the light of the results obtained by the single-droplet method. The main morphological properties of the powders (*i.e.*, area, circularity, solidity) were quantitatively characterized by image analysis.

4.3.2. EXPERIMENT STRATEGIES

The images of the dried particles were acquired by optical microscopy in bright field and phase contrast and then converted into a digital form (pixel matrix). A grey shade threshold was defined in accordance with user-specified criteria for the characterization of the main shape parameters of the objects identified in the images: such as area, circularity and solidity (these parameters were mentioned in

Chapter 2). Shape parameter characterization was carried out on a number of particles ranging between 500 and 900 for each sample.

4.3.3. RESULTS AND DISCUSSION

4.3.3.1. PARTICLE MORPHOLOGY OF DAIRY PROTEIN MIXES

The monodisperse drying tests were here performed on dairy protein suspensions with an overall protein concentration fixed at 6 w/w %, single or in mixture with WPI%_R = 50% and 80%. In **Figure 47**, a qualitative overview of the dried powders is presented, highlighting very specific morphological characteristics as a function of the physicochemical properties of the components. NPC particles exhibited an irregular and wrinkled surface **Figure 47 a**), whereas WPI ones (**Figure 47 b**) were round and hollow, in agreement with previous works in the literature (Sadek et al., 2014). Interestingly, at this concentration, the mixes with WPI%_R = 50% (**Figure 47 c**) showed a round, slightly buckled morphology, thus much closer to whey proteins than casein micelles. This preliminary observation highlighted a significant similarity to what already detected at the single-droplet scale (Lanotte et al., 2018; Yu et al., 2021) and, thus, suggested possible auto-stratification phenomena at droplet surface with WPI accumulation at the top layer. On the other hand, when comparing NPC and SC powders (**Figure 47 d**), we detected the presence of two classes of particles: i) small and very wrinkled (star-like shape), and ii) larger and more spherical. It is evident that, despite both samples exhibited a wrinkled surface, the ones with sodium caseinates exhibited less significant surface irregularities. Indeed, the statistical distribution of these two categories of particles in casein micelle and sodium caseinate powders were 28% and 72%, and 67% and 33%, respectively. The roundness of a large portion of SC dry particles, in analogy to what was observed in WPI-rich samples, could underline the key role played by the colloid size during the water removal process. Indeed, beyond an evident difference in terms of molecular composition, WPI and SC have comparable size than larger NPC micelles and this could lead to the formation of a more packed and rigid skin able to withstand the increasing drying-induced surface stresses.

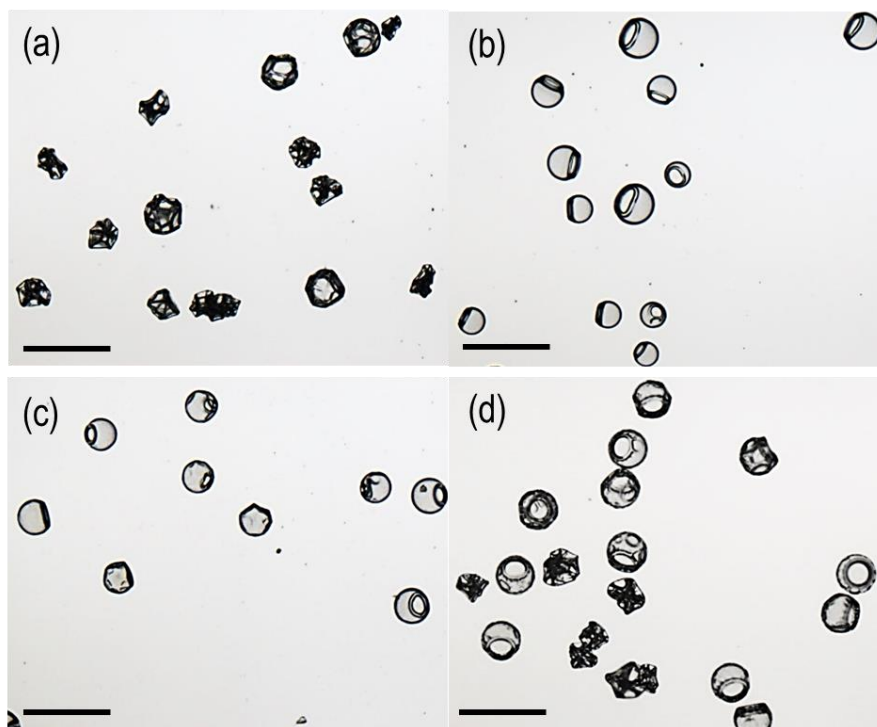


Figure 47 . Dry particles of NPC (a), WPI (b), WPI%_R = 50% (c) and SC (d). The scale bars correspond to 200 μ m.

4.3.3.2. ESTIMATION OF PARTICLE SHAPE PARAMETERS

All in all, this first qualitative analysis underlined that in WPI/NPC mixes, WPI properties at the colloid scale could have a stronger impact on powder characteristics than NPC ones. On the other hand, we also observed that the casein molecular structure influence particle size and shape. To better investigate and corroborate these outcomes, a systematic analysis of the area of particle projection, circularity and solidity was carried out in the following to quantify the main shape parameter in WPI/NPC and SC powders.

4.3.3.3. AREA DISTRIBUTION

First, an estimation of WPI, NPC (**Figure 48** a-b) and SC (**Figure 49**) dry particle area was carried out as a reference for the subsequent investigation of WPI/NPC mix powders. Despite evident qualitative and quantitative differences, we observed that all the single protein samples consisted of two main populations. In the case of WPI (**Figure 48** a), all particles exhibited their typical round and hollow shape. However, the area distribution highlighted the presence of a predominant population with a smaller cross-section area and a minor fraction (red arrow) characterized by larger one. In NPC powders (**Figure 48** b), two different morphologies were detected by microscopy observation as already mentioned in the previous paragraph: i) small, wrinkled particles (green circle) and ii) deflated-balloon particles (blue circle). This qualitative classification was corroborated by the evaluation of the area distribution: despite an evident polydispersity compared to the WPI case, it showed two peaks

consistent with the shape classification (green arrow for wrinkled particles that are major, blue for deflated-balloon ones that are minor). As it concerns SC particles, the area distribution was less polydisperse than in the case of casein micelles and most of all the fraction of bigger and deflated balloon particles (yellow arrow and circle) was significantly larger compared to smaller wrinkled ones (*i.e.*, the opposite of NPC area distribution).

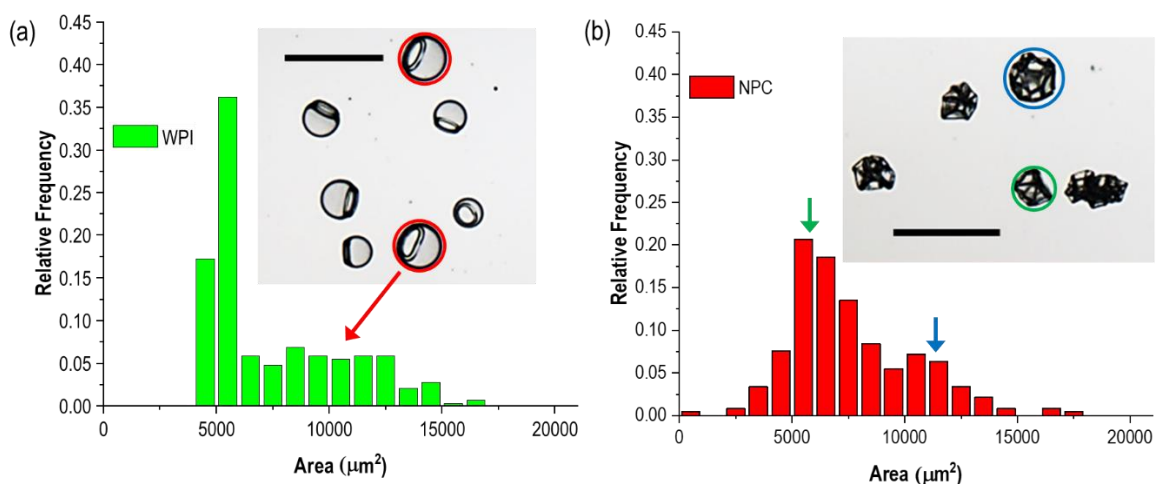


Figure 48. Cross-section area distribution of dry particles of WPI (a), and NPC (b) powders. Both curves are characterized by two peaks corresponding to two different populations differing by size and morphology, as shown in the corresponding images in the inset.

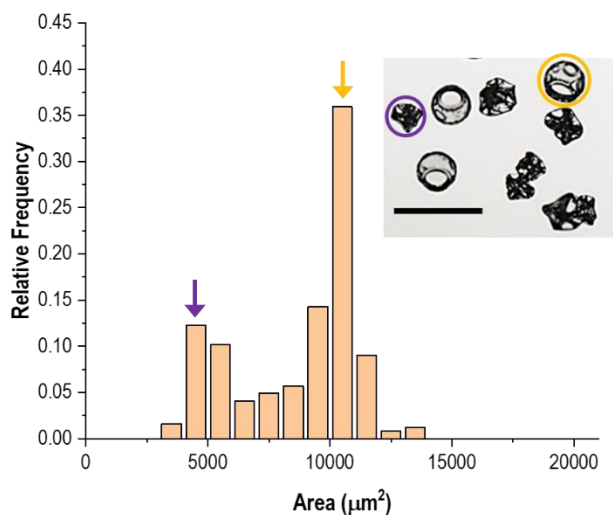


Figure 49. Cross-section area distribution of dry particles of SC powders. Similar to WPI and NPC case, the distribution is characterized by two peaks corresponding to two different populations, as illustrated in the corresponding images in the inset.

When comparing WPI and NPC to WPI/NPC mixes with $\text{WPI}\%_{\text{R}} = 50\%$ and $\text{WPI}\%_{\text{R}} = 80\%$ (Figure 50 a-b), the most glaring difference was the evident monodisperse area distribution measured in the mixes

(i.e., typical Gaussian distribution). This result reflected the qualitative observation of **Figure 47**, where only one population of dry particles was detected in the WPI/NPC mixes. Interestingly, the median values of the area distribution referring to $WPI\%_R = 50\%$ ($7500 \mu\text{m}^2$) and $WPI\%_R = 80\%$ ($6000\text{-}7500 \mu\text{m}^2$) were located in the middle region of the two peaks characterizing pure proteins distribution. To summarize, the measurement of the cross-section area underlined that the dry particles of both explored WPI/NPC mixes exhibited a hybrid shape with an average size larger than most single protein powders. Such a larger surface is probably associated to the characteristics of each of the two dairy colloids: on the one hand, NPC sponge-like structure enhanced an earlier sol-gel transition. On the other, the skin compactness due to WPI conferred an enhanced resistance to stress-induced surface deformation and avoided extensive wrinkling. This interpretation, based on the characterization of the shape indicators and therefore on a merely off-line analysis of powder properties, would anyway provide an indirect picture of the physical phenomena at the molecular scale. In particular, this would strengthen the hypothesis of protein organization at the air-liquid interface and, notably, of WPI external segregation, even for a quite rapid drying process like in monodisperse dryers.

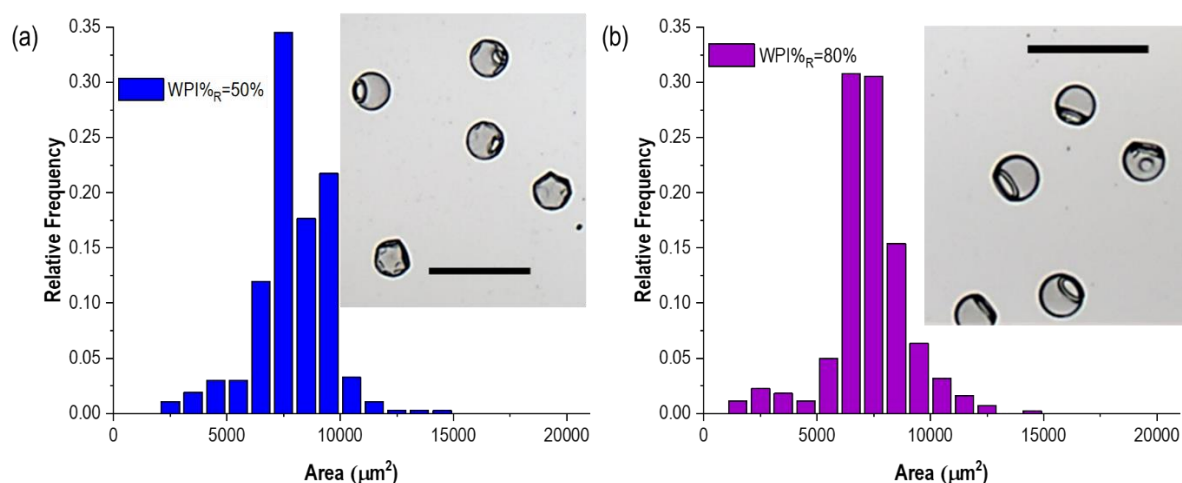


Figure 50. Cross-section area distribution of dry particles of $WPI\%_R=50\%$ and $WPI\%_R=80\%$.

4.3.3.4. CIRCULARITY

The circularity (C) was used to estimate particle shape in the two-dimension projection, and the value of circularity reflected how much a particle's shape deviates from a circle. Here, the particle circularity of pure dairy protein and WPI/NPC mixture samples was obtained by Image J analysis, and the result is presented in **Figure 51** a-b. The histogram referring to NPC and SC powders showed a large dispersity (0.25-0.925) that efficiently depicted their significant and non-repeatable deformation. Furthermore, the C frequency of NPC and SC in the range 0.85 to 1 were 34% and 60%, respectively. Therefore, SC particles presented a rounder edge compared to NPC ones. On the other hand, WPI and WPI/NPC mixtures exhibited a similar narrow-dispersed distribution (0.825-0.925) with a high median value (\approx

0.9). It is worth pointing out that, in these samples, the presence of the ‘jar opening’ induced by vacuole formation contributed to lower the circularity value, which otherwise would have been even closer to 1.

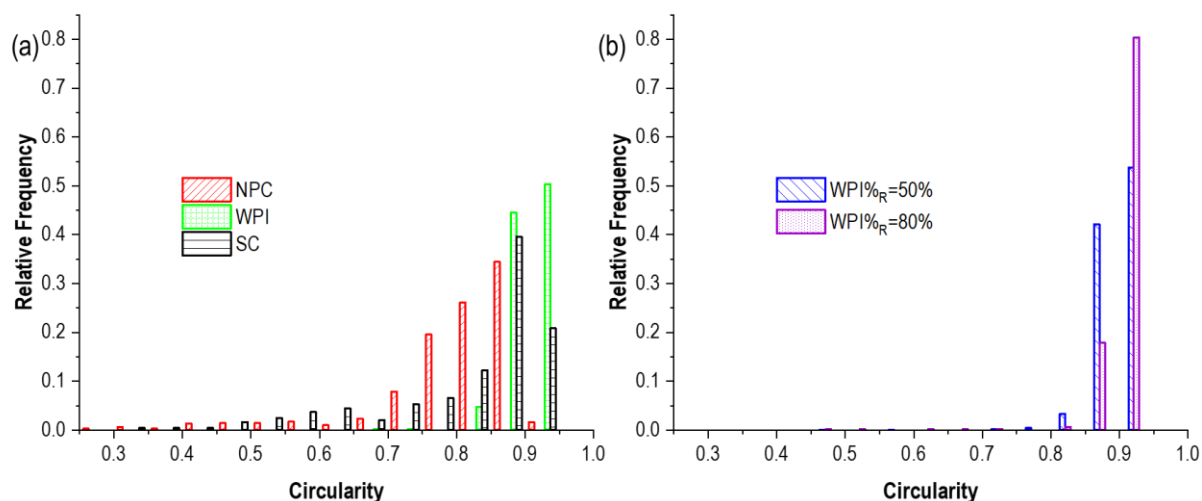


Figure 51. Distribution of the circularity in pure protein (a) and WPI/NPC mix (b) powders.

4.3.3.5. SOLIDITY

The Solidity (S) is the measurement of the overall concavity of a particle. We used solidity to explore the characteristic of particle surfaces. For example, the solidity is equal to 1 when a particle presents a perfectly smooth surface. In contrast, the particle shows a rough outline if the particle solidity is close to 0. The solidity of NPC and SC particles was in the range of 0.75 to 0.95, as illustrated in **Figure 52**, thus further underlining the irregularity and the roughness of casein powder surface irrespective of the molecular structure. Additionally, the distribution histogram related to particle solidity confirmed the similarity between WPI and WPI/NPC mix morphology. Indeed, both powders were characterized by a high median value close to 1 for most of the population. These results suggest that net of the slight surface bumps, the particle shape in WPI/NPC mixes is smooth and regular as WPI ones. These outcomes are in agreement with what observed in **Figure 36** for WPI/NPC pendant droplets, where mixes exhibited the same smooth and regular structure on the top layer of the skin at the end of the evaporation.

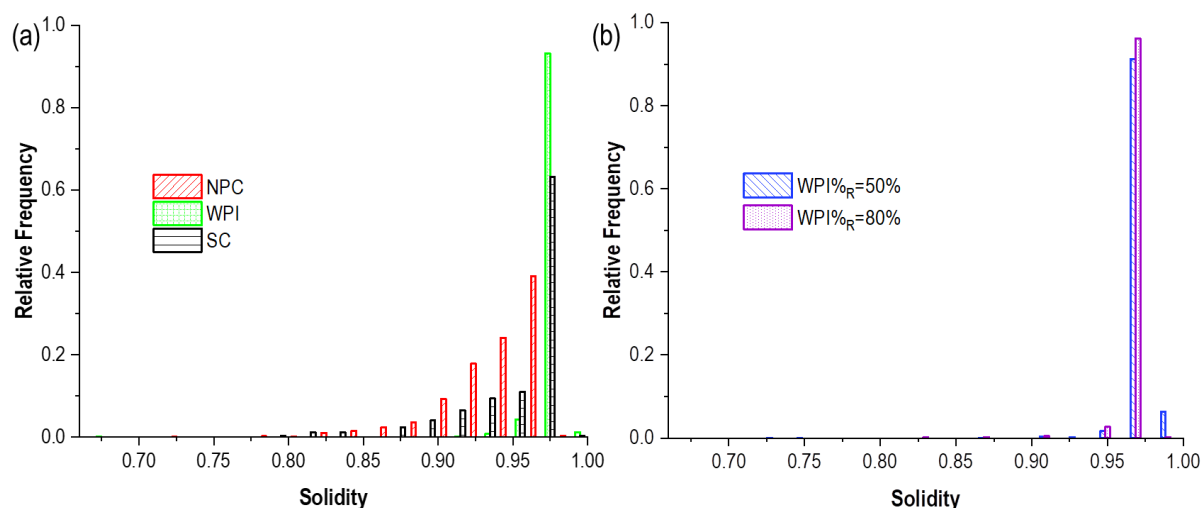


Figure 52. Distribution of the solidity in pure protein (a) and WPI/NPC mix (b) powders.

4.3.4. CONCLUSIONS

In this section, we observed the particle morphology of single SC, WPI, NPC and WPI/NPC in mix samples produced by a monodispersed spray dryer. In addition, the quantitative distribution of the key morphological parameters of the dry particles (cross-section area, circularity, and solidity) was determined to investigate possible phenomena of surface organization induced by the drying process, in analogy to what was observed at the single droplet scale. Two main results were highlighted:

1) WPI/NPC mixes exhibited a hybrid round shape, with slight bumps on the surface, thus quite similar to pure WPI powders. This similarity was confirmed also by the evaluation of particle circularity and solidity. Consequently, it is likely to predict protein segregation and, in particular, a small-on-top stratification also in flying droplets obtained by monodisperse spray drying, despite the significant rapidity of the drying process (few seconds).

2) NPC and SC dry particles, although both irregular and wrinkled, displayed evident differences in terms of roundness. Indeed, the vast majority of NPC powders consisted of star-like small, wrinkled particles, whereas SC ones were mainly composed of larger and round particles, similar to deflated balloons. This could be linked to the different skin properties induced by protein size in the initial dispersions. Small SC colloids, in analogy to WPI ones, would tend to form a regular compact skin able to withstand the surface instabilities leading to the typical buckling phenomena of casein micelles.

In general, the outcomes obtained by monodisperse spray drying method showed interesting similarities with the results presented in the sections 4.1 and 4.2 on the drying of single droplets of dairy protein suspensions. Therefore, this could pave the way to further and more systematic investigation resulting in the tight control of powder morphology and functional properties.

4.4. COUPLING REACTION ENGINEERING AND ENERGY MAP APPROACHES

4.4.1. INTRODUCTION

Drying is a central processing way in order to preserve biological materials, but as food raw material present a complex composition, structure and thereafter physicochemical behavior, the basic understanding of drying applied to food has not been fully established (Heldman & Lund, 1992; Rahman, 1995). Spray drying is one of the most popular approaches in the manufacture of powdered products. In the last decades, several research groups have been studying spray drying modeling in the practical utility of dimensioning and operating spray dryers in various applications. Among the different modelling approaches, the computational fluid dynamic has become yet a powerful tool in the spray drying process with the technology advance, and it can be used to optimize the spray dryer operation (L. Huang et al., 2004; Nijdam et al., 2004). However, it is necessary in the detailed simulation of the spray dryer to consider both the drying characteristic of the single droplet and wide dryer simulations incorporating computational fluid dynamics (Chen & Lin, 2005, 2005; L. X. Huang et al., 2005; Langrish & Fletcher, 2001; S. X. Q. Lin & Chen, 2002; Southwell et al., 2001). In view of correctly taking account of product-process interactions, the specific behavior of the product should be integrated as differences between formulas can be pretty significant (Chen & Xie, 1997). Lin and Chen adopted the glass filament method to study the drying history of a single droplet in isothermal drying air conditions and describe the product behavior as a function of water content through a normalized activation energy curve. They named this approach the reaction engineering approach (REA). Furthermore, the REA model predicted well the droplet drying history under variable drying conditions and has been validated experimentally first for skim and whole milk, latter on other dairy fluids such as cream and whey or milk protein concentrate (Chen & Lin, 2005; Chew et al., 2014; S. X. Q. Lin & Chen, 2002, 2007; Patel & Chen, 2008). Overall and regardless of the product, it has been shown that the experimental data were in good agreement with the REA predictions.

From the physical point of view, water evaporation leads to the phase transition from the liquid phase to the solid phase. Upon drying, the droplet moisture moves toward the environment, inducing the air interface to recede and the solutes to concentrate at the interface. Furthermore, this receding interface pushes the solutes toward the droplet center, as a result of the concentration gradient of solute and solvent developing in the droplet with evaporation progress. The consequences of such spatial and temporal heterogeneities are multiple. A model based on the momentum balance on the colloids and the fluid, known as the energy map model (Bacchin, 2017), can be helpful to describe the colloid interaction with the air-liquid interface, the receding interface being accounted for with a

moving energy map during the drying process. In previous work, Bacchin et al. (Bacchin et al., 2018)) established the energy map model describing the impact of colloidal-interface interactions in dynamic permeable flow through a semipermeable interface. In order to describe the non-equilibrium transfer, they used an energy barrier to represent the interface, the colloid having to overcome the energy barrier to be transported to the other side of the membrane. Moreover, the repulsion between colloids and the interface can be described by the interfacial pressure minus the water activity. The interfacial pressure is linked to the bulk's colloidal osmotic pressure when the interface is close to the equilibrium condition.

As such, REA and energy map approaches rely on similar concept: evaporation needs to overcome the water's activation energy at the interface. Therefore, coupling the REA and EMM could help to understand the droplet drying behavior from the physical point of view, all along with a prediction of the final product characteristics.

In this work, we applied the REA model to NPC in order to establish the relationship between the moisture content and the required energy for evaporation. The glass filament method (mass measurements) was used to measure the drying kinetics of NPC droplets and obtain the master normalized activation energy curve of the REA model. On the other hand, we considered the phase diagram of NPC proposed by Bouchoux et al. (Bouchoux, Cayemitte, et al., 2009) that links the moisture content and the interface's osmotic pressure in order to apply the energy map model. Finally, the two approaches were implemented and compared.

4.4.2. MODELLING STRATEGIES

4.4.2.1. ESTABLISHMENT OF THE NORMALIZED ACTIVATION ENERGY MASTER CURVE

The Reaction Engineering Approach was proposed by Dong and Xie in 1997(Chen & Xie, 1997). They expressed the idea that evaporation is an activation process that can take place when the energy barrier to transfer liquid water to vapor is exceeded. As we know, the driving force of evaporation is the vapor density gradient between the droplet interface and the hot surrounding air. Thus, the drying rate can be linked to the vapor density at the droplet surface:

$$\frac{d_m}{dt} = h_m A (\rho_{v,s} - \rho_{v,b}) \quad (\text{Eq. 10})$$

Where dm/dt and A refer to drying rate ($\text{kg}\cdot\text{s}^{-1}$) and droplet surface area (m^2), respectively. h_m stands for mass transfer coefficient ($\text{m}\cdot\text{s}^{-1}$), that can be obtained from the modified Ranz Marshall correlation(Chen & Xie, 1997):

$$Sh = \frac{h_m d_p}{D} = 1.63 + 0.54 Re^{1/2} Sc^{1/3} \quad (\text{Eq. 11})$$

Sh , Re and Sc being the Sherwood, Reynolds and Schmidt numbers, respectively. The Sherwood number (Sh) is a dimensionless number used in mass-transfer operation. It represents the ratio of the convective mass transfer to the rate of diffusive mass transport. The Reynolds number (Re) is the ratio of inertial forces to viscous forces within a fluid that is subjected to relative internal movement due to different fluid velocities. It characterizes the flow close to the droplet surface throughout the drying process. The Schmidt number (Sc) is the ratio of the shear component for diffusivity viscosity/density to the diffusivity for mass transfer. It is physically related to the relative thickness of the hydrodynamic layer and mass-transfer boundary layer.

Moreover, $\rho_{v,s}$ and $\rho_{v,b}$ are corresponding to the vapor concentration (kg.m^{-3}) at the droplet-air interface and of the bulk air, respectively. Interestingly, during the drying process, the vapor density at droplet surface is variable, but it can be described as a function of the saturated vapor density at the surface temperature:

$$\rho_{v,s} = \varphi \rho_{v,sat}(T_s) \quad (\text{Eq. 12})$$

Where T_s refers to the surface temperature, which equals the droplet temperature (T_d) during the drying process ($Bi < 0,1$; (Chen & Peng, 2005)). The fractionality coefficient (φ) corresponds to the surface water activity, establishing the relationship between the vapor density at the droplet surface and the saturated vapor density ($\rho_{v,sat}$) that can be calculated as a function of T_s :

$$\rho_{v,sat} = 4.844 \times 10^{-9} \times (T_s - 273)^4 - 1.4807 \times 10^{-7} \times (T_s - 273)^3 + 2.6572 \times 10^{-5} \times (T_s - 273)^2 - 4.8613 \times 10^{-5} \times (T_s - 273)^1 + 8.342 \times 10^{-3} \quad (\text{Eq. 13})$$

φ can be correlated to the activation energy of evaporation using the Arrhenius equation:

$$\varphi = \exp\left(-\frac{\Delta E_v}{RT_d}\right) \quad (\text{Eq. 14})$$

Where ΔE_v and R are the apparent activation energy (J.mol^{-1}) of droplet evaporation and gas constant number ($8.314 \text{ J.mol}^{-1}.\text{K}^{-1}$). Therefore, the drying rate can be rewritten considering Eq. 10, 12 and 14:

$$\frac{dm}{dt} = h_m A (\rho_{v,sat}(T_s) \exp\left(-\frac{\Delta E_v}{RT_d}\right) - \rho_{v,b}) \quad (\text{Eq. 15})$$

dm/dt , T_d and A can be obtained from single droplet drying experiments, while h_m and $\rho_{v,sat}$ can be calculated using Eq. 11 and 13, respectively. Finally, the apparent activation energy (ΔE_v) is obtained:

$$\Delta E_v = -RT_d \ln\left(\frac{\frac{dm}{dt} \times \frac{1}{h_m A} + \rho_{v,b}}{\rho_{v,sat}}\right) \quad (\text{Eq. 16})$$

In the ideal condition, at the end of the drying process, droplet moisture content reaches equilibrium humidity (near to zero), and the apparent activation energy tends to a maximum. Therefore, the drying rate (dm/dt) equals 0, and Eq. 16 can be modified in order to calculate the maximum value of apparent activation energy.

$$\Delta E_{v,b} = -RT_d \ln\left(\frac{\rho_{v,b}}{\rho_{v,sat}}\right) \quad (\text{Eq. 17})$$

The relative apparent activation energy is obtained by normalizing ΔE_v by $\Delta E_{v,b}$. As a result, the relationship between relative activation energy ($\Delta E_v/\Delta E_{v,b}$) and moisture content of droplets can be obtained:

$$\frac{\Delta E_v}{\Delta E_{v,b}} = f(X - X_b) \quad (\text{Eq. 18})$$

Where X refers to the droplet moisture content (w/w), and X_b to the equilibrium moisture content. Eq. 18 reflects the energy to overcome to evaporate water from droplets as a function of moisture content. Extensive work of XD Chen group has shown that this relationship is a master curve of the drying behavior of the material, that applies satisfactory regardless of the initial solid content of sample and the drying temperature conditions.

4.4.2.2. VALIDATION OF THE NORMALIZED ACTIVATION ENERGY MASTER CURVE THROUGH PREDICTION OF DROPLET TEMPERATURE

In order to validate the fit of the characteristic master curve, droplet drying history was predicted and compared with experimental data. For this purpose, the energy conservation equation was established considering that the droplet internal energy equals the heat transfer energy induced by temperature difference between hot air and droplet surface, minus the energy consumed for water evaporation:

$$mC_{p,d} \frac{dT_d}{dt} = hA(T_b - T_d) - \Delta H_l m_s \frac{dX}{dt} \quad (\text{Eq. 19})$$

Where m , m_s , $C_{p,d}$ and ΔH_l stand for droplet mass (kg), dry matter content mass (kg), specific capacity of the droplet ($J.kg^{-1}.K^{-1}$) and the latent heat of evaporation ($J.K^{-1}$), respectively. h is the heat transfer coefficient ($W.m^{-2}.K^{-1}$) given by the correlation:

$$h = (2.04 + 0.62Re^{\frac{1}{2}}Pr^{\frac{1}{3}}) \frac{k_b}{d_p} \quad (\text{Eq. 20})$$

Re and Pr being the Reynolds and Prandtl numbers, respectively. The Prandtl number is defined as the ratio of momentum diffusivity to thermal diffusivity.

The prediction of droplet drying history using the REA model was obtained as following: Firstly, the mass and heat transfer coefficient were calculated using Eq. 11 and 20. Moreover, the saturated vapor density was calculated with the initial droplet temperature (Eq. 13). Secondly, the activation energy of the initial droplet was calculated by Eq. 16 with droplet mass and saturated vapor density. Next, the vapor density of the droplet surface was calculated by combining Eq. 12, 13 and 14. Moreover, the drying rate (dm/dt) was further determined by Eq. 10. The next stage consisted in calculating dT/dt (Eq. 19) and predict the droplet temperature for the next interval (time interval considered: 0.5 s). It should be noticed that the droplet area for the next interval can also be determined from the relationship between diameter shrinkage and droplet moisture. Finally, the drying history of the droplets during the drying process was predicted from this iterative calculation.

4.4.2.3. COUPLING THE TWO MODELLING APPROACHES BY LINKING WATER ACTIVITY AND THE INTERFACIAL PRESSURE

During the drying process, droplet shrinkage tends to accumulate the NPC molecule at the interface. Thus, extra energy is needed for bringing solute to the concentrated interface as this latter repels NPC molecules. The energy cost per volume unit is given by the integration across the interface of the additional pressure ($\int \phi d\Pi_{ic}$), and the contribution of this energy to the chemical potential of water ($V_{wl} \int \phi d\Pi_{ic}$), leads to define the water activity related to the interfacial pressure (Π_{ic}) as (Bacchin, personal communication):

$$a_{w\ int} = e^{\frac{-V_{wl} \int \phi d\Pi_{ic}}{kT}} \quad (\text{Eq. 20})$$

The evaporation rate is linked to the water activity related to the interfacial pressure and the volume fraction close to the interface. It should be highlighted that at close-to-equilibrium conditions, the thermodynamic (reversible) colloid pressure gradient ($\nabla\Pi_{cc}$, that corresponds to the colloid-colloid interaction) offset the interfacial pressure ($\phi \nabla\Pi_{ic}$, that corresponds to the colloid-interface interaction):

$$\int \phi d\Pi_{ic} = - \int d\Pi_{cc} \quad (\text{Eq. 21})$$

Thus, the water activity is directly linked to the colloidal osmotic pressure in bulk (Bacchin, personal communication):

$$a_w = e^{\frac{-V_{wl} \Pi_{cc\ th}}{kT}} \quad (\text{Eq. 22})$$

Therefore, the droplet interfacial water activity can be described in a dynamic way (on the equilibrium state) when the vertical concentration variation exists close to the interface. Another way to define

the water activity as a function of the interfacial pressure is to consider the fluid depression that should exist close to the interface. Broadly, this approach considering interfacial pressure is very similar to the reaction engineering approach. As already mentioned, evaporation is an activation process that needs to overcome an energy barrier for water evaporation. The energy barrier relates to the interface pressure ($\Delta E_v = V_{wl} \int \phi d\Pi_{ic}$, V_{wl} being the molar volume of water, equal to $1.8 \cdot 10^{-5} \text{ mol.m}^{-3}$). It should be noticed that the surface relative humidity is then equivalent to the water activity at the interface given by Eq. 14. Reaching the equilibrium condition upon drying, the interfacial pressure is close to the osmotic pressure, and the energy barrier can be rewritten as:

$$\Delta E_v = V_{wl} \Pi_{cc} \quad (\text{Eq. 23})$$

Additionally, coupling the relative activation energy of NPC droplet variation with moisture content, described by Eq. 18, with Eq. 23, give access to the relationship between moisture content and osmotic pressure:

$$\Pi_{cc} = \Delta E_{v,b} f(X - X_b) \quad (\text{Eq. 24})$$

4.4.3. RESULTS AND DISCUSSION

4.4.3.1. NPC DROPLET DRYING CURVE

The drying history of NPC droplet (temperature, mass and diameter) was obtained at different drying temperatures using suspended single droplet drying experiment (**Figure 53**). **Figure 53.a** presents the drying temperature and droplet mass variation with time, that were linked through the coupled heat and mass transfer and presented opposite evolution as expected. At the beginning of drying, droplet temperature rapidly increased to the wet-bulb temperature when it met hot air and kept this value all along the constant rate drying stage. Indeed, droplet weight curve reduced with a linear tendency at the early drying stage. Moreover, the higher the drying temperature, the shorter the constant rate drying stage. At the end of the constant rate drying stage, the evaporation rate slowed down and the mass curve reached a plateau. Conversely, the temperature curve raised toward that of hot air, finally reaching a plateau at an asymptotic value 1 to 3°C below that latter.

In fact, the temperature of hot air has two different applications in drying: heating droplets to increase temperature and overcoming the latent heat of moisture evaporation. As the initial droplet contained abundant free moisture, most of the energy was used to evaporate water from the droplet, apart a small part transferred to the droplet internal energy. Therefore, droplet mass reduced faster, and the temperature slightly raised. However, with drying continuation, the evaporation rate started to decrease because of limiting moisture content at the surface and skin development impeding the

water transfer to this latter. Thus, more energy was used to heat droplets, which induced a rapid increase of the temperature to grow rapidly until the droplet temperature reached the drying temperature. Last, the temperature finally kept constant because almost no water could be evaporated from the droplet at the end of drying.

Droplet diameter presented a similar behavior regardless of the drying temperature (**Figure 53b**): as expected, it decreased at a rate depending on the drying temperature before arriving at the final plateau, at a value higher with increasing drying temperature. The insert in **Figure 53b**. (insert 1 to 5 with increasing time) illustrate the droplet shape at the different slope changes of the diameter curve. The initial droplet presented a spherical shape and shrunk homogenously at the beginning (insert 1). First slope change matched with the droplet bottom vertical extension (insert 2): the droplet bottom evaporated faster and formed a local gelation area, affecting the droplet surface tension force. With drying continuation, a gelled layer covered the droplet surface, and vertical extension stopped (insert 3). Then the droplet shape started to shrink due to the droplet solidification; simultaneously, the droplet diameter curve slope changed again (insert 4). Last, the droplet diameter kept a final stable value (insert 5).

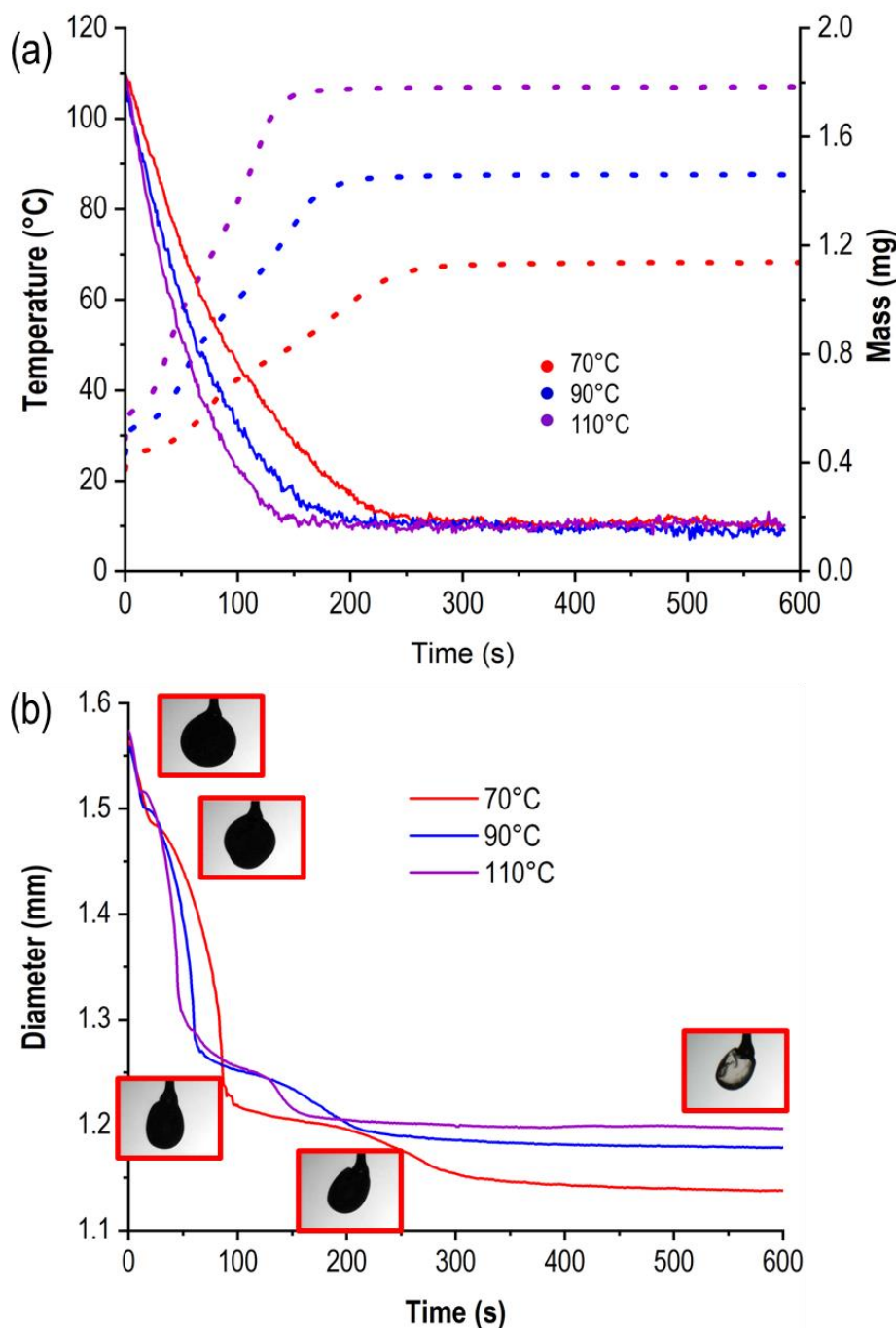


Figure 53 : (a) Temperature, mass and diameter of NPC droplet (10 w/w %) evolution at different drying temperatures (70°C, 90°C and 110°C). Each line is the average result of 3~5 repetitions. The inset droplet images were obtained from the video of droplet drying at 70°C.

4.4.3.2. RELATIVE ACTIVATION ENERGY CURVE OF NPC DROPLET

The activation energy of water evaporation was calculated with Eq. 16, then ratioed with the equilibrium activation energy. The relative activation energy variation with droplet moisture content ($X - X_b$) is described in Figure 54. The moisture content (X) was calculated by the fitted mass data (Table curve software). It should be noticed that regardless of the drying temperature, the $\Delta E_v/\Delta E_{v,b}$ evolution

of NPC droplets were merged (**Figure 54 a**). Therefore, the relative activation curve of NPC droplets can be resumed to a general trend and fitted with an empirical equation, picturing the drying behavior of casein micelles:

$$\frac{\Delta E_v}{\Delta E_{v,b}} = 1.03 e^{-0.66(X-X_b)^{0.63}} \quad (\text{Eq. 25})$$

In comparison, the unified correlation obtained for skim and whole milk (Chen and Lin, 2005) showed higher values of the coefficient in the exponential:

$$\frac{\Delta E_v}{\Delta E_{v,b}} = 0.98 e^{-1.35(X-X_b)^{0.93}} \quad (\text{Eq. 26})$$

The corresponding fit of the NPC master curve is presented in **Figure 54 b**. It is very representative of the curves previously reported for other dairy fluids (Chen & Lin, 2005; Chew et al., 2014). Overall, the fitting curve showed a good agreement with experimental data. Moreover, the $\Delta E_v/\Delta E_{v,b}$ curve can be divided into three different stages. During the early drying stage, $\Delta E_v/\Delta E_{v,b}$ reached its starting point (transient stage) and rose slowly up to a moisture content of around 8 kg.kg⁻¹. This observation illustrates that the ‘energy barrier’ needed to be overcome for water evaporation at the first drying stage is low, as the moisture removal from the droplet can freely occur. As evaporation progressed ($1 < X-X_b < 8$ kg.kg⁻¹), $\Delta E_v/\Delta E_{v,b}$ presented a continuous increase tendency, reflecting the increasing resistance to moisture evaporation from the droplet, casein micelle gradually concentrating and forming a gelled layer on the droplet surface. As the droplet gradually solidified at the end of the drying stage, the activation energy drastically increased until the moisture content of the particle reached equilibrium ($X-X_b < 1$ kg.kg⁻¹).

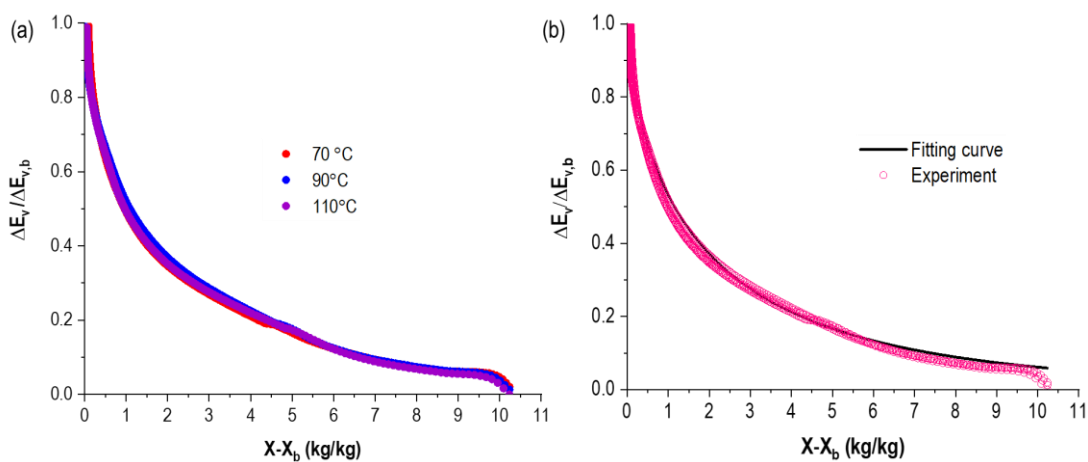


Figure 54 : (a) Relative activation energy variation as a function of moisture content at three drying temperatures, (b) Fit of the $\Delta E_v/\Delta E_{v,b}$ master curve (black solid line) with experimental data.

4.4.3.3. PREDICTION OF DROPLET DRYING HISTORY BY REA

In order to verify the prediction ability of this master curve, we used mass and energy transfer equations to predict the droplet drying history at the three drying temperatures considered (**Figure 55**). It can be seen that the prediction data closely followed the experiment result. Specifically, the transition of mass curves was accurately predicted. In general, the mass profiles of prediction were better predicted than temperature. However, the prediction curve of temperature can be used to describe different heating stages. Therefore, the master curve of NPC is well designed to precisely predict the water removal history during the drying process.

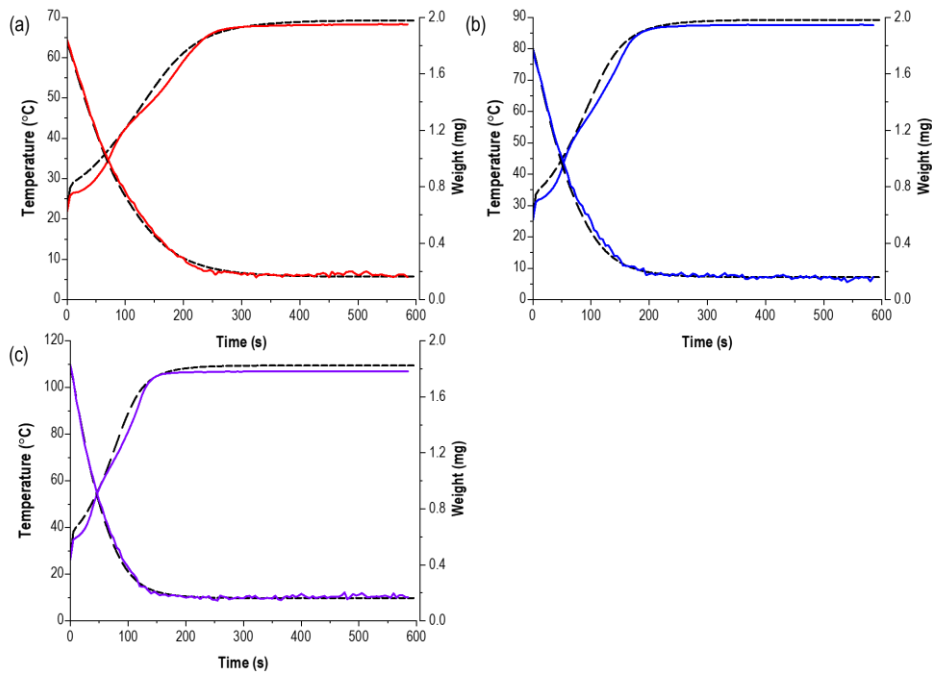


Figure 55 : Fit of temperature and mass at 70°C (a), 90°C (b) and 110°C (c).

4.4.3.4. COUPLING THE REA AND ENERGY MAP(REA-EMM)

Bouchoux et al. (Bouchoux, Cayemitte, et al., 2009) studied the osmotic pressure evolution in different phase transitions and built a model to describe the osmotic pressure (Π) variation with sample concentration:

$$\Pi = \left(1 - \frac{C}{C^*}\right)^{-4} * 14C \quad (\text{Eq. 27})$$

Where C and C^* refer to the sample NPC concentration and the critical concentration ($750 \text{ g}\cdot\text{L}^{-1}$) considered on Bouchoux's work. The volume concentration of NPC was converted in mass concentration of moisture content X , and then the osmotic pressure of NPC with X was deduced from Eq. 27 (**Figure 56 a**). The osmotic pressure kept a low value in the dilute state (close packing transition;

$5 < X < 6.7 \text{ kg.kg}^{-1}$), gently increased in the transition region ($3 < X < 5 \text{ kg.kg}^{-1}$), then rapidly rose when NPC arrived at the concentrated state ($X < 3 \text{ kg.kg}^{-1}$).

Besides, the interfacial osmotic pressure of the NPC droplet can be calculated at a given moisture condition, combining Eq. 23 and 24 (**Figure 56 b**). Π_{cc} presented a continuously increased tendency with the NPC droplet drying process. As evidence, the order of magnitudes of osmotic pressure ($\Pi_{cc} > 1000\Pi$) was strongly different according to REA and EMM approaches. This shift can rely on different reasons:

- i) The NPC powder used in the single droplet experiments included around 15% non-casein constituents (whey protein, non-protein nitrogen, lactose and minerals), that were concentrated in the final particle with evaporation. These constituents present a low molecular weight, and their concentration should therefore substantially impact the osmotic pressure; in contrast, Bouchoux et al. (2009 a) used dialysis to concentrate the casein micelle, keeping constant the non-casein constituents' concentration.
- ii) Moreover, Bouchoux et al. (Bouchoux, Cayemitte, et al., 2009) forced the NPC dialysis to a predetermined osmotic pressure Π up to an equilibrium state. In this regard, Π_{cc} was calculated at non-equilibrium conditions all along the drying dynamics.

In order to fill this gap, we aimed at studying the impact of the non-casein constituents on the osmotic pressure and measure the osmotic pressure of the NPC used in this study closer to the equilibrium state through dynamic vapor sorption (DVS) experiments. This is the purpose of next paragraph.

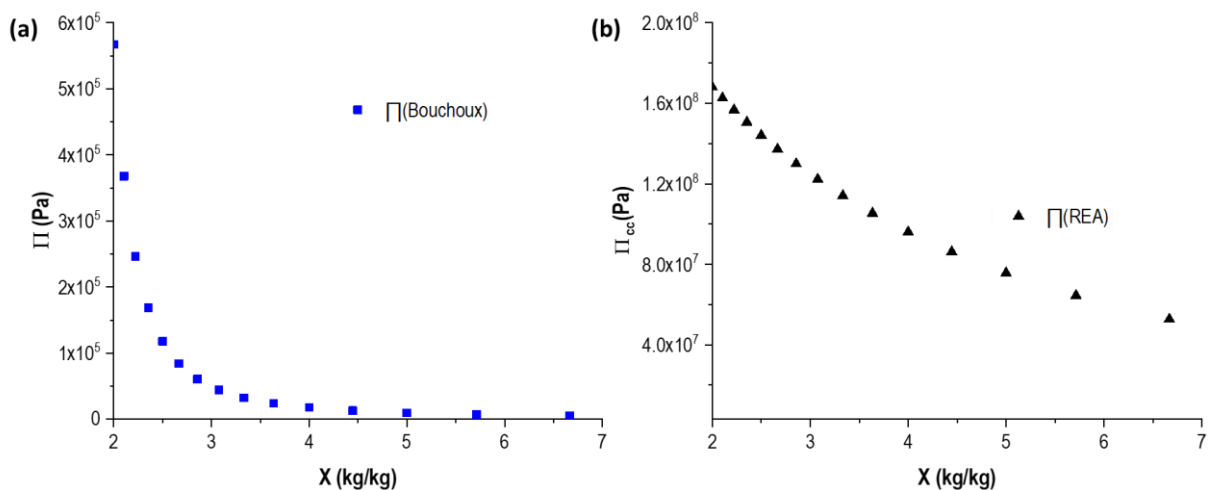


Figure 56 : Osmotic pressure of NPC as a function of moisture content calculated by EMM from Bouchoux et al. (2009a) data (a) and REA (b).

4.4.3.5. OSMOTIC PRESSURE OBTAINED FROM SORPTION ISOTHERM

The osmotic pressure at the equilibrium was deduced from the NPC sorption isotherm obtained from DVS measurement. In this experiment, the mass of NPC powder was measured at different saturated vapor conditions and corresponding moisture content was further deduced (Table 16). Using the non-simplified Van't Hoff equation to describe the osmotic pressure is another way to express the water activity. Therefore, the osmotic pressure was calculated with Eq. 22, and Π variation with X was subsequently obtained. Besides, the osmotic pressure was also calculated by the REA model at the same X values, and both approaches plotted on the same graph (**Figure 57**). Although the Π values stand in the same range, the REA ones were approx. one decade higher than the ones calculated from the sorption approach. One explanation could be that the REA approach considers the pressure exerted at the particle interface at a non-equilibrium state, whereas the sorption approach refers to the overall pressure at the equilibrium (no differences from the surface to the core of the particle).

Table 16. Water activity, mass of NPC, moisture content during NPC sorption.

a_w	0	0.1	0.2	0.3	0.4	0.5	0.6	0.7	0.8	0.9	0.95
Mass (g)	9.32	9.52	9.64	9.75	9.90	10.08	10.26	10.44	10.77	11.62	12.42
X (kg.kg⁻¹)	0	0.021	0.035	0.047	0.062	0.082	0.100	0.121	0.155	0.247	0.333

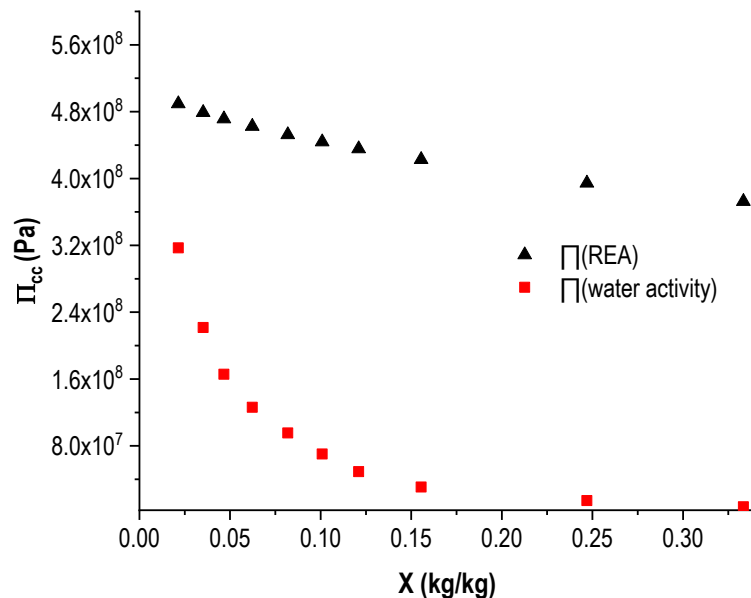


Figure 57 : Comparison of osmotic pressure calculated by different approaches at the same condition

4.4.4. CONCLUSIONS

In this work, we obtained the master normalized activation energy curve of NPC and checked the satisfactorily prediction ability of REA model based on this value. Further, the REA and EMM were applied to the drying of NPC solution to describe the osmotic pressure variation with the moisture content at the droplet interface. However, the osmotic pressure obtained from the REA model was more than 3 decades higher than that extracted from the phase diagram of NPC proposed by Bouchoux et al. (2009a). This difference in the order of magnitude might be due to the concentration of small non-casein solutes (salts, lactose) that have a significant contribution to the osmotic pressure in our NPC, or because of difference in equilibrium / non-equilibrium conditions at which osmotic pressure was considered. Last, we used the water activity to determine the osmotic pressure of the NPC powder at an equilibrium state. Although the result better matched with the REA approach, the order of magnitude was still one decade lower than that of this latter. Therefore, more work is needed to achieve our goal. One perspective would be to consider a purified source of NPC (diafiltration or dialysis), in order to avoid the influence of small non-casein solutes on osmotic pressure.

GENERAL CONCLUSION AND PERSPECTIVES

Conclusions

This work focused on the droplet-particle formation process in mixes of milk proteins (whey protein and casein micelles), which are essential ingredients with high nutrition and function in infant formula milk powder, whose characteristics strongly influence the final quality of the powder. Skin layer formation and evolution were investigated in different drying stages (early drying stage of sol-gel transition, later sol-gel transition stage and the solidification stage) with different experiment setups (tensiometer, pendant single droplet drying setup). Moreover, the effect of composition, controlled by varying the protein ratio, and concentration of whey protein and caseins micelles on the droplet drying history were studied with different instruments (high-speed camera, microscopy, microbalance and scanning electron microscopy). Shape factors of dairy mixes powder obtained from monodispersed spray drying were analyzed by the image analysis method. Furthermore, the reaction engineering approach model of NPC was established based on the glass filament single droplet drying experiment. Therefore, the simple conclusion of this project can be divided into five different parts.

Part 1: The small-on-top segregation of WPI on the droplet top layer during the drying-induced skin formation and evolution.

In the WPI/NPC droplet drying process, the morphological evolution and drying kinetics with time highlighted the crucial role played by WPI in the drying dynamics despite being the minor component of the suspension in terms of volume fraction. Indeed, when the whey protein composition arrived at a critical value ($20\% < \text{WPI}\%_{\text{RC}} < 50\%$) in the initial suspension, the WPI colloids confer to droplets a rigid skin with higher resistance to buckling. This enhanced mechanical performance indicates that WPI may have external separation caused by drying, as shown in previous work on binary system suspensions consisting of model colloids. This hypothesis of protein stratification during the drying process was verified by direct observation of the skin layer structure of WPI/NPC particle by SEM, and the result highlighted WPI molecule accumulation on the top surface (small-on-top auto-arrangement). The segregation behavior of WPI and NPC under certain conditions was interpreted in the light of the ZJD model for binary systems. According to this theory, the accumulation of colloids on the droplet surface throughout water evaporation led to increased osmotic pressure, thus favoring the motion of smaller macromolecules to the air-liquid surface. Surprisingly, although WPI and NPC exhibited different structure and physicochemical properties that could influence the droplet drying process, the size ratio of the two proteins was the main parameter to control the stratification. We also showed by oscillatory drop tensiometer that the small-on-top re-arrangement could also be driven by aging surface gelation.

This suggests that evaporation is not a prerequisite for colloid auto-stratification but rather the development of local concentration gradients near the droplet surface.

Part 2: Do the protein structure and resulting physicochemical properties impact the drying behavior of binary mixes droplet (whey protein and caseins)?

We replaced the NPC micelles with SC in the suspensions because NPC and SC consist of α , β , κ -casein, but with different structural forms. When comparing the drying process of NPC and SC, the results illustrated that, despite glaring structural differences, the chemical characteristics of NPC and SC macromolecules provided similar high deformability to droplet skin and a significant attenuation of the delamination at the borders. On the other hand, the global shrinkage of the droplets, which is influenced by the achievement of the sol-gel transition at the air-liquid interface, was strongly affected by the average colloid size, as evidenced by the consistency of final apex height in WPI/SC samples (proteins with comparable size) and the significant decrease with $WPI\%_R$ in WPI/NPC mixes. However, the observation of droplet profile modification during the drying process does not allow to gather any possible evidence of self-stratification in WPI/SC, thus paving the way to further ongoing investigation (confocal microscopy, SEM).

Part 3: Impact of overall protein concentration (c_p) on drying droplets of dairy protein.

In this part, we explored the effect of protein concentration, ranging from 6 w/w % to 14 w/w %, on particle morphology with different $WPI\%_R$. The results underlined a decreasing droplet diameter reduction with higher concentration, which resulted in the transition from border delamination to simple shrinkage. This behavior was interpreted in the light of the effective composition of the powders used for sample preparation. Indeed, the WPI powders do not consist of whey proteins only, but they include also around 5% of caseins. Therefore, droplets with higher concentration corresponded also to higher casein molecule amount, which favored the adhesion between the substrate and droplet border and, consequently, mitigated the delamination behavior. Additionally, a higher final apex height was measured in dried droplets with increasing c_p . This tendency was explained by the earlier occurrence of the sol-gel transition with increasing protein concentration due to the achievement of a critical colloid concentration at droplet surface. All in all, these outcomes showed that sample composition ($WPI\%_R$) affects sol-gel transition dynamics at droplet surface and triple-line, but these phenomena are strongly attenuated with increasing concentration due to crowding effects and to the physico-chemical properties of NPC micelles. This global overview on the impact of suspension composition and concentration on droplet final morphology led to the

construction of a first phase diagram able to predict dairy particle shape depending on the initial dispersion characteristics (c_p and $WPI\%_R$).

Part 4: Comparison of shape characteristics between particles produced by single droplet approach and monodisperse spray drying.

WPI, NPC, and WPI/NPC mix powders were produced by monodisperse dryers. The key shape parameters (area distribution, circularity, and solidity) of the dry particles were observed by optical microscopy and characterized by image analysis. A similar approach was used to also investigate the morphology of SC powders and to make a comparison with the WPI/NPC samples. Interestingly, the single droplet drying in pendant configuration and the drying flying droplet approach resulted in very good agreement. Indeed, WPI/NPC powders obtained by monodisperse spray drying displayed a hybrid shape with significant similarities to the round hollow shape typical of whey proteins, thus suggesting a possible protein auto-stratification even after rapid drying process (few seconds). On the other hand, the observation of SC particles highlighted a more significant roundness compared to NPC ones. This analogy with WPI samples underlined the possible key role played by protein size on skin formation and surface instabilities.

Part 5: Coupling the REA model and EMM of NPC.

The relationship between the relative activation energy and moisture content was established during the drying process based on the glass filament single droplet drying experiment. Coupling the REA and EMM, we obtained an equation (REA-EMM) that can picture the interfacial osmotic pressure of droplet variation with moisture content in the drying process. This modeling aims to link to phase transition with drying kinetics. However, the value of osmotic pressure calculated with REA-EMM was 1000 times more than the literature introducing NPC's osmotic pressure at different phase regions. Moreover, the osmotic pressure of NPC at equilibrium condition obtained from sorption isotherm was closer to the result obtained from the REA-EMM equation. It should be highlighted that the material includes around 15% non-casein small solutes, and the concentration of these later (mostly salts and lactose) positively affects the osmotic pressure within the whole particle. Furthermore, the REA-EMM model overestimated the osmotic pressure evolution during the drying process by solely considering the interfacial osmotic pressure, and not consider the osmotic pressure in the particle center part. This work only provides some preliminary results to connect the phase transition with drying kinetics.

Perspectives

The innovative results of this Ph.D. project represent a first step towards the full understanding of the skin formation mechanisms in drying dairy protein mixes. In the next future, the experimental activity will be devoted to the further characterization of the different stages of the sol-gel transition at droplet surface, using both single pendant droplet and flying monodisperse methods, and to the investigation of the physics of drying-induced stratification, shedding light on the specific role of each protein on the final interfacial structure.

For example, it will be crucial to visualize and quantify the internal flows in the droplets during the evaporation, by specifically labeling a portion of the whey proteins and the caseins in the mixes, using the protocol already tested at the STLO in Rennes. Previous studies have shown good results for the labelling of β -lactoglobulin with FITC and the labelling of α s1-casein with RITC. These probes can be used jointly, as their excitation wavelengths are 488 and 543 nm, respectively, while their emission wavelengths are 525 and 580 nm, respectively. It should first be established that their use in mixture does not lead to non-radiative emission transfer between the two probes (Fröster Resonance Emission Transfer). In addition, it would be interesting to explore the opportunity of using alternative probes to FITC and RITC, since a wide range of less photosensitive and brighter probes is currently available. For example, Dubert-Ferrandon et al (Dubert-Ferrandon et al., 2006) used Alexa Fluor 594 and Alexa Fluor 488 to label casein micelles and whey proteins, respectively. Preliminary studies will be performed to identify the best probes for selective labelling of milk proteins. The choice of the probes will take into account also the question of sensitivity to temperature, which could have consequences on their stability and brightness, in view of drying tests with MDS. From this point of view, Bowey et al (Bowey & Neufeld, 2009) reported images of particles containing both FITC-labelled insulin and RITC-labelled alginate after spray drying at an inlet temperature of 150°C. Once the probe optimization achieved, it will be crucial to characterize the convective flows inside the drops and the deposit of the proteins at the air-liquid interface leading to the formation of the outer skin. In addition to labelled proteins, latex or silica microbeads could be dispersed in the suspensions and used as tracers in order to perform a Particle Image Velocimetry (PIV) analysis and to quantify the evolution of the convective flows during the drying process.

Another challenging topic will be to investigate the dynamics of protein deposit and organization at droplet surface in the early stage of the evaporation process. The research will be devoted to the study of the evolution of the air/liquid interface when the first particles get captured up to the formation of coupled thin layers (i.e., thickness lower than 100 nm) (de Gennes, 2002; Okuzono et al., 2006). This stage, induced by the evaporation, acts as the precursor of the structural outer skin. Investigations

using SANS (Small Angle Neutron Scattering; SOLEIL) in the geometry of a planar film will aim to quantify the time variation of concentration in solutes at the evaporation surface. Experimental results will be combined to a non-linear advection-diffusion equation that predicts the evolution of the concentration of non-volatile solutes (Boulogne et al., 2014).

REFERENCES

- Acharya, K. R., Ren, J., Stuart, D. I., Phillips, D. C., & Fenna, R. E. (1991). Crystal structure of human α -lactalbumin at 1.7 Å resolution. *Journal of Molecular Biology*, 221(2), 571–581.
- Adhikari, B., Howes, T., Bhandari, B. R., & Truong, V. (2000). Experimental studies and kinetics of single drop drying and their relevance in drying of sugar-rich foods: A review. *International Journal of Food Properties*, 3(3), 323–351.
- Alamilla-Beltran, L., Chanona-Perez, J. J., Jimenez-Aparicio, A. R., & Gutierrez-Lopez, G. F. (2005). Description of morphological changes of particles along spray drying. *Journal of Food Engineering*, 67(1–2), 179–184.
- Anandharamakrishnan, C., & Ishwarya, S. (2015). *Spray Drying Techniques for Food Ingredient Encapsulation: Anandharamakrishnan/Spray Drying Techniques for Food Ingredient Encapsulation*.
- Arai, S., & Doi, M. (2012). Skin formation and bubble growth during drying process of polymer solution. *The European Physical Journal E*, 35(7), 57. <https://doi.org/10.1140/epje/i2012-12057-2>
- Audebert, A., Saint-Jalmes, A., Beaufile, S., Lechevalier, V., Le Floch-Fouéré, C., Cox, S., Leconte, N., & Pezennec, S. (2019). Interfacial properties, film dynamics and bulk rheology: A multi-scale approach to dairy protein foams. *Journal of Colloid and Interface Science*, 542, 222–232.
- Bacchin, P. (2017). An energy map model for colloid transport. *Chemical Engineering Science*, 158, 208–215. <https://doi.org/10.1016/j.ces.2016.10.024>
- Bacchin, P., Brutin, D., Davaille, A., Di Giuseppe, E., Chen, X. D., Gergianakis, I., Giorgiutti-Dauphiné, F., Goehring, L., Hallez, Y., Heyd, R., Jeantet, R., Le Floch-Fouéré, C., Meireles, M., Mittelstaedt, E., Nicloux, C., Pauchard, L., & Saboungi, M.-L. (2018). Drying colloidal systems: Laboratory models for a wide range of applications. *The European Physical Journal E*, 41(8), 94. <https://doi.org/10.1140/epje/i2018-11712-x>

References

- Baker, E. N., & Baker, H. M. (2009). A structural framework for understanding the multifunctional character of lactoferrin. *Biochimie*, 91(1), 3–10. <https://doi.org/10.1016/j.biochi.2008.05.006>
- Baker, P., Santos, T., Neves, P. A., Machado, P., Smith, J., Piwoz, E., Barros, A. J., Victora, C. G., & McCoy, D. (2021). First-food systems transformations and the ultra-processing of infant and young child diets: The determinants, dynamics and consequences of the global rise in commercial milk formula consumption. *Maternal & Child Nutrition*, 17(2), e13097.
- Batchelor, G. K., & Shen, C. (1985). Thermophoretic deposition of particles in gas flowing over cold surfaces. *Journal of Colloid and Interface Science*, 107(1), 21–37.
- Ben, X.-M. (2008). Nutritional management of newborn infants: Practical guidelines. *World Journal of Gastroenterology: WJG*, 14(40), 6133.
- Bhandari, B. R., & Howes, T. (1999). Implication of glass transition for the drying and stability of dried foods. *Journal of Food Engineering*, 40(1–2), 71–79.
- Bindels, J. (1992). Artificial feeds for infants — human milk substitutes: Current composition and future trends.
- Blanchard, E., Zhu, P., & Schuck, P. (2013). Infant formula powders. In *Handbook of food powders* (pp. 465–483). Elsevier.
- Bode, L. (2012). Human milk oligosaccharides: Every baby needs a sugar mama. *Glycobiology*, 22(9), 1147–1162.
- Bornaz, S., Novak, G., & Parmentier, M. (1992). Seasonal and regional variation in triglyceride composition of French butterfat. <https://doi.org/10.1007/BF02541049>
- Bouchoux, A., Cayemite, P.-E., Jardin, J., Gésan-Guiziou, G., & Cabane, B. (2009). Casein Micelle Dispersions under Osmotic Stress. *Biophysical Journal*, 96(2), 693–706. <https://doi.org/10.1016/j.bpj.2008.10.006>
- Bouchoux, A., Debbou, B., Gésan-Guiziou, G., Famelart, M.-H., Doublier, J.-L., & Cabane, B. (2009). Rheology and phase behavior of dense casein micelle dispersions. *The Journal of Chemical Physics*, 131(16), 165106. <https://doi.org/10.1063/1.3245956>

References

- Bouchoux, A., Gésan-Guiziou, G., Pérez, J., & Cabane, B. (2010). How to Squeeze a Sponge: Casein Micelles under Osmotic Stress, a SAXS Study. *Biophysical Journal*, 99(11), 3754–3762. <https://doi.org/10.1016/j.bpj.2010.10.019>
- Boulogne, F., Pauchard, L., Giorgiutti-Dauphiné, F., Botet, R., Schweins, R., Sztucki, M., Li, J., Cabane, B., & Goehring, L. (2014). Structural anisotropy of directionally dried colloids. *EPL (Europhysics Letters)*, 105(3), 38005.
- Bouman, J., Venema, P., de Vries, R. J., van der Linden, E., & Schutyser, M. A. I. (2016). Hole and vacuole formation during drying of sessile whey protein droplets. *Food Research International*, 84, 128–135. <https://doi.org/10.1016/j.foodres.2016.03.027>
- Bowey, K. E., & Neufeld, R. (2009). Alginate microparticles produced by spray drying for oral insulin delivery. *Masters Abstracts International*, 49(02).
- Brenna, J. T., Varamini, B., Jensen, R. G., Diersen-Schade, D. A., Boettcher, J. A., & Arterburn, L. M. (2007). Docosahexaenoic and arachidonic acid concentrations in human breast milk worldwide. *The American Journal of Clinical Nutrition*, 85(6), 1457–1464.
- Briard, V., Leconte, N., Michel, F., & Michalski, M. (2003). The fatty acid composition of small and large naturally occurring milk fat globules.
- Brownlow, S., Cabral, J. H. M., Cooper, R., Flower, D. R., Yewdall, S. J., Polikarpov, I., North, A. C., & Sawyer, L. (1997). Bovine β -lactoglobulin at 1.8 Å resolution—Still an enigmatic lipocalin. *Structure*, 5(4), 481–495.
- Brownsey, G. J., Noel, T. R., Parker, R., & Ring, S. G. (2003). The glass transition behavior of the globular protein bovine serum albumin. *Biophysical Journal*, 85(6), 3943–3950.
- Brutin, D., Sobac, B., & Nicloux, C. (2012). Influence of substrate nature on the evaporation of a sessile drop of blood. *Journal of Heat Transfer*, 134(6).
- Bylund, G. (1995). *Dairy processing handbook: Tetra Pak Processing Systems AB*.
- Calapaj, G. (1968). An electron microscope study of the ultrastructure of bovine and human casein micelles in fresh and acidified milk.

References

- Carić, M. (1994). Concentrated and dried dairy products. VCH Publishers Inc.
- Chatterton, D. E., Nguyen, D. N., Bering, S. B., & Sangild, P. T. (2013). Anti-inflammatory mechanisms of bioactive milk proteins in the intestine of newborns. *The International Journal of Biochemistry & Cell Biology*, 45(8), 1730–1747.
- Chen, X. D. (2008). The basics of a reaction engineering approach to modeling air-drying of small droplets or thin-layer materials. *Drying Technology*, 26(6), 627–639.
- Chen, X. D., & Lin, S. (2005). Air drying of milk droplet under constant and time - dependent conditions.
- Chen, X. D., & Peng, X. (2005). Modified Biot number in the context of air drying of small moist porous objects. *Drying Technology*, 23(1–2), 83–103.
- Chen, X. D., & Xie, G. Z. (1997). Fingerprints of the drying behaviour of particulate or thin layer food materials established using a reaction engineering model. *Food and Bioproducts Processing*, 75(4), 213–222.
- Chever, S., Mejean, S., Dolivet, A., Mei, F., Den Boer, C. M., Le Barzic, G., Jeantet, R., & Schuck, P. (2017). Agglomeration during spray drying: Physical and rehydration properties of whole milk/sugar mixture powders. *LWT-Food Science and Technology*, 83, 33–41.
- Chew, J. H., Liu, W., Fu, N., Gengenbach, T., Chen, X. D., & Selomulya, C. (2014). Exploring the drying behaviour and particle formation of high solids milk protein concentrate. *Journal of Food Engineering*, 143, 186–194.
- Chierici, R., Sawatzki, G., Tamisari, L., Volpato, S., & Vigi, V. (1992). Supplementation of an adapted formula with bovine lactoferrin. 2. Effects on serum iron, ferritin and zinc levels.
- Chilliard, Y., Ferlay, A., & Doreau, M. (2001). Effect of different types of forages, animal fat or marine oils in cow's diet on milk fat secretion and composition, especially conjugated linoleic acid (CLA) and polyunsaturated fatty acids. -forages%2C-animal-fat-or-Chilliard-Ferlay
- CNIEL. (2016). L'économie laitière en chiffres – édition 2016. Calameo.Com.
- CNIEL. (2020). L'économie laitière en chiffres—Édition 2020. Calameo.Com.

References

- Croguennec, T., Li, N., Phelebon, L., Garnier-Lambrouin, F., & Gésan-Guiziou, G. (2012). Interaction between lactoferrin and casein micelles in skimmed milk.
- Cuilliere, M. L., Tregot, V., Bene, M. C., Faure, G., & Montagne, P. (1999). Changes in the κ -casein and β -casein concentrations in human milk during lactation. *Journal of Clinical Laboratory Analysis*, 13(5), 213–218.
- Dahbi, L., Alexander, M., Trappe, V., Dhont, J. K. G., & Schurtenberger, P. (2010). Rheology and structural arrest of casein suspensions. *Journal of Colloid and Interface Science*, 342(2), 564–570.
- Dalgleish, D. G., & Law, A. J. R. (1988). Sodium caseinates—Composition and properties of different preparations. *International Journal of Dairy Technology*, 41(1), 1–4.
- de Gennes, P. G. (2002). Solvent evaporation of spin cast films: “Crust” effects. *The European Physical Journal E*, 7(1), 31–34. <https://doi.org/10.1140/epje/i200101169>
- De Kruif, C. G., & Holt, C. (2003). Casein micelle structure, functions and interactions. In *Advanced dairy chemistry—1 proteins* (pp. 233–276). Springer.
- De Wit, J. N. (1998). Nutritional and functional characteristics of whey proteins in food products. *Journal of Dairy Science*, 81(3), 597–608.
- Deegan, R. D. (2000). Pattern formation in drying drops. *Physical Review E*, 61(1), 475–485. <https://doi.org/10.1103/PhysRevE.61.475>
- Deegan, R. D., Bakajin, O., Dupont, T. F., Huber, G., Nagel, S. R., & Witten, T. A. (1997). Capillary flow as the cause of ring stains from dried liquid drops. *Nature*, 389(6653), 827–829. <https://doi.org/10.1038/39827>
- Dickinson, E. (2013). Stabilising emulsion-based colloidal structures with mixed food ingredients. *Journal of the Science of Food and Agriculture*, 93(4), 710–721.
- Dubert-Ferrandon, A., Niranjana, K., & Grandison, A. S. (2006). A novel technique for differentiation of proteins in the development of acid gel structure from control and heat treated milk using confocal scanning laser microscopy. *Journal of Dairy Research*, 73(4), 423–430.

References

- Engfer, M., Stahl, B., Finke, B., Sawatzki, G., & Daniel, H. (2000). Human milk oligosaccharides are resistant to enzymatic hydrolysis in the upper gastrointestinal tract.
- European Union. (2016). Infant and follow-on formula—Composition and information.
<http://publications.europa.eu/resource/cellar>
- FAO. (2020). Overview of global dairy market developments in 2020.
- FAO. (2021). Food and Agriculture Organization of the United Nations.
- Farrell Jr, H. M., Jimenez-Flores, R., Bleck, G. T., Brown, E. M., Butler, J. E., Creamer, L. K., Hicks, C. L., Hollar, C. M., Ng-Kwai-Hang, K. F., & Swaisgood, H. E. (2004). Nomenclature of the proteins of cows' milk—Sixth revision. *Journal of Dairy Science*, 87(6), 1641–1674.
- Fitzpatrick, J. J., Hodnett, M., Twomey, M., Cerqueira, P. S. M., O'flynn, J., & Roos, Y. H. (2007). Glass transition and the flowability and caking of powders containing amorphous lactose. *Powder Technology*, 178(2), 119–128.
- Foerster, M., Gengenbach, T., Woo, M. W., & Selomulya, C. (2016). The impact of atomization on the surface composition of spray-dried milk droplets B *Biointerfaces*.
- Forge, V., Wijesinha, R. T., Balbach, J., Brew, K., Robinson, C., Redfield, C., & Dobson, C. (1999). Rapid collapse and slow structural reorganisation during the refolding of bovine alpha-lactalbumin.
- Fortini, A., Martín-Fabiani, I., De La Haye, J. L., Dugas, P.-Y., Lansalot, M., D'Agosto, F., Bourgeat-Lami, E., Keddie, J. L., & Sear, R. P. (2016). Dynamic stratification in drying films of colloidal mixtures. *Physical Review Letters*, 116(11), 118301.
<https://doi.org/10.1103/PhysRevLett.116.118301>
- Fox, M., Akkerman, C., Straatsma, H., & De Jong, P. (2010). Energy reduction by high dry matter concentration and drying. *New Food*, 2010, 60–63.
- Fox, P. F., & Brodtkorb, A. (2008). The casein micelle: Historical aspects, current concepts and significance. *International Dairy Journal*, 18(7), 677–684.
- FranceAgriMer. (2019). Les exportations françaises de produits laitiers sur les 30 dernières années (1988-2018).

References

- Fu, N., Woo, M. W., & Chen, X. D. (2011). Colloidal transport phenomena of milk components during convective droplet drying. *Colloids and Surfaces B: Biointerfaces*, 87(2), 255–266.
- Fu, N., Woo, M. W., Selomulya, C., & Chen, X. D. (2013). Shrinkage behaviour of skim milk droplets during air drying. *Journal of Food Engineering*, 116(1), 37–44.
- Fu, X., Huck, D., Makein, L., Armstrong, B., Willen, U., & Freeman, T. (2012). Effect of particle shape and size on flow properties of lactose powders. *Particuology*, 10(2), 203–208.
- Gaiani, C., Schuck, P., Scher, J., Desobry, S., & Banon, S. (2007). Dairy powder rehydration: Influence of protein state, incorporation mode, and agglomeration. *Journal of Dairy Science*, 90(2), 570–581.
- Giorgiutti-Dauphiné, F., & Pauchard, L. (2016). Painting cracks: A way to investigate the pictorial matter. *Journal of Applied Physics*, 120(6), 065107.
- Goedhart, A. C., & Bindels, J. G. (1994). The composition of human milk as a model for the design of infant formulas: Recent findings and possible applications. *Nutrition Research Reviews*, 7(1), 1–23.
- Gopal, P. K., & Gill, H. S. (2000). Oligosaccharides and glycoconjugates in bovine milk and colostrum. *British Journal of Nutrition*, 84(S1), 69–74.
- Griko, Y., & Remeta, D. P. (1999). Energetics of solvent and ligand - induced conformational changes in α - lactalbumin.
- Habibnejad-korayem, M., Zhang, J., & Zou, Y. (2021). Effect of particle size distribution on the flowability of plasma atomized Ti-6Al-4V powders. *Powder Technology*, 392, 536–543.
- Havea, P., Singh, H., & Creamer, L. K. (2001). Characterization of heat-induced aggregates of β -lactoglobulin, α -lactalbumin and bovine serum albumin in a whey protein concentrate environment.
- Head, D. A. (2006). Modeling the elastic deformation of polymer crusts formed by sessile droplet evaporation. *Physical Review E*, 74(2), 021601.
- Heine, W. (1999). The significance of tryptophan in infant nutrition.

References

- Heine, W. E., Klein, P. D., & Reeds, P. J. (1991). The importance of α -lactalbumin in infant nutrition. *The Journal of Nutrition*, 121(3), 277–283.
- Heldman, D. R., & Lund, D. B. (1992). *Handbook of Food Engineering*. Marcel Dekkar. Inc. New York. USA.
- Hemar, Y., Banjar, W., Otter, D., & Yang, Z. (2021). Viscosity, size, structural and interfacial properties of sodium caseinate obtained from A2 milk. *Colloids and Surfaces A: Physicochemical and Engineering Aspects*, 614, 126163.
- Holland, J., Deeth, H., & Alewood, P. (2006). Resolution and characterisation of multiple isoforms of bovine κ - casein by 2 - DE following a reversible cysteine - tagging enrichment strategy.
- Holt, C. (1992). Structure and stability of bovine casein micelles. *Advances in Protein Chemistry*, 43, 63–151.
- Howard, M. P., Nikoubashman, A., & Panagiotopoulos, A. Z. (2017). Stratification in Drying Polymer–Polymer and Colloid–Polymer Mixtures. *Langmuir*, 33(42), 11390–11398.
<https://doi.org/10.1021/acs.langmuir.7b02074>
- Hu, H., & Larson, R. G. (2005). Analysis of the Effects of Marangoni Stresses on the Microflow in an Evaporating Sessile Droplet. *Langmuir*, 21(9), 3972–3980. <https://doi.org/10.1021/la0475270>
- Huang, L., Kumar, K., & Mujumdar, A. S. (2004). Simulation of a spray dryer fitted with a rotary disk atomizer using a three-dimensional computational fluid dynamic model. *Drying Technology*, 22(6), 1489–1515.
- Huang, L. X., Passos, M. L., Kumar, K., & Mujumdar, A. S. (2005). A three-dimensional simulation of a spray dryer fitted with a rotary atomizer. *Drying Technology*, 23(9–11), 1859–1873.
- IDF. (2020). *The World Dairy Situation 2020*, Bulletin of the International Dairy Federation 506/2020
- Innis SM (1993) Essential fatty acid requirements in human nutrition. Dairyreporter.Com.
- Innis, S. (1992). Human milk and formula fatty acids.
- Iversen, C., & Forsythe, S. (2004). Isolation of *Enterobacter sakazakii* and other Enterobacteriaceae from powdered infant formula milk and related products.

References

- Jeantet, R. (2016). Inactivation of Food Modifying Agents. *Handbook of Food Science and Technology* 2: Food Process Engineering and Packaging, 115–150.
- Jeantet, R., & Croguennec, T. (2018). Chapitre 4: Du lait au fromage : aspects biochimiques (Issue 4ième Edition, p. 1001 pages). Editions Tec & Doc Lavoisier.
- Jeness, R., Larson, B., Mcmeekin, T., Swanson, A. M., Whitnah, C. H., & Whitney, R. (1956). *Nomenclature of the Proteins of Bovine Milk*.
- JENSEN, R. G., & NEWBURG, D. S. (1995). Bovine milk lipids. In *Handbook of milk composition* (pp. 543–575). Elsevier.
- Kelly, A. L., O'Connell, J. E., & Fox, P. F. (2003). Manufacture and properties of milk powders. In *Advanced Dairy Chemistry—1 Proteins* (pp. 1027–1061). Springer.
- Kim, E. H.-J., Chen, X. D., & Pearce, D. (2005). Effect of surface composition on the flowability of industrial spray-dried dairy powders. *Colloids and Surfaces B: Biointerfaces*, 46(3), 182–187.
- Kim, E. H.-J., Chen, X. D., & Pearce, D. (2009). Surface composition of industrial spray-dried milk powders. 2. Effects of spray drying conditions on the surface composition. *Journal of Food Engineering*, 94(2), 169–181.
- Koga, S., & Inasawa, S. (2019). Packing structures and formation of cracks in particulate films obtained by drying colloid–polymer suspensions. *Colloids and Surfaces A: Physicochemical and Engineering Aspects*, 563, 95–101. <https://doi.org/10.1016/j.colsurfa.2018.11.066>
- Langrish, T. A. G., & Fletcher, D. F. (2001). Spray drying of food ingredients and applications of CFD in spray drying. *Chemical Engineering and Processing: Process Intensification*, 40(4), 345–354.
- Lanotte, L. (2020). The drying of milk at the laboratory scale: From the industrial need to the scientific challenge. In *Drying in the Dairy Industry* (pp. 261–274). CRC Press.
- Lanotte, L., Boissel, F., Schuck, P., Jeantet, R., & Le Floch-Fouéré, C. (2018). Drying-induced mechanisms of skin formation in mixtures of high protein dairy powders. *Colloids and Surfaces A: Physicochemical and Engineering Aspects*, 553, 20–27. <https://doi.org/10.1016/j.colsurfa.2018.05.020>

References

- Le Floch-Fouéré, C., Lanotte, L., Jeantet, R., & Pauchard, L. (2019). The solute mechanical properties impact on the drying of dairy and model colloidal systems. *Soft Matter*, 15(30), 6190–6199. <https://doi.org/10.1039/C9SM00373H>
- Le Maux, S., Bouhallab, S., Giblin, L., Brodkorb, A., & Croguennec, T. (2014). Bovine β -lactoglobulin/fatty acid complexes: Binding, structural, and biological properties. *Dairy Science & Technology*, 94(5), 409–426.
- Lin, S. X. Q., & Chen, X. D. (2002). Improving the glass-filament method for accurate measurement of drying kinetics of liquid droplets. *Chemical Engineering Research and Design*, 80(4), 401–410.
- Lin, S. X. Q., & Chen, X. D. (2007). The reaction engineering approach to modelling the cream and whey protein concentrate droplet drying. *Chemical Engineering and Processing: Process Intensification*, 46(5), 437–443.
- Lin, Y., Kelly, A. L., O'Mahony, J. A., & Guinee, T. P. (2017). Effect of heat treatment during skim milk powder manufacture on the compositional and processing characteristics of reconstituted skim milk and concentrate. *International Dairy Journal*, 78, 53–64.
- Liu, D. Z., Dunstan, D. E., & Martin, G. J. (2012). Evaporative concentration of skimmed milk: Effect on casein micelle hydration, composition, and size. *Food Chemistry*, 134(3), 1446–1452.
- Liu, W., Midya, J., Kappl, M., Butt, H.-J., & Nikoubashman, A. (2019). Segregation in Drying Binary Colloidal Droplets. *ACS Nano*, 13(5), 4972–4979. <https://doi.org/10.1021/acsnano.9b00459>
- Loveday, S. M., Creamer, L. K., Singh, H., & Rao, M. A. (2007). Phase and rheological behavior of high-concentration colloidal hard-sphere and protein dispersions. *Journal of Food Science*, 72(7), R101–R107.
- Lucena, M. E., Alvarez, S., Menéndez, C., Riera, F. A., & Alvarez, R. (2006). Beta-lactoglobulin removal from whey protein concentrates: Production of milk derivatives as a base for infant formulas. *Separation and Purification Technology*, 52(2), 310–316.
- Ma, X., & Chatterton, D. E. (2021). Strategies to improve the physical stability of sodium caseinate stabilized emulsions: A literature review. *Food Hydrocolloids*, 106853.

References

- Makepeace, D. K., Fortini, A., Markov, A., Locatelli, P., Lindsay, C., Moorhouse, S., Lind, R., Sear, R. P., & Keddie, J. L. (2017). Stratification in binary colloidal polymer films: Experiment and simulations. *Soft Matter*, 13(39), 6969–6980.
- Mansouri, S., Suriya Hena, V., & Woo, M. W. (2016). Narrow tube spray drying. *Drying Technology*, 34(9), 1043–1051.
- Martin, G. J., Williams, R. P. W., & Dunstan, D. E. (2007). Comparison of casein micelles in raw and reconstituted skim milk. *Journal of Dairy Science*, 90(10), 4543–4551.
- McCarthy, N. A., Gee, V. L., Hickey, D. K., Kelly, A. L., O'Mahony, J. A., & Fenelon, M. A. (2013). Effect of protein content on the physical stability and microstructure of a model infant formula. *International Dairy Journal*, 29(1), 53–59.
- McCarthy, N. A., Kelly, A. L., O'Mahony, J. A., Hickey, D. K., Chaurin, V., & Fenelon, M. A. (2012). Effect of protein content on emulsion stability of a model infant formula. *International Dairy Journal*, 25(2), 80–86.
- McSweeney, S. L. (2008). Emulsifiers in Infant Nutritional Products. In G. L. Hasenhuettl & R. W. Hartel (Eds.), *Food Emulsifiers and Their Applications: Second Edition* (pp. 233–261). Springer. https://doi.org/10.1007/978-0-387-75284-6_8
- McSweeney, S. L., Mulvihill, D. M., & O'Callaghan, D. M. (2004). The influence of pH on the heat-induced aggregation of model milk protein ingredient systems and model infant formula emulsions stabilized by milk protein ingredients. *Food Hydrocolloids*, 18(1), 109–125.
- Min, D. B., Lee, S. H., Lindamood, J. B., Chang, K. S., & Reineccius, G. A. (1989). Effects of packaging conditions on the flavor stability of dry whole milk. *Journal of Food Science*, 54(5), 1222–1224.
- Montagne, D.-H., Dael, P. V., Skanderby, M., & Hugelshofer, W. (2009). Infant Formulae – Powders and Liquids. 294–331. <https://doi.org/10.1002/9781444322729.ch9>

References

- Murphy, E. G., Tobin, J. T., Roos, Y. H., & Fenelon, M. A. (2011). The effect of high velocity steam injection on the colloidal stability of concentrated emulsions for the manufacture of infant formulations. *Procedia Food Science*, 1, 1309–1315.
- Mylonas, E., & Svergun, D. I. (2007). Accuracy of molecular mass determination of proteins in solution by small-angle X-ray scattering. *Journal of Applied Crystallography*, 40(s1), s245–s249. <https://doi.org/10.1107/S002188980700252X>
- NAZAROWEC-WHITE, & Farber, J. M. (1999). Phenotypic and genotypic typing of food and clinical isolates of *Enterobacter sakazakii*. *Journal of Medical Microbiology*, 48(6), 559–567.
- Nguyen, V. X., & Stebe, K. J. (2002). Patterning of Small Particles by a Surfactant-Enhanced Marangoni-Bénard Instability. *Physical Review Letters*, 88(16), 164501. <https://doi.org/10.1103/PhysRevLett.88.164501>
- Nigen, M., Gaillard, C., Croguennec, T., Madec, M.-N., & Bouhallab, S. (2010). Dynamic and supramolecular organisation of α -lactalbumin/lysozyme microspheres: A microscopic study. *Biophysical Chemistry*, 146(1), 30–35. <https://doi.org/10.1016/j.bpc.2009.10.001>
- Nijdam, J. J., Guo, B., Fletcher, D. F., & Langrish, T. A. G. (2004). Challenges of simulating droplet coalescence within a spray. *Drying Technology*, 22(6), 1463–1488.
- Nijdam, J. J., & Langrish, T. A. G. (2006). The effect of surface composition on the functional properties of milk powders. *Journal of Food Engineering*, 77(4), 919–925.
- Nunes, J. S., Bohórquez, S. J., Meeuwisse, M., Mestach, D., & Asua, J. M. (2014). Efficient strategy for hard nano-sphere usage: Boosting the performance of waterborne coatings. *Progress in Organic Coatings*, 77(10), 1523–1530.
- Nuzzo, M., Millqvist-Fureby, A., Sloth, J., & Bergenstahl, B. (2015). Surface composition and morphology of particles dried individually and by spray drying. *Drying Technology*, 33(6), 757–767.
- O’Callaghan DM, & John. (2011). Dehydrated Dairy Products | Infant Formulae. *Encyclopedia of Dairy Sciences*, 12, 135–145.

References

- Okuzono, T., Ozawa, K., & Doi, M. (2006). Simple Model of Skin Formation Caused by Solvent Evaporation in Polymer Solutions. *Physical Review Letters*, 97(13), 136103.
<https://doi.org/10.1103/PhysRevLett.97.136103>
- Özkan, N., Withy, B., & Chen, X. D. (2003). Effects of time, temperature, and pressure on the cake formation of milk powders. *Journal of Food Engineering*, 58(4), 355–361.
- Patel, K. C., & Chen, X. D. (2007). Production of spherical and uniform-sized particles using a laboratory ink-jet spray dryer. *Asia-Pacific Journal of Chemical Engineering*, 2(5), 415–430.
- Patel, K. C., & Chen, X. D. (2008). Sensitivity analysis of the reaction engineering approach to modeling spray drying of whey proteins concentrate. *Drying Technology*, 26(11), 1334–1343.
- Patton, S., & Huston, G. E. (1986). A method for isolation of milk fat globules. *Lipids*, 21(2), 170–174.
<https://doi.org/10.1007/BF02534441>
- Pauchard, L. (2006). Patterns caused by buckle-driven delamination in desiccated colloidal gels. *EPL (Europhysics Letters)*, 74(1), 188.
- Pauchard, L., Abou, B., & Sekimoto, K. (2009). Influence of Mechanical Properties of Nanoparticles on Macrocrack Formation. *Langmuir*, 25(12), 6672–6677. <https://doi.org/10.1021/la9001384>
- Pauchard, L., & Allain, C. (2003). Mechanical instability induced by complex liquid desiccation. *Comptes Rendus Physique*, 4(2), 231–239. [https://doi.org/10.1016/S1631-0705\(03\)00027-6](https://doi.org/10.1016/S1631-0705(03)00027-6)
- Phipps, L. W. (1985). The high pressure dairy homogenizer (Vol. 6). National Institute for Research in Dairying.
- Piatkowski, M., Taradaichenko, M., & Zbicinski, I. (2015). Energy consumption and product quality interactions in flame spray drying. *Drying Technology*, 33(9), 1022–1028.
- Qi, P. X. (2007). Studies of casein micelle structure: The past and the present. *Le Lait*, 87(4–5), 363–383.
- Rahman, S. (1995). *Food Properties Handbook* CRC Press Inc Boca Raton. Florida.

References

- Raju, L. T., Chakraborty, S., Pathak, B., & Basu, S. (2018). Controlling self-assembly and topology at micro–nano length scales using a contact-free mixed nanocolloid droplet architecture. *Langmuir*, 34(18), 5323–5333.
- Rastogi, V., Melle, S., Calderon, O. G., García, A. A., Marquez, M., & Velev, O. D. (2008). Synthesis of light-diffracting assemblies from microspheres and nanoparticles in droplets on a superhydrophobic surface. *Advanced Materials*, 20(22), 4263–4268.
- Relkin, P. (1996). Thermal unfolding of β - lactoglobulin, α - lactalbumin, and bovine serum albumin. A thermodynamic approach.
- Rogers, S., Wu, W. D., Lin, S. X. Q., & Chen, X. D. (2012). Particle shrinkage and morphology of milk powder made with a monodisperse spray dryer. *Biochemical Engineering Journal*, 62, 92–100.
- Roos, Y. (2002). Importance of glass transition and water activity to spray drying and stability of dairy powders.
- Sadek, C., Li, H., Schuck, P., Fallourd, Y., Pradeau, N., Le Floch-Fouéré, C., & Jeantet, R. (2014). To What Extent Do Whey and Casein Micelle Proteins Influence the Morphology and Properties of the Resulting Powder? *Drying Technology*, 32(13), 1540–1551.
<https://doi.org/10.1080/07373937.2014.915554>
- Sadek, C., Pauchard, L., Schuck, P., Fallourd, Y., Pradeau, N., Le Floch-Fouéré, C., & Jeantet, R. (2015). Mechanical properties of milk protein skin layers after drying: Understanding the mechanisms of particle formation from whey protein isolate and native phosphocaseinate. *Food Hydrocolloids*, 48, 8–16. <https://doi.org/10.1016/j.foodhyd.2015.01.014>
- Sadek, C., Schuck, P., Fallourd, Y., Pradeau, N., Jeantet, R., & Le Floch-Fouéré, C. (2016). Buckling and collapse during drying of a single aqueous dispersion of casein micelle droplet. *Food Hydrocolloids*, 52, 161–166. <https://doi.org/10.1016/j.foodhyd.2015.06.016>

References

- Sadek, C., Schuck, P., Fallourd, Y., Pradeau, N., Le Floch-Fouéré, C., & Jeantet, R. (2015). Drying of a single droplet to investigate process–structure–function relationships: A review. *Dairy Science & Technology*, 95(6), 771–794. <https://doi.org/10.1007/s13594-014-0186-1>
- Sadek, C., Tabuteau, H., Schuck, P., Fallourd, Y., Pradeau, N., Le Floch-Fouéré, C., & Jeantet, R. (2013). Shape, Shell, and Vacuole Formation during the Drying of a Single Concentrated Whey Protein Droplet. *Langmuir*, 29(50), 15606–15613. <https://doi.org/10.1021/la404108v>
- Sandler, N., & Wilson, D. (2010). Prediction of granule packing and flow behavior based on particle size and shape analysis. *Journal of Pharmaceutical Sciences*, 99(2), 958–968.
- Santos, D., Maurício, A. C., Sencadas, V., Santos, J. D., Fernandes, M. H., & Gomes, P. S. (2018). Spray drying: An overview. Pignatello, R.(Comp.). *Biomaterials-Physics and Chemistry-New Edition*. InTech. UK, 9–35.
- Schuck, P., Jeantet, R., Bhandari, B., Chen, X. D., Perrone, Í. T., de Carvalho, A. F., Fenelon, M., & Kelly, P. (2016). Recent advances in spray drying relevant to the dairy industry: A comprehensive critical review. *Drying Technology*, 34(15), 1773–1790.
- Schulz, M., & Keddie, J. L. (2018). A critical and quantitative review of the stratification of particles during the drying of colloidal films. *Soft Matter*, 14(30), 6181–6197. <https://doi.org/10.1039/C8SM01025K>
- Sear, R. P., & Warren, P. B. (2017). Diffusiophoresis in non-adsorbing polymer solutions: The Asakura-Oosawa model and stratification in drying films. *ArXiv:1709.00704 [Cond-Mat]*. <https://doi.org/10.1103/PhysRevE.96.062602>
- Selomulya, C., & Fang, Y. (2013). Food powder rehydration. In *Handbook of food powders* (pp. 379–408).
- Sharma, A., Jana, A. H., & Chavan, R. S. (2012). Functionality of milk powders and milk-based powders for end use applications—A review. *Comprehensive Reviews in Food Science and Food Safety*, 11(5), 518–528.

References

- Sibrant, A. L. R., & Pauchard, L. (2017). Effect of the particle interactions on the structuration and mechanical strength of particulate materials. *EPL (Europhysics Letters)*, 116(4), 49002.
- Singh, H. (2007). Interactions of milk proteins during the manufacture of milk powders. *Le Lait*, 87(4–5), 413–423.
- Sobac, B., & Brutin, D. (2014). Desiccation of a sessile drop of blood: Cracks, folds formation and delamination. *Colloids and Surfaces A: Physicochemical and Engineering Aspects*, 448, 34–44. <https://doi.org/10.1016/j.colsurfa.2014.01.076>
- Southwell, D. B., Langrish, T. A. G., & Fletcher, D. F. (2001). Use of computational fluid dynamics techniques to assess design alternatives for the plenum chamber of a small spray dryer. *Drying Technology*, 19(2), 257–268.
- Stunda-Zujeva, A., Irbe, Z., & Berzina-Cimdina, L. (2017). Controlling the morphology of ceramic and composite powders obtained via spray drying—a review. *Ceramics International*, 43(15), 11543–11551.
- Thompson, D. K., & Kharb, S. (2007). Aspects of infant food formulation. *Comprehensive Reviews in Food Science and Food Safety*, 6(4), 79–102.
- Trueman, R. E., Lago Domingues, E., Emmett, S. N., Murray, M. W., Keddie, J. L., & Routh, A. F. (2012). Autostratification in Drying Colloidal Dispersions: Experimental Investigations. *Langmuir*, 28(7), 3420–3428. <https://doi.org/10.1021/la203975b>
- Trueman, R. E., Lago Domingues, E., Emmett, S. N., Murray, M. W., & Routh, A. F. (2012). Auto-stratification in drying colloidal dispersions: A diffusive model. *Journal of Colloid and Interface Science*, 377(1), 207–212. <https://doi.org/10.1016/j.jcis.2012.03.045>
- van Tulleken, C., Wright, C., Brown, A., McCoy, D., & Costello, A. (2020). Marketing of breastmilk substitutes during the COVID-19 pandemic. *The Lancet*, 396(10259).
- Varnam, A. H., & Sutherland, J. P. (1994). Dehydrated Dairy Products | Infant Formulae. In *Milk and Milk Products* (pp. 42–102).

References

- Vehring, R. (2008). Pharmaceutical particle engineering via spray drying. *Pharmaceutical Research*, 25(5), 999–1022.
- Wal, J.-M. (2002). Cow's milk proteins/allergens. *Annals of Allergy, Asthma & Immunology*, 89(6), 3–10.
- Walstra, P. (1990). On the stability of casein micelles.
- Walstra, P., Geurts, T., Noomen, A., Jellema, A., & Boekel, M. (1999). *Dairy Technology: Principles of Milk Properties and Processes*.
- Walstra, P., Walstra, P., Wouters, J. T., & Geurts, T. J. (2005). *Dairy science and technology*. CRC press.
- Westergaard, V. (2004). Milk powder technology evaporation and spray drying GEA process engineering engineering for a better world preface to fifth edition.
- World Health Organization. (2006). *Enterobacter sakazakii and Salmonella in powdered infant formula: Meeting report*. World Health Organization.
- Wu, W. D., Patel, K. C., Rogers, S., & Chen, X. D. (2007). Monodisperse droplet generators as potential atomizers for spray drying technology. *Drying Technology*, 25(12), 1907–1916.
- Yano, Y. F. (2012). Kinetics of protein unfolding at interfaces. *Journal of Physics: Condensed Matter*, 24(50), 503101. <https://doi.org/10.1088/0953-8984/24/50/503101>
- You, X., Zhou, Z., Liao, Z., Che, L., Chen, X. D., Wu, W. D., Woo, M., & Selomulya, C. (2014). Dairy milk particles made with a mono-disperse droplet spray dryer (MDDSD) investigated for the effect of fat. *Drying Technology*, 32(5), 528–542.
- Yu, M., Le Floch-Fouéré, C., Pauchard, L., Boissel, F., Fu, N., Chen, X. D., Saint-Jalmes, A., Jeantet, R., & Lanotte, L. (2021). Skin layer stratification in drying droplets of dairy colloids. *Colloids and Surfaces A: Physicochemical and Engineering Aspects*, 620, 126560.
- Zang, D., Yu, Y., Chen, Z., Li, X., Wu, H., & Geng, X. (2017). Acoustic levitation of liquid drops: Dynamics, manipulation and phase transitions. *Advances in Colloid and Interface Science*, 243, 77–85.

References

- Zhang, C., Quek, S. Y., Fu, N., Liu, B., Kilmartin, P. A., & Chen, X. D. (2019). A study on the structure formation and properties of noni juice microencapsulated with maltodextrin and gum acacia using single droplet drying. *Food Hydrocolloids*, 88, 199–209.
- Zhou, J., Jiang, Y., & Doi, M. (2017). Cross-interaction drives stratification in drying film of binary colloidal mixtures. *Physical Review Letters*, 118(10), 108002.
<https://doi.org/10.1103/PhysRevLett.118.108002>

THESIS OUTPUTS

Publication

Yu M, Le Floch-Fouéré C, Pauchard L, Boissel F, Fu N, Chen XD, Saint-Jalmes A, Jeantet R, Lanotte L. 2021. Skin formation in drying droplets of dairy colloids. *Coll Surf A 620*, article 126560, 1-9

Yu M, Le Floch-Fouéré C, Lee J, Boissel F, Jeantet R, Lanotte L. 2022, Phase Diagram of Dairy Protein Mixes Obtained by Single Droplet Drying Experiments. *Foods* 11, 562. <https://doi.org/10.3390/foods1104056>

Oral Presentations

Yu M, Le Floch-Fouéré C, Pauchard L, Boissel F, Fu N, Chen XD, Saint-Jalmes A, Jeantet R, Lanotte L. 2021. Skin formation in drying droplets of dairy proteins. 12th NIZO Dairy Conference, Innovations in Dairy Ingredients, October 5th – 7th. Oral presentation

Yu M, Le Floch-Fouéré C, Pauchard L, Boissel F, Fu N, Chen XD, Saint-Jalmes A, Jeantet R, Lanotte L. 2021. Skin layer stratification in drying droplets of dairy colloids. 35th Conference of the European Colloid & Interface Society (ECIS), September 5th - 10th, Athens, Greece. Oral presentation

Yu M, Le Floch-Fouéré C, Boissel F, Pauchard L, Saint-Jalmes A, Jeantet R, Lanotte L. 2021. Drying dynamics in complex mixes of dairy proteins. Annual European Rheology Conference (AERC 2021) in Cyberspace, April 13th-14th. Oral presentation

Yu M, Jeantet R, Le Floch-Fouéré C, Lanotte L. 2019. Characterization of the droplet particle transition in dairy colloidal mixes: The impact of the molecular scale on particle morphology. 2nd SLAMM conference (Solliciter LA Matière Molle), November 18th-21st, Roscoff, France. Oral presentation

LIST OF FIGURES

Figure 1. Global milk equivalent per capita annual consumption (left axis; kg/(year.inhabitant)) and world population (right axis; million inhabitant) between 2010 and 2019 (IDF, 2020) ...	4
Figure 2. Cow's milk production growth in 2019 (IDF, 2020)	5
Figure 3. Key exporters at the global scale. Left: market share in 2019; right: top exporters (mlt of milk equivalent) in between 2010 and 2019 (IDF, 2020).....	6
Figure 4. World trade: Main dairy products exported (mlt) in between 2010 and 2019 (IDF, 2020). SMP: skim milk powder; WMP: whole milk powder.....	6
Figure 5. China dairy imports (left axis and coloured areas; x 1000 t milk equivalent) and milk production (right axis and green curve; x 1000 t milk) from 2000 to 2019 (FAO, 2020). SMP: skim milk powder; WMP: whole milk powder.....	8
Figure 6. Country milk formula category sales volumes (kg) per child in 2019 v. 14-year compounding annual growth rate (CAGR; %) for 2005–2019; weighted markers represent infant/child population sizes (P. Baker et al., 2021).	9
Figure 7. The casein micelle. A : Transmission electron micrograph image of bovine casein micelles (Qi, 2007). B: The nanocluster model structure proposed by de Kruif and Holt (2003); black dots correspond to CCP nanoclusters. C: Sponge like model structure proposed by Bouchoux et al. (2010).	14
Figure 8. Tridimensional representation of β -lactoglobulin (A) (Brownlow et al., 1997) and α -lactalbumin (B) (Acharya et al., 1991).....	16
Figure 9. Generalized powdered IMF and manufacturing process (adapted from (Montagne et al., 2009)). Dotted lines indicate alternative processing route.	22
Figure 10. Illustrative scheme of an industrial plant for the production of dairy powders.	26
Figure 11. A) Generation of monodisperse droplets in MDSD spray dryers. (Foerster 2016) B) Puffed and C) wrinkled dry particles obtained by monodisperse dryers varying feeding solution composition and operating parameters (e.g. temperature) (Rogers et al., 2012).30	30
Figure 12. A) GFM setup: 1- Main support; 2- Glass filament box; 3- Heater for temperature control; 4- Drying chamber; 5- Glass filament; 6- Video camera; 7- By-pass switch; 8) Mesh block; 9- Heaters. B) Milk droplet shrinkage with time and skin formation (S. X. Q. Lin & Chen, 2002).	32
Figure 13. A) Competition between diffusive Brownian motion and drying-induced front receding at droplet air-liquid interface. B) Onset of interfacial sol-gel transition for high evaporation rates (Lanotte, 2020).....	35

Figure 14. A) Schematic representation of a pendant drying droplet and definition of its base radius (r_b), cap radius (r_c) and apex height (z). B) Representation of dimensionless values (X/X_0) for base radius, cap radius, height, and mass of single droplet of WPI (filled dots). C) Representation of dimensionless values (X/X_0) for base radius, cap radius, height of single droplet of NPC (filled dots) and a single droplet of pure water (empty dots). Characteristic times represent the beginning of the buckling of droplet at t_B , and vacuole formation at t_V . Adapted from Sadek et al. (2013, 2016). 36

Figure 15. Sketch of the triple line as a boundary of solid substrate, liquid droplet and surrounding air. 37

Figure 16. WPI (A) and NPC (B) shape evolution with time. Final particle of WPI (c) and NPC(d) observation by SEM (Sadek, Pauchard, et al., 2015). 38

Figure 17. Diagram WPI and NPC skin rheological regimes as a function of the drying time (Sadek et al, 2015). 39

Figure 18. A) Micrographs of different WPI/NPC particles obtained by MDSD drying (objective: x10, scale bar =100 μm); B) Image of WPI/NPC particle obtained by pendant single droplet drying experiment (objective: x10, scale bar =200 μm) (Sadek et al., 2014). 41

Figure 19. A) Internal part of dry WP skin layer observed by SEM. B) Normalized Ca mass percentage on the internal (IN) and the external (OUT) part of WP/CM mixes skin layer (Lanotte et al., 2018)..... 42

Figure 20. Research strategy of the PhD project 44

Figure 21. (a) Top view of the PDMS substrate, cylindrical pillars (blue circle) were separated from each other by a 50 μm center-to-center distance. (b) a scanning electron microscopy image of the cylindrical pillars (20 μm diameter, 10 μm height (Sadek et al., 2013)..... 49

Figure 22. Profile observation device, ① high-speed camera, ② drying glass chamber (8*8*8 cm^3), ③ background light, ④ glass support (grey area), ⑤ PDMS substrate (green square), ⑥ zeolites (empty circle)..... 50

Figure 23 . A pendant droplet on the substrate. Base diameter (D) is the radius at contact line with substrate and the apex height (H) is the maximum height from the substrate to the top of the droplet. 51

Figure 24: Droplet top view setup. Zeolites (circle shape) were put on the bottom of the box, the support (grey rectangle) was used to provide droplet pendant configuration. PDMS substrate (green square) and glass slide (yellow rectangle) were used to hold droplets. .. 54

Figure 25. Profile (①) and top (②) view of a WPI particle; W_f refers to the foot width. Scale bar is 200 μm 54

Figure 26 . Droplet mass measurement device, ①micro-balance, ②zeolites, ③ support 55

Figure 27 . Image of a dry droplet obtained by SEM. (a) Half particle deposited on the conductive tape, δ_s is the shell thickness of particle. (b) Zoom of the skin section structure. The scale bar of (a) and (b) is 100 μm and 10 μm , respectively. 56

Figure 28. (a) droplet oscillatory process: a droplet (blue circle) first compresses to a smaller volume (green dash circle) and recovers to its initial one, then expands into a big drop (black dash circle). (b) Preliminary oscillatory test of droplets with different frequencies and strain amplitude percentages. The droplet area difference of big and small is defined as A, the initial droplet area is A_0 58

Figure 29. Viscoelastic modulus (E) of WPI/NPC particle variation with frequency when we fix the strain amplitude percentage at 12.5% (a); we fixed the frequency at 20 s, the E changing as function of amplitude percentage(b)..... 59

Figure 30 . Monodisperse spray dryer sketch. ① droplet generator with the detail components are shown in red rectangle, ②drying chamber and ③ the collection plate. 60

Figure 31. Various shapes at different circularity (A) and solidity (B). 61

Figure 32. Schematic of single droplet drying setup: 1. Air-pressure controller. 2. Drying tower. 3. Air storage tank. 4. Flow regulator. 5. Heater. 6. Temperature controller of drying air flow. 7. Drying chamber. 8. High-speed camera. 9. Droplet suspension module for droplet diameter measurement. 10. Temperature measuring glass filament. 11. Weight measuring glass filament. 63

Figure 33. Morphological evolution of WPI/NPC droplets during the evaporation process as a function of $\text{WPI}\%_R$. The image sequences are intended only to summarize the main drying-induced shape changes, without providing a quantitative comparison between the duration of the different stages. The scale bar is equal to 500 μm 69

Figure 34: Evolution of the mass loss ($-\text{dm}/\text{dt}$) with time in WPI/NPC droplets with $\text{WPI}\%_R=0\%$, 50%, 100%. In the inset, the black triangles refer to the overall drying time (t_{dry}) and the blue stars to the half-life drying time ($t_{1/2}$) for all the mixes 71

Figure 35. Onset and duration of the buckling stage (Δt_{gel} , purple rectangles), and of the final drying of remaining water (Δt_{dry} , yellow rectangles) as a function of $\text{WPI}\%_R$. In the inset, typical curves referring to base diameter (D) and apex height (H) time evolution is presented for WPI suspensions. From these curves, the value of Δt_{gel} has been deduced for all WPI/NPC mixes. 73

Figure 36 Particle shell structure captured by SEM: A) Skin layer of a dry droplet. The white frame highlights the region of interest for the investigation of skin structure; Shell structure of

droplets of WPI (B), NPC (C), and mixes with $WPI\%_R=50\%$ (D). The scale bars correspond to $10\ \mu\text{m}$.	74
Figure 37. Evolution of the complex viscoelastic modulus (E) with time in WPI/NPC droplets with different $WPI\%_R$. In the inset, the elastic (E') and the viscous part (E'') of the complex modulus are presented for $WPI\%_R=0\%$, 50% , and 100% .	77
Figure 38. Schematic representation of the molecular structure of casein micelles (NPC) and sodium caseinates (SC).	78
Figure 39. Qualitative comparison between WPI/SC and WPI/NPC dry droplets for different $WPI\%_R$.	79
Figure 40. Diameter reduction percentage in WPI/SC and WPI/NPC dry droplets as a function of $WPI\%_R$.	80
Figure 41. Normalized final apex height of WPI/SC and WPI/NPC dry droplets as a function of $WPI\%_R$.	81
Figure 42. Evolution of normalized droplet base diameter (D/D_{max} – top curves) and apex height (H/H_{max} – bottom curves) with time for WPI samples with different protein concentration (c_p).	85
Figure 43. Estimation of the diameter reduction ($\Delta D\%$) as a function of $WPI\%_R$ at the end of the drying process in WPI/NPC droplets with $c_p = 6\ \text{w/w}\%$, $10\ \text{w/w}\%$, and $14\ \text{w/w}\%$.	87
Figure 44. A) Definition of the foot width (w_f) at the end of the evaporation process in WPI/NPC droplets. 1) Profile and 2) top view projections in a WPI droplet. Scale bar equal to $200\ \mu\text{m}$. B) Measure of w_f as a function of $WPI\%_R$ for $c_p = 8\ \text{w/w}\%$, and $12\ \text{w/w}\%$.	89
Figure 45. Evaluation of the impact of $WPI\%_R$ on WPI/NPC droplet final normalized height (H_f/H_{max}) for dispersions with $c_p = 6\ \text{w/w}\%$, $10\ \text{w/w}\%$, $14\ \text{w/w}\%$.	90
Figure 46. Phase diagram of the main shape characteristics of dried WPI/NPC droplets as a function of protein overall concentration (c_p) and sample composition ($WPI\%_R$). I: Wrinkled surface, no border detachment, vacuole formation; II: Hybrid shape, significant delamination, vacuole formation; III: smooth interface, border detachment, vacuole formation; IV: smooth surface, significant delamination, no vacuole formation.	91
Figure 47. Dry particles of NPC (a), WPI (b), $WPI\%_R = 50\%$ (c) and SC (d). The scale bars correspond to $200\ \mu\text{m}$.	95
Figure 48. Cross-section area distribution of dry particles of WPI (a), and NPC (b) powders. Both curves are characterized by two peaks corresponding to two different populations differing by size and morphology, as shown in the corresponding images in the inset.	96

Figure 49. Cross-section area distribution of dry particles of SC powders. Similar to WPI and NPC case, the distribution is characterized by two peaks corresponding to two different populations, as illustrated in the corresponding images in the inset. 96

Figure 50. Cross-section area distribution of dry particles of WPI%_R=50% and WPI%_R=80%. 97

Figure 51. Distribution of the circularity in pure protein (a) and WPI/NPC mix (b) powders. 98

Figure 52. Distribution of the solidity in pure protein (a) and WPI/NPC mix (b) powders. 99

Figure 53 : (a) Temperature, mass and diameter of NPC droplet (10 w/w %) evolution at different drying temperatures (70°C, 90°C and 110°C). Each line is the average result of 3~5 repetitions. The inset droplet images were obtained from the video of droplet drying at 70°C. 107

Figure 54 : (a) Relative activation energy variation as a function of moisture content at three drying temperatures, (b) Fit of the $\Delta E_v/\Delta E_{v,b}$ master curve (black solid line) with experimental data. 108

Figure 55 : Fit of temperature and mass at 70°C (a), 90°C (b) and 110°C (c). 109

Figure 56 : Osmotic pressure of NPC as a function of moisture content calculated by EMM from Bouchoux et al. (2009a) data (a) and REA (b). 110

Figure 57 : Comparison of osmotic pressure calculated by different approaches at the same condition 111

LIST OF TABLES

Table 1. Overall production of the main dairy powders between 2014 and 2018 (CNIEL, 2020)..	7
Table 2. Protein composition of cow milk (g.L^{-1}) (adapted from Jeantet & Croguennec, 2018)..	12
Table 3. Physicochemical characteristics of bovine caseins (Jeantet & Croguennec, 2018).....	13
Table 4. Physicochemical characteristics of main bovine whey proteins (Jeantet & Croguennec, 2018)	15
Table 5. Distribution of macroelements (mg.L^{-1}) between the soluble phase and the colloidal phase at pH 6.65 and at room temperature (Jeantet & Croguennec, 2018).....	17
Table 6. Human milk composition in comparison to cow milk (data from (1) Thompkinson & Kharb, 2007, (2) Brenna et al., 2007, (3) Bode L (2012), (4) Gopal & Gill (2000), (5) Chatterton et al., 2013, (6) Farrell et al., 2004, (7) Cuillière et al., 1999, (8) Jeantet & Croguennec, 2018) ...	18
Table 7. Advantages and drawbacks of wet-mixing and dry blending (adapted from Montagne et al., 2009)	20
Table 8. Raw materials typically used in infant milk formulae (Adapted from Montagne et al., 2009; Thompkinson and Kharb, 2007 and European Union, 2016).....	23
Table 9 : Overall volume fraction (ϕ_p) and WPI volume fraction (ϕ_{WPI}) as a function of overall protein concentration c_p and WPI percentage $\text{WPI}\%_{\text{R}}$	49
Table 10. Monodispersed drying conditions.	60
Table 11. Drying parameters of NPC droplet.....	62
Table 12. Overall protein volume fraction (ϕ_p), WPI volume fraction (ϕ_{WPI}), and average surface tension (γ) at the equilibrium in WPI/NPC droplets as a function of $\text{WPI}\%_{\text{R}}$	67
Table 13. Duration of Δt_{gel} and of the final drying of remaining water (Δt_{dry}) as a function of $\text{WPI}\%_{\text{R}}$	72
Table 14: C value calculated by ZJD model (Eq. 8) with different $\text{WPI}\%_{\text{R}}$	76
Table 15. Measured values of $\Delta D\%$ and H_i/H_{max} in drying WPI/NPC droplets with different c_p and $\text{WPI}\%_{\text{R}}$	87
Table 16. Water activity, mass of NPC, moisture content during NPC sorption.	111

Titre : Séchage de gouttes uniques et monodisperses de mélanges de protéines laitières

Mots clés : Séchage - Caséines – Protéines solubles – Peau – Transition sol-gel - Particule

Résumé :

Afin de garantir les propriétés des formules infantiles, un parfait contrôle du séchage est nécessaire. Mais comprendre la transition goutte à particule est difficile au sein d'enceintes fermées et au vu des cinétiques de séchage. Cette thèse vise à étudier la formation de la peau en surface de gouttes de mélange de protéines solubles (WPI) et micelles de caséine (NPC), qui influence la morphologie et les propriétés des particules. L'influence du rapport WPI/NPC ($WPI\%_R$) sur la formation de la peau, la morphologie des particules et la cinétique de séchage a été démontrée sur goutte unique. Au-delà d'un $WPI\%_R$ critique, les protéines solubles contrôlent les caractéristiques interfaciales, depuis la transition sol-gel jusqu'à solidification complète. 4 morphologies caractéristiques ont été observées selon un diagramme de phase validé en séchage monodisperse et fonction de la concentration protéique globale (C_p) et du

$WPI\%_R$. Ainsi, l'augmentation de C_p induit une transition sol-gel précoce, réduisant la contraction volumique et la délamination des particules. Par ailleurs, le remplacement des NPC par des caséinates de sodium dans les mélanges conduit à un comportement intermédiaire induit par leurs caractéristiques physico-chimiques et de taille. Enfin, un modèle préliminaire a été établi pour prédire la transition de phase des gouttelettes lors du séchage par atomisation.

Ce travail permet de mieux comprendre la phénoménologie du séchage des colloïdes laitiers, et plus généralement la physique de la structuration de l'interface de systèmes polydispersés. Ses perspectives concernent la formation de particules à partir de formulations plus complexes représentatives de produits nutritionnels.

Title : Drying of mixes of dairy protein using single and monodisperse droplet experiments

Keywords : Drying - Caseins - Whey proteins - Skin - Sol-gel transition - Particle

Abstract :

In order to guarantee the properties of infant formulas, perfect control of drying is necessary. It requires understanding the drop-to-particle transition, which is still difficult given the closed feature of drying chambers and the fast-drying kinetics. This thesis aims to study the skin formation on the surface of drops of mixture of whey proteins (WPI) and casein micelles (NPC), which effect the morphology and properties of the particles.

The impact of the WPI / NPC ($WPI\%_R$) ratio on skin formation, particle morphology and drying kinetics has been explored on single drop. Beyond a critical $WPI\%_R$ ratio, WPI control the interfacial characteristics, from the sol-gel transition to solidification, since WPI prefers to accumulate at outer layer of the skin. In addition, 4 characteristic morphologies were observed according to a phase diagram as a function of the overall concentration (C_p) and of the $WPI\%_R$.

ratio validated in monodisperse drying. Regardless of $WPI\%_R$, the increase in C_p induces an early sol-gel transition, with reduced shrinkage and delamination of the particles. Besides, replacing NPC with sodium caseinates (SC) in the mixes showed an intermediate behavior induced by their physico-chemical properties and their smaller size. Finally, a preliminary model was established to predict the droplet phase transition in spray drying chambers.

This work provides a better understanding of the phenomenology of the drying of dairy colloids, and more generally of the physics of the structuring of the interface of polydispersed systems. The perspectives of this study concern the formation of particles from more complex formulations representative of nutritional products.